AFOSR-1092

262348

CATALOGED BY ASTIA

The Effect of the Earth-Ionosphere Waveguide on Whistlers

by

J. H. Crary

Technical Report No. 9
July 17, 1961

61-4-4
NOX

RADIOSCIENCE LABORATORY

STANFORD ELECTRONICS LABORATORIES

STANFORD UNIVERSITY · STANFORD, CALIFORNIA

THE EFFECT OF THE EARTH-IONOSPHERE WAVEGUIDE ON WHISTLERS

by

J. H. Crary

Technical Report No. 9
July 17, 1961

Radioscience Laboratory
Stanford Electronics Laboratories
Stanford University
Stanford, California

ABSTRACT

A whistler is a natural audio-frequency electromagnetic signal which
results from the dispersion of broad-band energy radiated by lightning
discharges. Whistlers travel along discrete paths aligned with the earth's
magnetic field. Such a path takes the energy several thousand kilo-
meters out into space, and back to earth in the opposite hemisphere.
The space between the earth and the lower edge of the ionosphere acts as
a waveguide. The whistler then propagates in the earth-ionosphere wave-
guide to the receiver. Thus it should be possible to explain certain
properties of whistlers in terms of the properties of the waveguide. It
should also be possible to locate the point at which the energy enters
the waveguide (the exit point) by direction-finding (d-f) measurements at
spaced stations.

The first possibility is investigated by expressing the theoretical
intensity, polarization, and apparent direction of arrival of the received
signal as the sum of multiply-reflected rays propagating in the earth-
ionosphere waveguide. The boundaries of the guide are assumed to be
sharply bounded homogeneous media. The earth is described by a complex
dielectric constant. The ionosphere is described by the ql approximation
of the magneto-ionic theory, assuming a vertical, static, magnetic field.
The coupling introduced between the two polarization components of the
wave by the magnetic field in the ionosphere is included.

Curves (parametric in frequency, distance, and waveguide parameters)
of the response of a vertical monopole and of crossed loops are shown.
The ratio of the crossed-loop voltages and the null-bearing errors are
determined for comparison with experimental data.

Qualitative agreement is found between the calculated and the pre-
viously unexplained experimental data on crossed-loop voltage ratios.
Detailed agreement is not expected because of the dependence of the
Lissajous patterns on various waveguide parameters which are not known
with sufficient accuracy. It is possible that a detailed comparison
could be obtained from a large number of calculations, but the conditions
would probably not be unique.

From the theoretical work it was found that apparent lateral deviation of bearing can be caused by the presence of multiple rays, even though all the rays travel in the great-circle plane containing the source and the receiver.

Another new result is that either a normal vertical loop or vertical monopole may receive a higher field strength when multiple rays are present. This factor is significant in vlf field-strength measurements.

A two-station d-f experiment was performed, using crossed vertical loops, a vertical monopole, and a goniometer device. Exit points were located from average null bearings for ten whistlers. The geomagnetic latitudes of these locations were compared with the latitudes calculated independently from whistler-dispersion data. The individual latitude differences are as great as 18 degrees, although the average difference is only 3.1 degrees. The individual differences can be accounted for by the d-f errors for each location and therefore do not contradict the theory of whistler propagation.

Large differences in the null bearing occur for each whistler for different frequencies. Calculations using ray theory show that the null-bearing error in a loop system varies widely with frequency, because of polarization and apparent lateral-deviation error. An even wider variation in error is expected when distance and waveguide parameters are varied. The theoretical and the experimental results thus agree qualitatively. The results show that the average bearing tends to approach the true bearing, but that the accuracy is insufficient to warrant further d-f work with the present system. A system which uses only one type of antenna, and preferably responds to only one field component, is recommended. This system would eliminate the polarization and apparent lateral-deviation errors.

TABLE OF CONTENTS

TABLE OF CONTENTS (Cont'd)

LIST OF ILLUSTRATIONS

Figure   Page

ACKNOWLEDGEMENTS

I. INTRODUCTION

A. BACKGROUND

Whistlers are one of many types of natural electromagnetic noise occurring in the audible range of frequencies. They may frequently be detected by listening to the output of a sensitive audio amplifier connected to an antenna. Whistlers are gliding tones which descend in frequency across the audible range in about 1 sec.

The gliding tone results from the dispersion of lightning energy that travels along discrete paths believed to be aligned with the earth's magnetic field. This path takes the energy several thousand kilometers out into space and then back to earth in the opposite hemisphere. The action of free electrons in the presence of the magnetic field causes the velocity of propagation to vary markedly with frequency. At the lower frequencies this variation is given approximately by $D = t \sqrt{f}$, where t is the time in seconds after the originating impulse, f is the whistler frequency in cps, and D is the dispersion. The value of D depends upon the magnetic latitude of, and the ionization density along, the path. (Recent papers and reports are available which cover the history and details of whistlers.)[1--5]*

The whistler energy leaves the lower edge of the ionosphere at a point determined mainly by the location of such a path. The lower edge of the ionosphere and the earth's surface form a channel which acts like a waveguide at very low frequencies (vlf). The whistler is propagated in the earth-ionosphere waveguide from the exit point to the receiver. These considerations lead directly to a number of interesting possibilities for further research. Two of these areas of study were selected for discussion in this paper. The first of these is the explanation of certain characteristics of whistlers in terms of the properties of the earth-ionosphere waveguide; the second is the location of the exit point by direction-of-arrival measurements at two or more spaced stations. This information would provide a useful check on the determination of whistler-path location by other methods. It is the purpose of this report to

---

*Superscript numerals refer to references at end of report.

present the results of theoretical and experimental investigations in these two areas.

Ray theory is used to calculate the field intensity, apparent polarization, and apparent direction of arrival of the received signal for different distances, frequencies, and waveguide parameters. A two-station direction-finding (d-f) experiment was also performed. The calculated results are shown to be consistent with this and other experiments. In addition, the theoretical investigation showed that the mere presence of multiple rays can cause apparent lateral deviation at vlf (see p. 145). A new factor, which results in differences in field-strength measurements with vertical loops and monopoles in the presence of multiple rays, was also found.

B. PREVIOUS WORK

The wealth of experimental data on whistlers available in recent years, especially the multistation synoptic recordings made during the IGY[6] and the following periods, and the magneto-ionic-duct propagation studies,[7] provide overwhelming evidence of the existence of discrete paths or ducts of propagation. The magnetic latitude of such a path and the ionization density along the path may be calculated, on the assumption that the paths are aligned with the earth's dipole field. The results are quite reasonable, as shown by Smith,[4] and provide models of ionization density variation with height along the paths.

The earliest known measurements of direction-of-arrival and polarization of whistlers were undertaken by the author, beginning in late 1955.[1,8] In the first experiment an attempt was made to compare the amplitudes and phases of the voltages induced in a pair of crossed vertical loopes. These voltages were recorded on a dual-channel tape recorder. The amplifiers and tape-recording channels were equalized in amplitude to within 0.1 db and in phase to within one degree over the useful frequency range. Lissajous patterns and waveforms were later photographed on continuously moving film.

The best results were obtained during the great magnetic disturbance of 4 March 1956. The crossed-loop antenna voltages produced by a whistler

were found to vary rapidly with frequency in relative phase and amplitude. The variations of axis ratio and orientation of the Lissajous-pattern ellipse were roughly sinusoidal in time, as previously reported.[1,9] The only conclusion that could be drawn was that the direction of arrival or polarization, or both, seemed to vary rapidly with the frequency of the whistler. Both directions of rotation of the ellipse were found to be present for these whistlers. A previous whistler recorded on 13 September 1955 at approximately 1204 UT was found to contain only one direction of rotation, although the crossed-loop Lissajous pattern varied from elliptical to linear in a similar manner. These results will be discussed on page 133.

Some of the early work on the directions of arrival proceeded from the assumption (shown in this report to be untenable) that the energy would arrive from the direction of the magnetic field. A thesis by Delloue[9*] reported partial confirmation of this expected result by narrow-band polarization and direction measurements at 5 kc. He stated that the directions of arrival tended to "circle around the magnetic field line" in some cases. He also stated that the direction of arrival appears to vary rapidly in most cases and this was attributed to "many small elementary whistlers, arriving, apparently, from different directions." The author then stated that the polarization varied rapidly. He attempted to interpret the observed polarization in terms of the ionization density in the outer atmosphere. Even when the effects of the earth-ionosphere waveguide are neglected, this interpretation may be criticized on the basis that the observed polarization should be the "limiting"[35] polariz-ation characteristic of the lower layers of the ionosphere. The observed rapid variation of apparent direction of arrival is exactly what would be expected when the effects of the earth-ionosphere waveguide are taken into account.

The crossed-loop Lissajous patterns for several whistlers were observed by the author on the night of 27 May 1959 between 0730 and 0755 UT. These patterns, sketched directly from the oscilloscope, were generally

elliptical in shape and some showed fairly consistent patterns, with some rapid changes in tilt or axis ratios. These results will be discussed further on page 147.

J. M. Watts was the first to suggest that goniometer[*] techniques could be applied to whistlers, and he made the first measurements of this type.[41] Further details are given on page 101.

In 1960, Ellis[10,11] reported d-f measurements of vlf noise associated with geomagnetic disturbances. The measurements were made with crossed vertical-loop antennas and a goniometer. Bearings from three stations in Hobart, Tasmania, and Camden and Adelaide, Australia, were reported, yielding a location for the source. Interpretations were made of the "null" ratios (maximum/minimum voltage ratios) of the goniometer in terms of the size of the source. A horizontal direction of arrival was assumed, thus eliminating the effect of polarization on the azimuth determination. However, this assumption is not valid, as the calculations given later in this report will demonstrate.

A different system is described by Cartwright[28] who assumes that the polarization is completely random. This view is questioned, since a characteristic polarization is probably present in at least some vlf noise. An example is the "hiss" (a type of vlf noise[1]) of 4 March 1956 at Stanford, in which a characteristic pattern was present in crossed-loop Lissajous patterns. The results given later will show that the polarization over a limited frequency range is not random.

---

[*] A goniometer is a device constructed to provide coupling between two circuits and an output as a sine-cosine function of the rotor position. It is constructed with two pairs of fixed plates and a rotor assembly, shaped to give sinusoidal coupling. The rotor assembly consists of two sections that are 90 deg apart in position on the shaft. One section meshes with each set of fixed plates, so that sine-cosine coupling is obtained.

C. PRESENT WORK

It has been shown that the effect of the earth-ionosphere waveguide
on whistler and other vlf signals is of great interest. By means of ray
theory and several simplifying assumptions a theoretical method is developed
that yields values for the magnitude and polarization of the electric
field and the apparent angles of arrival of the wave as seen by the antenna
system. The antenna-induced voltages and certain ratios of voltages that
are important to the d-f system are also calculated. The response of a
d-f system, utilizing a goniometer, is also calculated for positions of
the goniometer for 0 to 180° in 10° steps. The results are presented
in curves, and are discussed in comparison with available experimental
data, which include those mentioned in previous work and the results of
a d-f experiment that utilized goniometer systems at two spaced stations
to determine exit-point locations from the observed null bearings.

A general discussion of exit-point location by means of inverse
loran (see p. 100) and d-f methods for vlf is presented. In addition, a
new sensing method designed for the goniometer system is described.
Sense (removal of 180° ambiguity) is obtained by adding the output of
a vertical monopole antenna to the goniometer output. The new method
also improves the theoretical bearing accuracy and null ratio for ellip-
tically polarized waves.

The response and errors of the goniometer system, with and without
sense, are calculated for various conditions of wave polarization and
elevation angle of arrival. Some of the results of an experimental d-f
program are also presented and discussed.

The conclusions drawn from the theoretical results are given, theoreti-
cal and experimental data are compared, and recommendations for future
work are made.

D. CONTRIBUTIONS OF THE PRESENT WORK

It is the purpose of this report to present the ray-theory (geo-
metrical-optics) method selected for the calculation of the effect of
the earth-ionosphere waveguide on whistlers and other vlf signals, and

the results of the use of the model. This model is the first one to in-
clude the total field excited by an elliptically polarized wave and the
effect of the coupling between the horizontal (perpendicular) and vertical
(parallel) components of the field resulting from the presence of the
earth's magnetic field. The results show that this relatively simple
model can explain most of the experimental results, including field-
strength variations, apparent polarization, and apparent arrival angles.
This agreement gives significant support to the duct theory of propagation.
There is no theory that would explain most of the experimental results in
terms of a signal arriving directly at the receiver from the direction of
the magnetic field. Furthermore, these results provide for the first
time a basis for evaluating the performance of antenna systems used in
whistler observation and for estimating the effective area of a whistler.
They also provide values of transmission loss from the whistler mode to
the antenna that may be used to evaluate the various losses in the ex-
citation and transmission of whistler-mode signals.

The equations of the total field and the antenna response also show
that the response of different antennas is often not compatible with the
assumption that the total received field is a plane wave, although the
ray components which make it up are essentially plane waves. It is also
shown that a vertical monopole may "see" a larger vertically polarized
field component than a normal loop antenna under these conditions. The
difference in the response of the normal and abnormal loops is also shown
to cause apparent lateral deviation at vlf. This effect is similar to,
but distinct from, polarization error.

To test the hypothesis that whistler signals generally arrive from
the direction of the magnetic field, a calculation was performed at a
distance such that the n = 0 ray is parallel to the earth's magnetic
field at the geomagnetic latitude of Stanford (44°N). The characteristics
of the actual signal calculated for this case show that the polarization
and the phase shift between crossed-loop antenna voltages is relatively
constant as a function of frequency. These results show that the experi-
mental results generally are inconsistent with the premise that the
energy arrives from the direction of the magnetic field.

II. THE CALCULATION OF THE CHARACTERISTICS OF WAVEGUIDE SIGNALS

A. THE AVAILABLE METHODS AND THE CHOICE OF A MODEL

It is now necessary to develop a model for the calculation of the
characteristics of whistler-mode signals. Two general methods — "ray
theory"[14,26] and "mode theory"[45] — have been used in the calculation of
the vertical component of vlf field strengths for a path between two
points on the ground.

The mode theory utilizes a series of solutions to Maxwell's equations
matching the boundary conditions to represent the wave traveling in the
guide. Flat-earth geometry* is usually assumed. The same assumptions
about the boundary conditions are made in both methods of solution.

The ray-theory uses the principles of geometrical optics in the
solution of propagation problems. The use of geometrical optics is
strictly valid in solving refraction and reflection problems only for
the case of λ approaching zero. It can be applied to other cases of re-
flection, however, when the reflecting or refracting medium may be con-
sidered to have slowly varying properties.[36]

Each method has some general advantages. Ray theory generally re-
quires few rays for short distances, while mode theory requires a large
number of modes. At long distances the reverse tends to be true. The
exact number of modes or rays necessary to describe the field for a given
distance depends, of course, on the electrical characteristics of the
ionosphere and the ground, and on the frequency of the wave. For long
distances, mode theory has the advantage over ray theory in the case of
the calculation of transmission from point to point on the ground. Be-
yond the critical distance (around 1000 km) the first skywave component
is in the shadow region and a diffracted wave exists at the receiving
antenna. Special calculations are required for an accurate solution for
the diffracted ray in this region. This problem is discussed on page 23.

One further factor gives the ray theory a definite advantage for
this particular problem. The majority of mode-theory[12-14] treatments
deal only with the vertical component of the electric field of the wave,
although some later work considers the horizontal component of the field.

---

*Some work by Wait and Spies, showing that the curvature cannot be
neglected in mode calculations, has recently been published.[44]

To a slightly lesser extent the same is true of the ray theory. However, it is very difficult in mode theory to take account of the coupling introduced between the two polarizations by the earth's magnetic field in the ionosphere. This coupling can be handled simply in the ray theory. The necessary ray-theory expressions for the complete field are much simpler to derive and calculate, and reflection coefficients that include the effects of both vertical and horizontal field components are already available. For these reasons, the ray theory was chosen for this problem.

B. ASSUMPTIONS

It is now necessary to make several simplifying assumptions, as follows:

1. Each individual ray component may be considered a plane wave in the antenna area, and the antenna is considered to be in the far field. In the near field the ratio of E/H is no longer constant and the antenna-response equations lose accuracy. Thus the problem is restricted to distances beyond the order of one half the wavelength. This restriction will be violated for short distances at the lower end of the whistler spectrum, since the wavelength at 2 kc is 150 km. The results obtained, however, can still be significant in terms of gross behavior of the whistler signals. For this reason the calculations will be carried into this range for the purpose of comparison with the available experimental data. Over most of the ranges of frequency and distance of interest, however, the wave may be considered plane and the equations given may be applied with very little error.

2. The quasi-longitudinal (ql) approximation is valid for this problem. According to Budden,[12] the ql approximation is valid where

$$\left| y_T^4 / 4 y_L^2 \ (1-x-jz)^2 \right| \ll 1 \tag{2.1}$$

This may be expressed as

$$\left| \text{Tan } \theta \, \sin \theta \right| \ll \frac{2f}{f_L} \left| \left(1 - \frac{f_o^2}{f^2} - j\frac{\nu}{2\pi f} \right) \right| , \qquad (2.2)$$

where θ is the angle between the wave normal and the static magnetic field, and

$$y_T = y_H \, \sin \theta .$$

$$y_L = y_H \, \cos \theta$$

$$y_H = \frac{f}{f_H}$$

$$x = \frac{f_o^2}{f^2}$$

$$z = \frac{\nu}{2\pi f}$$

$$f_o = \left(\frac{Ne^2}{4\pi^2 \, m\kappa_o} \right)^{1/2} = \text{plasma frequency (cycles/sec)}$$

$$f_H = \frac{\mu' \, He}{2\pi m} = \text{gyrofrequency (cycle/sec)}$$

$N =$ electron density (number/m^3)

$e =$ electronic charge (coulombs)

$m =$ electronic mass (kg)

$H =$ strength of static magnetic field (amp/meter)

$f =$ wave frequency (cps)

$\nu =$ collision frequency (collisions/sec)

$\kappa_o =$ permitivity of free space (farad/meter)

$\mu' =$ permeability of free space (hy/meter)

Rationalized mks units will be used except where otherwise noted. This restriction will be most critical at the higher frequencies because of the f^2 in the denominator of the second term. When $f = 20$ kc (the highest frequency of interest here) and for a typical summer-night-model

ionosphere (see page 37), the result is:

$$\left| \tan \theta \sin \theta \right| \ll 8 \qquad (2.3)$$

When 5% error is chosen, the result is:

$$\sin \theta \tan \theta = 0.4$$
$$\theta \cong 35°$$

The angle of refraction in the ionosphere is complex. The best way to interpret this fact is to use the angle of the wave normal ψ, defined on p. 166. The maximum angle of refraction ψ_{cr} vs frequency is plotted in Fig. F-1. The value of ψ_{cr} for the summer-night-model ionosphere is approximately 28 deg. The angle between the earth's magnetic field and the vertical, measured in the same sense as ψ_{cr}, is 27.5 deg from the vertical at the latitude of Stanford ($44°$ geomagnetic). If propagation is toward the magnetic pole in the magnetic meridian the ql approximation is valid, since the wave normal will make small angles with the earth's field. This statement is also essentially true for directions on either side of the meridian where the rays make small angles with the field. The wave normal would have to be almost perpendicular to the field for propagation toward the equator. The ql approximation would be very poor for this direction. The region of validity increases rapidly as the frequency is decreased, however, and the approximation is valid for all directions up to $90°$ on either side of the direction of the magnetic pole, at the low end of the whistler range.

The exact conditions for validity are very sensitive to plasma frequency and collisional frequency. If the plasma frequency were doubled, which is not unreasonable for night-time conditions, the ql approximation becomes valid for essentially all directions. It must be recalled that the parameters used in the summer-night model were determined for this same approximation, to match experimental ground-to-ground propagation data for all directions of propagation in the 15- to 20-kc range. Therefore the range of application is probably greater in the upper frequency range than the inequality suggests.

It must also be considered that the longitudinal component of the gyrofrequency y_L is actually complex in the case of the lossy ionosphere, and its magnitude varies with the angle of refraction. Another result of the ql assumption is that y_L is represented by a real value with an effective magnitude determined to fit experimental results best. When the ql assumption is not make, a complete solution is necessary, in the manner of Yabroff,[17] for the case for which the refractive index is a function of the wave normal angle. This requirement would so complicate the calculations that they would be no longer practical. The justification for this assumption is, first, that previous results[14,26] of calculations using these assumptions for ground-to-ground propagation problems are consistent with experimental data; second, the results obtained in this report are consistent with the experimental data on whistlers.

3. The third assumption is that the lower edge of the ionosphere may be adequately represented by an equivalent homogeneous model with a sharp lower boundary. This assumption is very difficult to treat quantitatively. It is generally accepted that a sharp boundary approximation is reasonable if there is a large change in the properties of the medium within the distance of a fraction of a wavelength. There is a sharp gradient of electron density at the lower edge of the E layer, so that this condition is fulfilled over most of the frequency range of interest.

The homogeneous model may be used if the changes in the medium above the sharp boundary are slow enough that there is not a significant change in the properties of the medium within a distance of the order of a wavelength. A superposition of a number of these slabs of different properties may be used to describe a rapidly varying medium in the limit as the number of slabs becomes very large and their thickness very small.

In this report, one homogeneous medium is used. The medium, which approximates the ionosphere, must be sufficiently uniform that the wave is attenuated to the point of being negligible before it encounters a significant change. This uniformity would thus have to exist over a distance of at least the order of a wavelength. The wavelength in the medium decreases approximately inversely as the square root of the frequency. The actual distance over which the medium must not change significantly thus depends on the frequency, the refractive index, and the angle of refraction in the medium.

An actual quantitative statement of the criteria for the validity of this assumption has not been made and cannot be made with the present state of knowledge of propagation in a conductive, inhomogeneous medium. The only justification for this assumption is that the results are consistent with the available experimental data on ground-to-ground transmission[12,14,26] and whistlers.

4. The fourth assumption is that the ionosphere contains plane-wave energy, with all wave normals contained within a cone whose axis is normal to the boundary and whose half angle is equal to the "critical" angle for total internal reflection. Furthermore, it is assumed that the transmitted waves may be considered to radiate from a point source.

This fourth assumption probably does not completely describe the actual conditions, since the ionosphere is in general a lossy medium and the range of wave normals actually available to excite the waveguide may be restricted by the trapping characteristics of a duct. When a plane wave in a dielectric medium is incident on a lossy medium, the wave in the lossy medium is what Stratton[18] calls an "inhomogeneous plane wave."

The assumption of plane waves is the only practical assumption in the present state of knowledge.* The justification must again be the fact that the results are reasonable in view of experimental data.

The field at a receiving antenna will then consist of the sum of all the rays of significant amplitude that will propagate between the exit point and the antenna. The assumption that all necessary wave normals are present results in excitation for all these components.

5. It is assumed that all the energy in a set of sky-wave components is of the same frequency. Actually, the various rays contributing to a whistler signal at a given time are of slightly different frequency because of the frequency variation of the whistler and the difference in propagation times of the rays.

The maximum path difference between two adjacent-order rays, which occurs for vertical incidence, is of the order of 200 km (one round trip between earth and ionosphere). A typical dispersion of 100 $\sec^{\frac{1}{2}}$ yields

---

*A brief discussion of critical-angle phenomena and waves in lossy media is given on page 166.

a frequency difference of about 13 cps at 10 kc. The frequency difference decreases as the distance is increased and is about 4 cps at a distance of 500 km. A comparison of calculated and experimental data shows that this phenomenon is not generally important. Further discussion of beating is given on page 128.

This single-frequency assumption means essentially that the calculations may be performed on a steady-state basis, and it is not in general necessary to solve the transient problem. The transient problem is extremely complicated, and attempts to solve it do not appear to be warranted until the results of steady-state solutions have been more completely examined.

C. PATH GEOMETRY

It is now possible to formulate a system of equations for calculating the total field for the whistler-mode signal which arrives at a receiving antenna. The equations for the curved-earth geometry[20] will be used in order to determine the geometrical characteristics of the ray path itself. It is assumed that the earth is a perfect sphere of radius 6,367.39 km.[10]

Refer to Figs. 2.1 and 2.2 for an example of the ray geometry and for the notation. The angle θ_n, calculated from the path geometry, is determined by the virtual height of the ionosphere h', the ground distance D to the receiver (mks units will be used, except for h' and D in km), and the number of ionosphere reflections n.

The ionosphere angles of refraction θ_o and θ_e are then calculated from Snell's Law:

$$\mu_e \sin \theta_e = \mu_o \sin \theta_o = \sin \theta_n$$

where μ_o = the complex refractive index of the ordinary wave (see p. 16)

μ_e = the complex refractive index of the extraordinary wave.
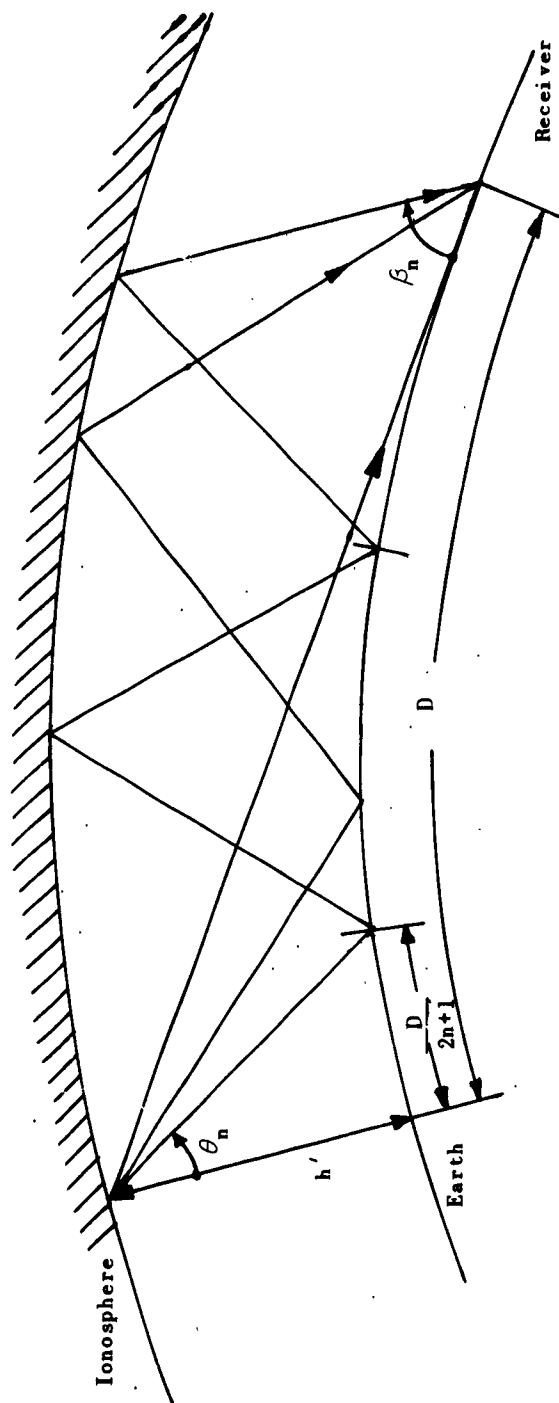
FIG. 2.1. TYPICAL RAY GEOMETRY FOR n = 0, 1, AND 2.
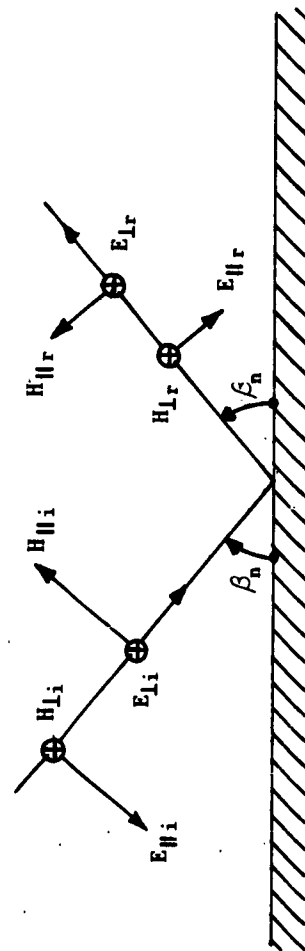
FIG. 2.2. FIELD COMPONENTS AND ANGLES AT THE EARTH'S SURFACE.

D. IONOSPHERE MODEL AND ITS REFRACTIVE INDEX

The next step is to define the ionosphere model and its refractive index. It will be recalled that we assumed for purposes of this problem that the ionosphere may be represented by a homogeneous medium with a sharp lower boundary and a vertical magnetic field.

With these assumptions, the refractive index of the medium has been expressed by Budden[12] as:

$$\mu^2 = 1 - j \ (\omega_r/\omega) \ \epsilon^{\pm j\tau} \tag{2.4}$$

$$= 1 \pm \omega_r/\omega \ \sin \tau - j\omega_r/\omega \ \cos \tau \tag{2.4a}$$

where

$$\tan \tau = \omega_L/\nu \tag{2.5}$$

$$\omega_r = \frac{\omega_o^2}{\sqrt{\nu^2 + \omega_L^2}} \tag{2.6}$$

$$\omega_o^2 = \frac{Ne^2}{\kappa_o m} \tag{2.7}$$

$$\omega_L = \frac{\mu'He}{m} \tag{2.8}$$

N = number of electrons per meter

e = charge of the electron in coulombs

m = mass of the electron in kg

κ_o = permittivity of free space in farad/meter

ν = collisional frequency in sec^{-1}

H = the earth's magnetic field in amp/meter^2

This expression for μ^2 is double valued, as is shown by the $\pm$ sign. The whistler mode corresponds to the + sign or the ordinary (o) mode.*

---

*The term ordinary is used here to conform to the reference from which this material was obtained. Modern practice,[35,36] however, is to label the whistler mode as the extraordinary mode.

The refractive index μ_o is then given by

$$\mu_o^2 = 1 + (\omega_r/\omega)(\sin \tau - j \cos \tau) \qquad (2.9)$$

The coordinate system and field components are shown in Fig. 2.3. The polarization for the case of a downcoming wave in the northern hemisphere is, then[12]

$$Q_o = \frac{E_{\perp o}}{E_{\parallel o}} = -j \qquad (2.10)$$

where the $\parallel$ and $\perp$ indicate that the electric field is parallel or perpendicular to the plane of incidence. Similarily, for the extraordinary (e) mode[12]

$$\mu_e^2 = 1 - (\omega_r/\omega)(\sin \tau + j \cos \tau) \qquad (2.11)$$

$$Q_e = \frac{E_{\perp e}}{E_{\parallel e}} = +j$$

The refractive-index expressions are thus stated in a convenient form as a function of the normalized parameters ω_r and τ.

E.   TRANSMISSION COEFFICIENTS

The expressions for the transmitted waves may now be written, assuming that the incident wave is plane and has the polarization of the "ordinary" or whistler component. Since the ql approximation is valid this wave will be circularly polarized. The polarization at the boundary will thus be such that it will excite a significant reflected wave only in the same mode, since the e mode requires the oppositely rotating circular polarization. The e mode will therefore be negligible under ql conditions.* The wave in the ionosphere has been given as:

---

*A discussion of the point is given in Appendix E.

- 16 -
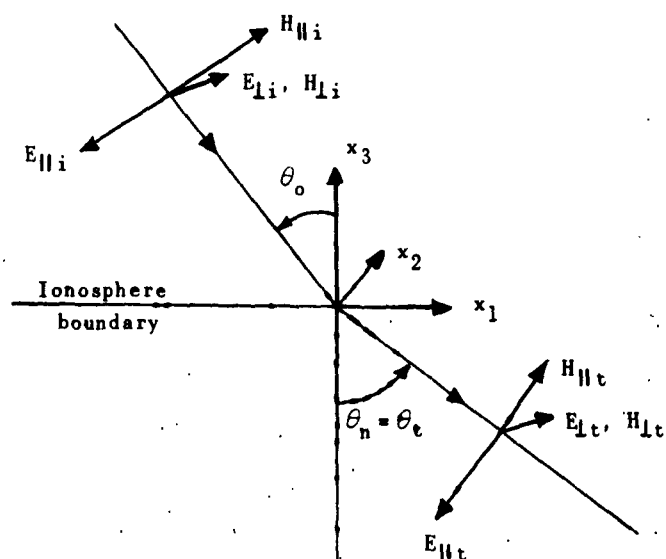
FIG. 2.3. THE COORDINATE SYSTEM AND FIELD COMPONENTS.

$$E_{\|o} = E_{\|i} \tag{2.13}$$

$$E_{\perp o} = Q_o E_{\|o} = E_{\perp i} \tag{2.14}$$

where o signifies the ordinary mode of propagation and the $\|$ and $\perp$ indicate whether the electric field is parallel to or perpendicular to the plane of incidence. The coordinate system is defined in Fig. 2.3. The $x_1 - x_2$ plane is the lower boundary of the model ionosphere, and the $x_1 - x_3$ plane is the plane of incidence. The transmitted components below the ionosphere may then be expressed by:

$$E_{\|t} = E_{\|i} \, T_{\|} \tag{2.15}$$

$$E_{\perp t} = E_{\perp i} \, T_{\perp} \tag{2.16}$$

where $T_{\|}$ and $T_{\perp}$ are the transmission coefficients which are to be determined. This is done by matching the four field components parallel to the boundary. These components are:

$$C_i E_{\|i} - E_{\|r} \, C_r = E_{\|t} C_t \tag{2.17}$$

$$E_{\perp i} + E_{\perp r} = E_{\perp t} \tag{2.18}$$

$$H_{\|i} \, C_i - H_{\|r} \, C_r = H_{\|t} \, C_t \tag{2.19}$$

$$H_{\perp i} + H_{\perp r} = H_{\perp t} \tag{2.20}$$

where C represents cos θ, and the subscripts i, r and t refer to the incident, reflected, and transmitted waves, respectively. In this case

$$\mu_i = \mu_r = \mu_o$$

and

$$C_1 = C_r = C_o$$

where the o refers to the ordinary mode of propagation. The ratios of the components of E to H may now be expressed by:

$$\frac{E_\parallel}{H_\perp} = \frac{E_\perp}{H_\parallel} = \sqrt{\mu'/k_1} = \eta_o/\mu_o \tag{2.21}$$

where

μ' = the permeability of free space,

k_1 = the permittivity of the medium.

We now substitute Eqs. (2.21) in (2.19) and (2.20) with the proper subscripts and divide by η_o, obtaining:

$$\mu_1 C_1 E_{\perp 1} - \mu_r C_r E_{\perp r} = C_t E_{\perp t} \tag{2.19a}$$

$$\mu_1 E_{\parallel 1} + \mu_r E_{\parallel r} = E_{\parallel t} \tag{2.20a}$$

Now, multiplying Eq. (2.17) by μ_r and Eq. (2.20) by C_r, and adding, yields:

$$E_{\parallel 1}(\mu_r C_1 + \mu_1 C_r) = \mu_r C_t E_{\parallel t} + C_r E_{\parallel t}$$

$$T_\parallel = \frac{E_{\parallel t}}{E_{\parallel 1}} = \frac{\mu_r C_1 + \mu_1 C_r}{\mu_r C_t + C_r} \tag{2.22}$$

Next, multiply Eq. (2.18) by $\mu_r C_r$ and add to Eq. (2.19a), yielding:

$$E_{\perp 1}(\mu_r C_r + \mu_1 C_1) = E_{\perp t}(C_r \mu_r + C_t)$$

$$T_\perp = \frac{E_{\perp t}}{E_{\perp 1}} = \frac{\mu_r C_r + \mu_1 C_1}{\mu_r C_r + C_t} \tag{2.23}$$

Now, for the whistler case $\mu_i = \mu_r = \mu_0$ and $C_i = C_r = C_0$, by Snell's law. Therefore, $T_\parallel$ and $T_\perp$ may be expressed as:

$$T_\parallel = \frac{C_0 \mu_0 + \mu_0 C_0}{\mu_0 C_t + C_0} = \frac{2\mu_0 C_0}{\mu_0 C_t + C_0} \qquad (2.24)$$

$$T_\perp = \frac{2\mu_0 C_0}{\mu_0 C_0 + C_t} \qquad (2.25)$$

F. RAY ADDITIONS

The resultant transmitted wave expressed by the preceding equations is then reflected n times from the earth and the ionosphere before arriving at the receiver. The reflections from the ionosphere are conveniently described by the reflection coefficients derived by Budden[12] and used by Wait.[13] There are four of these coefficients, designated $_\parallel R_\parallel$, $_\perp R_\perp$, $_\parallel R_\perp$, $_\perp R_\parallel$. The first subscript indicates whether the incident electric field is parallel or perpendicular to the plane of incidence, and the second similarly indicates the position of the reflected electric field. The existence of the cross-coupling terms $_\parallel R_\perp$ and $_\perp R_\parallel$ is due to the effect of the earth's magnetic field, which causes the characteristic waves in the ionosphere at vlf to be elliptically polarized in general. Thus, if the incident wave is linearly polarized, the reflected wave must contain some of the cross polarized component in order to match the boundary conditions. Some of the energy in a given linear polarization is therefore converted into a reflected component which has a polarization perpendicular to that of the incident wave.

The reflections from the earth are expressed in terms of the Fresnel reflection coefficients $R_\parallel$ and $R_\perp$. These are functions of the dielectric constant and conductivity of the ground, the wave frequency, and of the takeoff and/or arrival angle β_n, (hereafter referred to as the takeoff-arrival angle) measured from the horizontal. The subscripts on the coefficients $R_\parallel$ and $R_\perp$ indicate the polarization of both the incident and the reflected electric field at the ground.

The expression for the total field for each ray may now be given, using these six reflection coefficients and the transmission coefficients derived in Section II-E. Equations (2.15) and (2.16) express the transmitted fields as:

$$E_{\parallel t} = E_{\parallel 1} T_{\parallel} \qquad (2.15)$$

$$E_{\perp t} = E_{\perp 1} T_{\perp} \qquad (2.16)$$

The addition of components may now be expressed as:

$$_k E_{\parallel} = \,_{k-1} E_{\parallel} R_{\parallel \parallel \parallel} R_{\parallel} + \,_{k-1} E_{\perp} R_{\perp \perp} R_{\perp} \qquad (2.26)$$

$$_k E_{\perp} = \,_{k-1} E_{\parallel} R_{\parallel \parallel \parallel} R_{\perp} + \,_{k-1} E_{\perp} R_{\perp \perp} R_{\perp} \qquad (2.27)$$

Where

$$_0 E_{\parallel} = E_{\parallel t} \qquad (2.28)$$

$$_0 E_{\perp} = E_{\perp t} \qquad (2.29)$$

The subscript k is a dummy index which indicates that the calculation is performed repetitively n times (i.e., until k = n). The quantities $_k E_{\parallel}$ and $_k E_{\perp}$ for k = n, represent the fields of the n-hop ray uncorrected for path length. The fields are then corrected for path length by:

$$E_{\parallel}^{(n)} = \,_k E_{\parallel} \frac{\alpha_n}{R_n} \quad \cos \angle T_n + j \sin \angle T_n \qquad \text{when } k = n \qquad (2.30)$$

$$E_{\perp}^{(n)} = \,_k E_{\perp} \frac{\alpha_n}{R_n} \quad \cos \angle T_n + j \sin \angle T_n \qquad \text{when } k = n \qquad (2.31)$$

where

$E_{\parallel}^{(n)}$ = the parallel polarized component of the nth-order ray

$E_{\perp}^{(n)}$ = the perpendicular polarized component of the nth-order ray

α_n = the convergence coefficient of the nth-order ray

R_n = the propagation distance of the nth-order ray

$\angle T_n$ = the phase of the nth-order ray

R_n and $\angle T_n$ are defined in Appendix A.

This method of expressing the general n-hop component is analogous to finding the output of a multi-stage network by splitting it into a number of transfer functions, calculating the output of each section in turn, and using the output of that section as the input to the next.

The convergence coefficient α_n is a factor derived to account for the effect of the reflections from the concave ionosphere surface and the convex earth surface   In the ground-to-ground case, the coefficient expresses the net convergence due to n reflections from the ionosphere and n - 1 from the earth. The net convergence is generally very small in this case, except near the critical distance where the expressions become invalid and a higher-order approximation must be used. In the present case, the number of reflections from the earth and the ionosphere is equal and the two effects would tend to cancel each other. It is therefore reasonable to assume a value of unity for this coefficient. This will lead to some error in the calculation of a ray as its critical distance is approached. The error due to this factor is opposite in effect to that of neglecting the diffraction factor near the critical distance, and the resulting error is small.

G. CONVERGENCE OF THE SERIES OF RAYS

We have shown how the field is calculated as the sum of n sky-wave components. Each succeeding component is of lower amplitude than the previous one, due to the 1/R amplitude factor and the multiplication of further reflection coefficients, which are always less than unity in magnitude. Thus, a series is formed with terms of successively decreasing amplitude. It is now necessary to determine the point at which the series should be terminated. The method used is as follows: The six components for n = 0 through 5 are always calculated. The field from each component is resolved into its three axial components (see p. 24) and each axial component is added to the sum of that axial component built up by previous rays. The amplitude of the last ray is then compared with the amplitude of the sum for each of the three axial components in turn. The calculation is terminated when the amplitude of the last ray is less than a specified percentage of the smallest of the three sums.

This percentage was experimentally studied and the value of 1 per cent was adopted. The error in neglecting further components is less than 1 per cent in amplitude and about 0.1 degree in the angles calculated for all cases studied.

H.   CRITICAL DISTANCE EFFECTS

The critical distance is that which yields a value of zero for β_n, the takeoff-arrival angle at the earth's surface. When the critical distance for a given ray is exceeded, a diffracted field exists at the antenna. The expressions for the diffracted field are very complicated. Recently, Wait[21,22] has published approximate solutions to this problem. In order to preserve a reasonable simplicity in the over-all calculation, it was specified that the field for a given ray is not calculated if β_n is less than zero. The effect of the refracted field in the "shadow zone" is thus ignored. This limits the accuracy of the calculations for distances just beyond the critical distance. There is an additional effect on waves which have a low takeoff-arrival angle which is caused by the presence of the earth's surface. This effect was also ignored in order to maintain simplicity of the calculations. This effect is similar to that dealt with by Wait in his consideration of the "cutback" factor, which expresses the modification of the pattern of a radiating antenna at angles close to the earth's surface. Approximate solutions to similar problems also exist, but these were also discarded in order to preserve the essential simplicity of the calculations. The error due to these factors is believed to be small. No noticeable discontinuities appear at or near the critical distance, so that it appears reasonable that the results are useful near these critical distances.

I.   TOTAL FIELD AND ANTENNA RESPONSE

1.   GENERAL CONSIDERATIONS.   We have expressed the electric field due to all significant sky wave components. Each of these components arrives at an angle β_n, determined by its path geometry. The problem now is to determine the total field and the response of the antenna system to it.

Equations will be derived for the total electric field at the antenna, which is assumed to be small compared with the wavelength. It is important to realize at this point that the field which is effective in inducing a voltage in an antenna will not necessarily be the same as the total electric field present at the antenna. The type of antenna used determines the exact form of the field which will affect it. These differences in response for different types of antennas must be carefully considered when the form of the field to be calculated is determined.

2. TOTAL FIELD. First, we consider the problem of the behavior of the total electric field as a function of time in an area small with respect to a wavelength. It is commonly expected that the total field vector will describe a complicated, non-plane figure in space, even in the single-frequency case. This is not true, however. It can be shown that the figure is in general an ellipse contained in a plane whose orientation is readily described in terms of the component rays. A series of rays may thus be described by a single elliptically polarized field. We will therefore consider this problem in detail.

It is easily seen that the series of rays arriving at different angles β_n, and each containing a parallel and a perpendicular component of electric field, will have components in all three coordinate directions. Therefore, we first resolve the waves into these components:

$$E_{x1} = - \sum_n E_{\parallel}^{(n)} \sin \beta_n \qquad (2.32)$$

$$E_{x2} = \sum_n E_{\perp}^{(n)} \qquad (2.33)$$

$$E_{x3} = - \sum_n E_{\parallel}^{(n)} \cos \beta_n \qquad (2.34)$$

The coordinates are the same as in Fig. 2.3. The three resultant components are independent of one another in phase and amplitude.

Now, the position of the total field vector as a function of time must be determined. It has been previously assumed that the waves are all sinusoidal and of the same frequency. Let the origin of the coordinates be the base of the vector. The tip of the vector will then describe a pattern in three dimensions, with its displacement in each of the

coordinate directions given by Eqs. (2.32) to (2.34). Since the waves are sinusoidal, each of these displacements must be symmetrical about the origin, which means that the figure passes through the origin. Also, each component has the same number of maxima and minima per cycle, since the frequency is the same. These restrictions determine that the figure is a plane, whose orientation is determined only by the relative phases and amplitudes of the components. (This same conclusion is reached mathematically on page 26.)

Since the three axial components of field strength have independent phases and amplitudes, the figure which the field vector describes will, in the general case, be an ellipse. The simplest way to describe the resultant is to determine the orientation of the plane of this ellipse, and then rotate coordinates so that the ellipse can be described by two coordinates and two angles of rotation.

Consider the plane of the ellipse. This plane is most easily described by the direction cosines of its normal. Let these direction cosines be l, m, and n, in the x_1, x_2, and x_3 directions, respectively. The general equation of a plane is[23] then:

$$l x_1 + m x_2 + n x_3 = p \qquad (2.35)$$

where p is a constant equal to the length of the normal.

The coordinate values then may be replaced by the actual electric field strength values, which are sinusoidal functions of time. Let:

$$x_1 = E_{x_1} \sin \omega t = \overline{E_{x_1}} \sin \omega t \qquad (2.36)$$

$$x_2 = E_{x_2} \sin (\omega t + \theta_y) = \overline{E_{x_2}} \sin \omega t \qquad (2.37)$$

$$x_3 = E_{x_3} \sin (\omega t + \theta_z) = \overline{E_{x_3}} \sin \omega t \qquad (2.38)$$

where $\overline{E_{x_1}}$, $\overline{E_{x_2}}$, and $\overline{E_{x_3}}$ are complex numbers.

Then (2.35) becomes:

$$\sin \omega t \; (l \overline{E_{x_1}} + m \overline{E_{x_2}} + n \overline{E_{x_3}}) = p \qquad (2.39)$$

This equation can be satisfied only by p = 0 for all values of t. This means that the plane must pass through the origin, as we found previously.

Now let:

$$\bar{R}_y = \frac{x_2}{x_1} = R_y \left(\cos \theta_y + j \sin \theta_y\right) \tag{2.40}$$

$$\bar{R}_z = \frac{x_3}{x_1} = R_z \left(\cos \theta_z + j \sin \theta_z\right) \tag{2.41}$$

Now, from (2.39) for a solution to exist:

$$E_{x_1} \left(\ell + mR_y \cos \theta_y + nR_z \cos \theta_z\right) = 0 \tag{2.42}$$

$$E_{x_1} \left(mR_y \sin \theta_y + nR_z \sin \theta_z\right) = 0 \tag{2.43}$$

and

$$\ell^2 + m^2 + n^2 = 1 \tag{2.44}$$

from the properties of direction cosines. Now, multiply Eq. (2.42) by $\sin \theta_y$ and Eq. (2.43) by $\cos \theta_y$, yielding

$$\ell \sin \theta_y + mR_y \sin \theta_y \cos \theta_y + nR_z \sin \theta_y \cos \theta_z = 0 \tag{2.42a}$$

$$mR_y \sin \theta_y \cos \theta_y + nR_z \cos \theta_y \sin \theta_z = 0 \tag{2.43a}$$

Then, subtract Eq. (2.43a) from Eq. (2.42a), which results in:

$$\ell \sin \theta_y + nR_z \left(\sin \theta_y \cos \theta_z - \cos \theta_y \sin \theta_z\right) = 0 \tag{2.45}$$

This gives the relation between n and ℓ. Next, multiply Eq. (2.42) by $\sin \theta_z$ and Eq. (2.43) by $\cos \theta_z$, yielding:

$$\ell \sin \theta_z + mR_y \cos \theta_y \sin \theta_z + nR_z \sin \theta_z \cos \theta_z = 0 \tag{2.42b}$$

$$mR_y \sin \theta_y \cos \theta_z + nR_z \sin \theta_z \cos \theta_z = 0 \tag{2.43b}$$

Next, subtract Eq. (2.43b) from Eq. (2.42b), which yields:

$$l \sin \theta_z + mR_y (\cos \theta_y \sin \theta_z - \sin \theta_y \cos \theta_z) = 0 \quad (2.46)$$

The next step is to substitute Eq. (2.45) and Eq. (2.46) into Eq. (2.44), which yields an equation for l^2 alone:

$$l^2 \left[\frac{1 + R_y^2 \sin^2 \theta_y + R_z^2 \sin^2 \theta_z}{R_y R_z (\sin \theta_y \cos \theta_z - \cos \theta_y \sin \theta_z)} \right] = 1 \quad (2.47)$$

This equation, when rearranged, yields:

$$l^2 = \frac{R_y^2 R_z^2 (\sin \theta_y \cos \theta_z - \cos \theta_y \sin \theta_z)^2}{R_y^2 R_z^2 (\sin \theta_y \cos \theta_z - \cos \theta_y \sin \theta_z)^2 + R_y^2 \sin^2 \theta_y + R_z^2 \sin^2 \theta_z}$$

$$(2.48)$$

Then m and n are found from Eq. (2.45) and Eq. (2.46), which, when rearranged, yield:

$$m = \frac{l \sin \theta_z}{R_y (\sin \theta_y \cos \theta_z - \cos \theta_y \sin \theta_z)} \quad (2.49)$$

and

$$n = \frac{l \sin \theta_y}{R_z (\sin \theta_y \cos \theta_z - \cos \theta_y \sin \theta_z)} \quad (2.50)$$

Now, the elevation and azimuth angles of the normal, β_e and $\emptyset_e$ must be found. Refer to Fig. 2.4 for an illustration of the nomenclature. The direction of propagation of the ray is the positive x_1'' direction. The line a is the projection of the direction of propagation on the $x_1 - x_2$ plane. The angle $\emptyset_e$ is the angle of rotation in that plane. The angle $- \beta_e$ is the corresponding depression angle. It is readily apparent that:

- 27 -
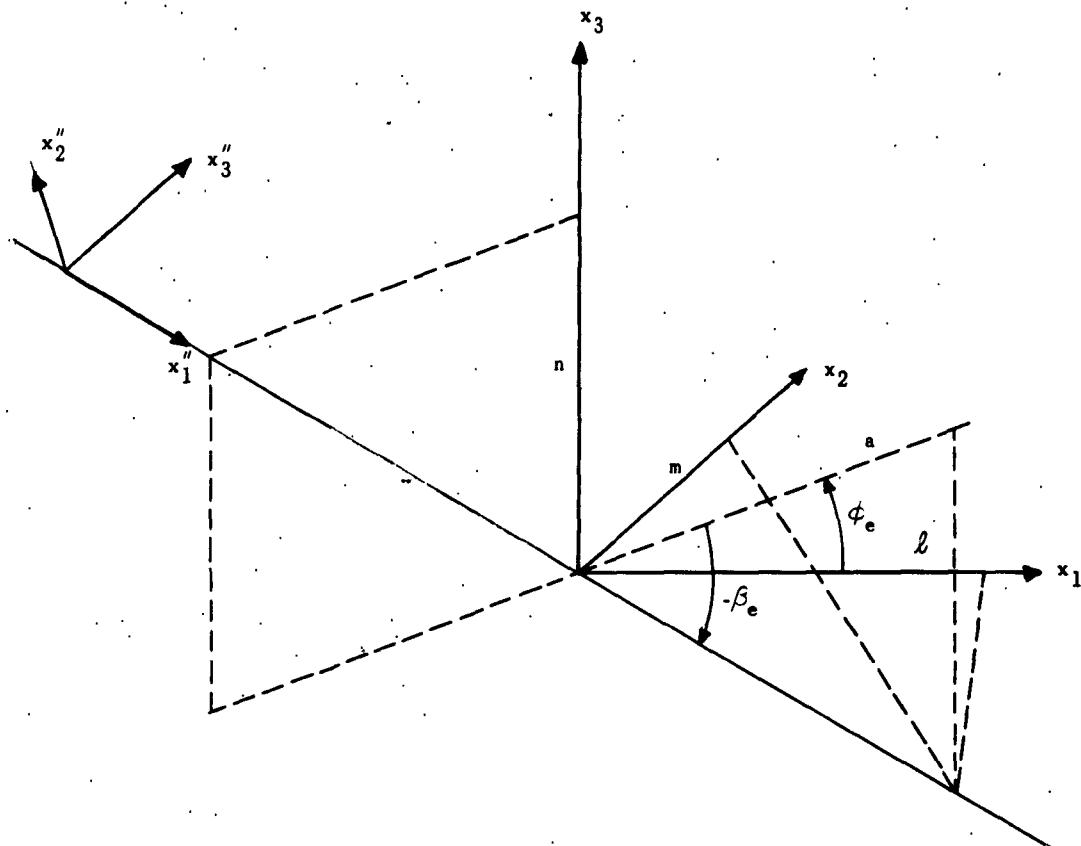
FIG. 2.4.   THE NEW COORDINATE SYSTEM AND ANGLES OF ROTATION.

$$\tan \phi_e = \frac{\sin \phi_e}{\cos \phi_e} = \frac{m}{a} \cdot \frac{a}{l} = \frac{m}{l}$$

$$a = \cos \beta_e = \sqrt{1 - n^2}$$

$$1 - \cos^2 \beta_e = \sin^2 \beta_e = 1 - (1 - n^2)$$

$$\sin \beta_e = \pm n \tag{2.51}$$

and

$$\tan \beta_e = \frac{\pm n}{\sqrt{1 - n^2}} \tag{2.52}$$

The next step is to rotate the coordinates, first about x_3 through an angle ϕ_e, which results in axes x_n'. Then we rotate the coordinates about x_2' through an angle β_e, which results in coordinates x_n''. These operations may be performed as follows: first, for each x_n substitute its proper replacement in the primed system.[13]

$$x_1' \cos \phi_e - x_2' \sin \phi_e = \overline{E}_{x_1} \tag{2.53}$$

$$x_1' \sin \phi_e + x_2' \cos \phi_e = \overline{E}_{x_2} \tag{2.54}$$

$$x_3' = \overline{E}_{x_3} \tag{2.55}$$

which expresses the first rotation of ϕ_e degrees about x_3.

Then replace each of the primed coordinates by its proper substitute in the double-primed system:

$$(x_1'' \cos \beta_e - x_3'' \sin \beta_e) \cos \phi_e - x_2'' \sin \phi_e = \overline{E}_{x_1} \tag{2.56}$$

$$(x_1'' \cos \beta_e - x_3'' \sin \beta_e) \sin \phi_e + x_2'' \cos \phi_e = \overline{E}_{x_2} \tag{2.57}$$

$$x_1'' \sin \beta_e + x_3'' \cos \beta_e = \overline{E}_{x_3} \tag{2.58}$$

which expresses the rotation of β_e degrees about x_2'. Now, rearranging and collecting terms yields:

$$x_1'' \cos \beta_e \cos \emptyset_e - x_2'' \sin \emptyset_e - x_3'' \sin \beta_e \cos \emptyset_e = \overline{E_{x_1}} \tag{2.59}$$

$$x_1'' \cos \beta_e \sin \emptyset_e + x_2'' \cos \emptyset_e - x_3'' \sin \beta_e \sin \emptyset_e = \overline{E_{x_2}} \tag{2.60}$$

$$x_1'' \sin \beta_e + x_3'' \cos \beta_e = \overline{E_{x_3}} \tag{2.61}$$

These equations are now in a form suitable for the solution of the system by determinants.

First, the denominator of the system is given by

$$D = \begin{vmatrix} \cos \beta_e \cos \emptyset_e & -\sin \emptyset_e & -\sin \beta_e \cos \emptyset_e \\ \cos \beta_e \sin \emptyset_e & \cos \emptyset_e & -\sin \beta_e \sin \emptyset_e \\ \sin \beta_e & 0 & \cos \beta_e \end{vmatrix} \tag{2.62}$$

$$= \sin \emptyset_e \left(\cos^2 \beta_e \sin \emptyset_e + \sin^2 \beta_e \sin \emptyset_e \right) + \cos \emptyset_e \left(\cos^2 \beta_e \cos \emptyset_e \right.$$

$$\left. + \sin^2 \beta_e \cos \emptyset_e \right) = \sin^2 \emptyset_e + \cos^2 \emptyset_e = 1 \tag{2.63}$$

Then x_1'' is given by

$$x_1'' = \begin{vmatrix} \overline{E_{x_1}} & -\sin \emptyset_e & -\sin \beta_e \cos \emptyset_e \\ \overline{E_{x_2}} & \cos \emptyset_e & -\sin \beta_e \sin \emptyset_e \\ \overline{E_{x_3}} & 0 & \cos \beta_e \end{vmatrix}$$

When normalized, this yields:

- 30 -

$$\overline{E}_{x_1} \begin{vmatrix} 1 & -\sin\emptyset_e & -\sin\beta_e \cos\emptyset_e \\ \overline{R_y} & \cos\emptyset_e & -\sin\beta_e \sin\emptyset_e \\ \overline{R_z} & 0 & \cos\beta_e \end{vmatrix} \qquad (2.64)$$

$$x_1'' = \overline{E}_{x_1} [\sin\emptyset_e (\overline{R_y} \cos\beta_e + \overline{R_z} \sin\beta_e \sin\emptyset_e) + \cos\emptyset_e (\cos\beta_e$$

$$+ \overline{R_z} \sin\beta_e \cos\emptyset_e)] = \overline{E}_{x_1} (\overline{R_y} \sin\emptyset_e \cos\beta_e + \overline{R_z} \sin\beta_e \sin^2\emptyset_e$$

$$+ \cos\emptyset_e \cos\beta_e + \overline{R_z} \sin\beta_e \cos^2\emptyset_e)$$

$$x_1'' = \overline{E}_{x_1} [R_z \sin\beta_e + \cos\beta_e (\overline{R_y} \sin\emptyset_e + \cos\emptyset_e) \qquad (2.65)$$

Similarly:

$$x_2'' = \begin{vmatrix} \cos\beta_e \cos\emptyset_e & \overline{E}_{x_1} & -\sin\beta_e \cos\emptyset_e \\ \cos\beta_e \sin\emptyset_e & \overline{E}_{x_2} & -\sin\beta_e \sin\emptyset_e \\ \sin\beta_e & \overline{E}_{x_3} & \cos\beta_e \end{vmatrix} =$$

$$E_{x_1} \begin{vmatrix} \cos\beta_e \cos\emptyset_e & 1 & -\sin\beta_e \cos\emptyset_e \\ \cos\beta_e \sin\emptyset_e & \overline{R_y} & -\sin\beta_e \sin\emptyset_e \\ \sin\beta_e & \overline{R_z} & \cos\beta_e \end{vmatrix} \qquad (2.66)$$

$$x_2'' = \overline{E}_{x_1} [-1 (\cos^2\beta_e \sin\emptyset_e + \sin^2\beta_e \sin\emptyset_e) + \overline{R_y} (\cos^2\beta_e \cos\emptyset_e$$

$$+ \sin^2\beta_e \cos\emptyset_e) - \overline{R_z} (-\sin\beta_e \cos\beta_e \sin\emptyset_e \cos\emptyset_e$$

$$+ \sin\beta_e \cos\beta_e \sin\emptyset_e \cos\emptyset_e)] \qquad (2.67)$$

$$x_2^{\,\prime\prime} = \overline{R_y}\ \cos\varnothing_e - \sin\varnothing_e$$

$$x_3^{\,\prime\prime} = \overline{E_{x_1}}\ \begin{vmatrix} \cos\beta_e\ \cos\varnothing_e & -\sin\varnothing_e & 1 \\[2mm] \cos\beta_e\ \sin\varnothing_e & \cos\varnothing_e & \overline{R_y} \\[2mm] \sin\beta_e & 0 & \overline{R_z} \end{vmatrix} \qquad (2.68)$$

$$= \overline{E_{x_1}}\ [\sin\varnothing_e\ (\overline{R_z}\ \cos\beta_e\sin\varnothing_e - \overline{R_y}\ \sin\beta_e)$$

$$+ \cos\varnothing_e(\overline{R_z}\ \cos\beta_e\ \cos\varnothing_e - \sin\beta_e)]$$

$$= \overline{E_{x_1}}\ [\overline{R_z}\ \cos\beta_e - \overline{R_y}\ \sin\beta_e\ \sin\varnothing_e - \sin\beta_e\ \cos\varnothing_e] \qquad (2.69)$$

$$x_3^{\,\prime\prime} = \overline{E_{x_1}}\ [\overline{R_z}\ \cos\beta_e - \sin\beta_e\ (\overline{R_y}\ \sin\varnothing_e + \cos\varnothing_e) \qquad (2.70)$$

The $x_1^{\,\prime\prime}$ axis is now aligned with the normal, and the $x_1^{\,\prime\prime}$ vector is, ideally, zero, or very small in an actual computation.

The polarization of this total field is then:

$$Q_n = \frac{x_2^{\,\prime\prime}}{x_3^{\,\prime\prime}} \qquad (2.71)$$

These four quantities, Q_n, β_e, $\varnothing_e$, and $\overline{E_{x_1}}$ then describe completely the total incident field.

3. ANTENNA RESPONSE. In order to compare the calculations with measurements, we must be able to express them in a manner that will yield induced antenna voltages. We will now consider the response of the crossed (mutually perpendicular) vertical loops and vertical monopole system most commonly used in whistler and vlf work. The coordinate system and field directions were shown in Fig. 2.3. Figure 2.2 shows the arrangement of the E and H components of the incident and reflected waves.

The response of a loop antenna to a sinusoidal wave is proportional to the time rate of change in the H field threading the loop. We will use the H field to determine the antenna response, and then express the result in terms of the E field. The response of a vertical-loop antenna, making an angle $\emptyset$ with the plane of incidence of the n-hop rays is given by:

$$v_\ell = K[(H_{\perp i} + H_{\perp r}) \cos \emptyset - (H_{\parallel i} \sin \beta_n - H_{\parallel r} \sin \beta_n) \sin \emptyset] \quad (2.72)$$

The subscripts i and r refer to the incident and reflected waves, respectively. This equation may then be expressed in terms of the E field by:

$$v_\ell = h'_\ell [E_{\parallel i}(1 + R_\parallel) \cos \emptyset - E_{\perp i}(1 - R_\perp) \sin \beta_n \sin \emptyset] \quad (2.73)$$

where $R_\parallel$ is the Fresnel ground reflection coefficient for parallel (vertical) polarization

$R_\perp$ is the Fresnel ground reflection coefficient for perpendicular (horizontal) polarization

h'_ℓ is the effective "height" of the loop antenna in meters

The effective height of the loop contains the constant factor K from the previous expression Eq. (2.72) as well as the factor expressing the ratio of E to H.

The preceding expression may then be generalized for a pair of crossed vertical loops and for a number of waves arriving at various elevation angles β_n to yield:

$$v_{ns} = h'_\ell (x_{3a} \cos \emptyset - x_{2a} \sin \emptyset) \quad (2.74)$$

$$v_{ew} = h'_\ell (x_{3a} \sin \emptyset + x_{2a} \cos \emptyset) \quad (2.75)$$

The vertical monopole antenna responds only to the parallel (or vertical) component of the total electric field, which is proportional to the sum of the incident and reflected waves as may be seen from Fig. 2.2. The induced voltage v_v in a vertical antenna is thus given by:

- 33 -

$$v_v = h'_v \, x_{3v} \qquad (2.76)$$

where:

$$x_{2a} = \sum_n E_\perp^{(n)} (1 - R_{\perp n}) \sin \beta_n \qquad (2.77)$$

$$x_{3a} = \sum_n E_\parallel^{(n)} (1 + R_{\parallel n}) \qquad (2.78)$$

$$x_{3v} = \sum_n E_\parallel^{(n)} (1 + R_{\parallel n}) \cos \beta_n \qquad (2.79)$$

4. THE ARRIVAL ANGLES AND POLARIZATION. We have now expressed the induced voltages in the three antennas as a function of the sum of the arriving waves. In order to simplify the interpretation of these results, we now seek an equivalent plane wave which will produce the same response voltages as the "complex" wave. Let us rewrite Eq. (2.74), (2.75), (2.76) in terms of an equivalent plane wave at the antenna, and use the subscript a to indicate this wave. We shall first define a polarization Q_a, which may be expressed as:

$$Q_a = X_a + jY_a = \frac{E_{\perp a}}{E_{\parallel a}} \qquad (2.80)$$

We must also define an effective vertical angle of arrival β_a and an effective azimuth angle of arrival $\emptyset_a$. Now, we write Eqs. (2.74), (2.75), (2.76) in terms of these equivalent antenna quantities, and combine them, which yields:

$$\frac{v_{ns}}{v_v} = v_1 = a_1 + jb_1 = \frac{(\cos \emptyset_a - Q_a \sin \beta_a \sin \emptyset_a)}{\cos \beta_a} \qquad (2.81)$$

$$\frac{v_{ew}}{v_v} = v_2 = a_2 + jb_2 = \frac{(\sin \emptyset_a + Q_a \sin \beta_a \cos \emptyset_a)}{\cos \beta_a} \qquad (2.82)$$

$$\frac{v_{ns}}{v_{ew}} = v_R = a_R + jb_R = \frac{(\cos \emptyset_a - Q_a \sin \beta_a \sin \emptyset_a)}{(\sin \emptyset_a + Q_a \sin \beta_a \cos \emptyset_a)} \qquad (2.83)$$

. Notice that the right hand side of these equations is written entirely in terms of the effective antenna quantities, while the left hand side is written entirely in terms of the actual fields present at the antenna.

We will now separate the real and imaginary parts, obtaining

$$a_1 = \frac{\cos \phi_a - X_a \sin \beta_a \sin \phi_a}{\cos \beta_a} \tag{2.84}$$

$$b_1 = \frac{-Y_a \sin \beta_a \sin \phi_a}{\cos \beta_a} = - Y_a \tan \beta_a \sin \phi_a \tag{2.85}$$

$$a_2 = \frac{\sin \phi_a + X_a \sin \beta_a \cos \phi_a}{\cos \beta_a} \tag{2.86}$$

$$b_2 = \frac{+ Y_a \sin \beta_a \cos \phi_a}{\cos \beta_a} = + Y_a \tan \beta_a \cos \phi_a \tag{2.87}$$

From Eq. (2.85) and Eq. (2.87) it is easily seen that:

$$\tan \phi_a = - \frac{b_1}{b_2} \tag{2.88}$$

Equations (2.84) and (2.86) yield:

$$\frac{\cos \phi_a - a_1 \cos \beta_a}{\sin \phi_a} = \frac{a_2 \cos \beta_a - \sin \phi_a}{\cos \phi_a} \tag{2.89}$$

$$\cos^2 \phi_a - a_1 \cos \beta_a \cos \phi_a = a_2 \cos \beta_a \sin \phi_a - \sin^2 \phi_a$$

$$\cos \beta_a (a_1 \cos \beta_a + a_2 \sin \phi_a) = \sin^2 \phi_a + \cos^2 \phi_a$$

$$\cos \beta_a = \frac{1}{a_2 \sin \phi_a + a_1 \cos \phi_a} \tag{2.90}$$

Equation (2.85) and (2.87) yield:

$$Y_a = - \frac{b_1}{\tan \beta_a \sin \emptyset_a} = \frac{b_2}{\tan \beta_a \cos \emptyset_a} \qquad (2.91)$$

and Eq. (2.84) and (2.86) yield:

$$X_a = \frac{\cos \emptyset_a - a_1 \cos \beta_a}{\sin \beta_a \sin \emptyset_a} = \frac{a_2 \cos \beta_a - \sin \emptyset_a}{\sin \beta_a \cos \emptyset_a} \qquad (2.92)$$

These sets of equations therefore enable the four unknown quantities $\emptyset_a$, β_a, X_a, and Y_a to be determined for a plane wave when voltages induced in the antennas are known. There are conditions for which the values of the fields x_{2a}, x_{3a}, and x_{3v} are not compatible with the assumption that the field present at the antennas is a plane wave. This phenomenon is discussed on p. 138.

5. GONIOMETER RESPONSE AND ANTENNA VOLTAGE RATIOS. The response of a goniometer system utilizing crossed vertical loops is derived on p.101. $\emptyset_g$ is the goniometer bearing angle for maximum signal measured clockwise from north. This corresponds to the plane of the electrically rotated loop lying in the plane of incidence and receiving maximum signal from a vertically polarized wave arriving from that direction. The calculations are arranged to give the antenna responses v_{ns} and v_{ew} in 10° steps for $\emptyset_g$ from 0 to 180°. This is equivalent to changing the direction of arrival in 10° steps in the opposite rotation. In addition, the ratios v_R, v_1, and v_2, which are defined by Eq. (2.81) to (2.83), are calculated for the specified values of $\emptyset_g$. They correspond to the quantities measured by Lissajous patterns when comparing the outputs of the ns and ew loop antennas and the vertical antenna on an oscillograph. v_R corresponds to the common d-f trace often used for sferics d-f systems at vlf. In all following calculations, it will be assumed that the North-South (ns) loop lies in the plane of incidence, and the East-West (ew) loop perpendicular to it. These are sometimes referred to as the "normal" and "abnormal" loops, respectively.

- 36 -

The majority of the curves showing the results of the calculations
are presented in this chapter. Similar curves are grouped together to
facilitate comparison. The discussion of these results is given in
Chapter V.

A.   THE CLASSIFICATION OF THE CALCULATIONS

There are seven independent variables involved in these calculations
which may be organized into three groups: (1) The normalized factors
ω_r, τ, and h', which describe the ionosphere model. (2) The ground con-
stants κ and σ. (3) The path and wave constants f and D. The calcul-
ations have been organized as follows: The ionosphere model has been
chosen from available literature (Wait,[13,14] Budden,[12] etc.) giving values
for typical conditions. The majority of the calculations were made
using the "summer night" constants. These are $\omega_r = 5 \times 10^5$, $\tau = 60°$,
and h' = 90 km. These values correspond to effective values of f_H, f_o
and ν for a homogeneous model. Since only ratios of f_H, f_o and ν are
specific, one must be assumed to find the others. The best reference
is f_H, since its value is essentially constant. If an effective f_H of
1.34 Mc is assumed, the values correspond to $f_o = 352.0$ kc, and
$\nu = 4.855 \times 10^6$. These are physically reasonable values for the night-
time layers. A "spring" night model might have been a little more
typical of the whistler characteristics discussed in this report but
these established values appeared to be the most reasonable starting
point. Most calculations were based on this model.

In additions, some calculations were made for the summer-day model.
This model was made up from Wait's[13,14] value of $\omega_r = 1.5 \times 10^5$, $\tau = 15°$,
and h' = 70 km. The last two values come from the available data on the
D-layer characteristics.[24,25] This corresponds to a value of $f_H = 1.35$
Mc, $f_o = 350$ kc, and $\nu = 3.165 \times 10^7$. The available information[24,25]
on D-layer characteristics contains a fairly wide range of choice for
these factors. The values were chosen to represent an equivalent homo-
geneous model, and probably most resemble the characteristics of the

actual layer some distance above the assumed virtual height of 70 km. Studies of the results for variations in ω_r, τ, and h' about the summer-night-model values were also made. This will be discussed further on p. 128.

The ground constants used were picked for values typical of three general cases for most of the calculations. These were (1) poor ground, $\kappa = 3.0$, $\sigma = 1 \times 10^{-4}$ mho/m, (2) average ground, $\kappa = 20$, $\sigma = 3 \times 10^{-2}$ mho/m and (3) sea water $\kappa = 80$, $\sigma = 4.5$ mho/m. These values were chosen from the constants given by Terman,[32] Wait[26] and others.[46] The majority of the calculations used the extreme values of poor ground and sea water, which seemed to be of the most interest and the most economical for calculation. The results for average ground would lie approximately mid-way between these two extremes. Some cases were calculated with ground constants $\kappa = 0$ and very large values of σ, which approaches perfect conductivity. It was soon determined that the computer program used would not handle values of σ greater than 1×10^{14}.

The electric field strength of the circularly polarized energy in the ionosphere $E_{||_1}$, was specified as $2 + j0$ for the majority of these calculations. This is an arbitrary normalizing factor, and the amplitude and phase of the total field and antenna response are relative to this value. The phase, of course, has an ambiguity of ± 360 p degrees, where p is an integer.

The values of f were chosen to cover the major part of the whistler range, from 500 cps to 20 kc. The values of D were chosen to cover the region of interest, which is zero to 2000 km. The latter value is the maximum distance mentioned by Storey[2,3] for most whistler sources. Most of the calculations were made as a function of frequency for a given distance. Values of $D = 0.1$, 500, 1000, 1500 and 2000 km were originally chosen as being typical in whistler work. The first was essentially vertical incidence. The next two lie well within the critical distance for most ionosphere models, and the last lies between, but well away from, the critical distances for the n = 0 and n = 1 components. One set of calculations for a fixed frequency was performed, covering a range of D from 0.1 to at least 12000 km. These results will be discussed on page 132.

The final set of calculations was performed for a distance of 47.23 km. This distance was chosen so that the n = 0 ray is parallel to the magnetic field direction for the latitude of Stanford ($44°N$ geomagnetic), in order to determine the characteristics of a signal arriving from the direction of the magnetic field. The calculated curves are presented together to facilitate comparison.

B. FIELD STRENGTH

The field strength data are presented in Figs. 3.1 to 3.21 and in 3.64. The plotted magnitude is, of course, relative to the magnitude of the electric field in the ionosphere. The absolute field strength cannot be determined without knowledge of the duct size. The calculations and curves therefore are suitable only for the study of variations in the field as a function of frequency, distance, and ionosphere and ground parameters. The same amplitude, frequency, and distance scales will be used, when the range of the results permits this, to facilitate comparison of different curves

1. DISTANCE VARIATIONS. Figures 3.1 through 3.7 show the magntiude of the field seen by the normal loop ($|v_{ns}|$ for $\emptyset_g = 0$) and the vertical monopole ($|v_v|$) as a function of frequency. The curves are calculated for poor ground and sea water, using the summer-night model ionosphere, for distances of 0.1, 500, 1000, and 2000 km. Figures 3.8 through 3.12 show the magnitudes of the fields seen by the normal and abnormal loops ($|v_{ns}|$ and $|v_{ew}|$ for $\emptyset_g = 0$) and by the vertical monopole as a function of distance for 5 kc and 15.5 kc. Figure 3.8 was plotted from results for poor-ground conditions, and the rest for sea water. Figures 3.8 through 3.10 were plotted from results calculated for the summer-night model ionosphere, and 3.11 and 3.12 for the summer-day model.

2. IONOSPHERE HEIGHT VARIATION. Figures 3.13 and 3.14 show the normal-loop and vertical-monopole fields as a function of frequency for poor ground at a distance of 500 km. The summer-night model ionosphere was used, except that h' was changed to 89 and 91 km, respectively, in Figs. 3.13 and 3.14.

FIG. 3.1. MAGNITUDE OF E FIELD RECEIVED BY NORMAL VERTICAL LOOP
AND MONOPOLE VS FREQUENCY, FOR SUMMER-NIGHT MODEL IONOSPHERE,
POOR GROUND, D = 0.1 km, AND ϕ_g = 0.

- 40 -

FIG. 3.2. MAGNITUDE OF E-FIELD RECEIVED BY NORMAL VERTICAL LOOP AND MONOPOLE VS FREQUENCY, FOR SUMMER-NIGHT MODEL IONOSPHERE, SEA WATER, D = 0.1 km, AND ϕ_g = 0.

- 41 -

10^0

10^{-1}

10^{-2}

10^{-3}

10^{-4}

$|E|$

0 1 2 3 4 5 6 7 8 9 10 11 12 13 14 15 16 17 18 19 20

f (kc)

$\tau = 60^o$

$\omega_r = 5 \times 10^5$

$h' = 90$ km

$\kappa = 3$

$\sigma = 1 \times 10^{-4}$ mho/m

⊙ $|v_{ns}|$ normal loop

☐ $|v_v|$ vertical

FIG. 3.3. MAGNITUDE OF E-FIELD RECEIVED BY NORMAL VERTICAL LOOP AND MONOPOLE VS FREQUENCY
FOR SUMMER-NIGHT MODEL IONOSPHERE, POOR GROUND, D = 500 km, AND $\phi_g = 0$.
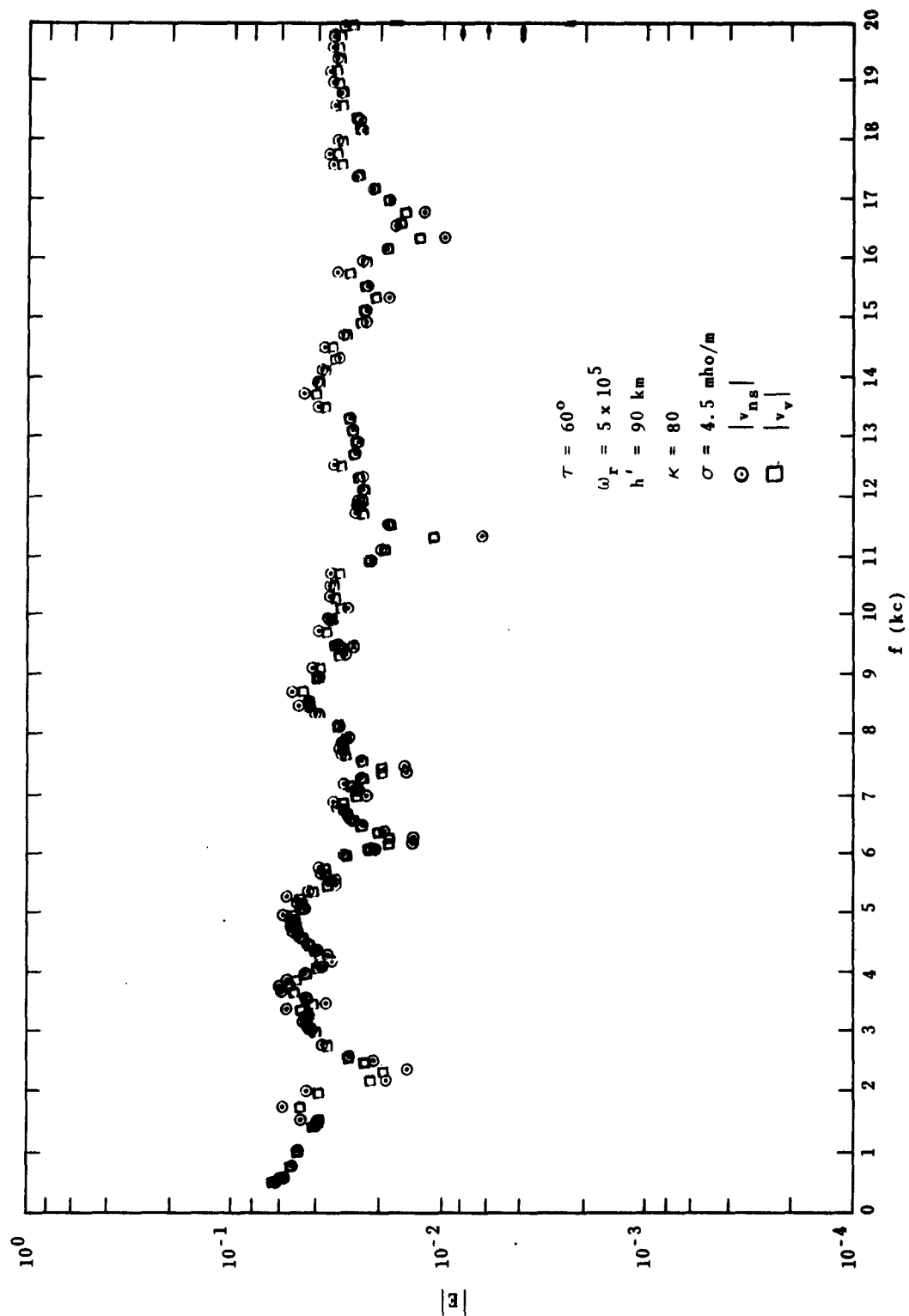
FIG. 3.4. MAGNITUDE OF E-FIELD RECEIVED BY NORMAL VERTICAL LOOP AND MONOPOLE VS FREQUENCY, FOR SUMMER-NIGHT MODEL IONOSPHERE, SEA WATER, D = 500 km, AND ϕ_g = 0.
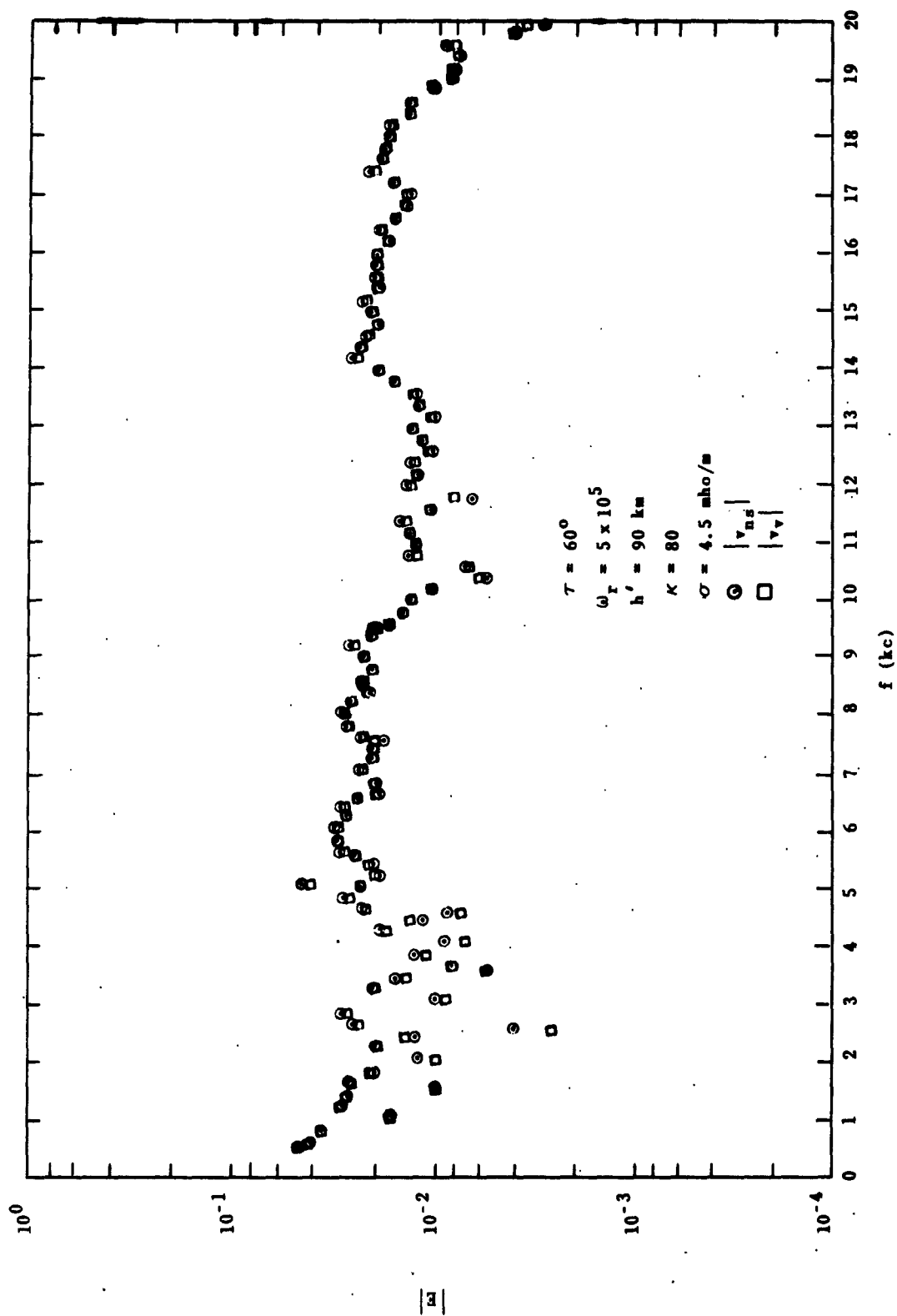
FIG. 3.5. MAGNITUDE OF E-FIELD RECEIVED BY NORMAL VERTICAL LOOP AND MONOPOLE VS FREQUENCY, FOR SUMMER-NIGHT MODEL IONOSPHERE, SEA WATER, D = 1000 km, AND ϕ_g = 0.
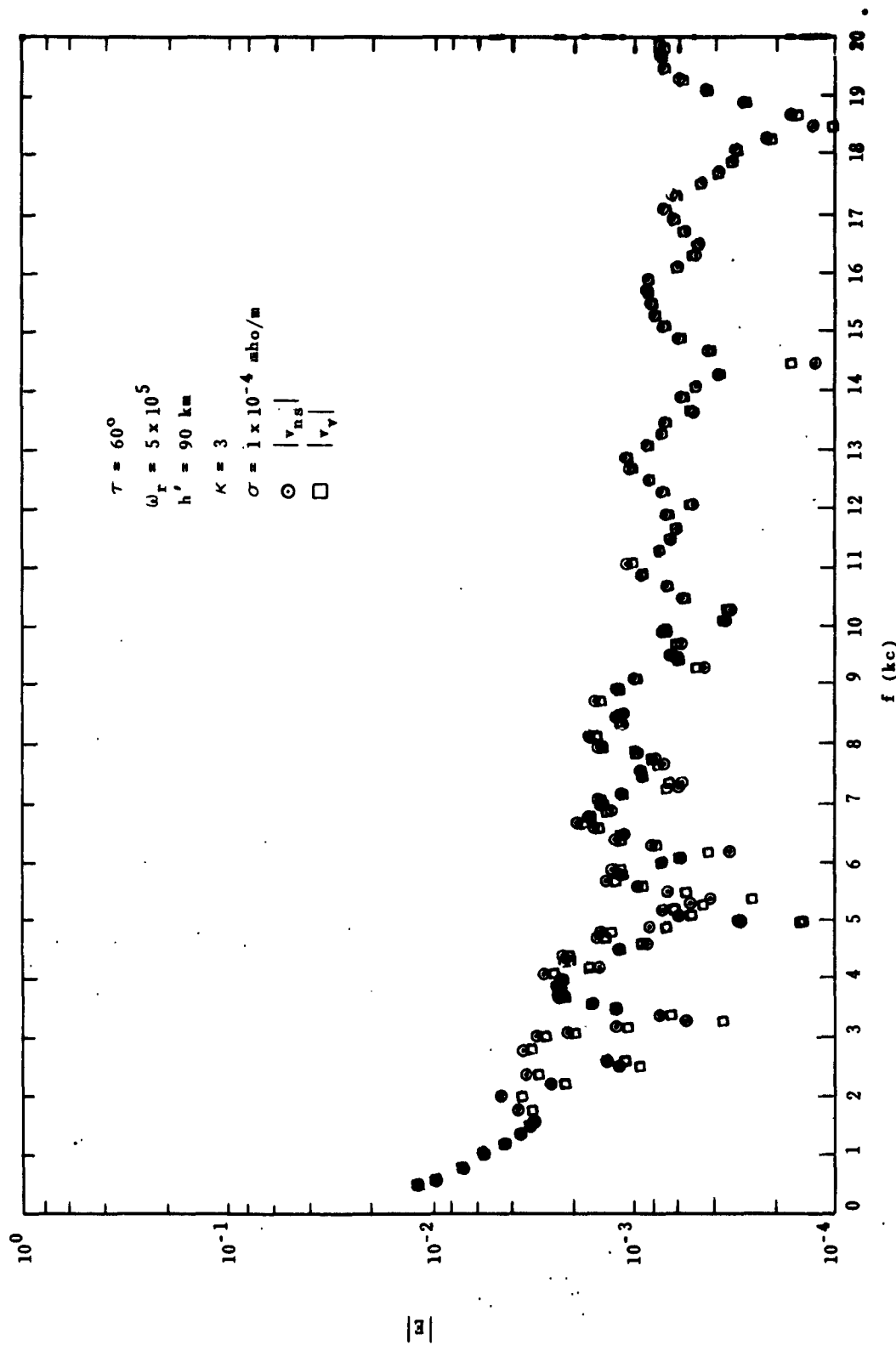
FIG. 3.6. MAGNITUDE OF E-FIELD RECEIVED BY NORMAL VERTICAL LOOP AND MONOPOLE VS FREQUENCY, FOR SUMMER-NIGHT MODEL IONOSPHERE, POOR GROUND, D = 2000 km, AND ϕ_g = 0.
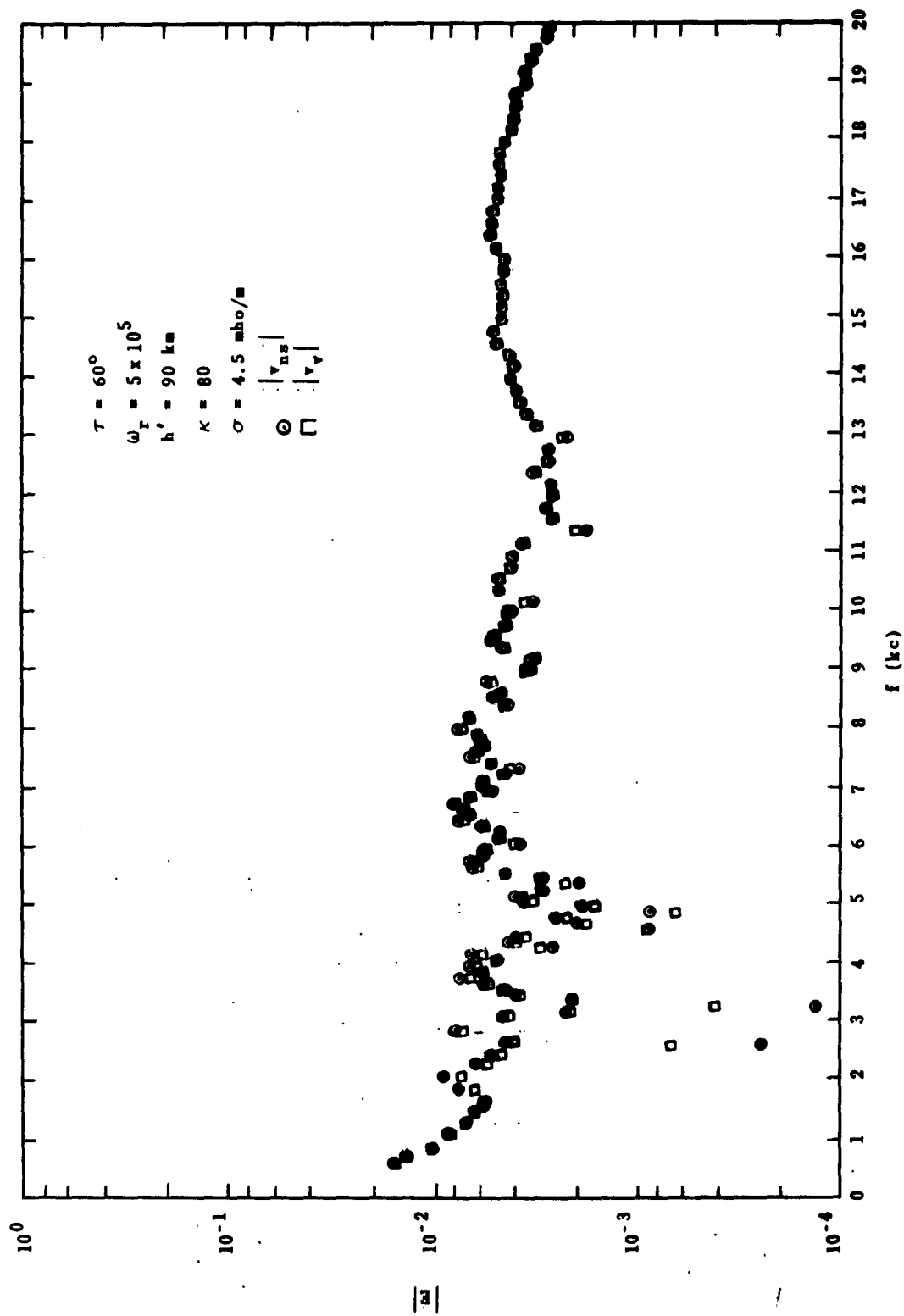
FIG. 3.7. MAGNITUDE OF E-FIELD RECEIVED BY NORMAL VERTICAL LOOP AND MONOPOLE VS FREQUENCY, FOR SUMMER-NIGHT MODEL IONOSPHERE, SEA WATER, $D = 2000$ km, AND $\phi_g = 0$.
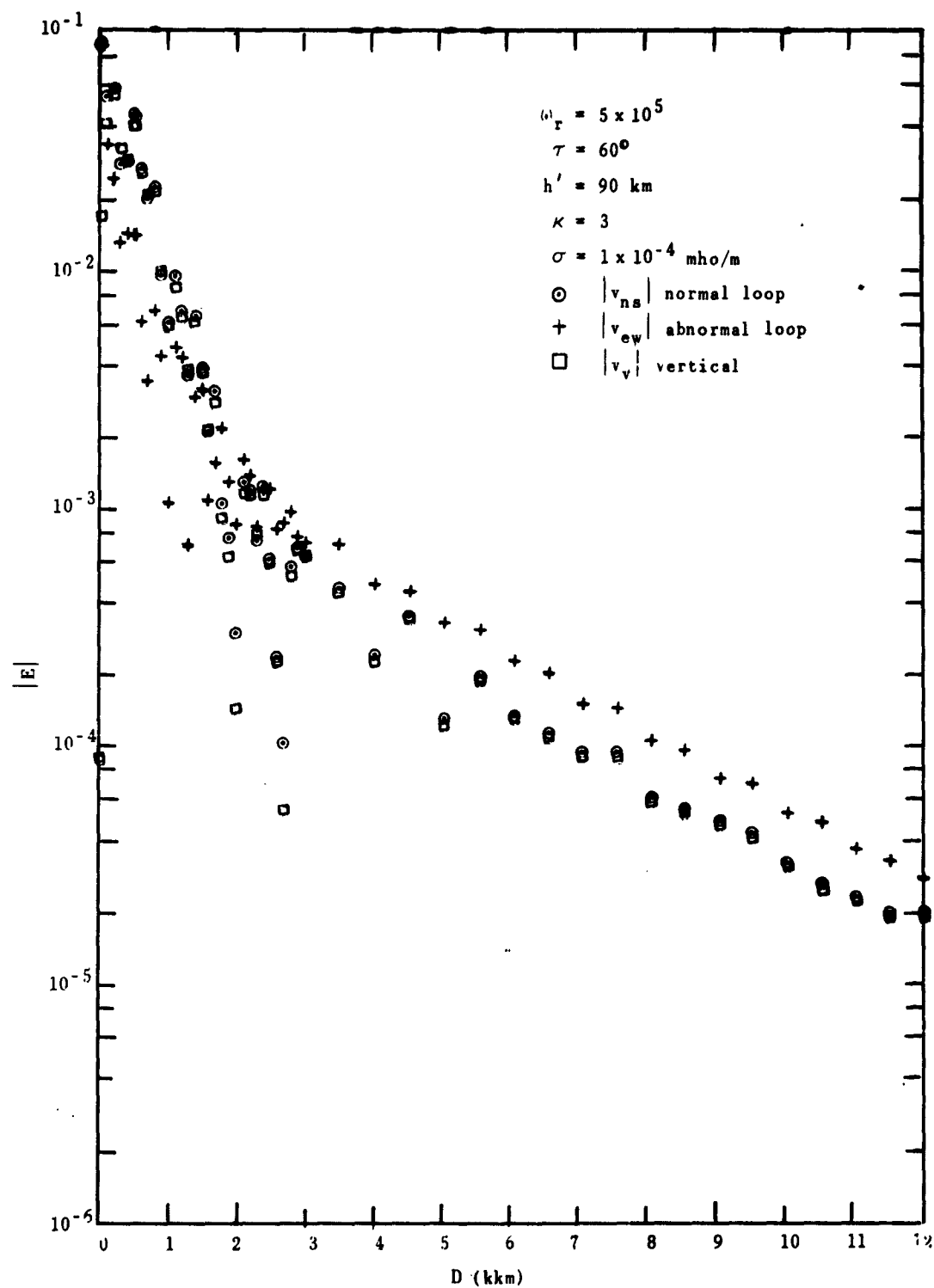
FIG. 3.8. MAGNITUDE OF E-FIELD RECEIVED BY NORMAL AND ABNORMAL
VERTICAL LOOPS AND MONOPOLE VS DISTANCE, FOR SUMMER-NIGHT MODEL
IONOSPHERE, POOR GROUND, $f = 5$ kc, AND $\phi_g = 0$.
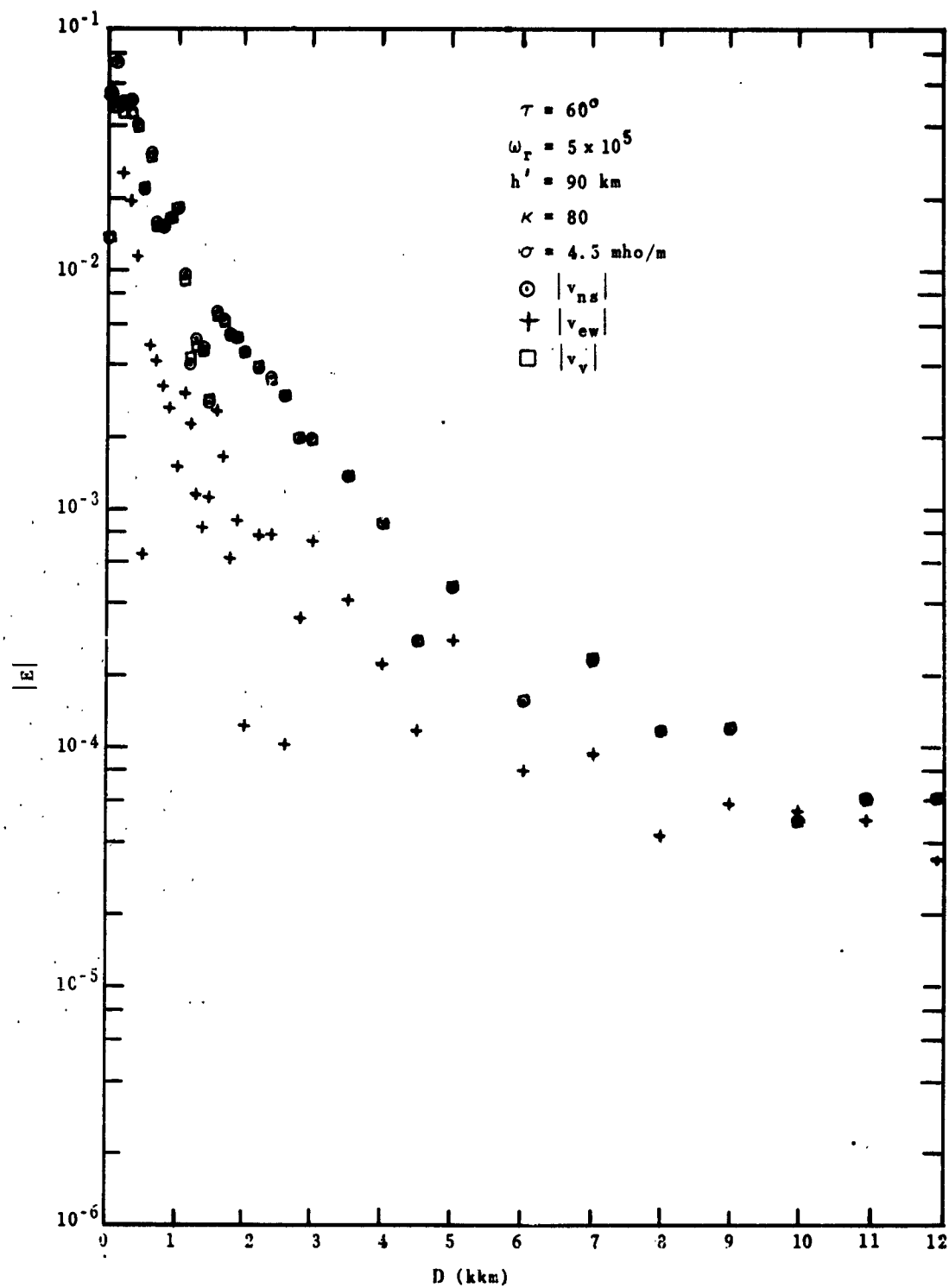
FIG. 3.9. MAGNITUDE OF E-FIELD RECEIVED BY NORMAL AND ABNORMAL VERTICAL
LOOPS AND MONOPOLE VS DISTANCE, FOR SUMMER-NIGHT MODEL IONOSPHERE, SEA
WATER, $f = 5$ kc, AND $\phi_g = 0$.

FIG. 3.10. MAGNITUDE OF E-FIELD RECEIVED BY NORMAL AND ABNORMAL VERTICAL
LOOPS AND MONOPOLE VS DISTANCE, FOR SUMMER-NIGHT MODEL IONOSPHERE, SEA
WATER, f = 15.5 kc, AND ϕ_g = 0.

10^{-1}

10^{-2}

10^{-3}

|E|

10^{-4}

10^{-5}

10^{-6}

0 1 2 3 4 5 6 7 8 9 10 11 12

D (kkm)

$\omega_r = 1.5 \times 10^5$

$\tau = 15^{\circ}$

$h' = 70$ km

$\kappa = 80$

$\sigma = 4.5$ mho/m

$\odot$ $|v_{ns}|$ normal loop

$+$ $|v_{ew}|$ abnormal loop

$\square$ $|v_v|$ vertical

FIG. 3.11.   MAGNITUDE OF E-FIELD RECEIVED BY NORMAL AND ABNORMAL
VERTICAL LOOPS AND MONOPOLE VS DISTANCE, FOR SUMMER-DAY MODEL
IONOSPHERE, SEA WATER, f = 5 kc, AND $\phi_g = 0$.

- 50 -

$\omega_p = 1.5 \times 10^5$

$\tau = 15°$

$h' = 70$ km

$\kappa = 80$

$\sigma = 4.5$ mho/m

⊙ $|v_{ns}|$ normal loop

+ $|v_{ew}|$ abnormal loop

□ $|v_v|$ vertical

$|E|$

D (kkm)
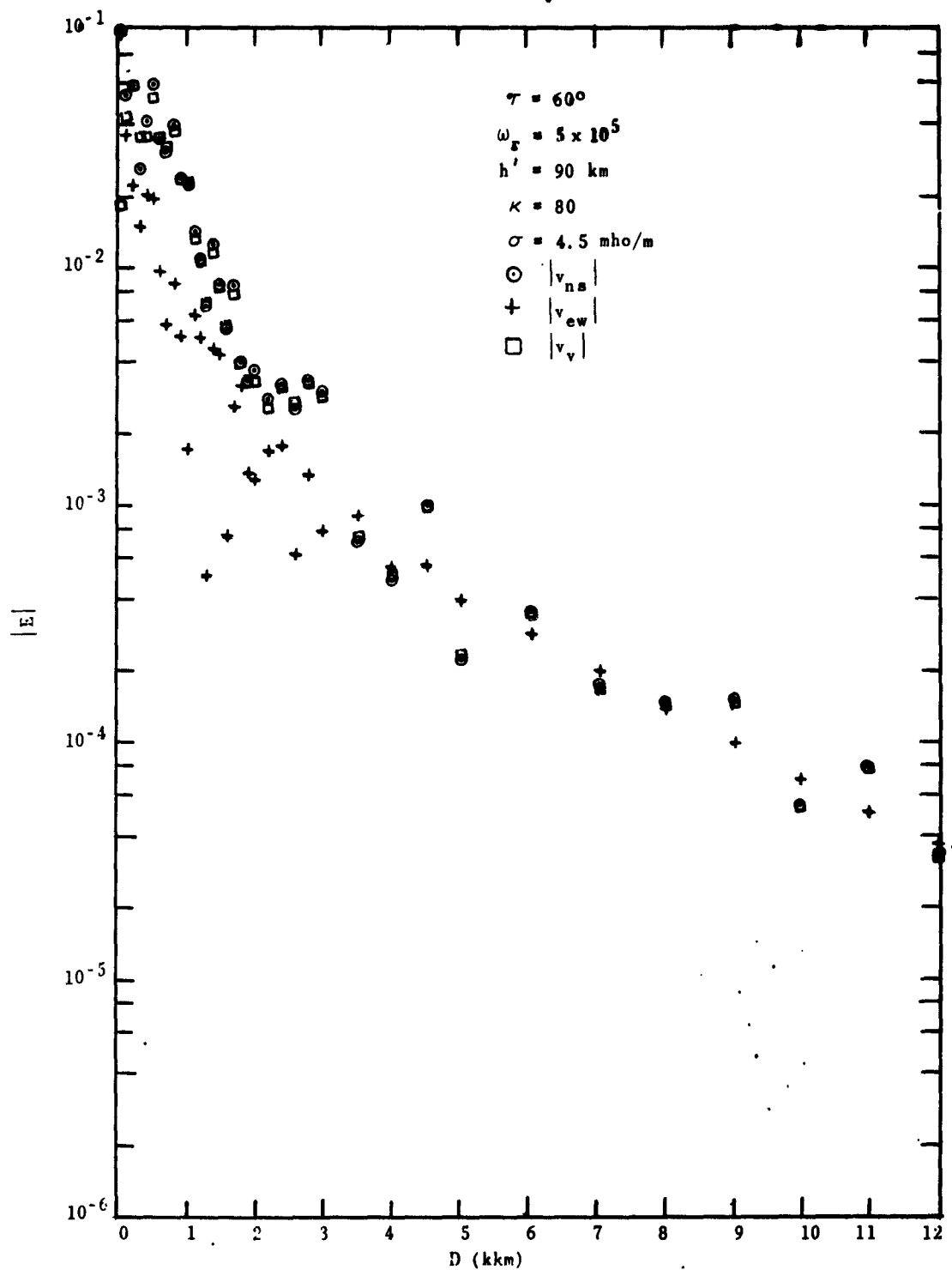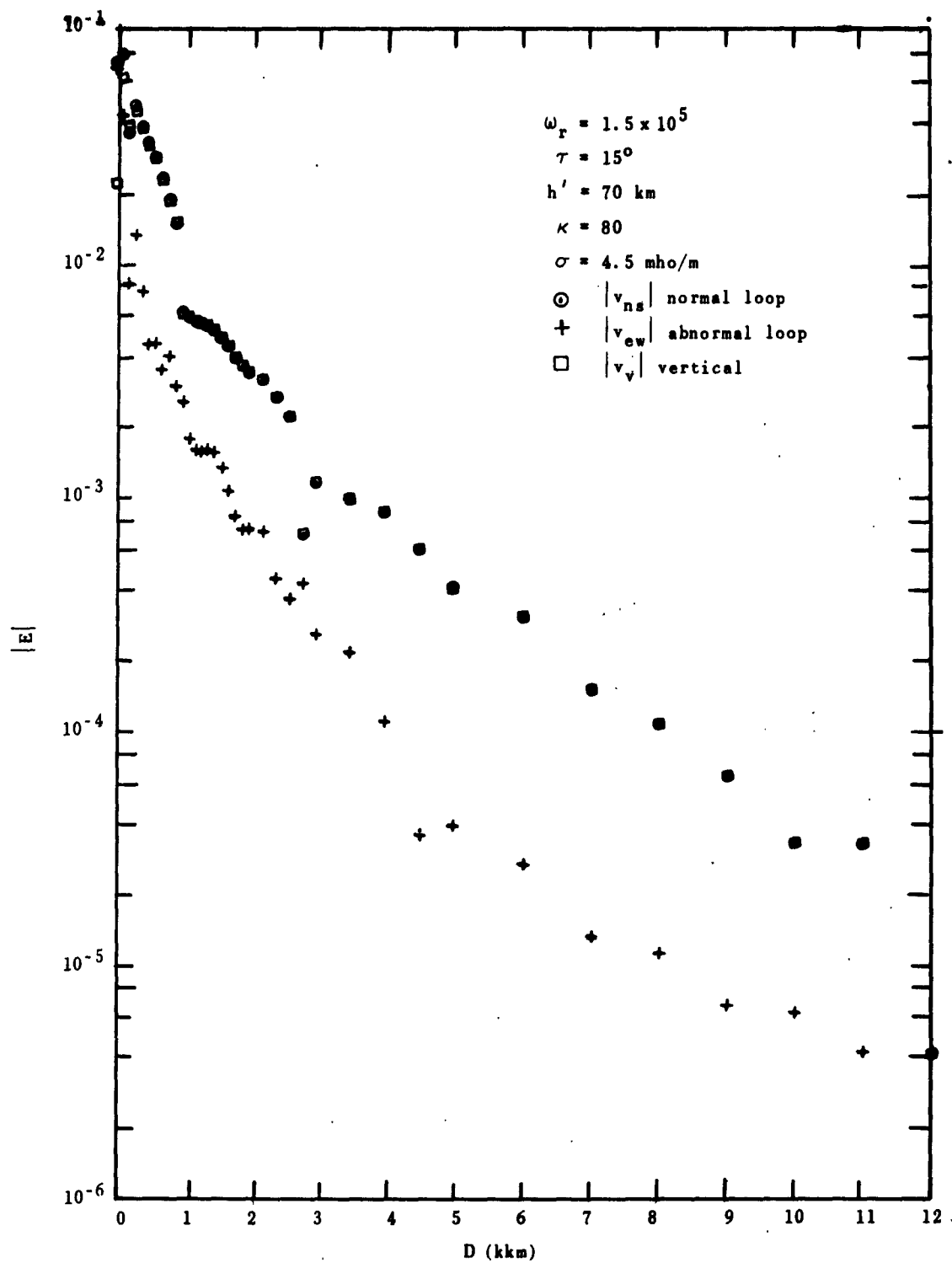
FIG. 3.12. MAGNITUDE OF E-FIELD RECEIVED BY NORMAL AND ABNORMAL
VERTICAL LOOPS AND MONOPOLE VS DISTANCE, FOR SUMMER-DAY MODEL
IONOSPHERE, SEA WATER, f = 15.5 kc, AND $\phi_g = 0$.
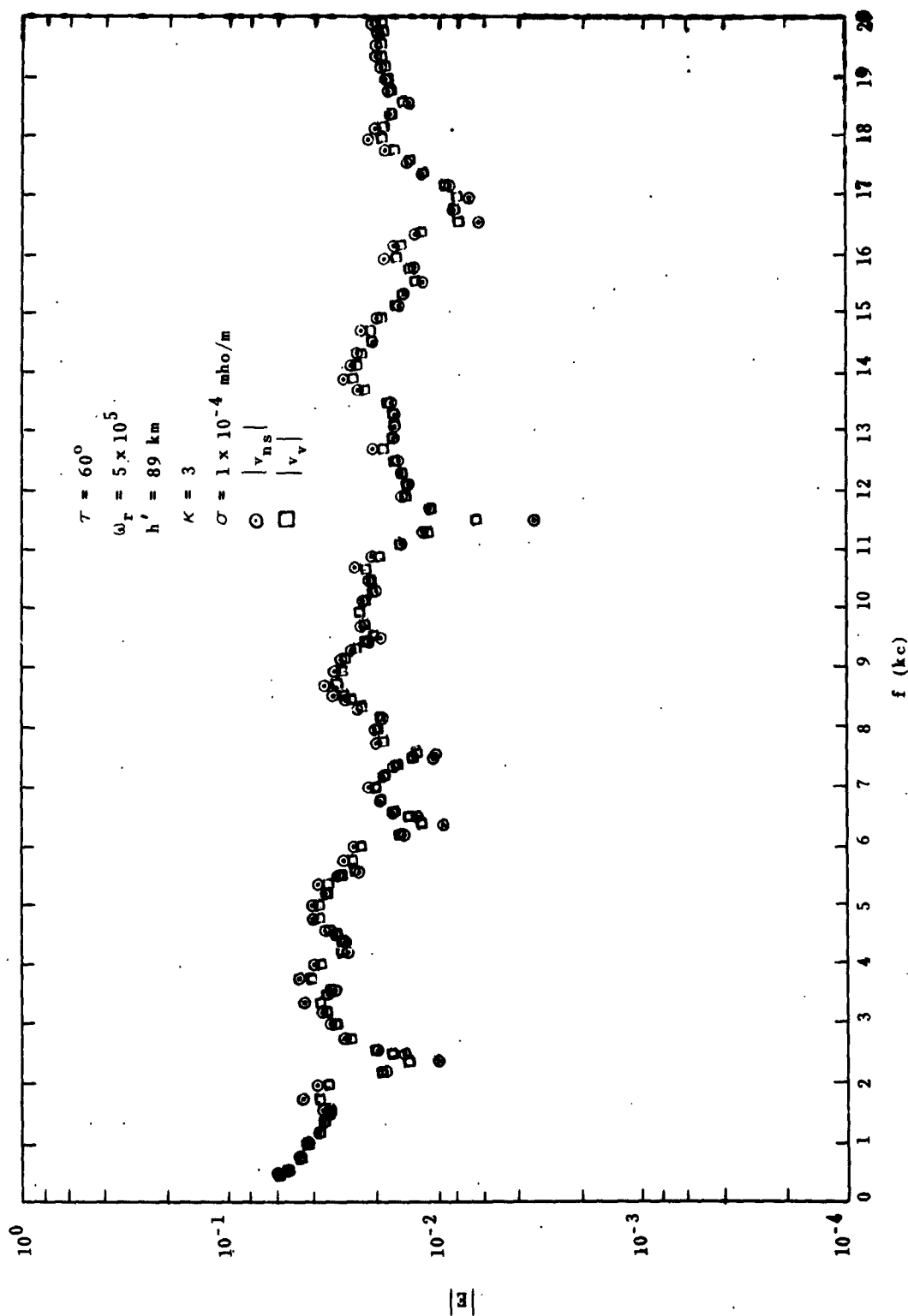
FIG. 3.13. MAGNITUDE OF E-FIELD RECEIVED BY NORMAL VERTICAL LOOP AND MONOPOLE VS FREQUENCY FOR SUMMER-NIGHT MODEL IONOSPHERE, EXCEPT $h' = 89$ km, POOR GROUND, $D = 500$ km, AND $\phi_g = 0$.
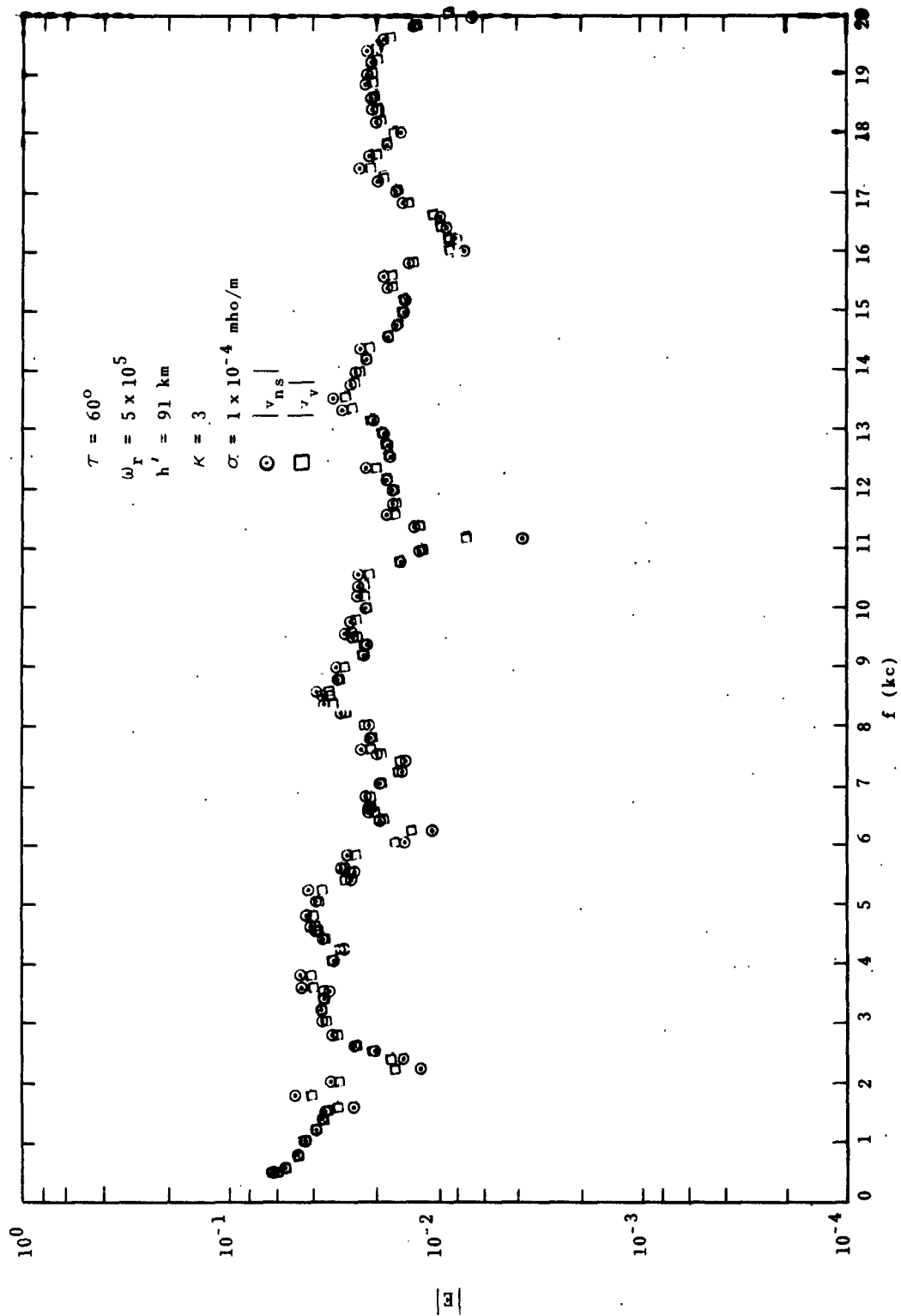
FIG. 3.14. MAGNITUDE OF E-FIELD RECEIVED BY NORMAL VERTICAL LOOP AND MONOPOLE VS FREQUENCY, FOR SUMMER-NIGHT MODEL IONOSPHERE EXCEPT $h' = 91$ km, POOR GROUND, $D = 500$ km, AND $\phi_g = 0$.
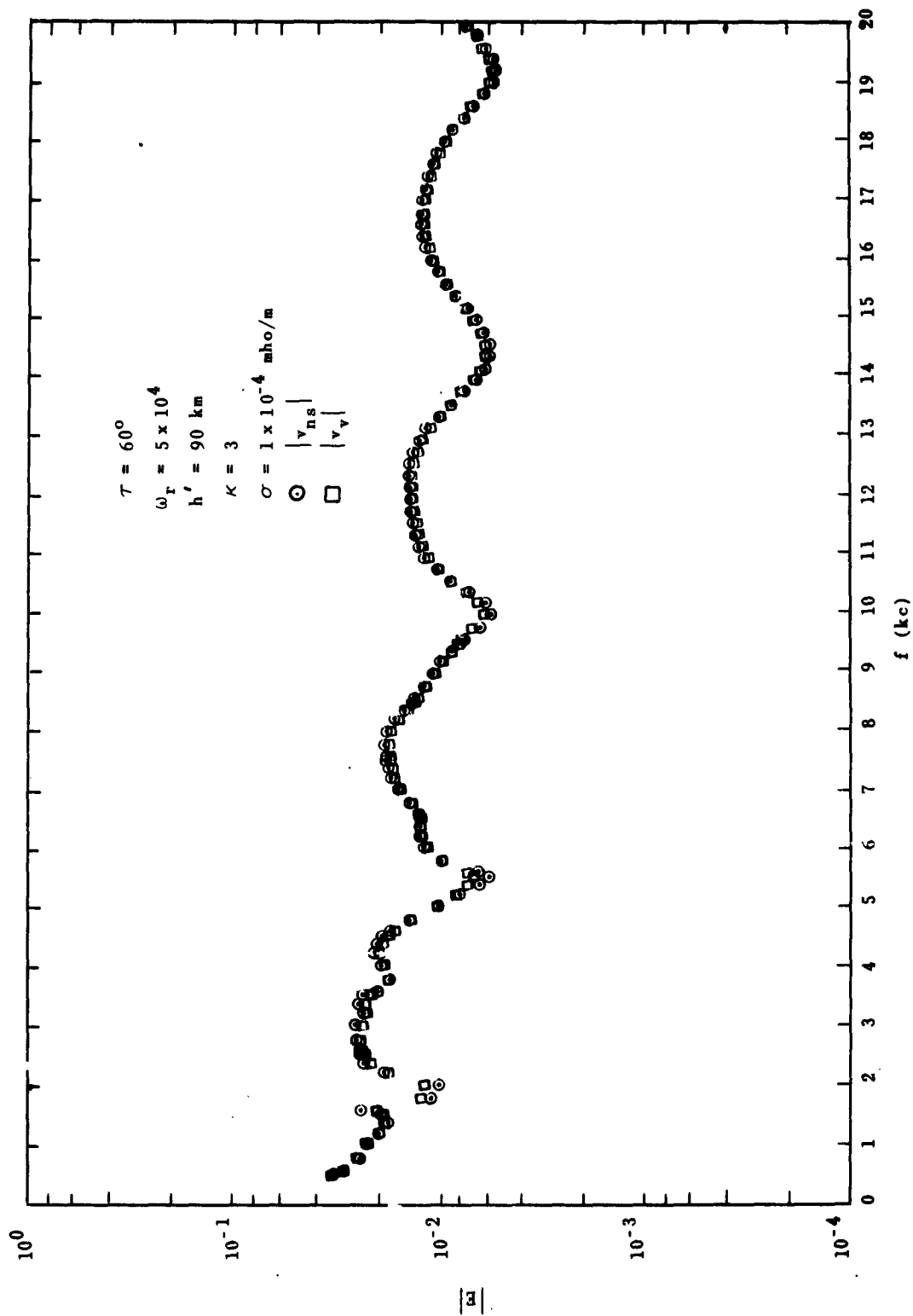
FIG. 3.15. MAGNITUDE OF E-FIELD RECEIVED BY NORMAL VERTICAL LOOP AND MONOPOLE VS FREQUENCY, FOR SUMMER-NIGHT MODEL IONOSPHERE EXCEPT $\omega_r = 5 \times 10^4$, POOR GROUND, D = 500 km, AND $\phi_g = 0$.

FIG. 3.16. MAGNITUDE OF E-FIELD RECEIVED BY NORMAL VERTICAL LOOP AND MONOPOLE VS FREQUENCY, FOR SUMMER-NIGHT MODEL IONOSPHERE, EXCEPT $\omega_r = 5 \times 10^6$, POOR GROUND, D = 500 km, AND $\phi_g = 0$.

$|\mathcal{E}|$

f (kc)

$\tau = 60^\circ$
$\omega_r = 5 \times 10^5$
$h' = 90$ km
$\kappa = 80$
$\sigma = 4.5$ mho/m
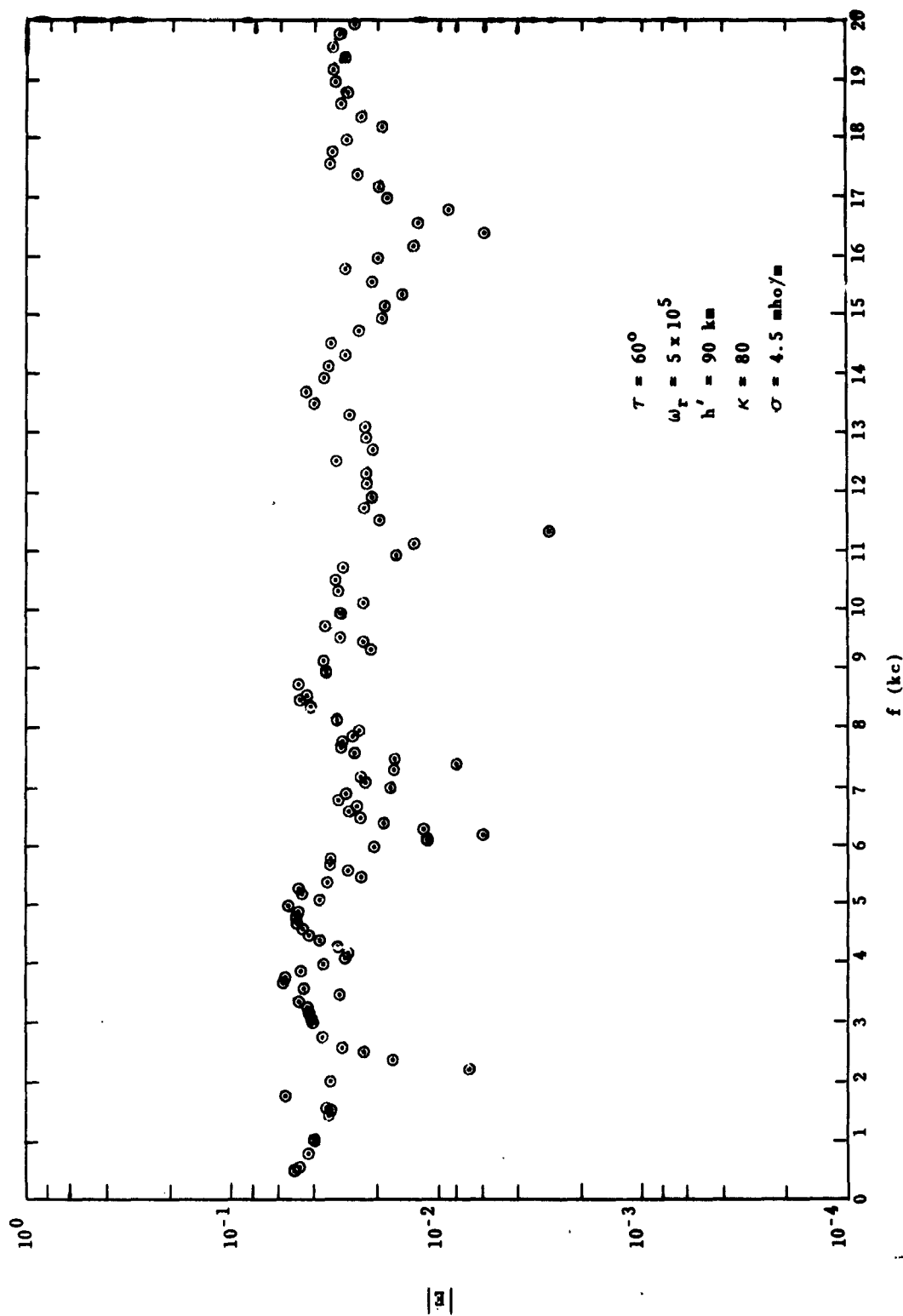
FIG. 3.17. MAGNITUDE OF E-FIELD RECEIVED BY NORMAL VERTICAL LOOP VS FREQUENCY FOR SUMMER-NIGHT MODEL IONOSPHERE, SEA WATER, D = 500 km, AND $\phi_g = 30$.
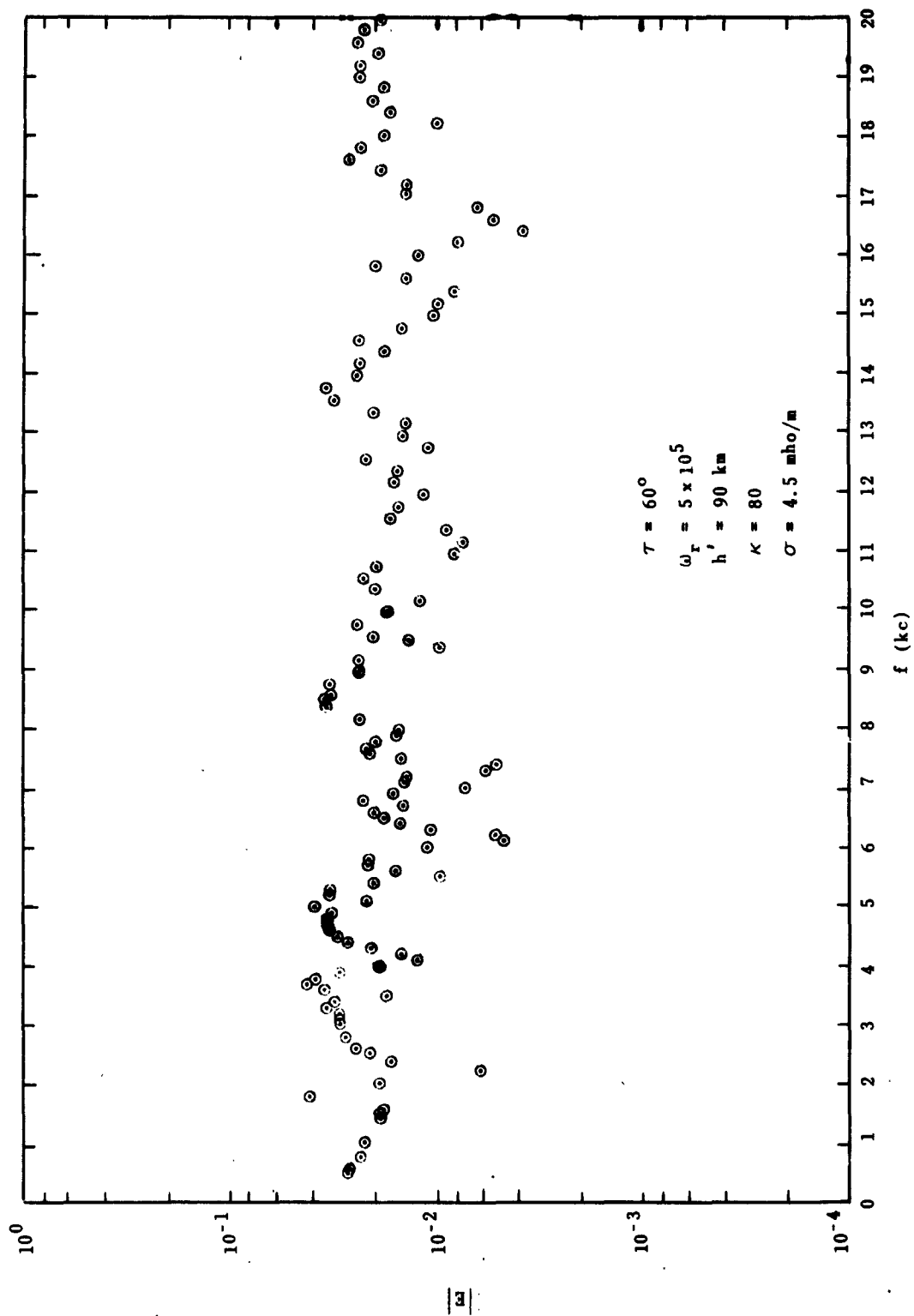
FIG. 3.18. MAGNITUDE OF E-FIELD RECEIVED BY NORMAL VERTICAL LOOP VS FREQUENCY FOR SUMMER-NIGHT MODEL IONOSPHERE, SEA WATER, D = 500 km, AND ϕ_g = 60.
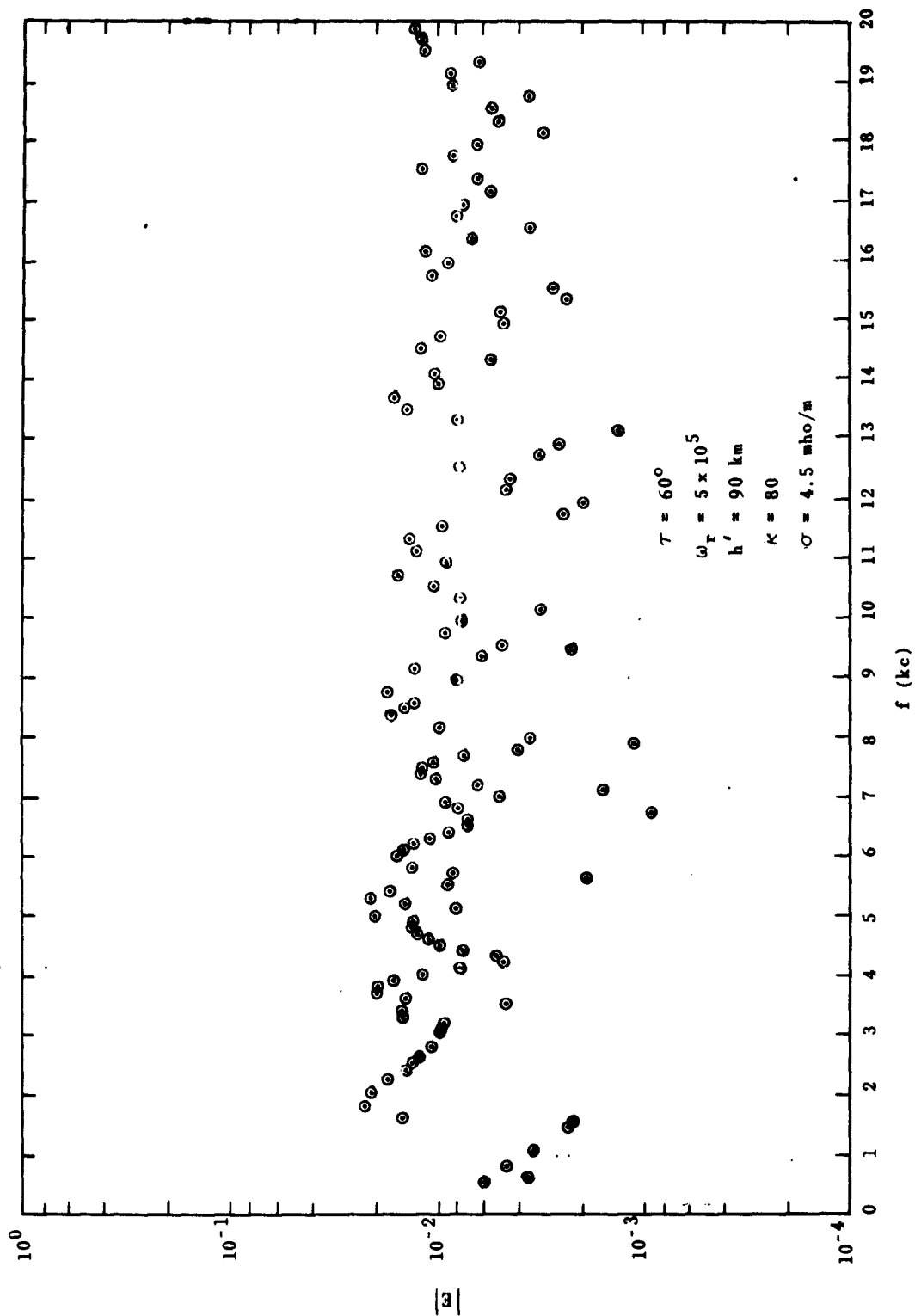
FIG. 3.19. MAGNITUDE OF E-FIELD RECEIVED BY NORMAL VERTICAL LOOP VS FREQUENCY FOR SUMMER-NIGHT MODEL IONOSPHERE, SEA WATER, D = 500 km, AND ϕ_g = 90.
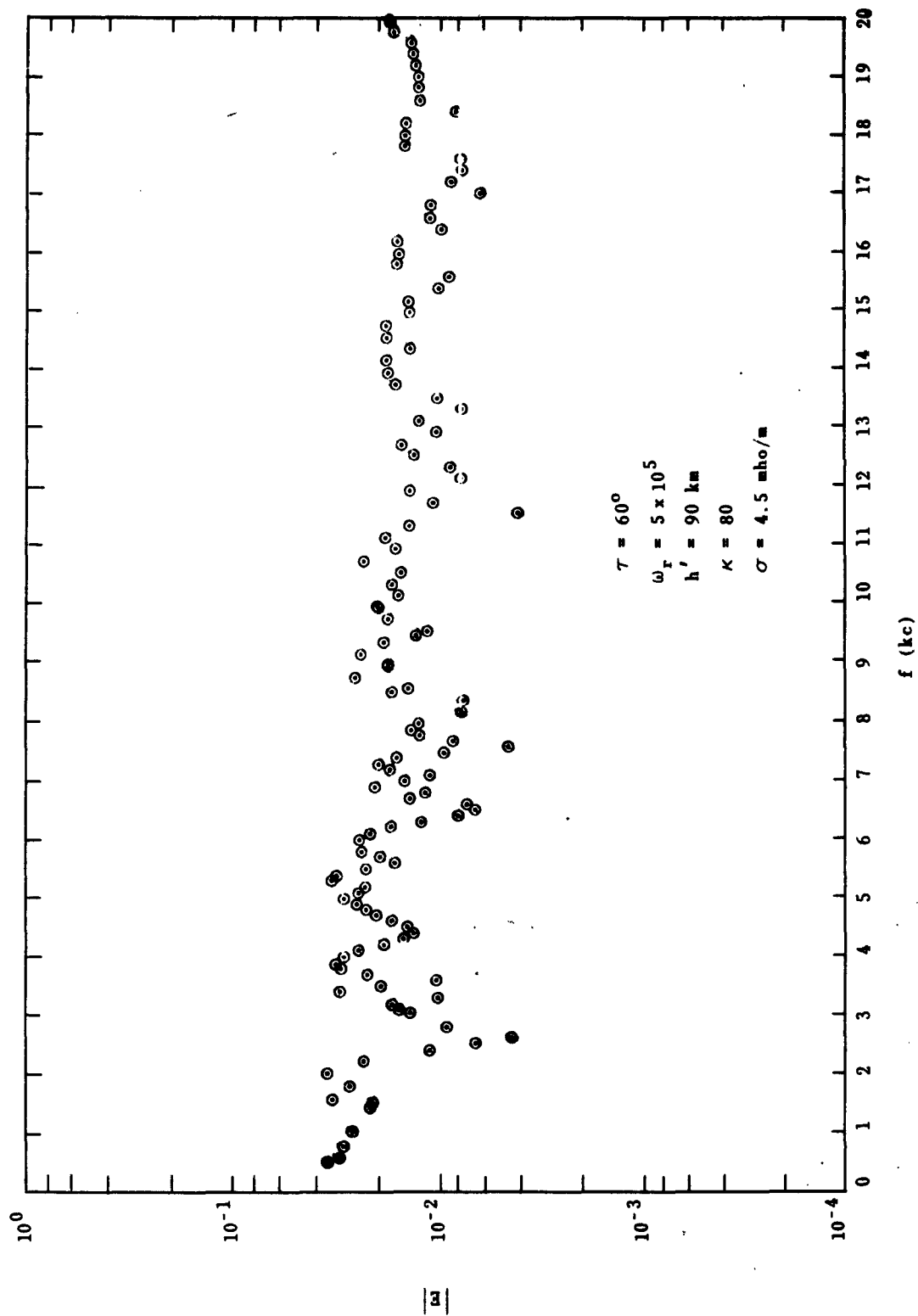
FIG. 3.20. MAGNITUDE OF E-FIELD RECEIVED BY NORMAL VERTICAL LOOP VS FREQUENCY FOR SUMMER-NIGHT MODEL IONOSPHERE, SEA WATER, D = 500 km, AND ϕ_g = 120.
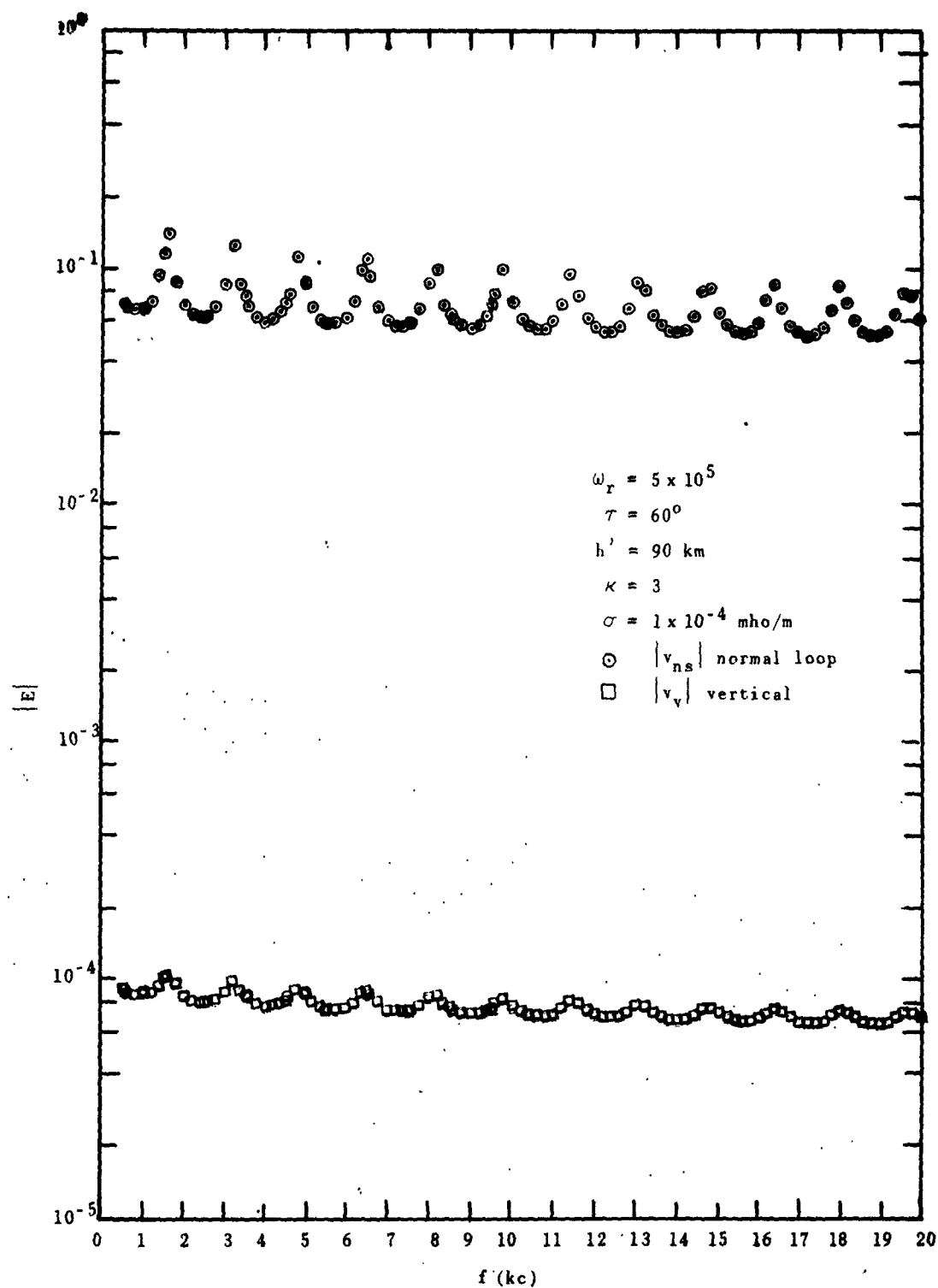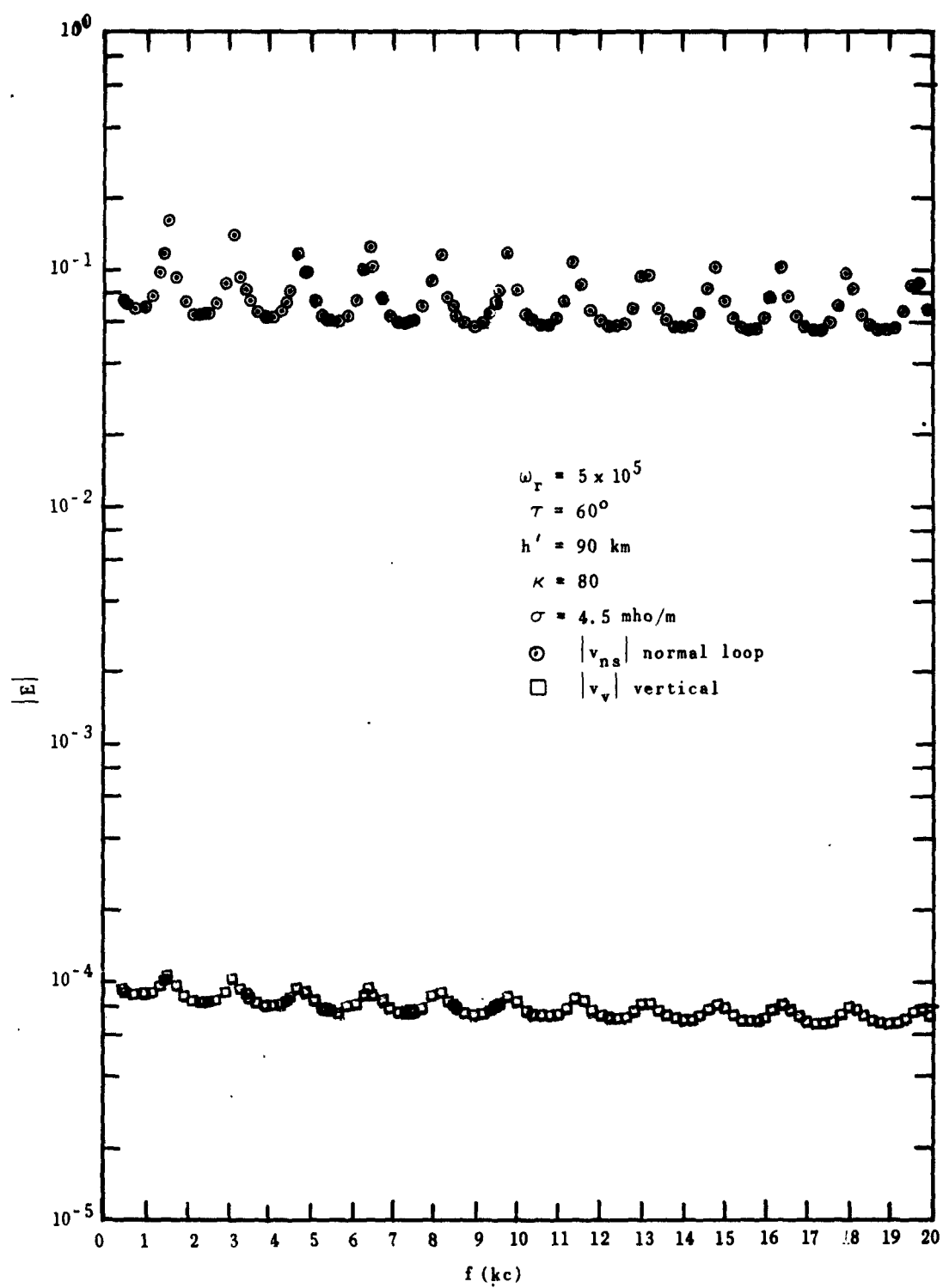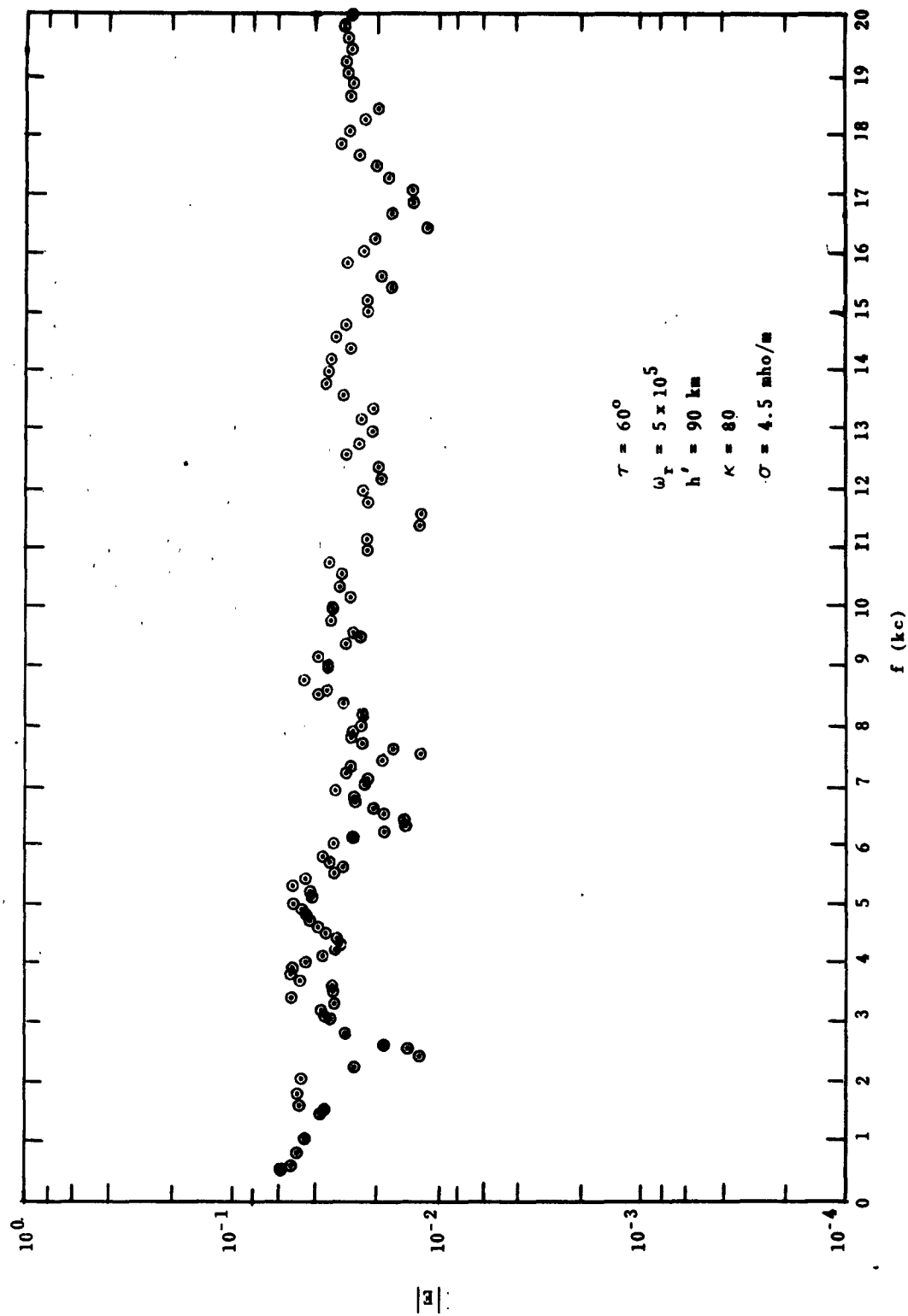
FIG. 3.21. MAGNITUDE OF E-FIELD RECEIVED BY NORMAL VERTICAL LOOP VS FREQUENCY FOR SUMMER-NIGHT MODEL IONOSPHERE, SEA WATER, D = 500 km, AND ϕ_g = 150.

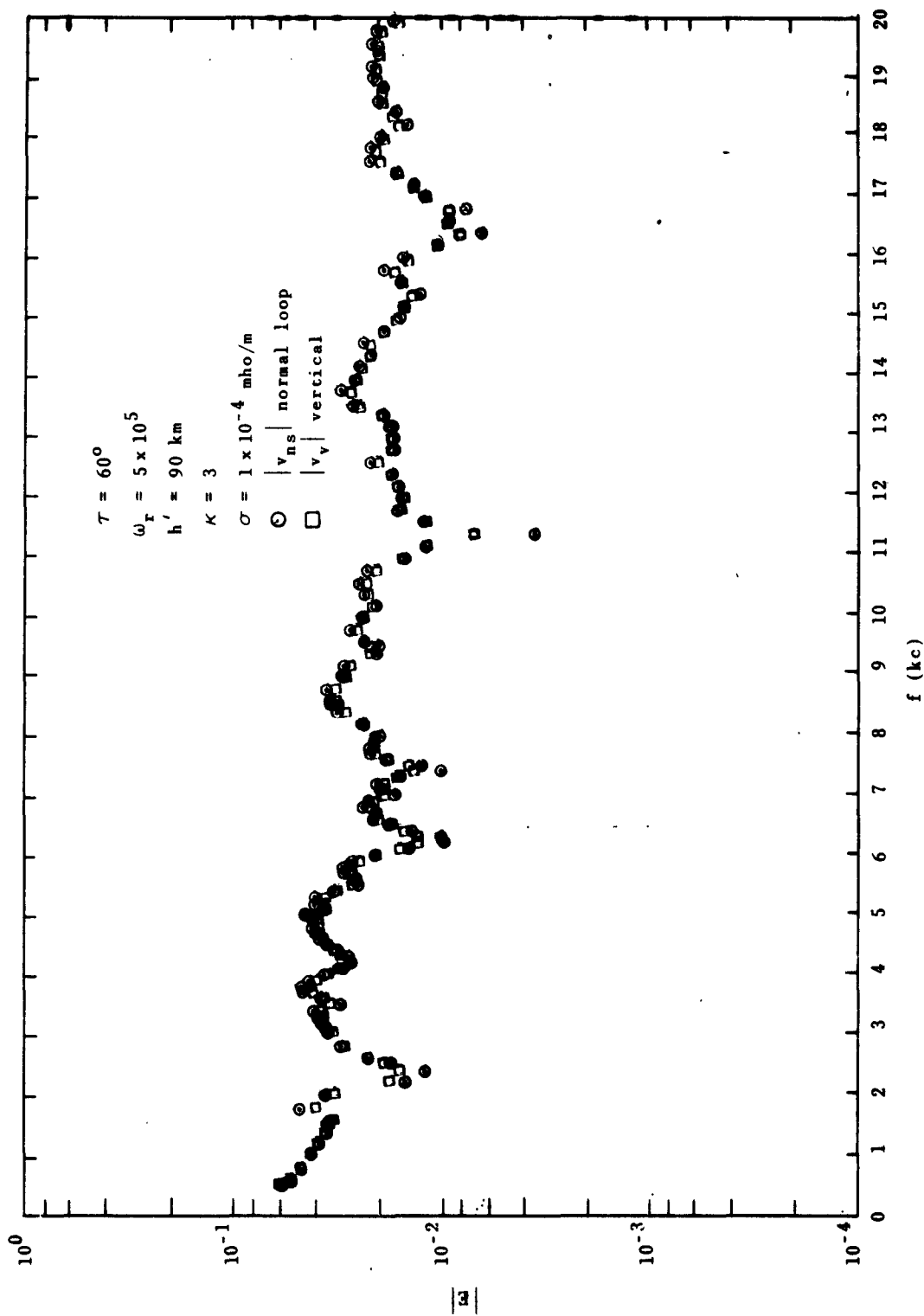3.   IONIZATION DENSITY VARIATION. Figures 3.15 and 3.16 are similar to Fig. 3.13 and Fig. 3.14 except that the values of ω_r have been changed instead of those of h'. The values used are 5×10^4 and 5×10^6 for Figs. 3.13 and 3.14, respectively, a factor of 10 lower and higher than for the summer-night model.

4.   RELATIVE BEARING VARIATION. Figures 3.17 through 3.21 show the field strength, as seen by the normal (ns) loop as a function of frequency for the summer-night model ionosphere and sea water at 500 km. The value of $\emptyset_g$ was increased, in 30-degree steps in each case, from 30 through 150 degrees. These curves show the effect of different bearings relative to a fixed loop.

C. CROSSED-LOOP VOLTAGE RATIO VARIATION WITH FREQUENCY

1.   DISTANCE VARIATION. Figures 3.22 through 3.30 show the values of the real and imaginary parts of $v_R (v_R = v_{ns}/v_{ew})$ as a function of frequency for various conditions. Figures 3.22 through 3.26 show the values calculated for the summer-night model ionosphere with sea water and poor ground conditions for 500, 1000, and 2000 km.

2.   IONOSPHERE HEIGHT VARIATION. Figures 3.27 and 3.28 show the values of the real and imaginary parts of v_R for poor ground at 500 km, using the summer-night model ionosphere except that h' was changed to 89 and 91 km, respectively.

3.   IONIZATION DENSITY VARIATION. Figures 3.29 and 3.30 show the values of the real and imaginary parts of v_R for the same conditions as 2, above, except that the values of ω_r were changed to 5×10^4 and 5×10^6, respectively, while h' was 90 km.

D. THE WAVE POLARIZATION Q_a

The values of the real and imaginary parts of Q_a, the polarization of the incoming wave as seen by the crossed loop and vertical system are presented as a function of frequency in Figs. 3.31 to 3.34. It will be recalled that Q_a is not defined for conditions for which there is no equivalent plane wave. No values are defined for these frequencies.
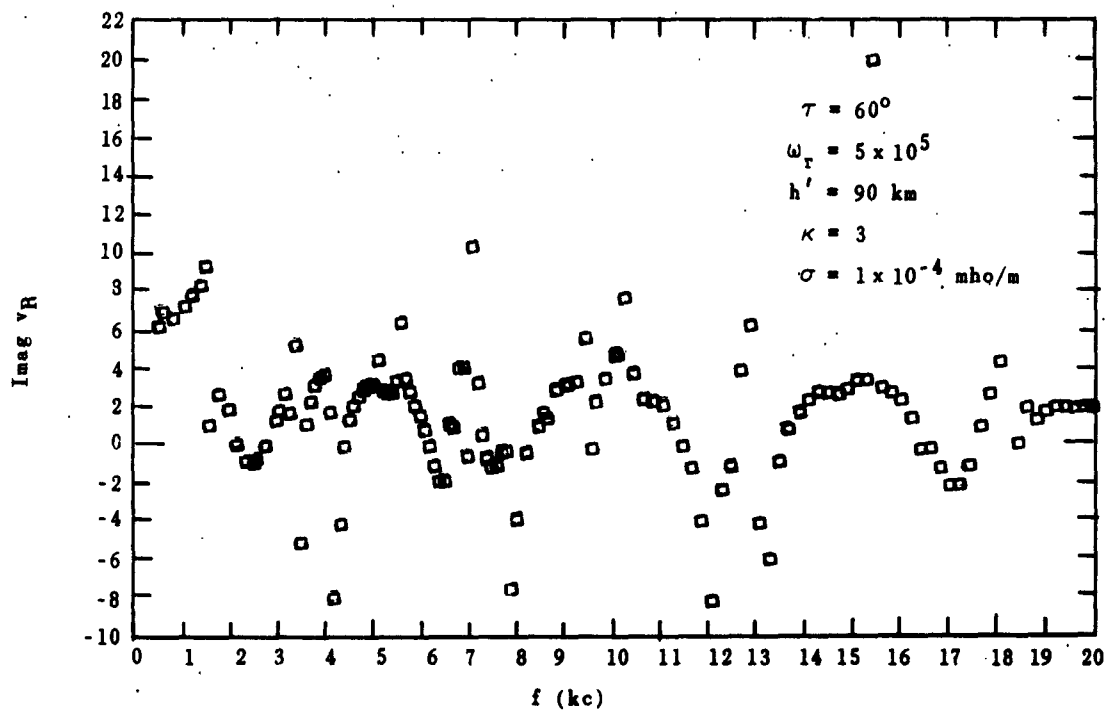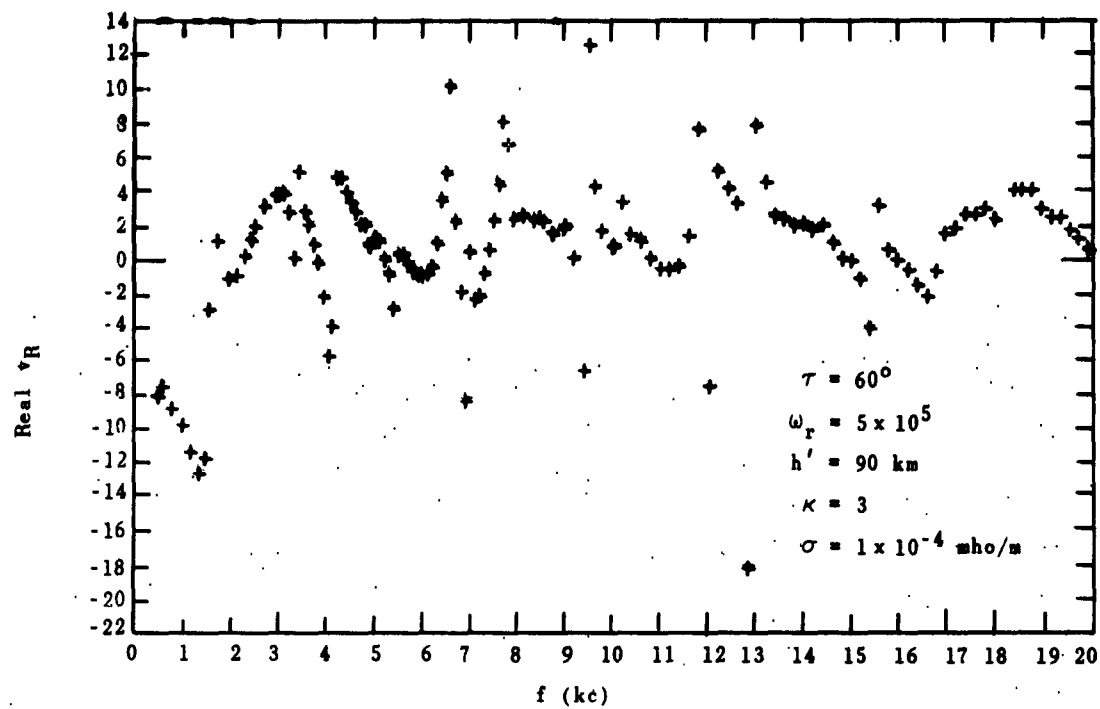
FIG. 3.22.   REAL AND IMAGINARY PARTS OF CROSSED-LOOP VOLTAGE RATIO
VS FREQUENCY FOR SUMMER-NIGHT MODEL IONOSPHERE, POOR GROUND,
D = 500 km, AND ϕ_g = 0.
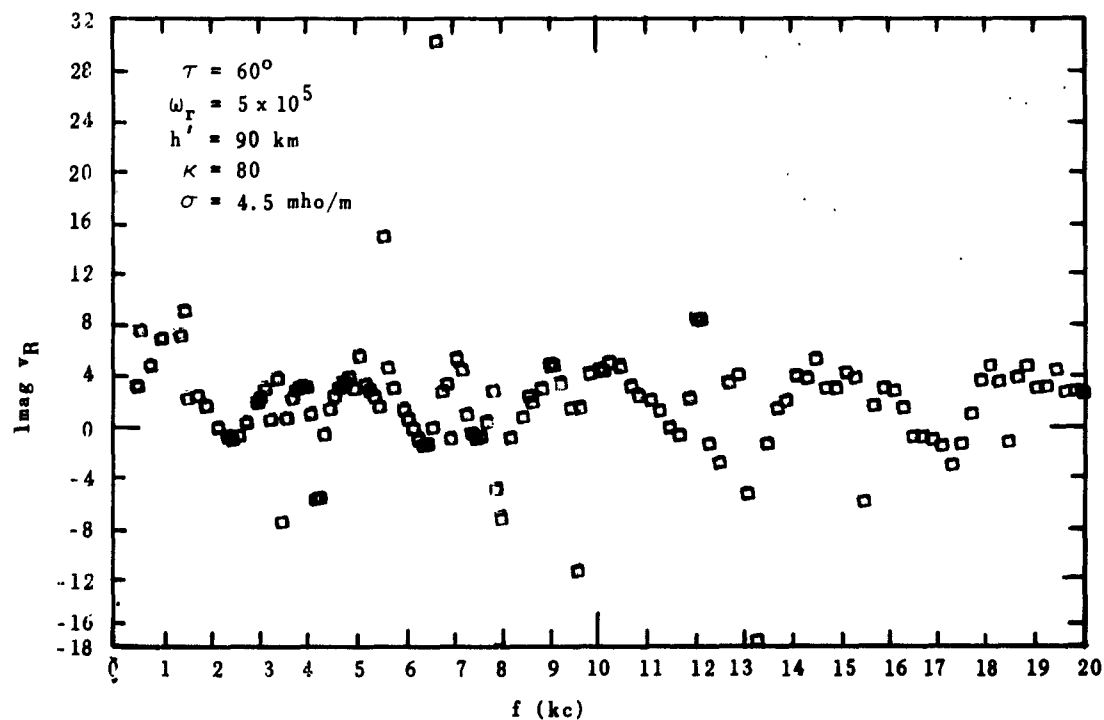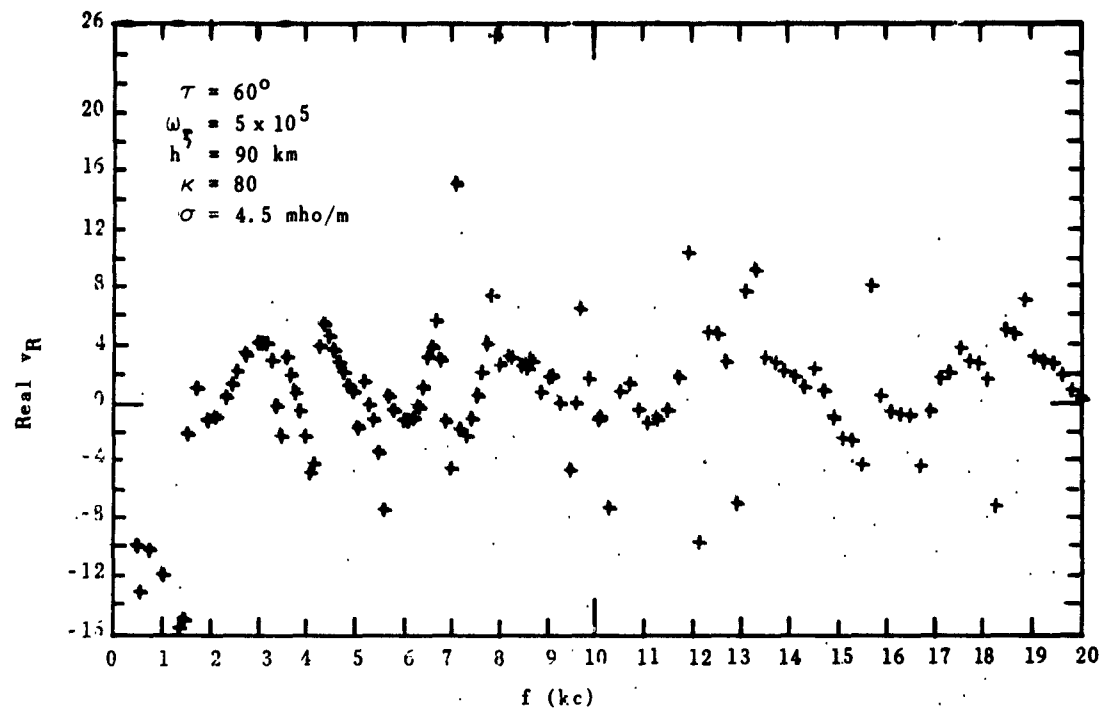
FIG. 3.23. REAL AND IMAGINARY PARTS OF CROSSED-LOOP VOLTAGE RATIO VS FREQUENCY, FOR SUMMER-NIGHT MODEL IONOSPHERE, SEA WATER, D = 500 km, AND ϕ_g = 0.

FIG. 3.24.   REAL AND IMAGINARY PARTS OF CROSSED-LOOP VOLTAGE RATIO
VS FREQUENCY FOR SUMMER-NIGHT MODEL IONOSPHERE, SEA WATER, D = 1000 km,
AND ϕ_g = 0.

The upper plot shows Real v_R versus f (kc) with parameters:

$$\tau = 60^{\circ}$$
$$\omega_r = 5 \times 10^5$$
$$h' = 90 \text{ km}$$
$$\kappa = 3$$
$$\sigma = 1 \times 10^{-4} \text{ mho/m}$$

The lower plot shows Imag v_R versus f (kc) with parameters:

$$\tau = 60^{\circ}$$
$$\omega_r = 5 \times 10^5$$
$$h' = 90 \text{ km}$$
$$\kappa = 3$$
$$\sigma = 1 \times 10^{-4} \text{ mho/m}$$
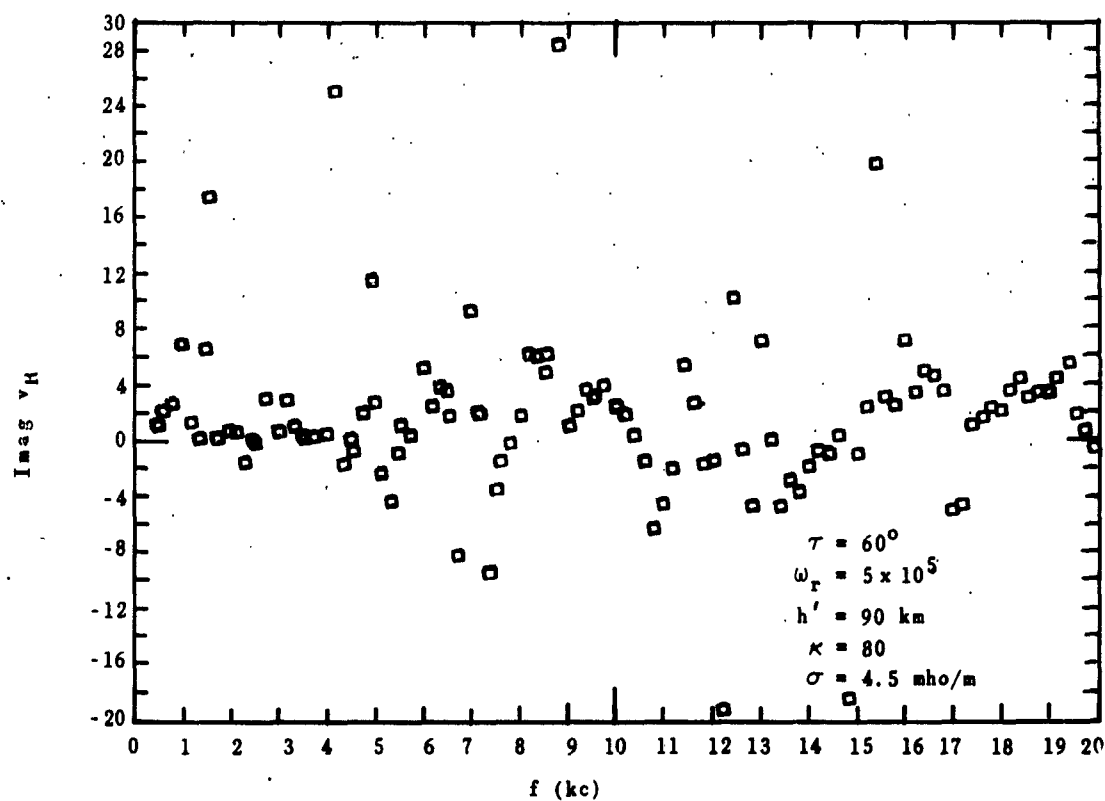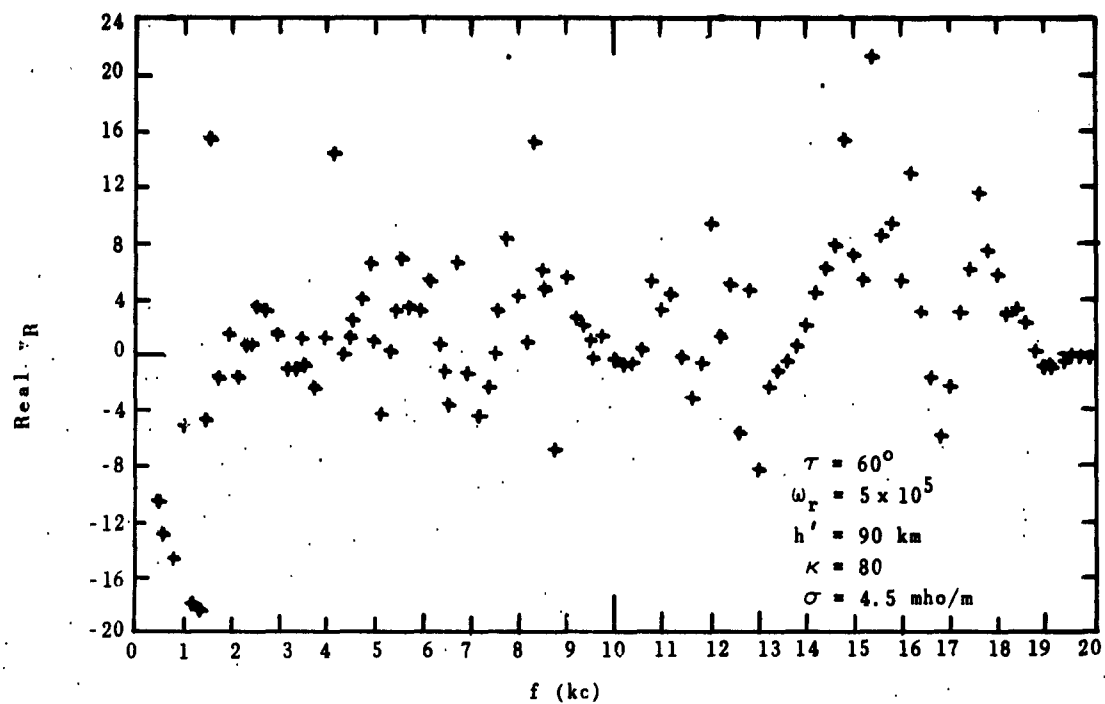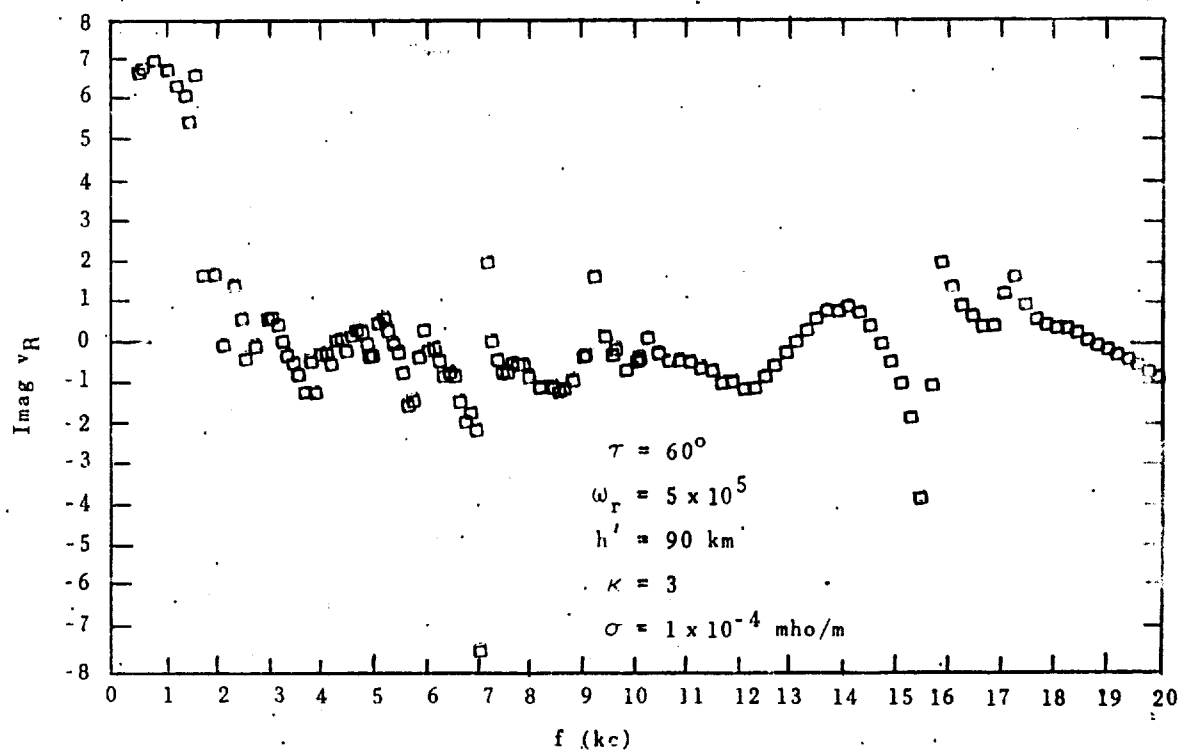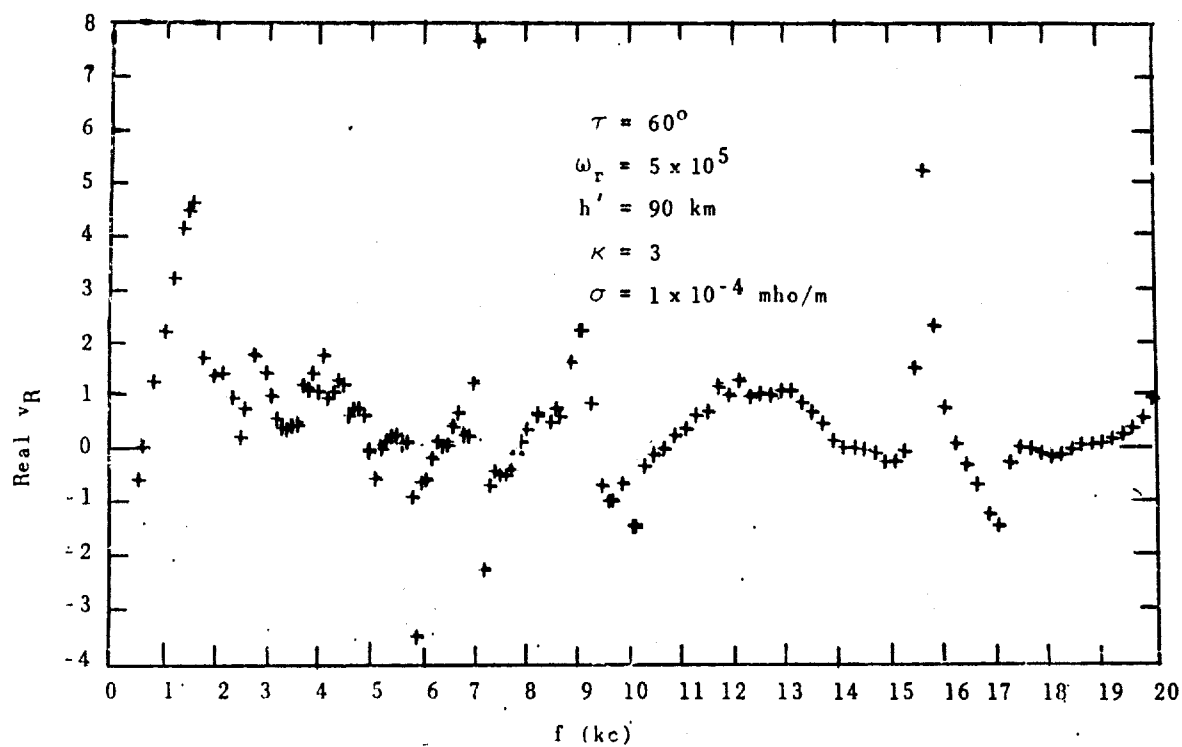
FIG. 3.25. REAL AND IMAGINARY PARTS OF CROSSED-LOOP VOLTAGE RATIO VS FREQUENCY FOR SUMMER-NIGHT MODEL IONOSPHERE, POOR GROUND, D = 2000 km, $\phi_s = 0$.

- 65 -
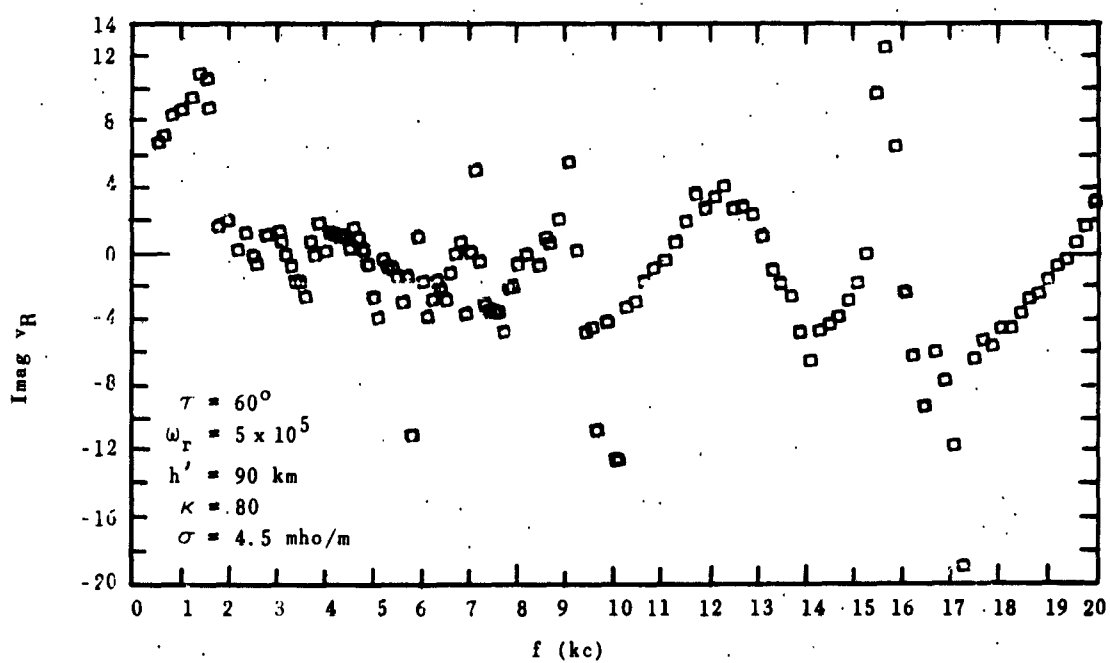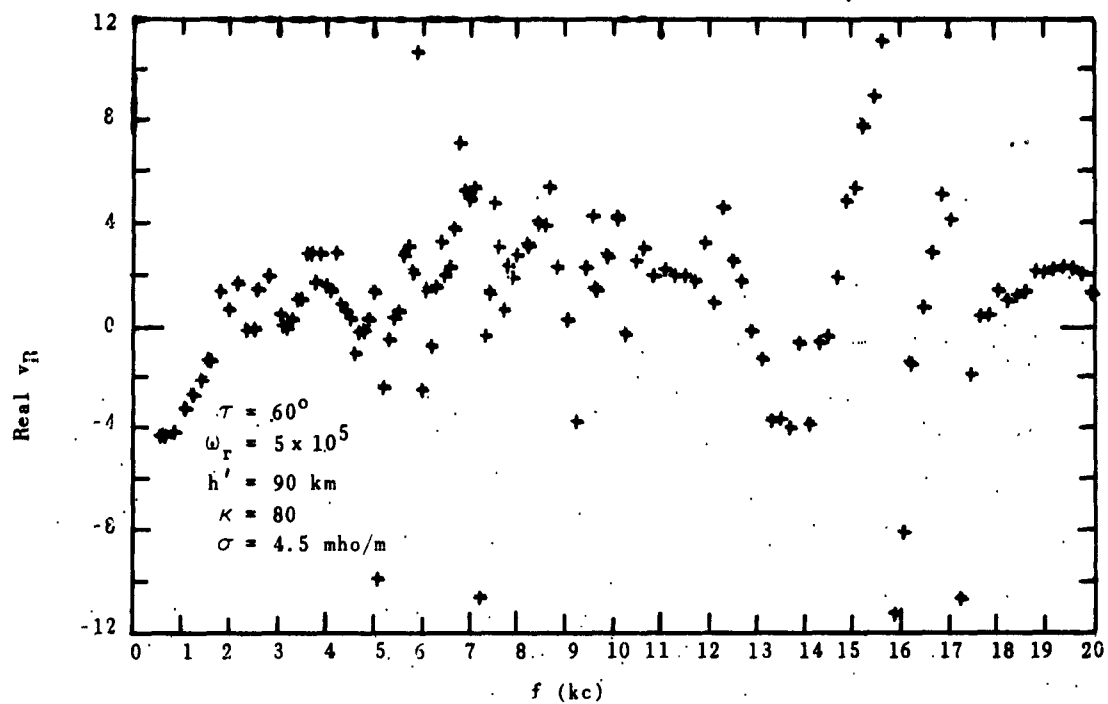
FIG. 3.26. REAL AND IMAGINARY PARTS OF CROSSED-LOOP VOLTAGE RATIO
VS FREQUENCY, FOR SUMMER-NIGHT MODEL IONOSPHERE, SEA WATER, D = 2000 km,
AND $\phi_g = 0$.
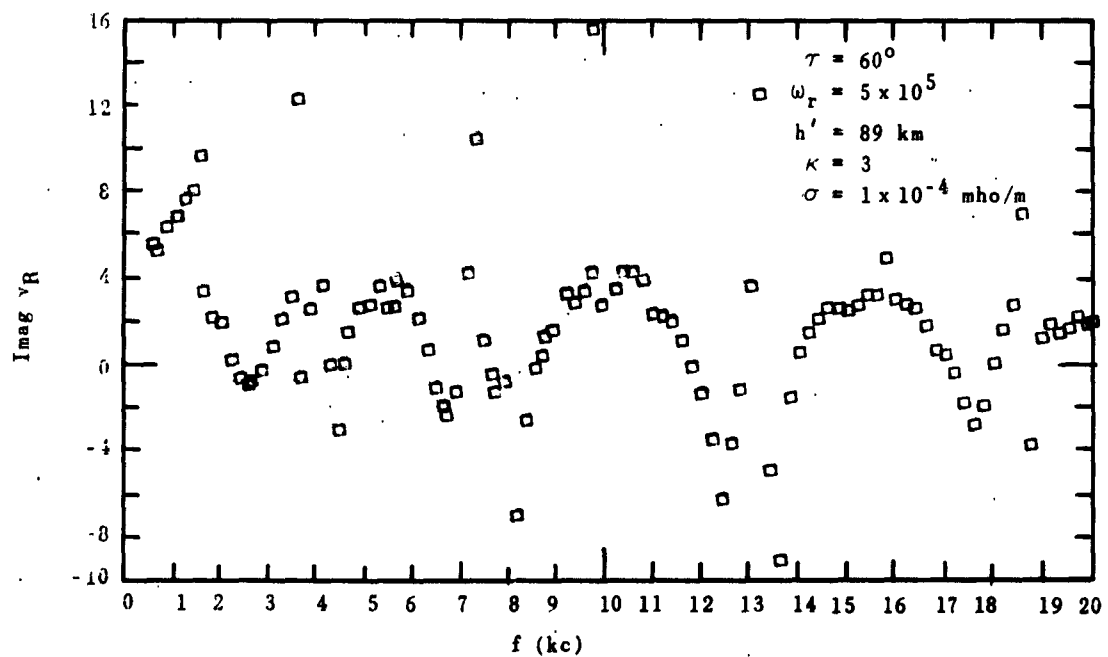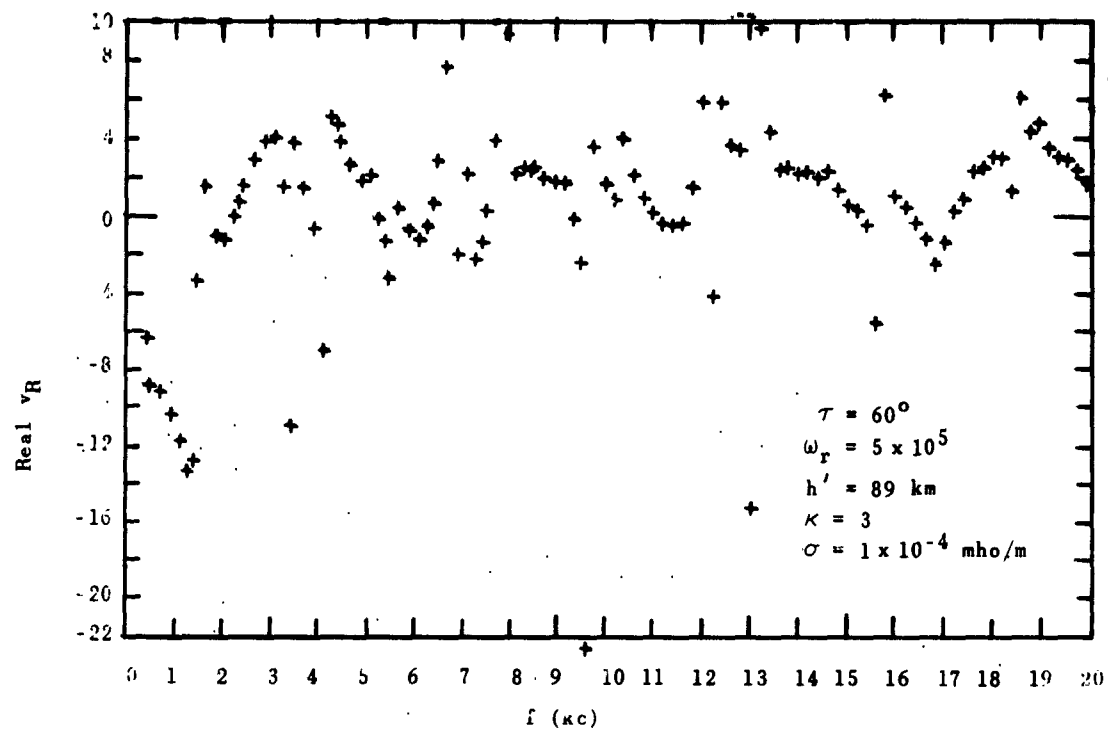
FIG. 3.27 REAL AND IMAGINARY PARTS OF CROSSED-LOOP VOLTAGE RATIO VS FREQUENCY, FOR SUMMER-NIGHT MODEL IONOSPHERE EXCEPT h' = 89 km, POOR GROUND, D = 500 km, AND $\phi_g = 0$.
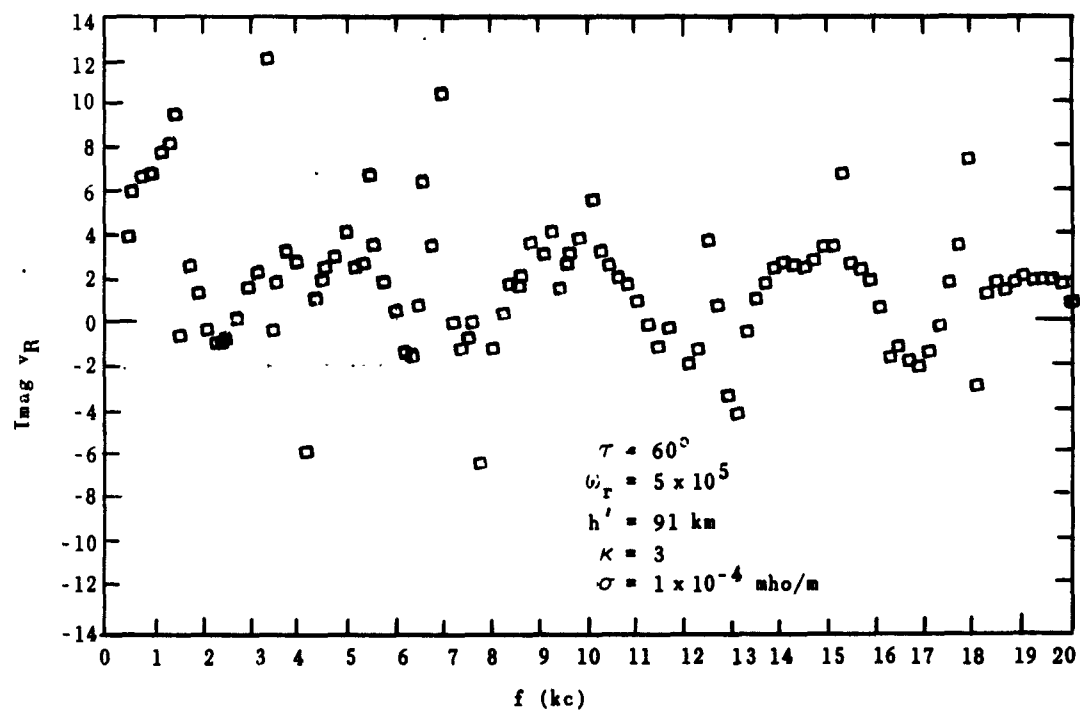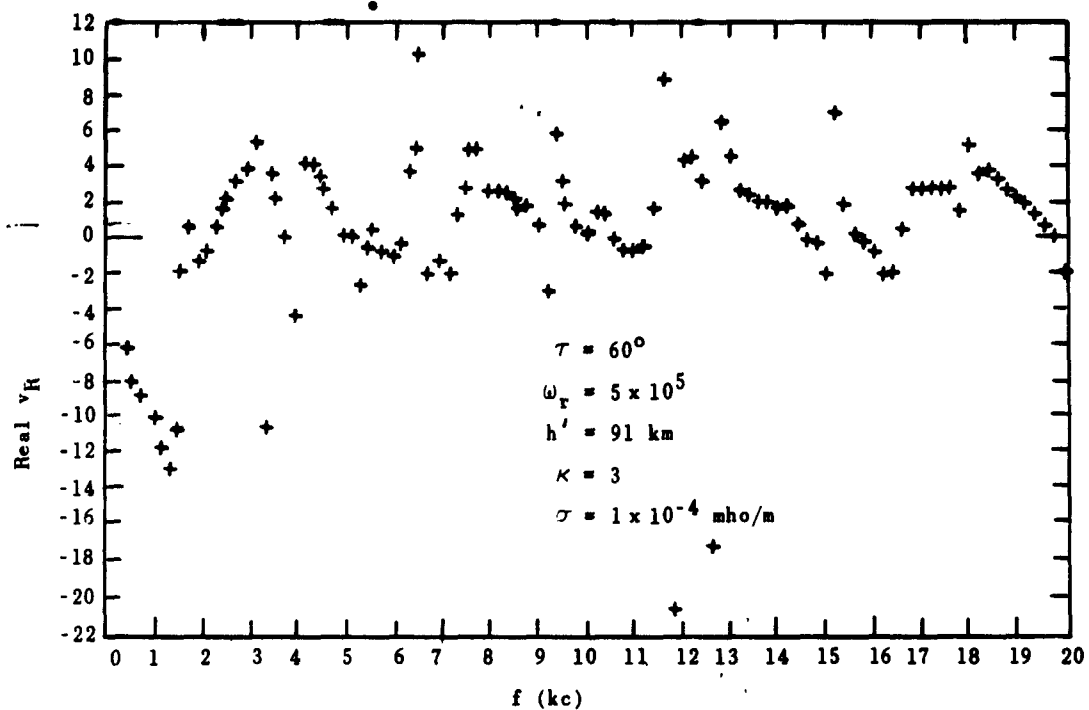
FIG. 3.28.   REAL AND IMAGINARY PARTS OF CROSSED-LOOP VOLTAGE RATIO
VS FREQUENCY, FOR SUMMER-NIGHT MODEL IONOSPHERE EXCEPT h' = 91 km,
POOR GROUND, D = 500 km, AND ϕ_g = 0.
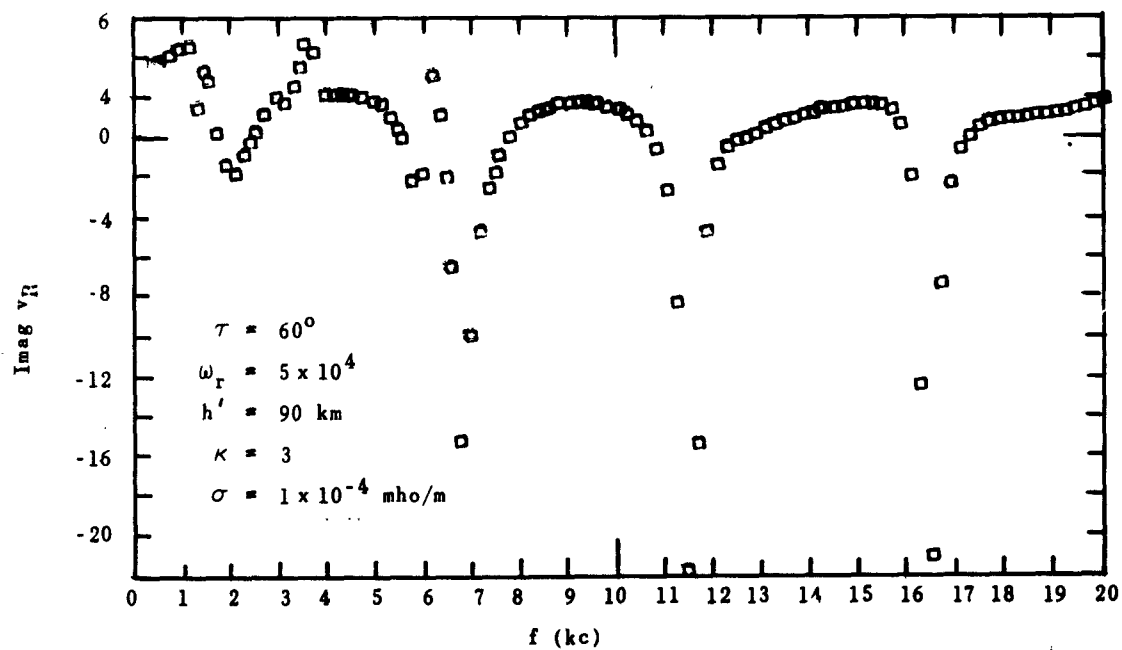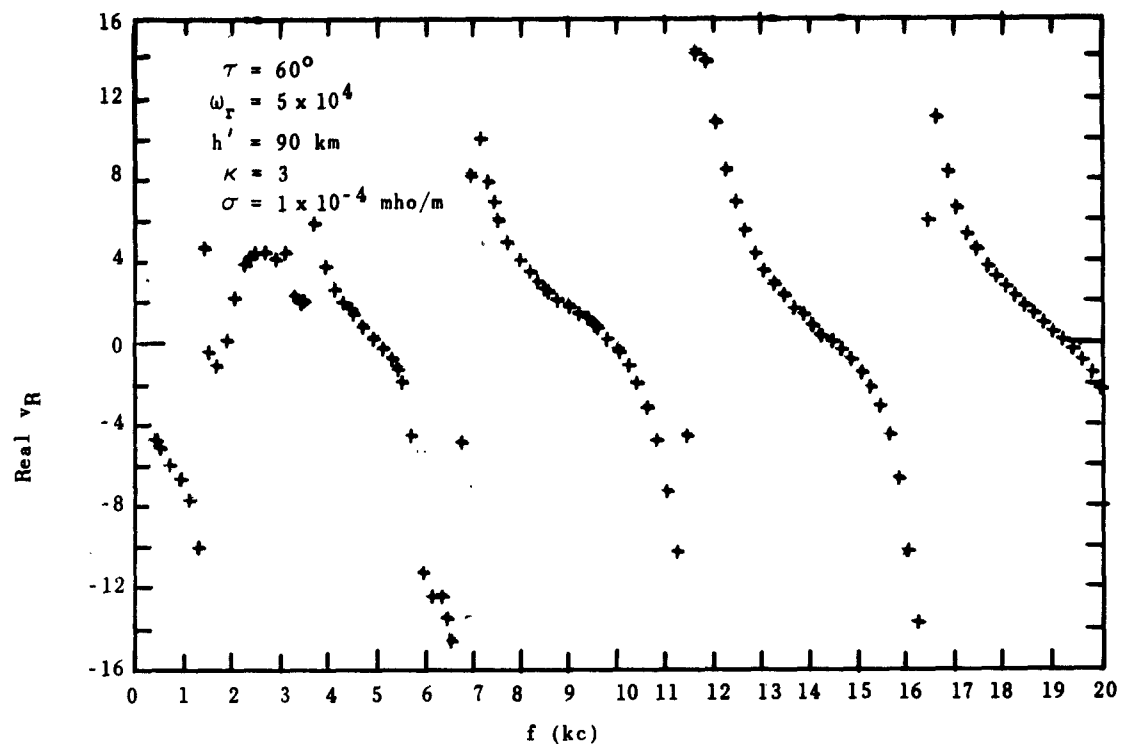
FIG. 3.29. REAL AND IMAGINARY PARTS OF CROSSED-LOOP VOLTAGE RATIO VS FREQUENCY, FOR SUMMER-NIGHT MODEL IONOSPHERE EXCEPT $\omega_r = 5 \times 10^4$, POOR GROUND, D = 500 km, AND $\phi_g = 0$.
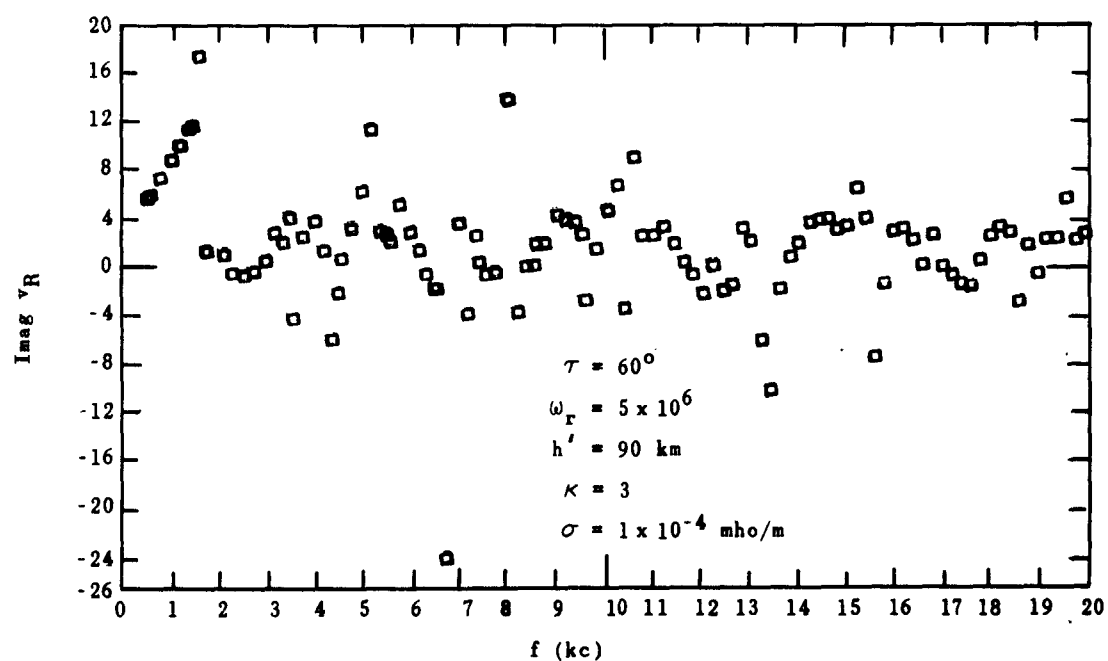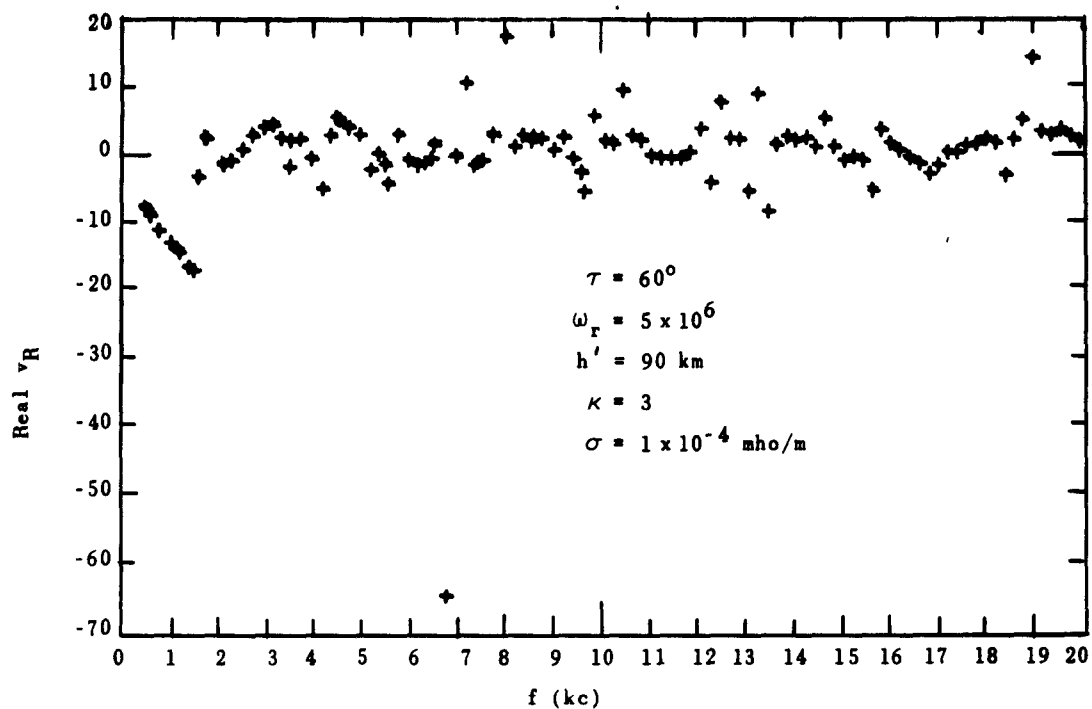
FIG. 3.30. REAL AND IMAGINARY PARTS OF CROSSED-LOOP VOLTAGE RATIO VS FREQUENCY, FOR SUMMER-NIGHT MODEL IONOSPHERE EXCEPT $\omega_r = 5 \times 10^6$, POOR GROUND, $D = 500$ km, AND $\phi_g = 0$.

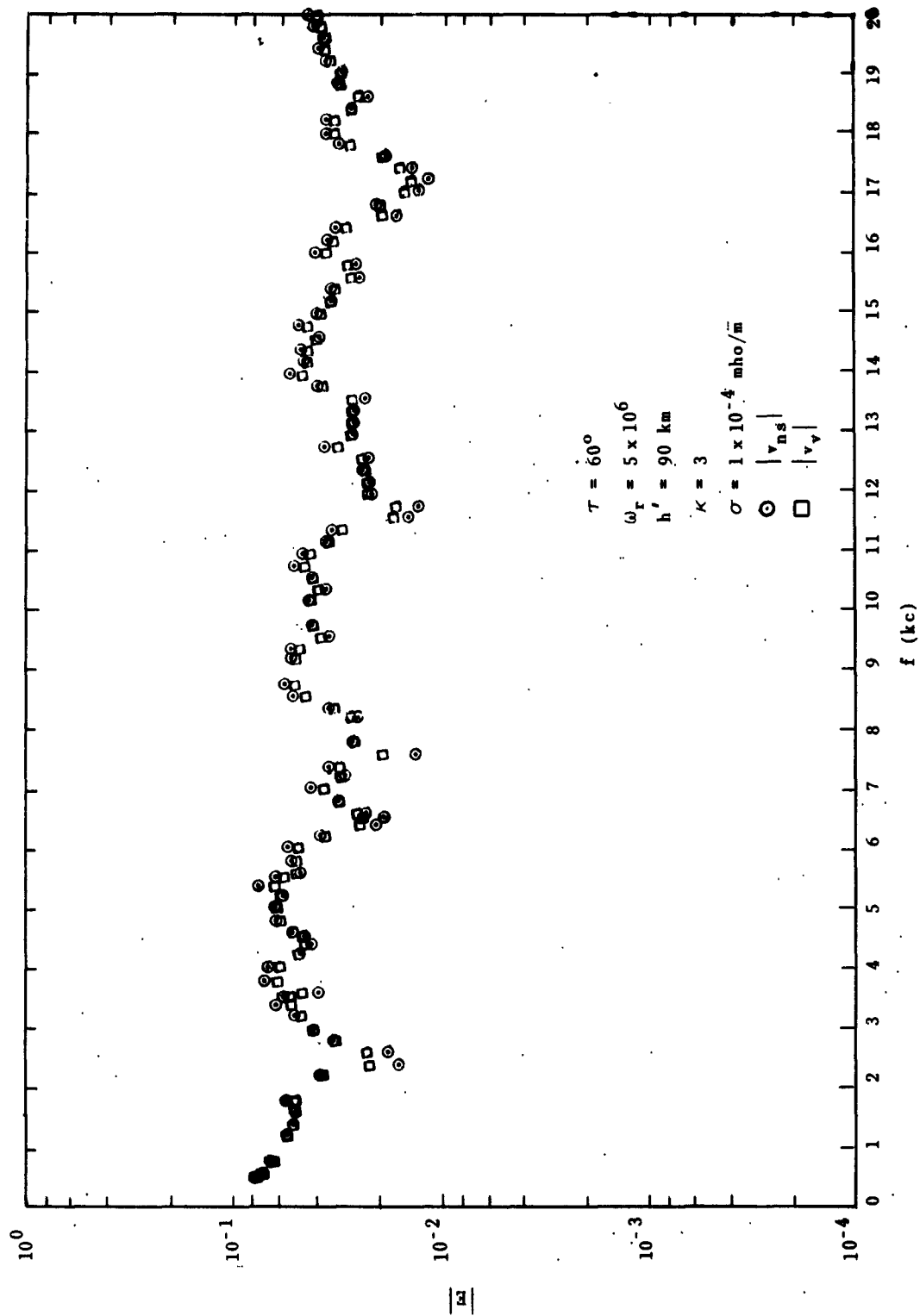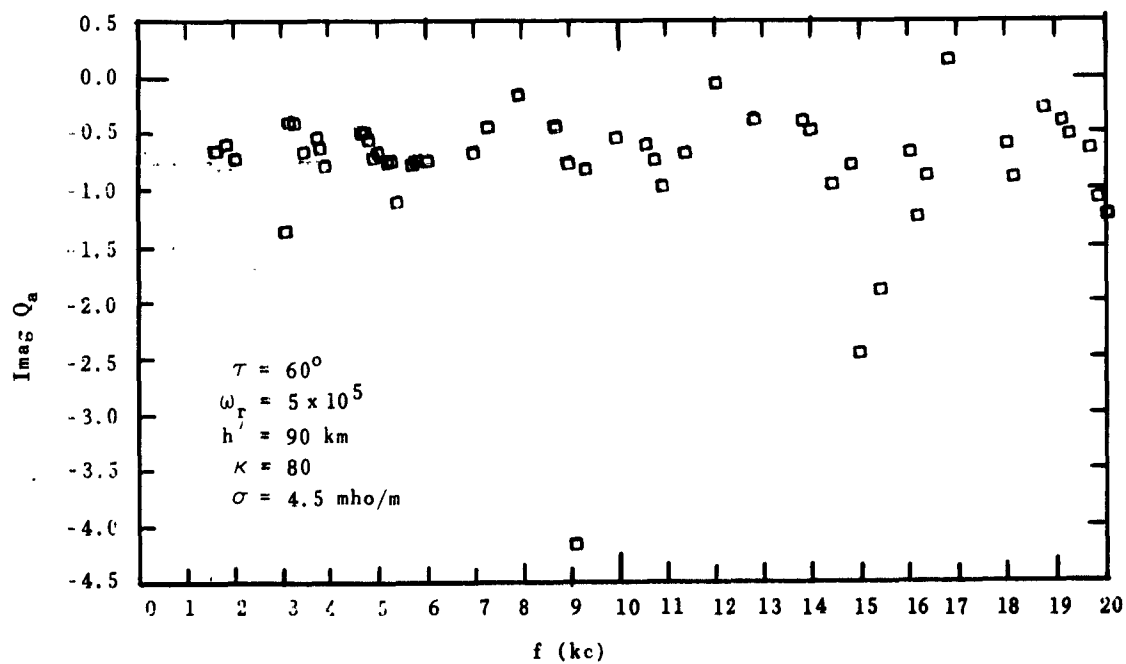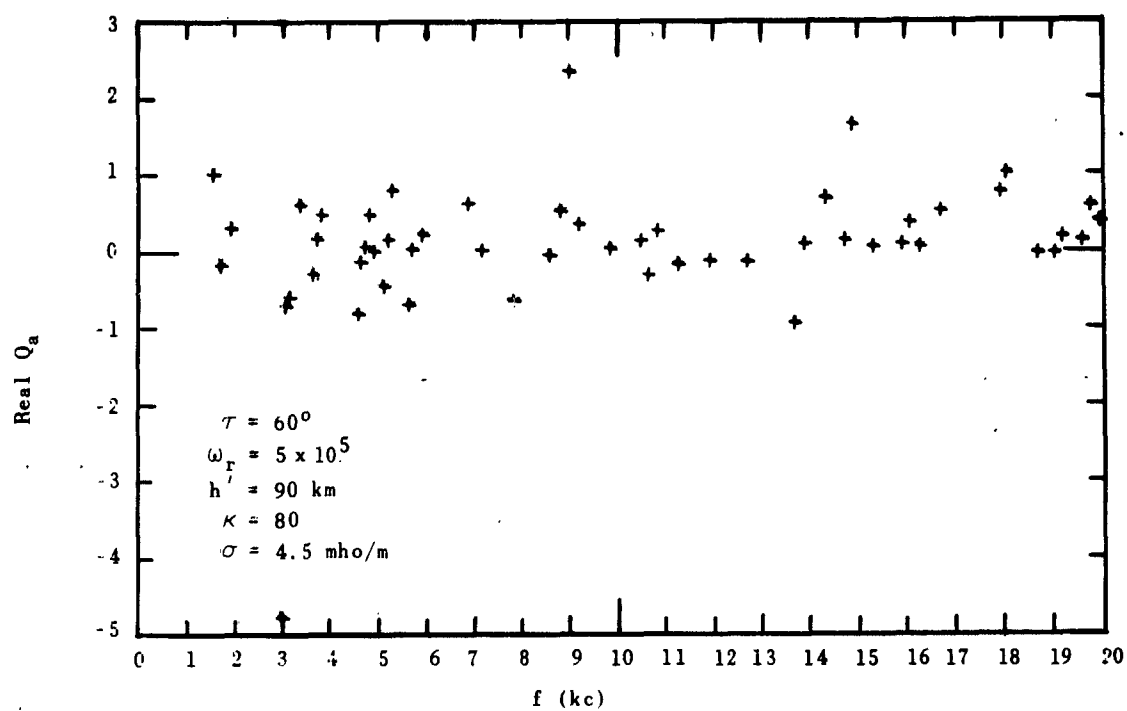FIG. 3.31. REAL AND IMAGINARY PARTS OF POLARIZATION Q_a AT ANTENNA VS FREQUENCY, FOR SUMMER-NIGHT MODEL IONOSPHERE, SEA WATER, D = 500 km.

8

7

6

5

4

3

2

1

0

-1

-2

Real Q_a

$\tau = 60^\circ$

$\omega_r = 5 \times 10^5$

$h' = 90$ km

$\kappa = 80$

$\sigma = 4.5$ mho/m

0 1 2 3 4 5 6 7 8 9 10 11 12 13 14 15 16 17 18 19 20

f (kc)

22

20

18

16

14

12

10

8

6

4

2

0

-2

-4

-5

Imag Q_a

$\tau = 60^\circ$

$\omega_r = 5 \times 10^5$

$h' = 90$ km

$\kappa = 80$

$\sigma = 4.5$ mho/m

0 1 2 3 4 5 6 7 8 9 10 11 12 13 14 15 16 17 18 19 20

f (kc)
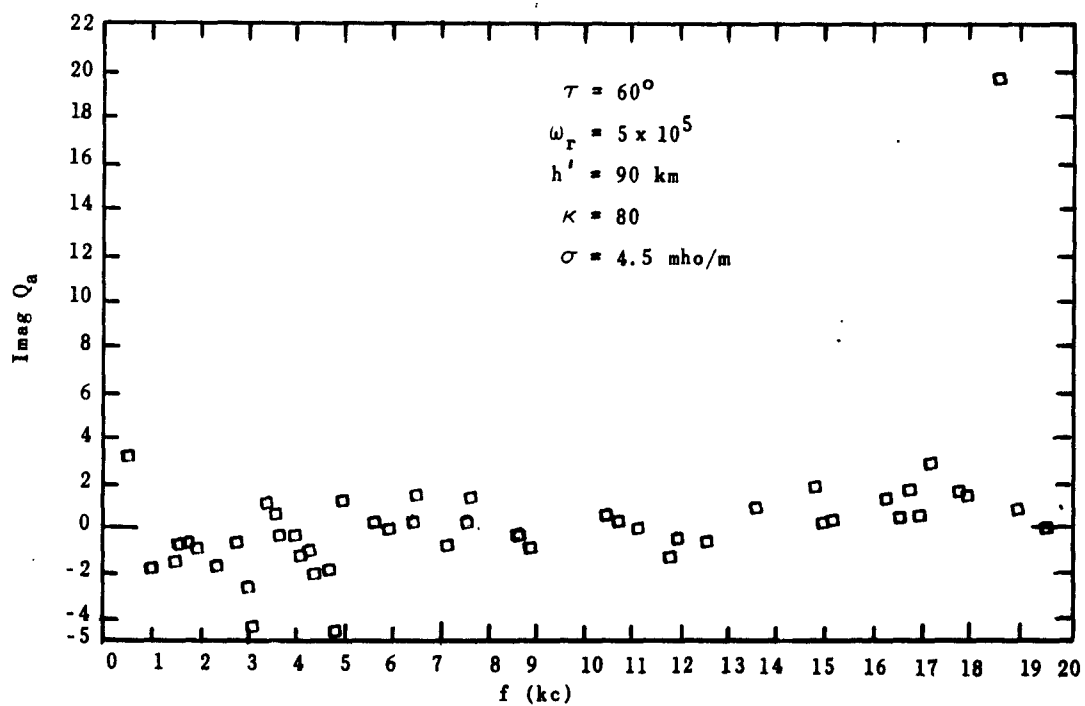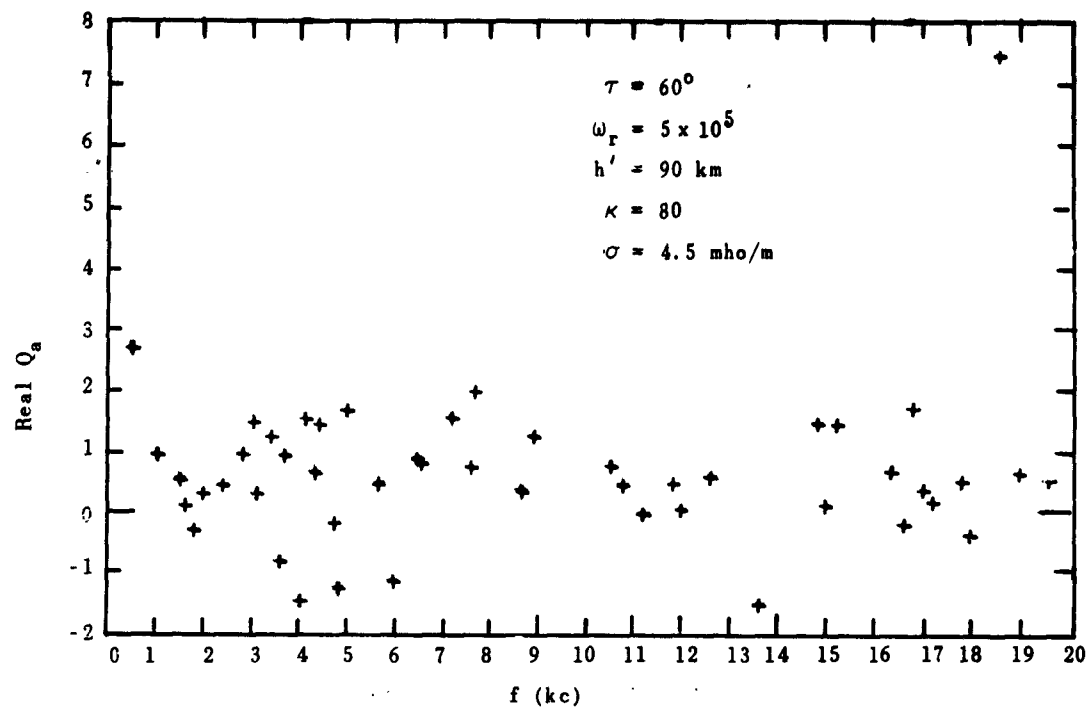
FIG. 3.32.   REAL AND IMAGINARY PARTS OF POLARIZATION Q_a AT ANTENNA
VS FREQUENCY, FOR SUMMER-NIGHT MODEL IONOSPHERE, SEA WATER, D = 2000 km.
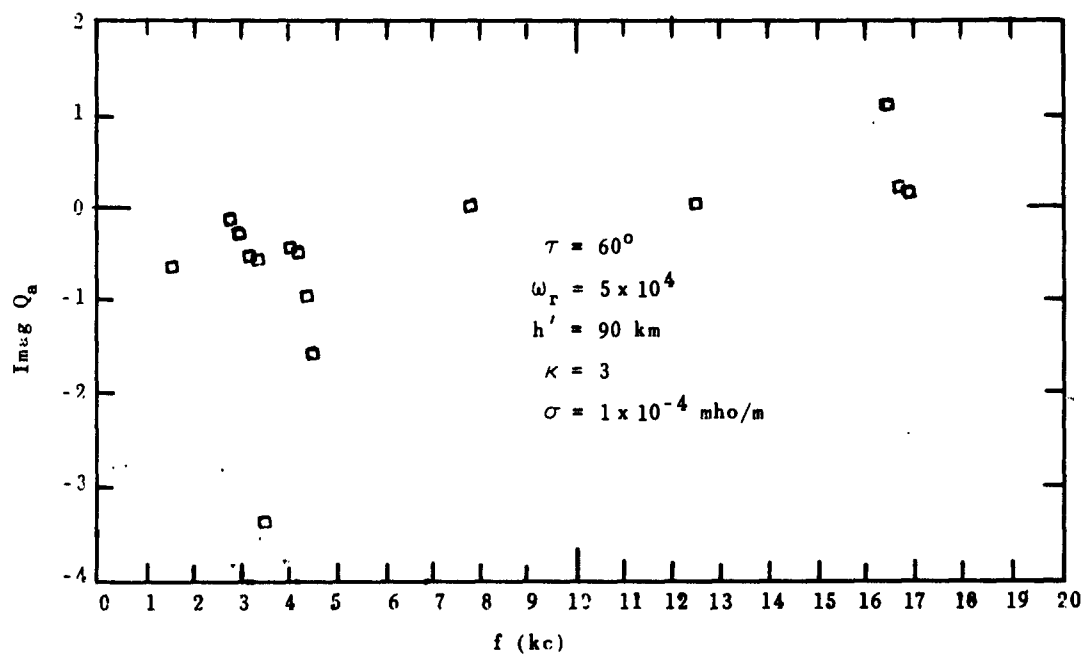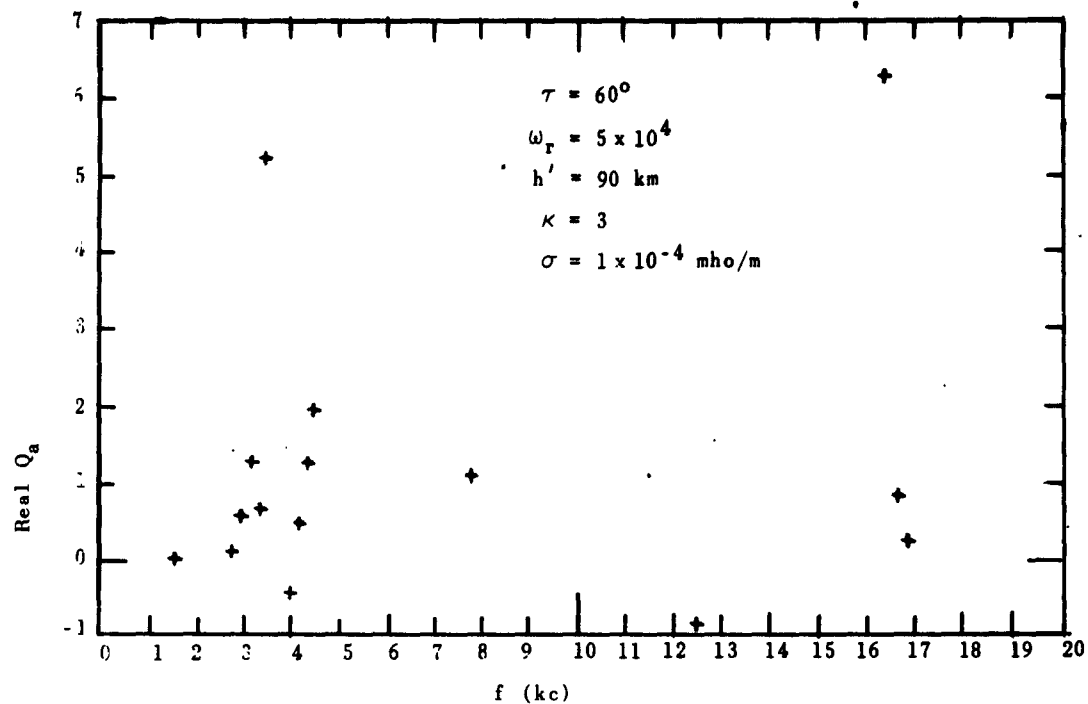
FIG. 3.33. REAL AND IMAGINARY PARTS OF POLARIZATION Q_a AT ANTENNA VS FREQUENCY, FOR SUMMER-NIGHT MODEL IONOSPHERE EXCEPT $\omega_r = 5 \times 10^4$, POOR GROUND, $D = 500$ km.
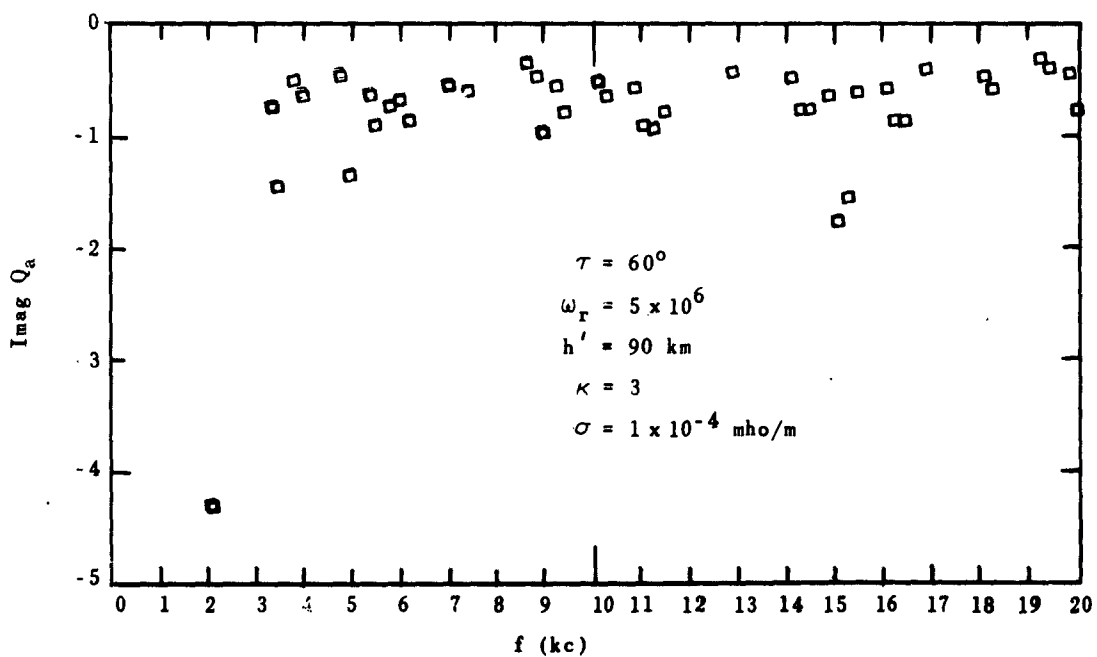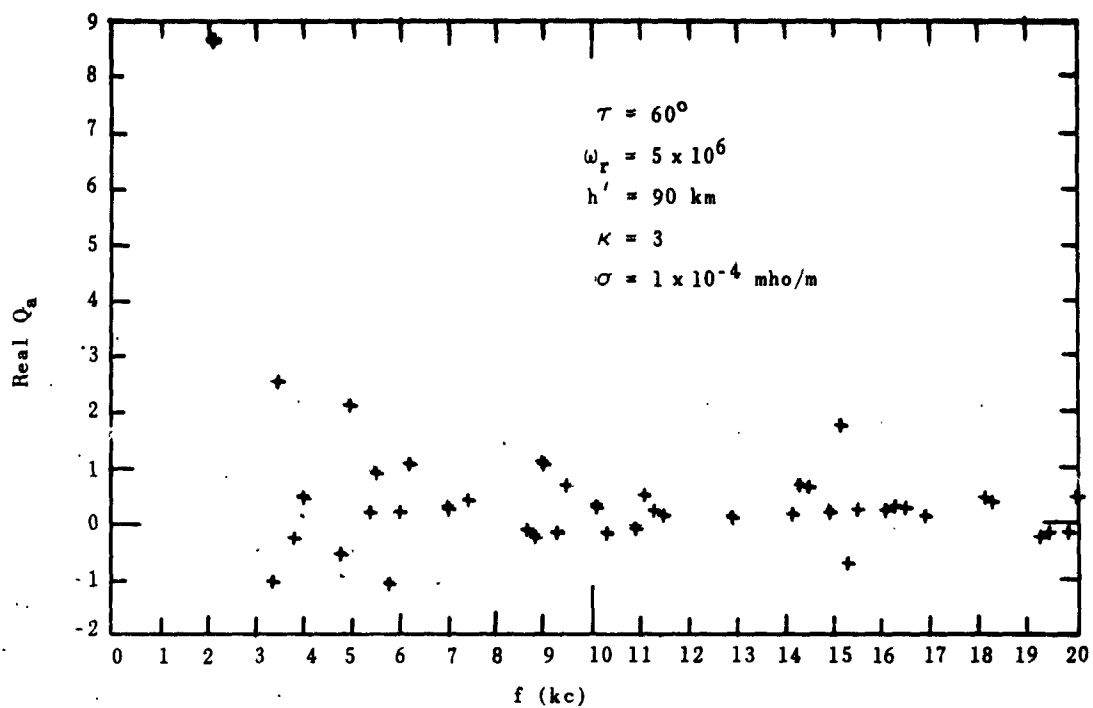
FIG. 3.34. REAL AND IMAGINARY PARTS OF POLARIZATION Q_a AT ANTENNA VS FREQUENCY, FOR SUMMER-NIGHT MODEL IONOSPHERE EXCEPT $\omega_r = 5 \times 10^6$, POOR GROUND, $D = 500$ km.

Figures 3.31 and 3.32 show the real and imaginary parts of Q_a for the summer-night model and sea water conditions, at 500 and 2000 km respectively. Figures 3.33 and 3.34 show these values for poor ground at 500 km. The summer-night model ionosphere is used, except that $\omega_r = 5 \times 10^4$ and 5×10^6, respectively.

E. THE APPARENT BEARING ANGLE ϕ_a.

Figures 3.35 through 3.45 show the values of ϕ_a vs frequency for poor ground and sea water conditions.

1. DISTANCE VARIATION. Figures 3.35 through 3.41 show the values of ϕ_a vs frequency for the summer-night model ionosphere at distances of 0.1, 500, 1000, and 2000 km.

2. IONOSPHERE HEIGHT VARIATIONS. Figures 3.42 and 3.43 show the calculated values of ϕ_a vs frequency for poor ground at 500 km. The summer-night model ionosphere was used, except that h' was changed to 89 and 91 km, respectively.

3. IONIZATION DENSITY VARIATIONS. Figures 3.44 and 3.45 show the values of ϕ_a vs frequency for poor ground conditions at 500 km. Summer-night model ionosphere conditions are used except that ω_r is changed to 5×10^4 and 5×10^6, respectively.

F. TRANSMISSION COEFFICIENTS

The calculated magnitude of the two transmission coefficients ($|T_{\parallel}|$ and $|T_{\perp}|$) is shown for frequencies of 0.5, 1, 5, 10, 15, and 20 kc. The curves are plotted as a function of θ_n, which is equivalent to θ_t, the angle of transmission into the waveguide. Figures 3.46 through 3.48 show $|T_{\parallel}|$ for three different ionization densities, and Figs. 3.49 through 3.51 show $|T_{\perp}|$ for these same conditions. The conditions are $\omega_r = 5 \times 10^4$, 5×10^5 (summer-night model) and 5×10^6, with $\tau = 60$ degrees.
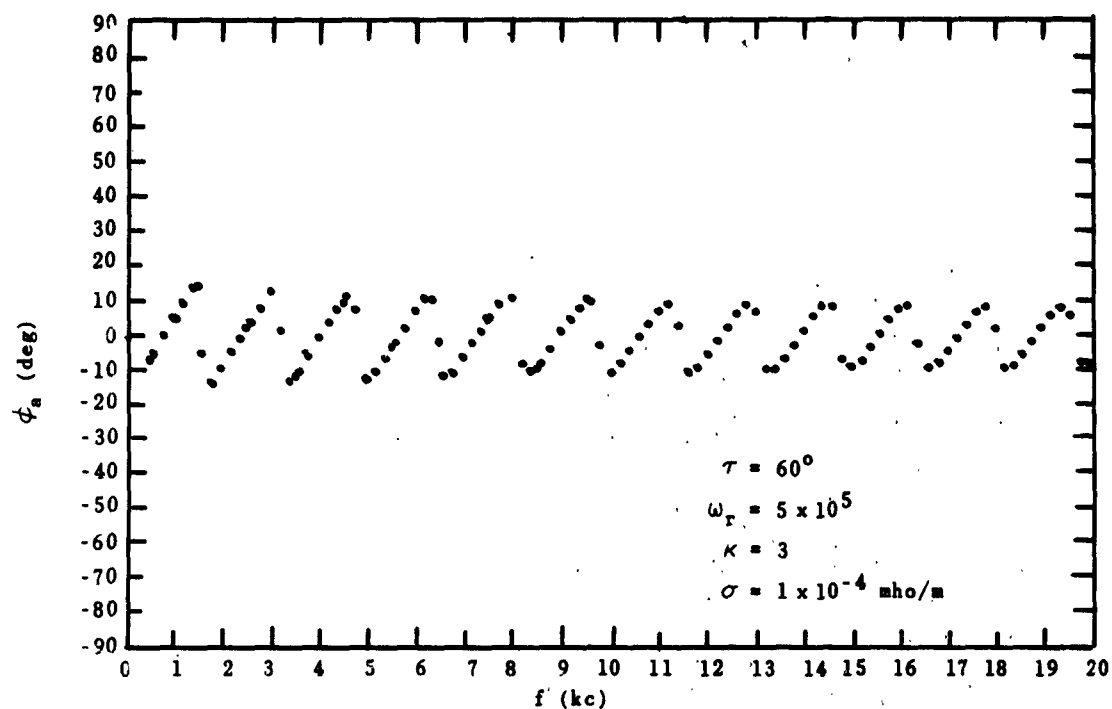
FIG. 3.35. LATERAL DEVIATION ANGLE ϕ_a VS FREQUENCY, FOR SUMMER-NIGHT MODEL IONOSPHERE, POOR GROUND, D = 0.1 km.
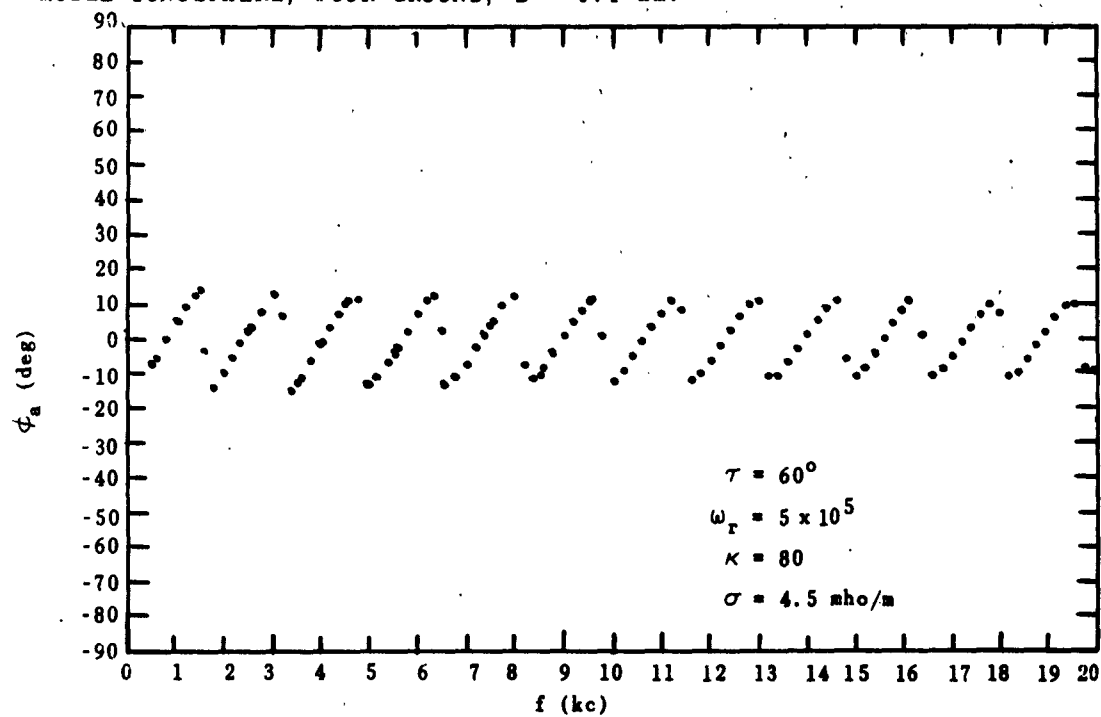
FIG. 3.36. LATERAL DEVIATION ANGLE ϕ_a VS FREQUENCY, FOR SUMMER-NIGHT MODEL IONOSPHERE, SEA WATER, D = 0.1 km.

- 76 -
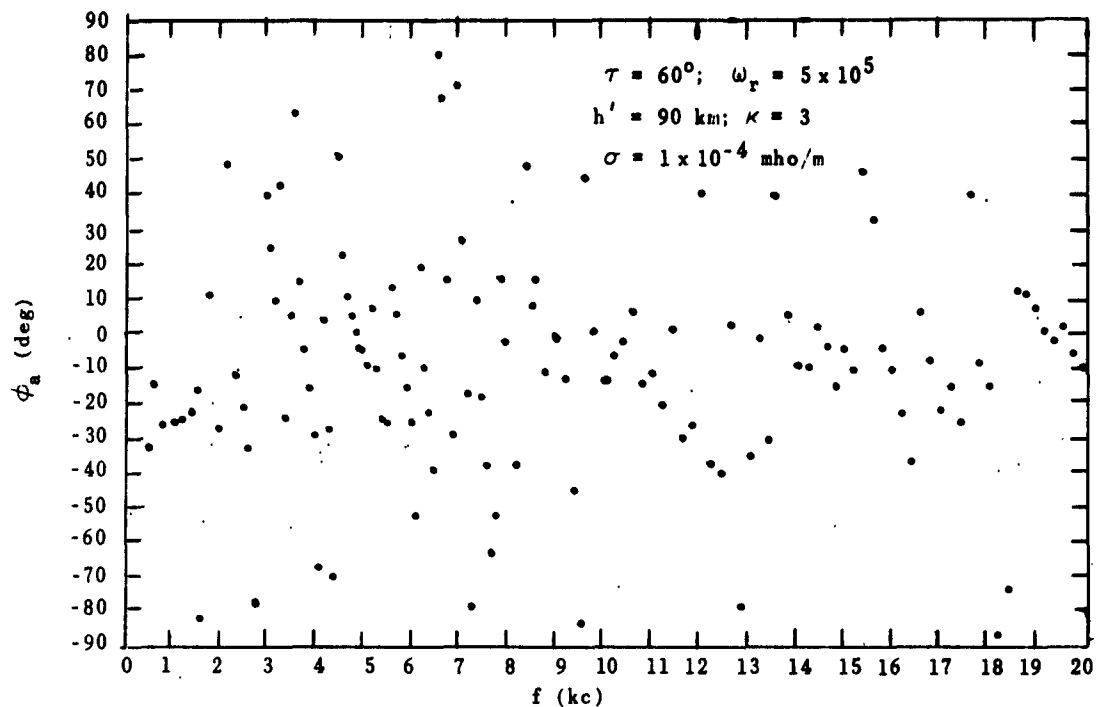
FIG. 3.37. LATERAL DEVIATION ANGLE ϕ_a VS FREQUENCY, FOR SUMMER-NIGHT MODEL IONOSPHERE, POOR GROUND, D = 500 km.
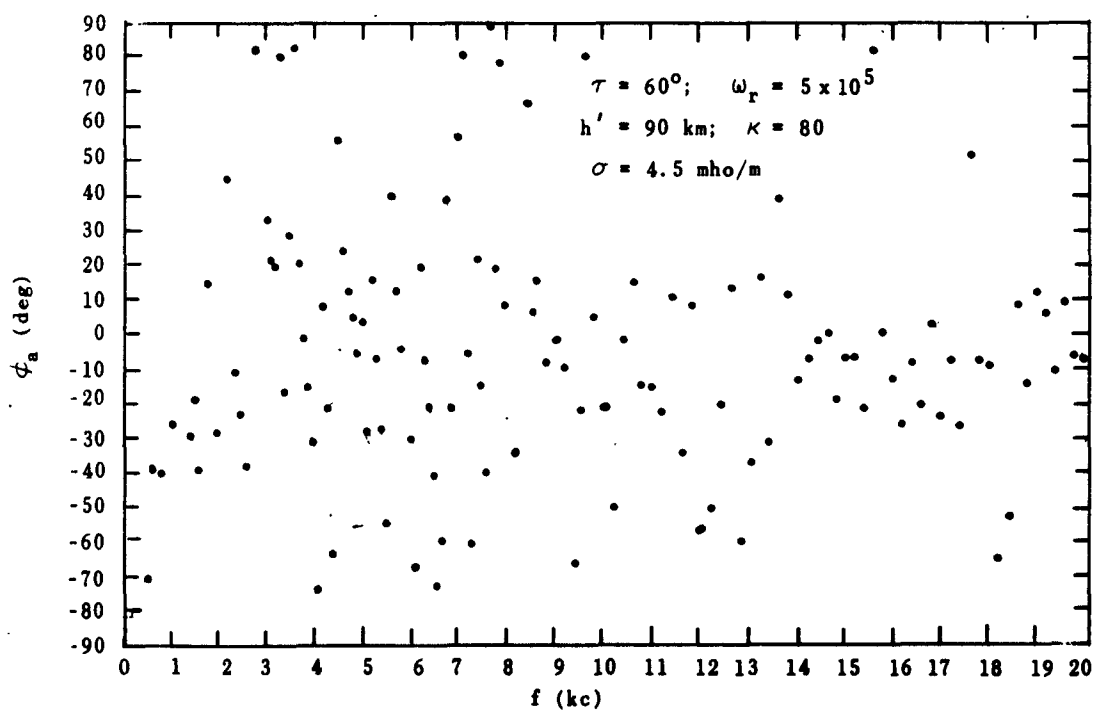
FIG. 3.38. LATERAL DEVIATION ANGLE ϕ_a VS FREQUENCY, FOR SUMMER-NIGHT MODEL IONOSPHERE, SEA WATER, D = 500 km.
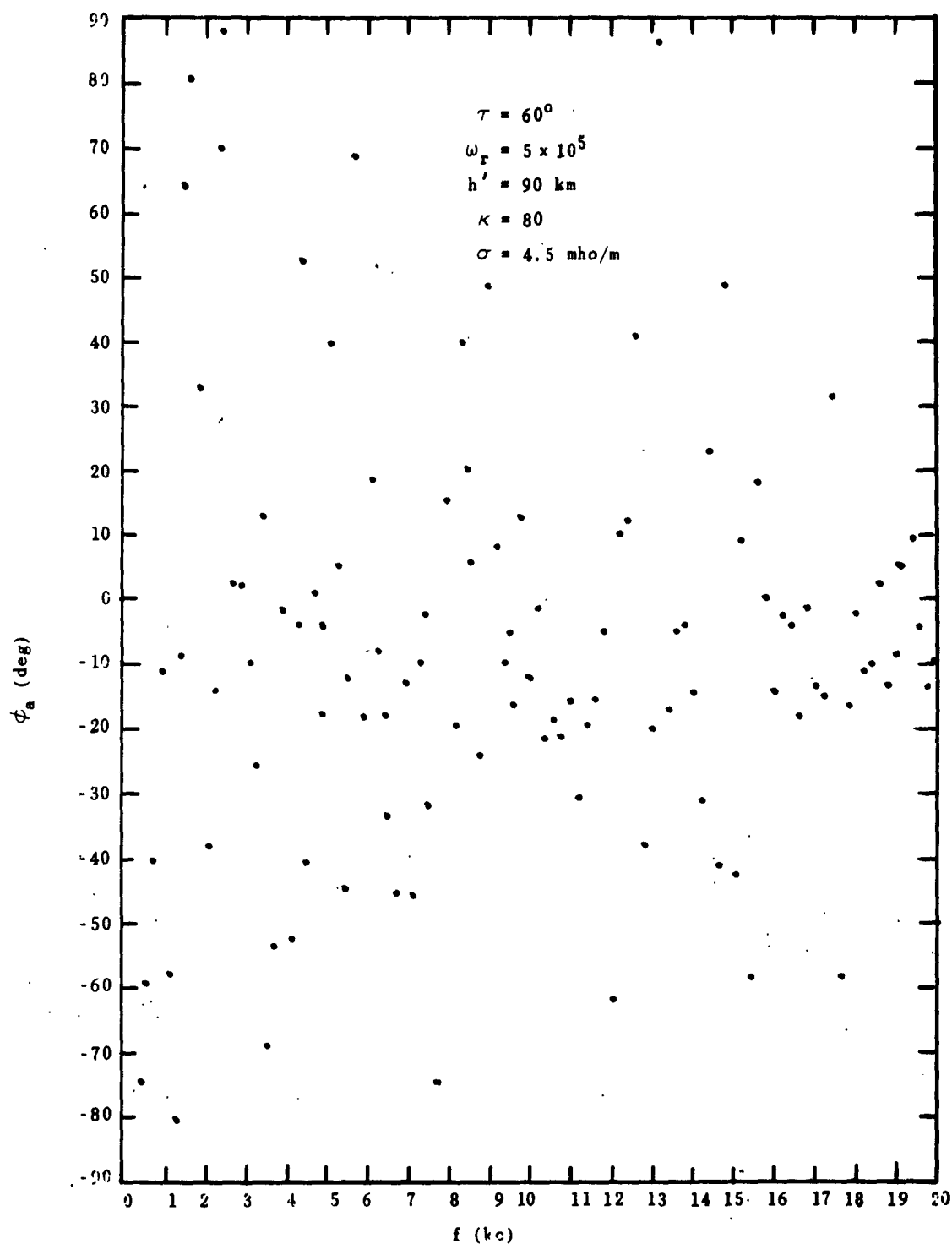
FIG. 3.39. LATERAL DEVIATION ANGLE ϕ_a VS FREQUENCY, FOR SUMMER-NIGHT MODEL IONOSPHERE, SEA WATER, D = 1000 km.
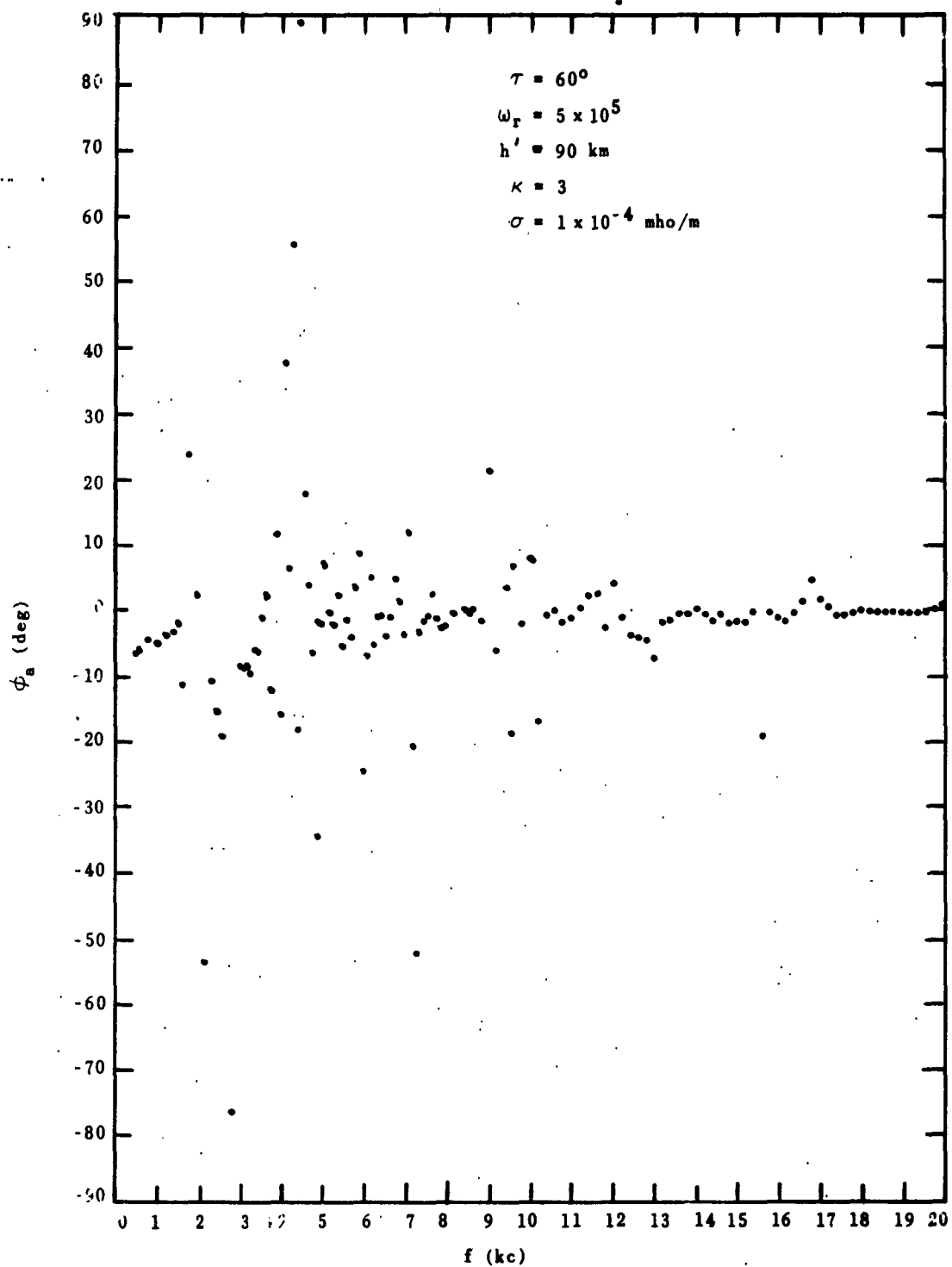
FIG. 3.40. LATERAL DEVIATION ANGLE ϕ_a VS FREQUENCY, FOR SUMMER-NIGHT MODEL IONOSPHERE, POOR GROUND, D = 2000 km.
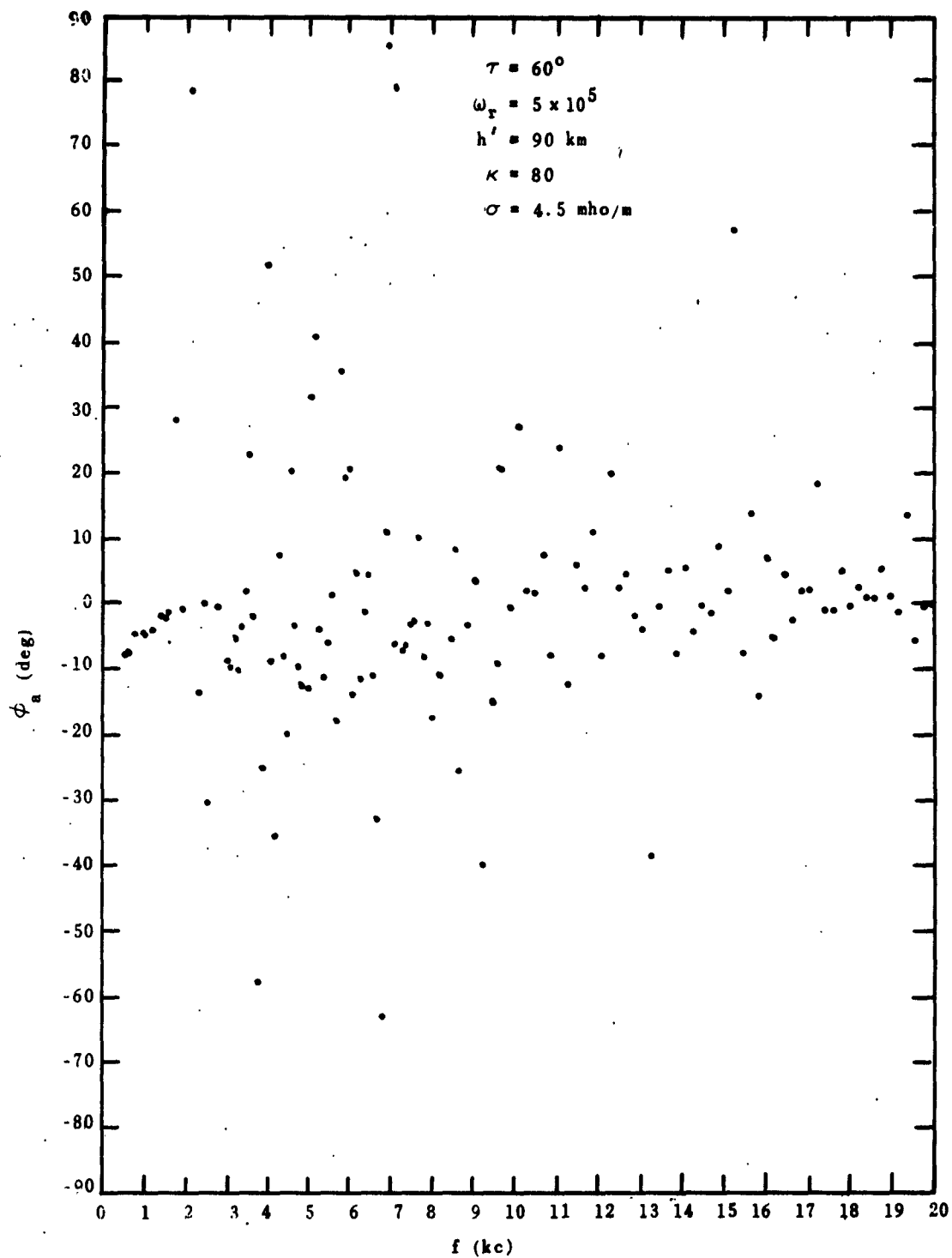
FIG. 3.41.   LATERAL DEVIATION ANGLE ϕ_a VS FREQUENCY FOR SUMMER-NIGHT
MODEL IONOSPHERE, SEA WATER, D = 2000 km.
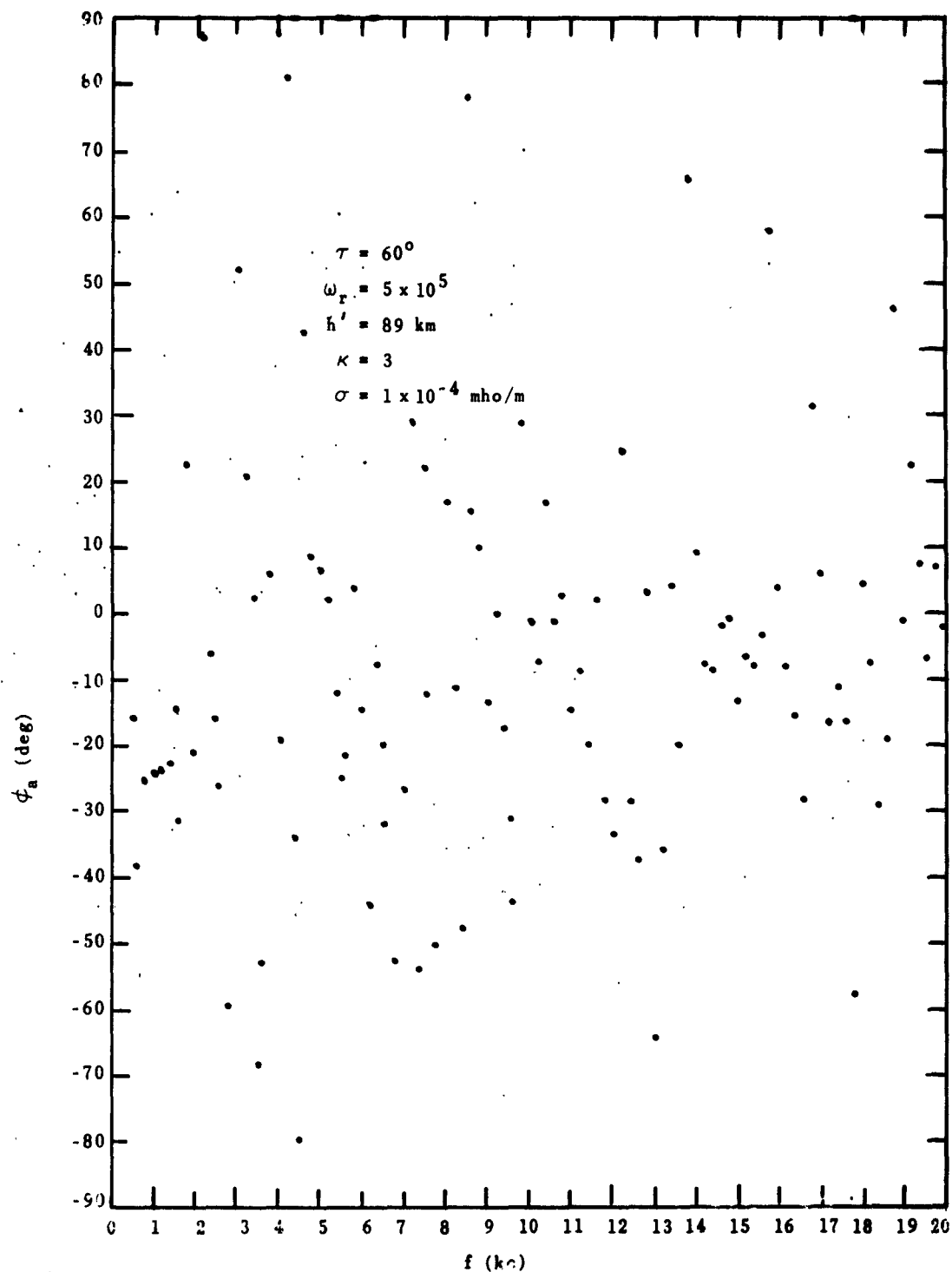
FIG. 3.42. LATERAL DEVIATION ANGLE ϕ_a VS FREQUENCY FOR SUMMER-NIGHT MODEL IONOSPHERE EXCEPT h' = 89 km, POOR GROUND, D = 500 km.
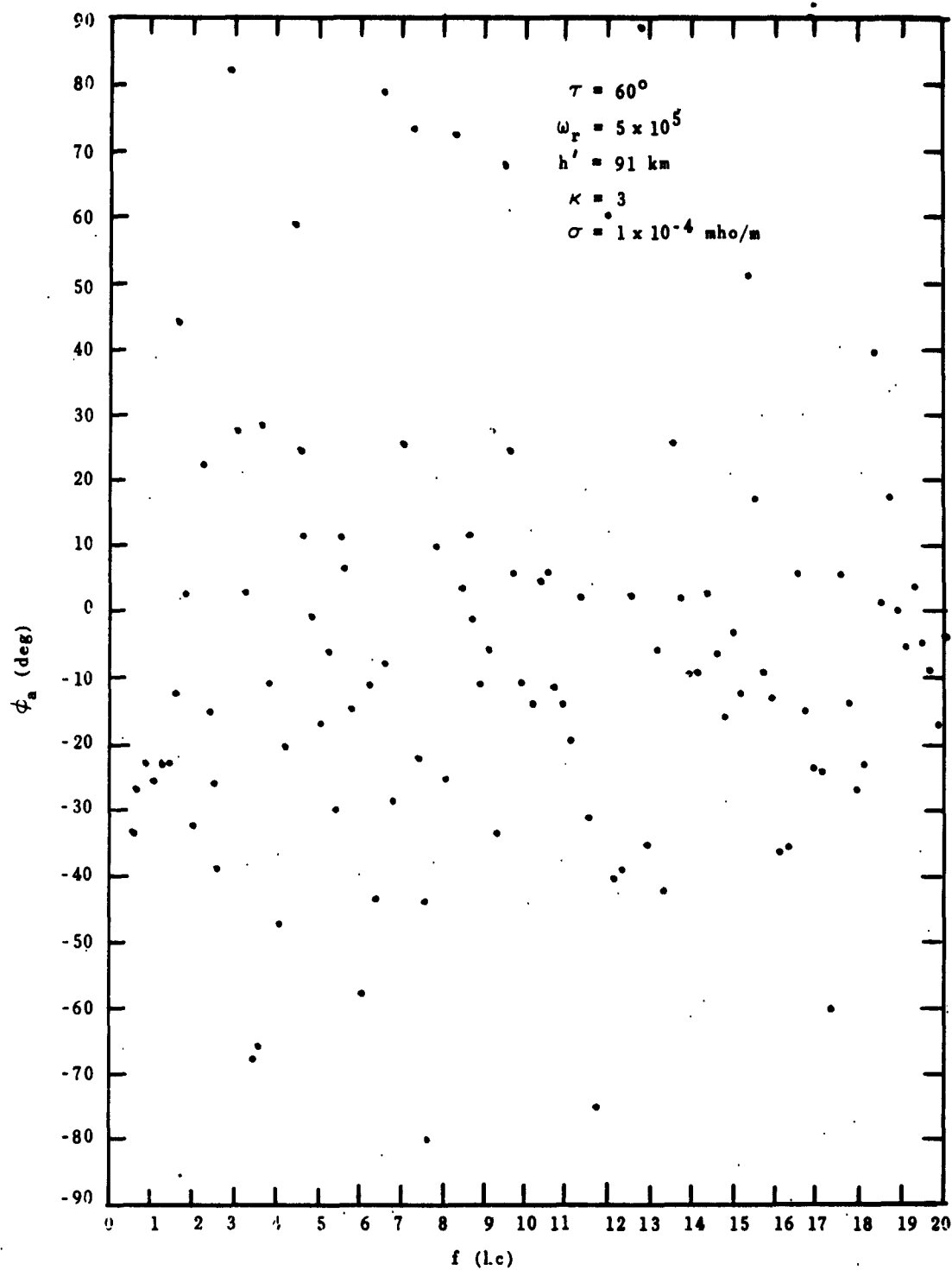
FIG. 3.43. LATERAL DEVIATION ANGLE ϕ_a VS FREQUENCY FOR SUMMER-NIGHT MODEL IONOSPHERE EXCEPT $h' = 91$ km, POOR GROUND, D = 500 km.
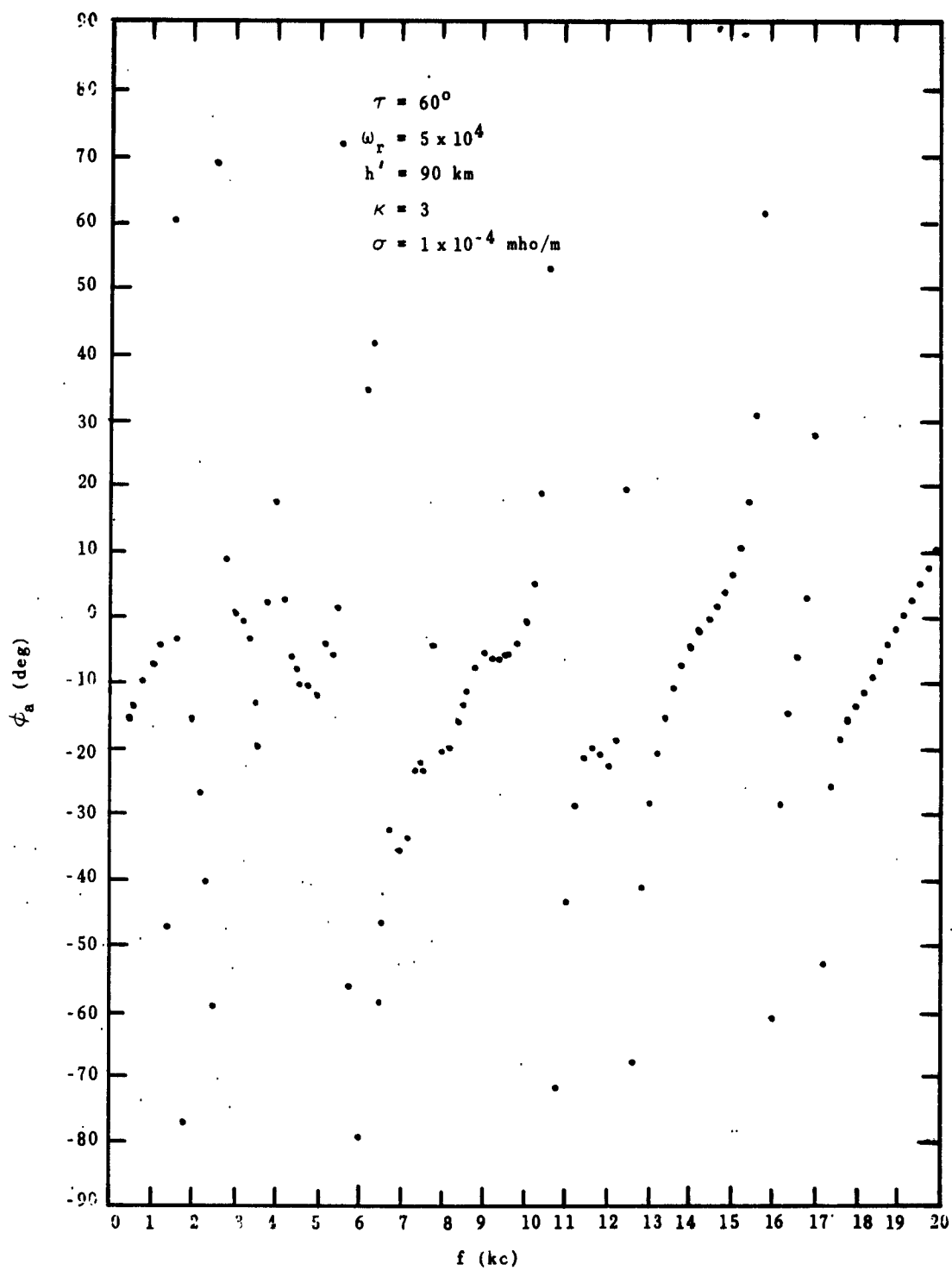
FIG. 3.44. LATERAL DEVIATION ANGLE ϕ_a VS FREQUENCY, FOR SUMMER-NIGHT
MODEL IONOSPHERE EXCEPT $\omega_r = 5 \times 10^4$, POOR GROUND, D = 500 km.
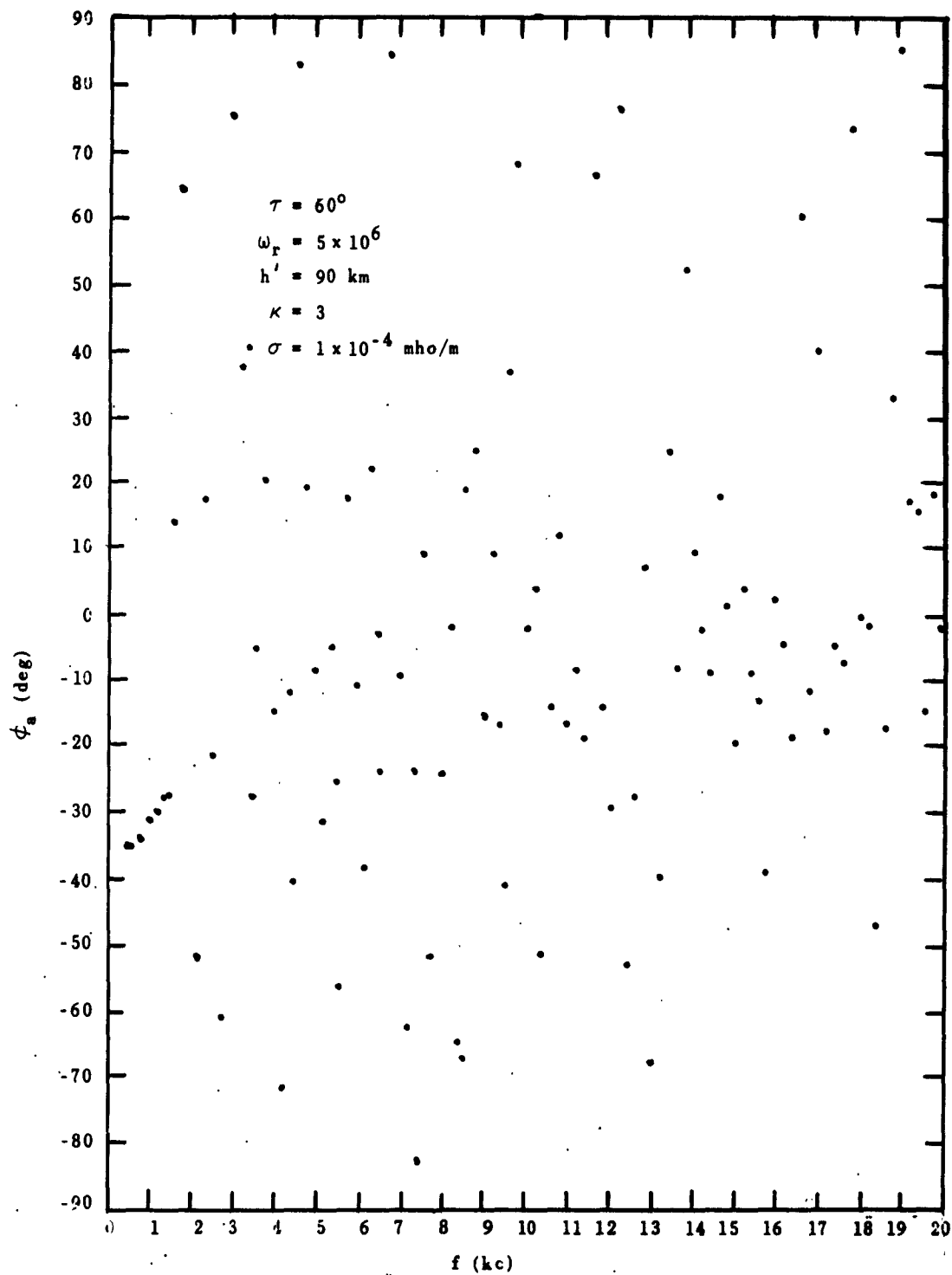
FIG. 3.45. LATERAL DEVIATION ANGLE ϕ_a VS FREQUENCY, FOR SUMMER-NIGHT MODEL IONOSPHERE EXCEPT $\omega_r = 5 \times 10^6$, POOR GROUND, D = 500 km.
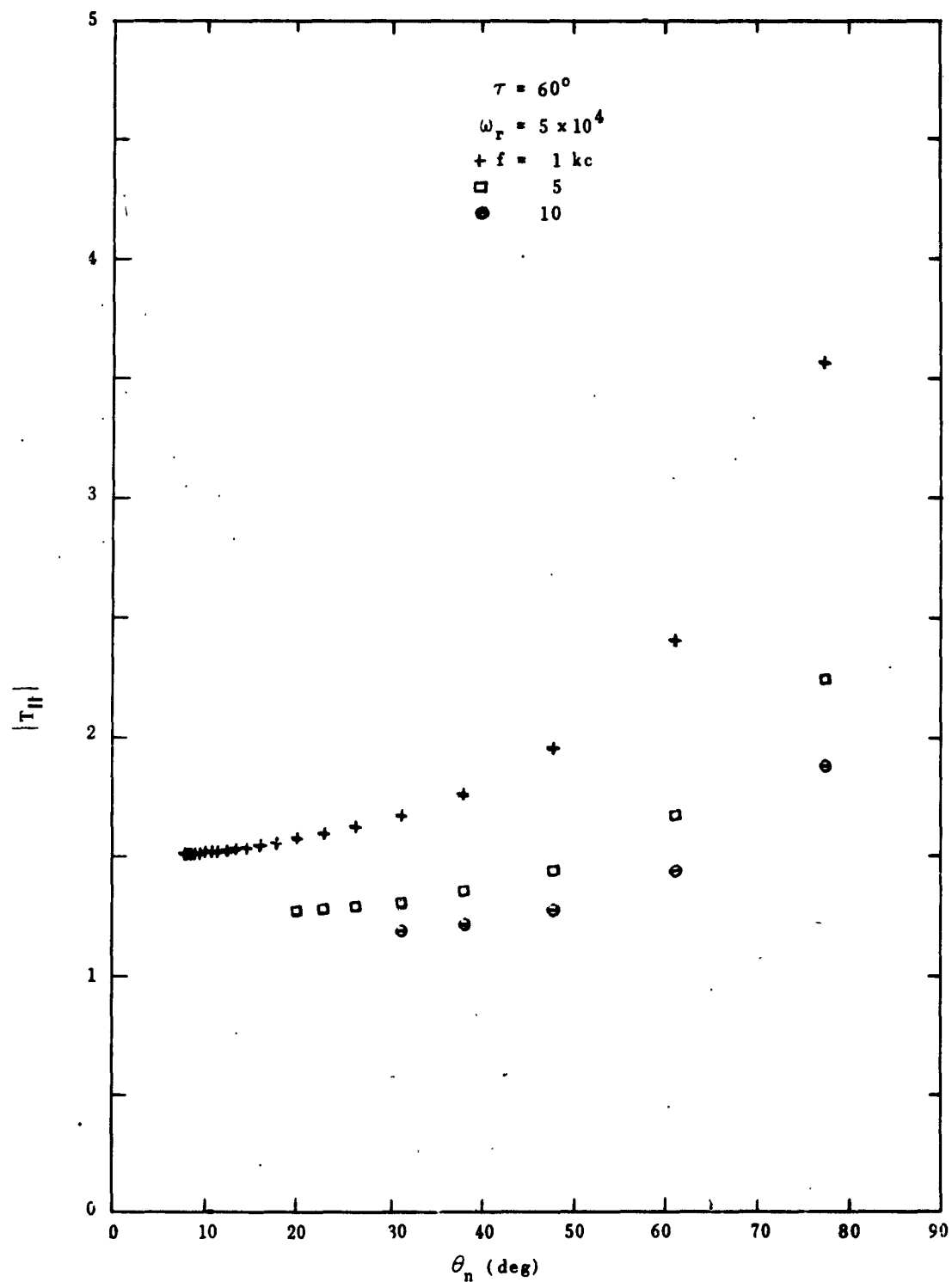
FIG. 3.46. MAGNITUDE OF TRANSMISSION COEFFICIENT
$T_{\parallel}$ VS θ_n FOR $\tau = 60°$, $\omega_r = 5 \times 10^4$.
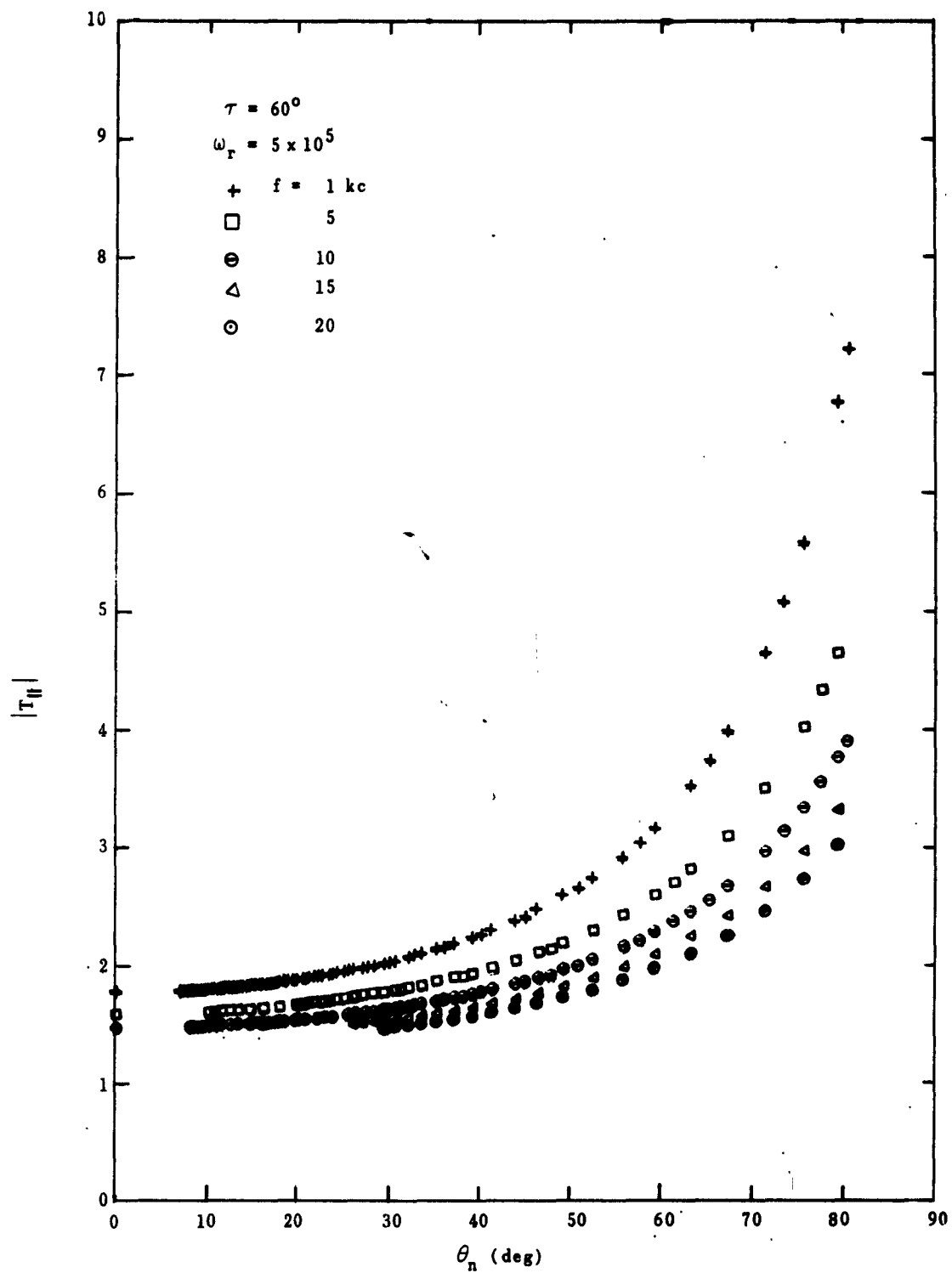
FIG. 3.47. MAGNITUDE OF TRANSMISSION COEFFICIENT $T_{||}$ VS θ_n FOR $\tau = 60°$, $\omega_r = 5 \times 10^5$ (SUMMER-NIGHT MODEL IONOSPHERE).
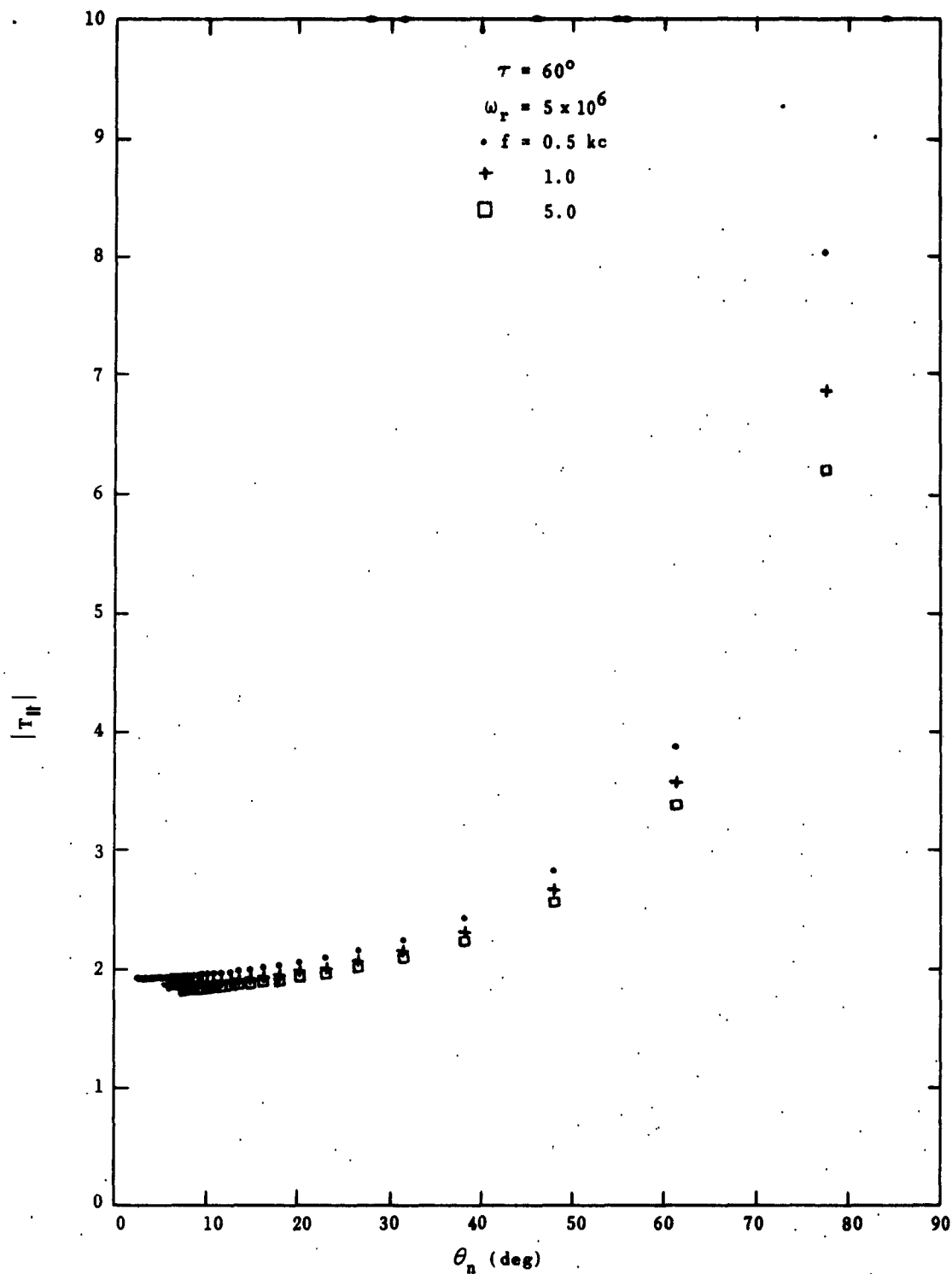
FIG. 3.48. MAGNITUDE OF TRANSMISSION COEFFICIENT $T_{\parallel}$ VS θ_n FOR $\tau = 60°$, $\omega_r = 5 \times 10^6$.
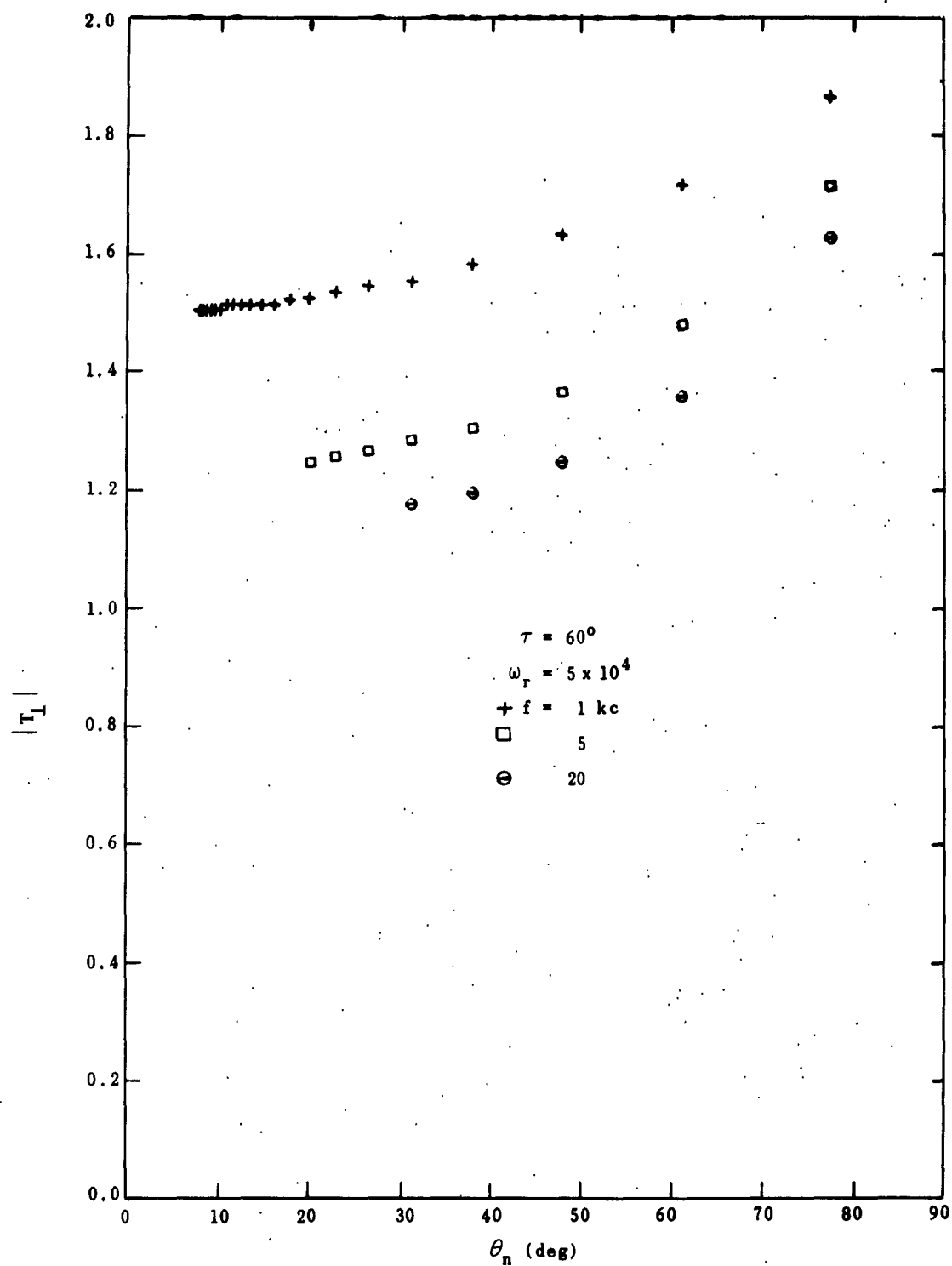
FIG. 3.49. MAGNITUDE OF TRANSMISSION COEFFICIENT $T_\perp$ VS θ_n FOR $\tau = 60°$, $\omega_r = 5 \times 10^4$.
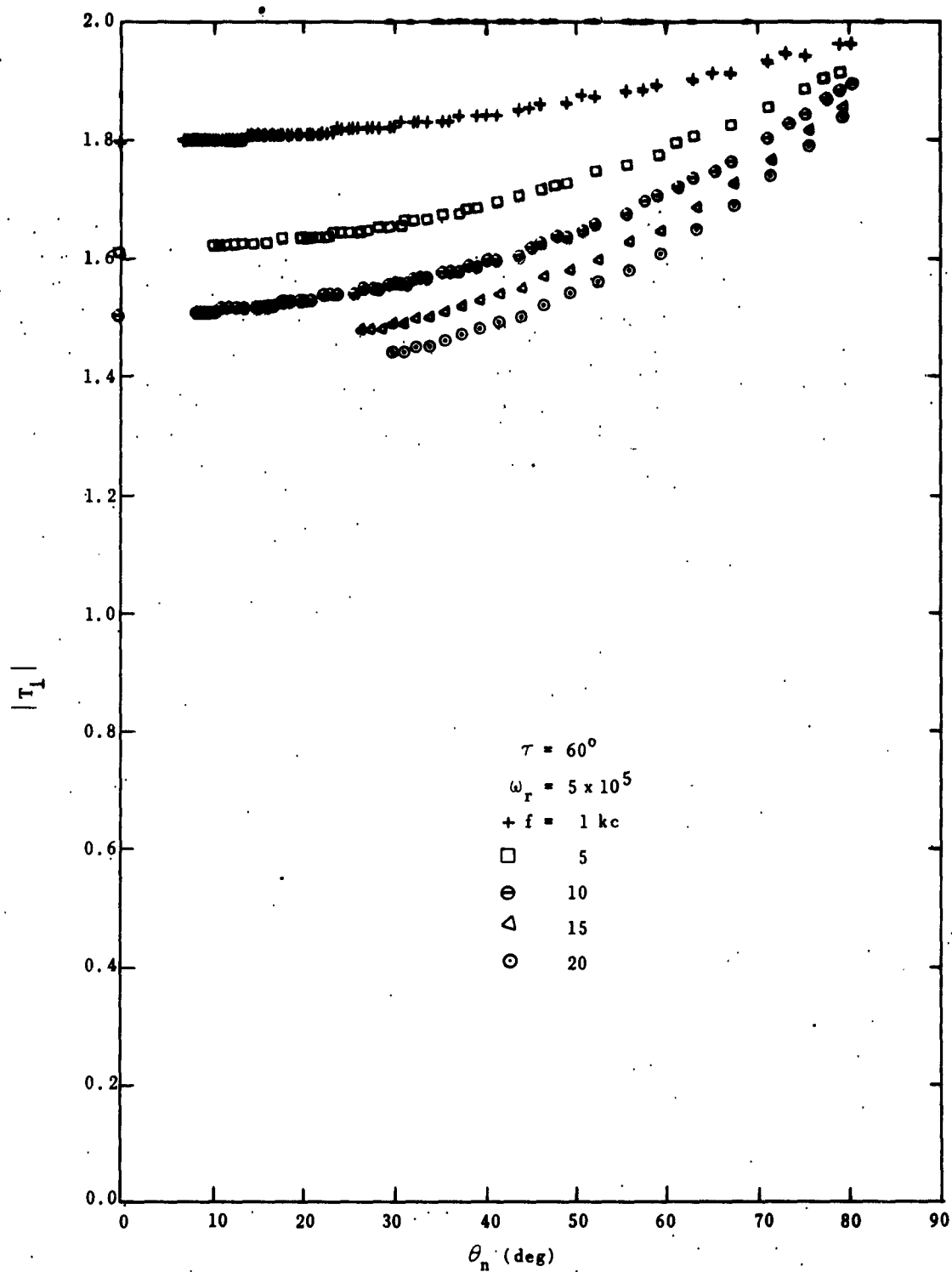
FIG. 3.50. MAGNITUDE OF TRANSMISSION COEFFICIENT $T_\perp$ VS θ_n FOR $\tau = 60°$, $\omega_r = 5 \times 10^5$ (SUMMER-NIGHT MODEL IONOSPHERE).
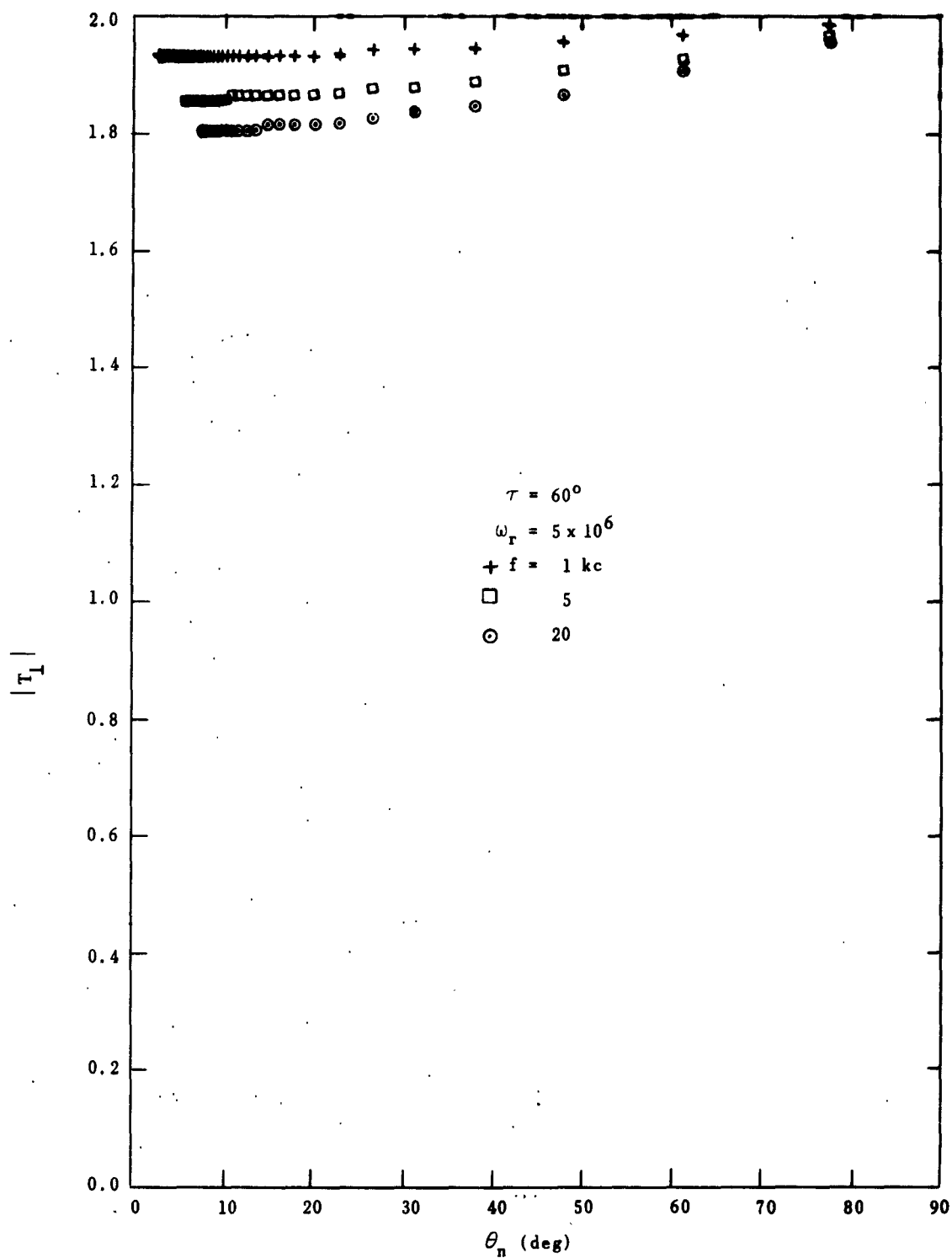
FIG. 3.51.   MAGNITUDE OF TRANSMISSION COEFFICIENT
$T_\perp$ VS θ_n FOR $\tau = 60°$, $\omega_r = 5 \times 10^6$.

G. IONOSPHERE REFLECTION COEFFICIENTS

The calculated magnitudes of the ionosphere reflection coefficients are shown in Figs. 3.52 through 3.59 as a function of the ionosphere angle of incidence θ_n for frequencies of 0.5, 1, 5, 10, 15, and 20 kc. They are grouped by ionosphere conditions. Figures 3.52 through 3.55 show the values for $\omega_r = 5 \times 10^4$, and Figs. 3.56 through 3.59 show those for $\omega_r = 5 \times 10^5$ (summer-night model), with $\tau = 60$ degrees.

H. GROUND REFLECTION COEFFICIENTS

The calculated magnitude of the two ground reflection coefficients is shown in Figs. 3.60 through 3.63 as a function of β_n, the takeoff-arrival angle at the earth's surface. Frequencies of 0.5, 1, 5, 10, 15, and 20 kc are generally shown. Figures 3.60 and 3.61 show the values for poor ground, and Figs. 3.62 and 3.63 show the values for sea water.

I. THE CHARACTERISTICS OF A WAVE ARRIVING FROM THE MAGNETIC FIELD DIRECTION

The curves in Figs. 3.64 and 3.65 were calculated for a distance of 47.23 km. At this distance the n = 0 ray is parallel to the earth's magnetic field at the geomagnetic latitude of Stanford (44°N). Summer-night model ionosphere and sea water conditions were used. The calculated magnitude of the field seen by the antennas is shown as a function of frequency in Fig. 3.64. Figure 3.65 shows the real and imaginary parts of v_R for the same conditions.
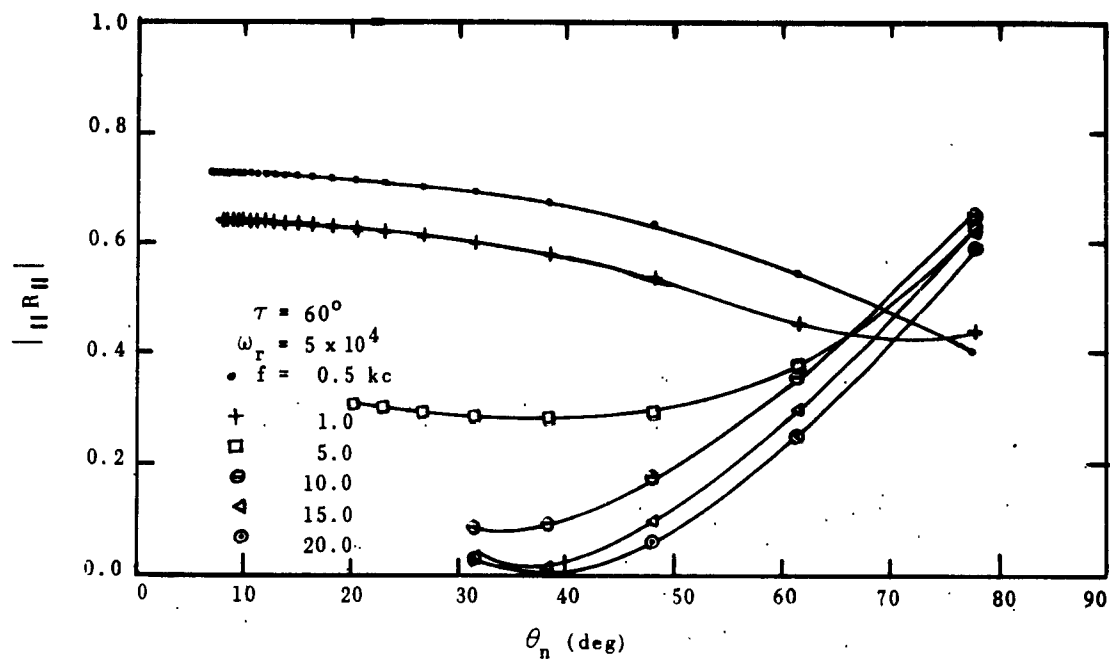
FIG. 3.52. MAGNITUDE OF IONOSPHERE REFLECTION COEFFICIENT $_{||}R_{||}$ VS θ_n, FOR $\tau = 60°$, AND $\omega_r = 5 \times 10^4$.
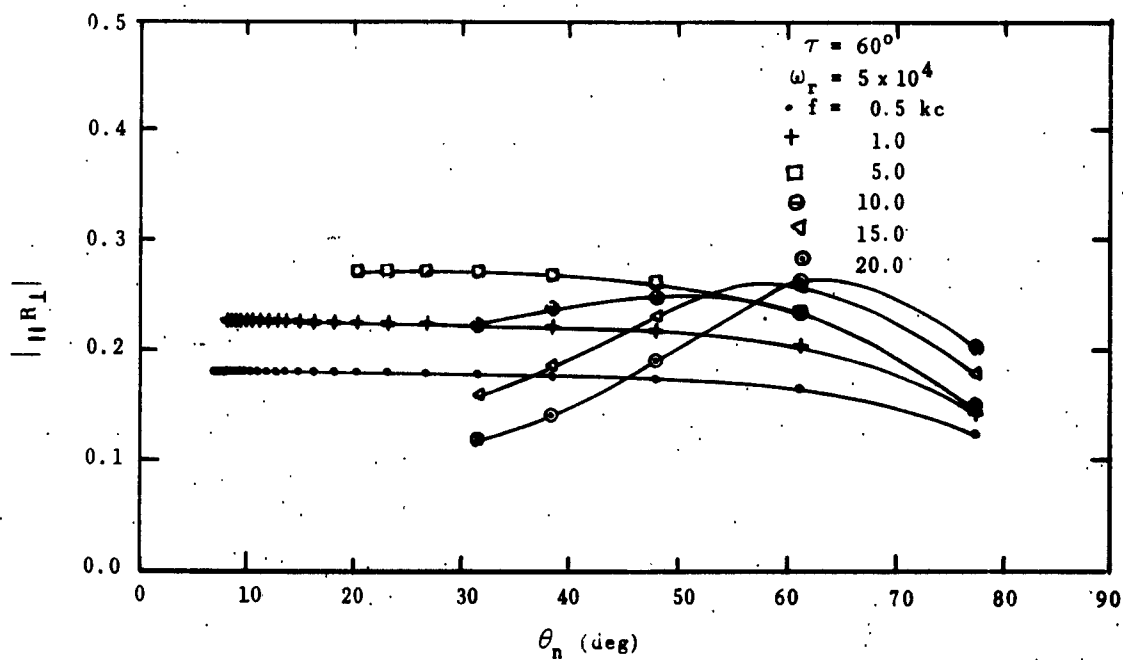
FIG. 3.53. MAGNITUDE OF IONOSPHERE REFLECTION COEFFICIENT $_{||}R_{\perp}$ VS θ_n, FOR $\tau = 60°$, AND $\omega_r = 5 \times 10^4$.
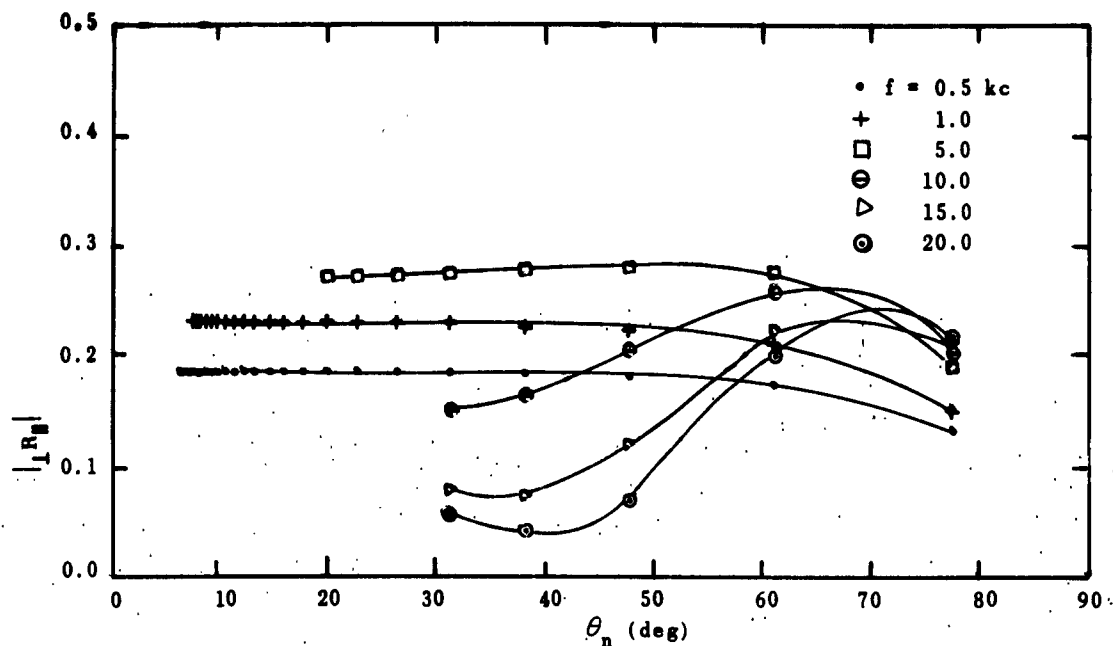
FIG. 3.54. MAGNITUDE OF IONOSPHERE REFLECTION COEFFICIENT $_{\perp}R_{||}$ VS θ_n, FOR $\tau = 60°$, AND $\omega_r = 5 \times 10^4$.
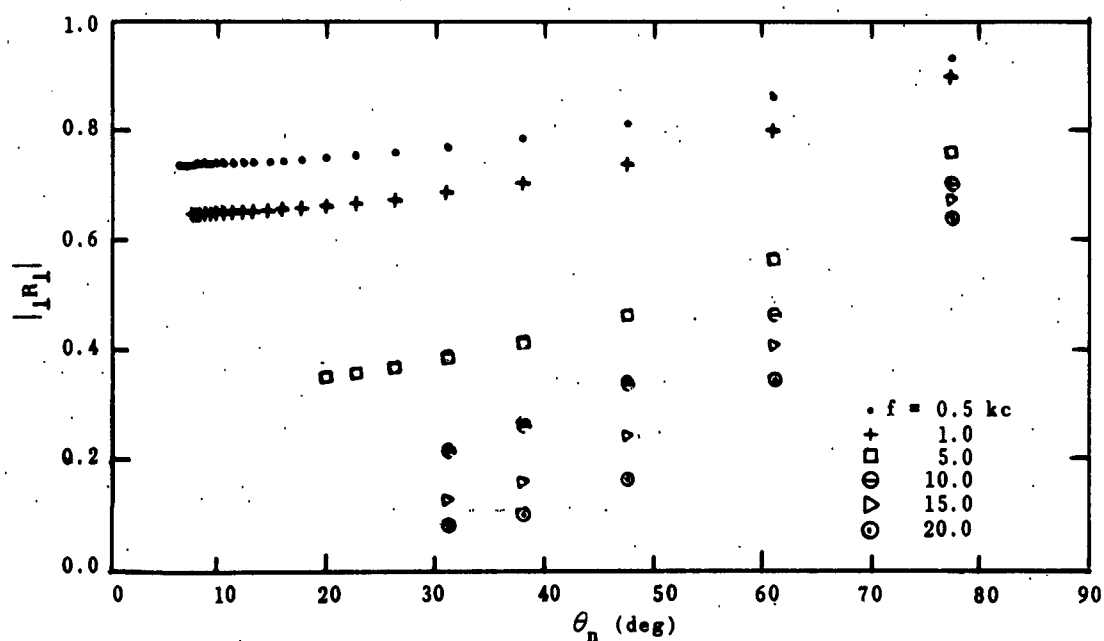
FIG. 3.55. MAGNITUDE OF IONOSPHERE REFLECTION COEFFICIENT $_{\perp}R_{\perp}$ VS θ_n, FOR $\tau = 60°$, AND $\omega_r = 5 \times 10^4$.
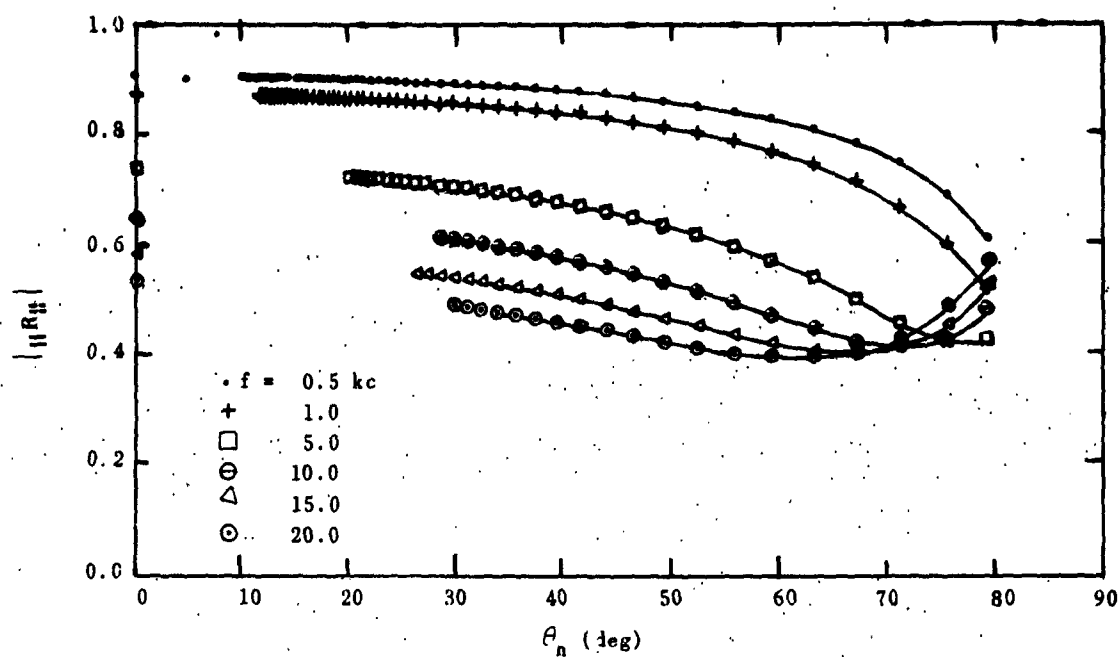
FIG. 3.56. MAGNITUDE OF IONOSPHERE REFLECTION COEFFICIENT $_{\parallel}R_{\parallel}$ VS θ_n, FOR $\tau = 60°$, AND $\omega_r = 5 \times 10^5$ (SUMMER-NIGHT MODEL IONOSPHERE).
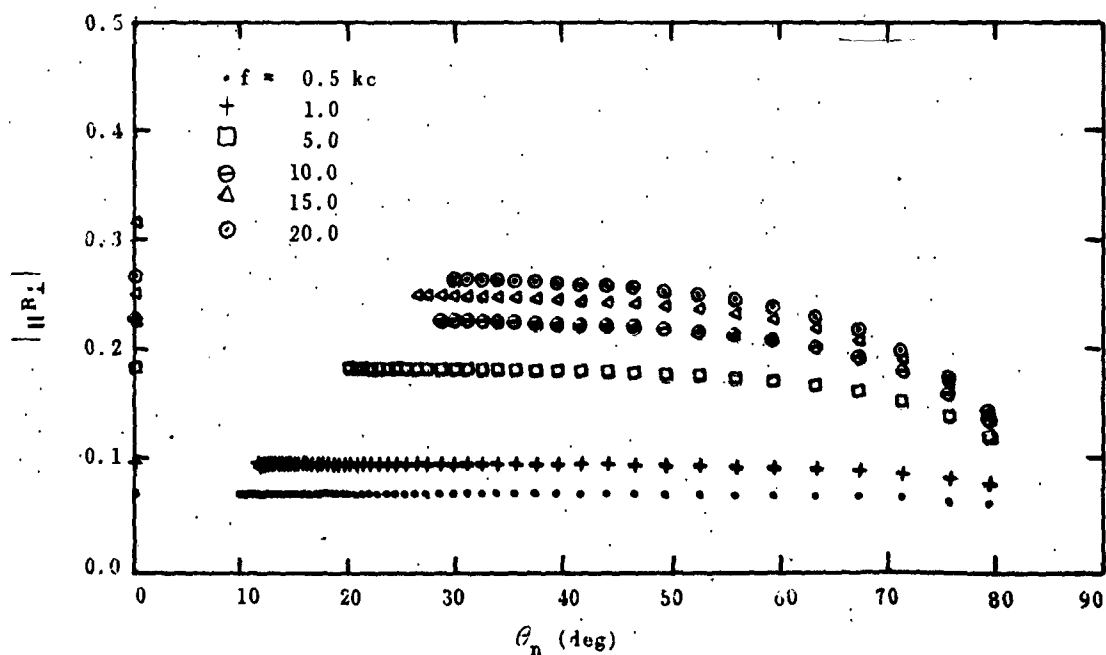
FIG. 3.57. MAGNITUDE OF IONOSPHERE REFLECTION COEFFICIENT $_{\parallel}R_{\perp}$ VS θ_n, FOR $\tau = 60°$, $\omega_r = 5 \times 10^5$ (SUMMER-NIGHT MODEL IONOSPHERE).

- 94 -
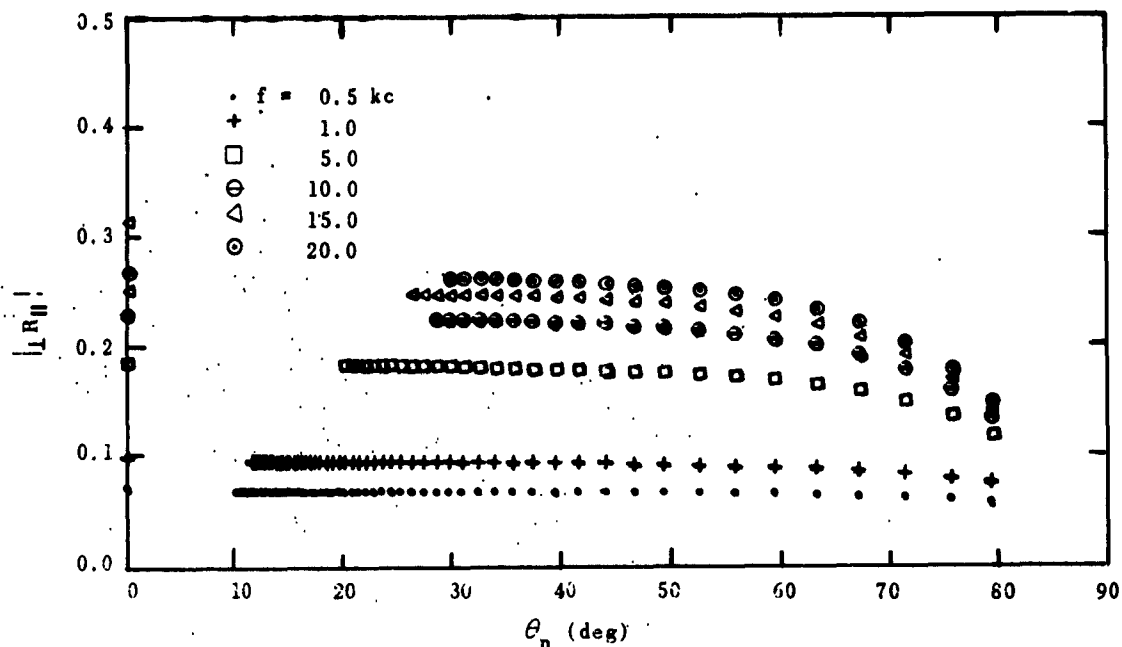
FIG. 3.58. MAGNITUDE OF IONOSPHERE REFLECTION COEFFICIENT $_\perp R_\parallel$ VS θ_n, FOR $\tau = 60°$, $\omega_r = 5 \times 10^5$ (SUMMER-NIGHT MODEL IONOSPHERE).
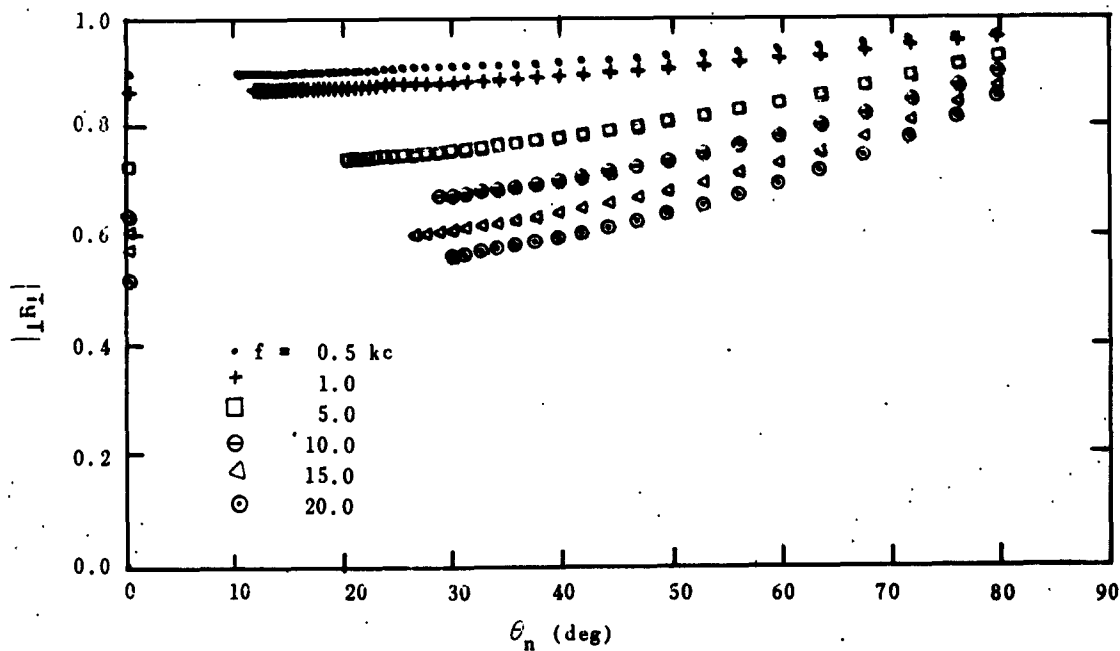
FIG. 3.59. MAGNITUDE OF IONOSPHERE REFLECTION COEFFICIENT $_\perp R_\perp$ VS θ_n, FOR $\tau = 60°$, $\omega_r = 5 \times 10^5$ (SUMMER-NIGHT MODEL IONOSPHERE).
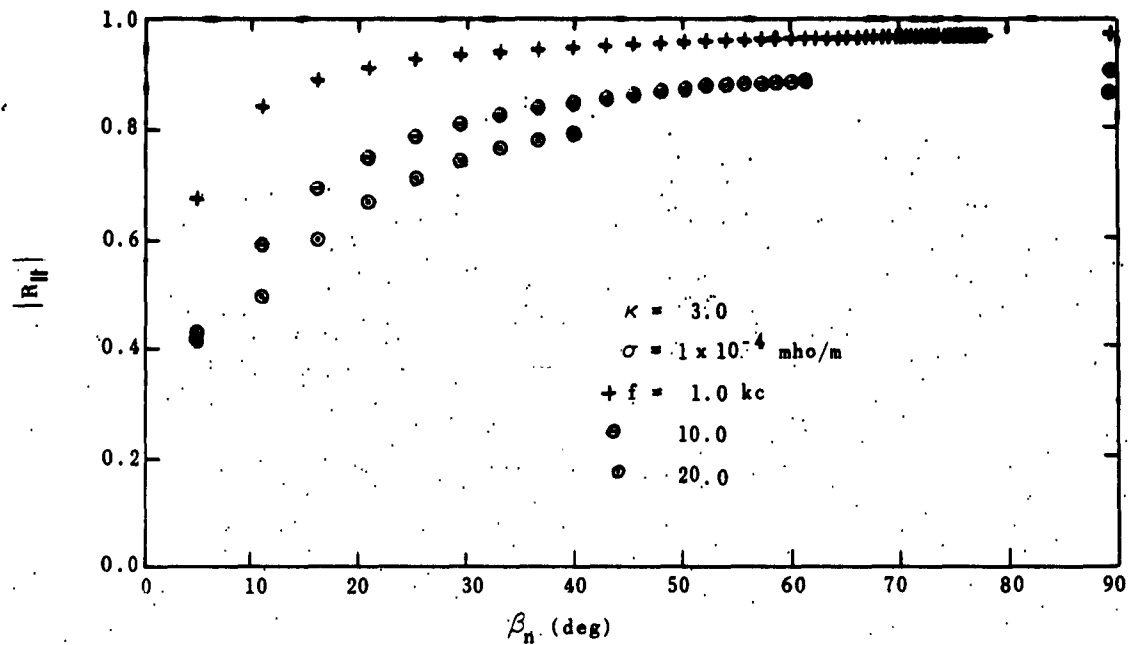
FIG. 3.60. MAGNITUDE OF GROUND REFLECTION COEFFICIENT
$R_{\parallel}$ VS β_n, FOR POOR GROUND, $\kappa = 3.0$, $\sigma = 1 \times 10^4$ mho/m.
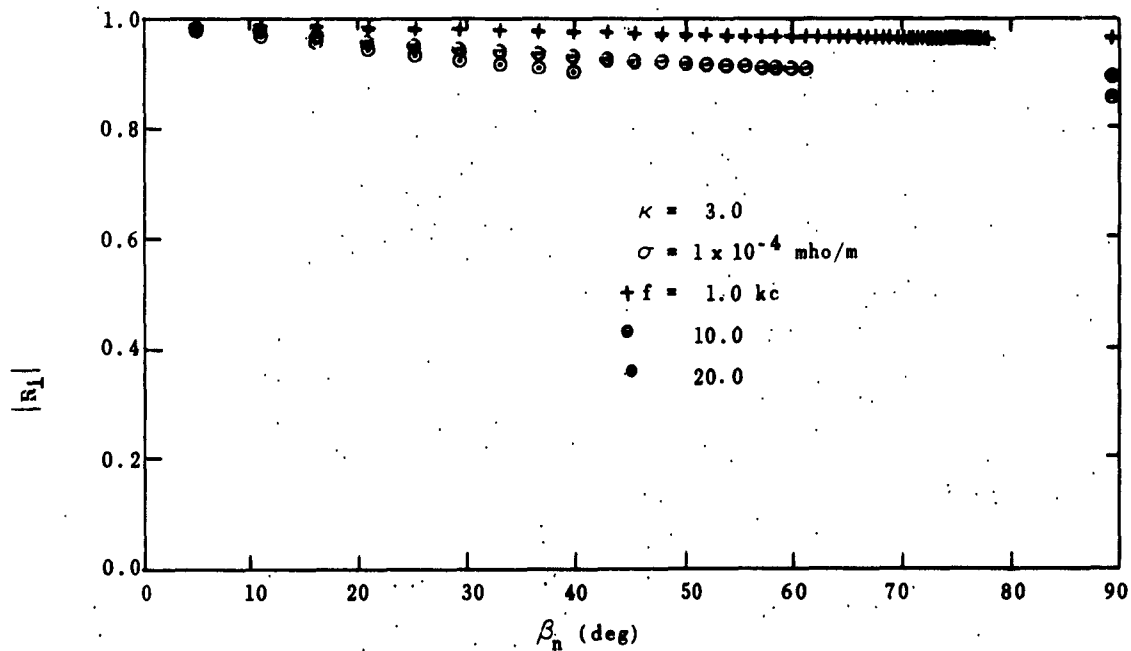
FIG. 3.61. MAGNITUDE OF GROUND REFLECTION COEFFICIENT
$R_\perp$ VS β_n, FOR POOR GROUND, $\kappa = 3.0$, $\sigma = 1 \times 10^4$ mho/m.
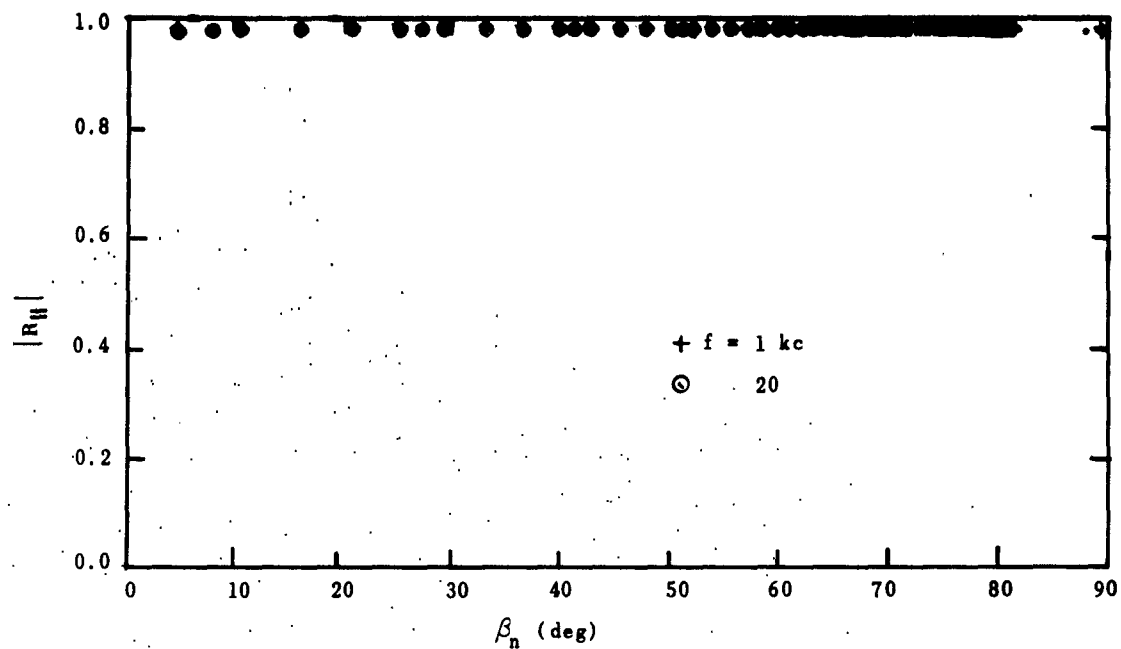
FIG. 6.62. MAGNITUDE OF GROUND REFLECTION COEFFICIENT $R_{\parallel}$ VS β_n FOR SEA WATER, $\kappa = 80.0$, $\sigma = 4.5$ mho/m.
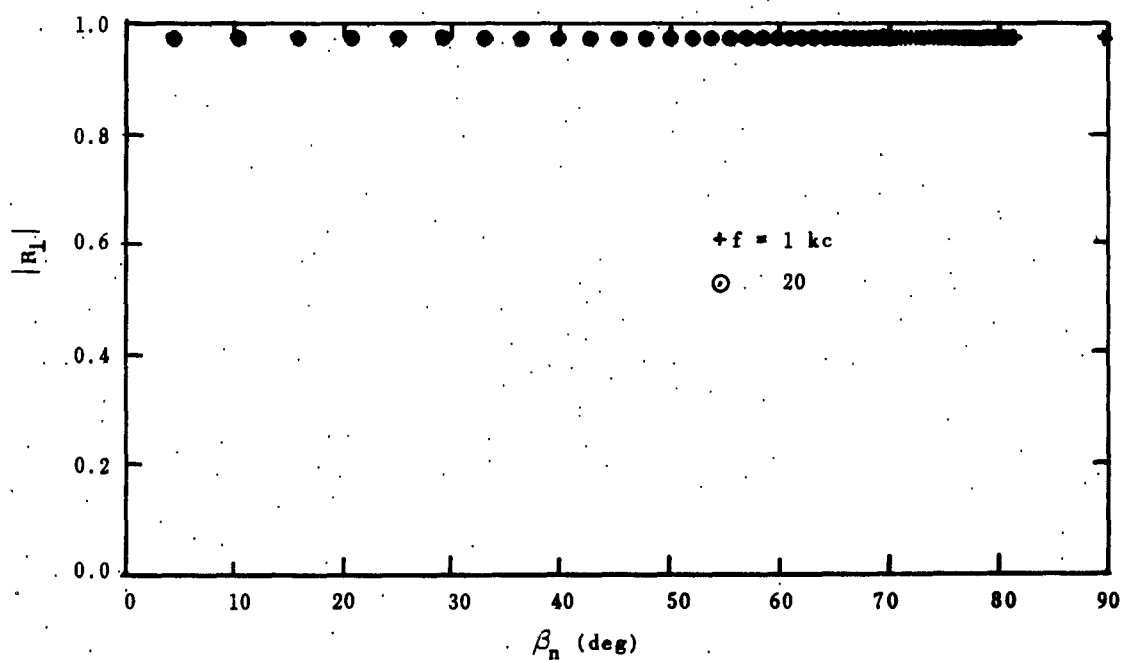
FIG. 3.63. MAGNITUDE OF GROUND REFLECTION COEFFICIENT $R_{\perp}$ VS β_n FOR SEA WATER, $\kappa = 80.0$, $\sigma = 4.5$ mho/m.
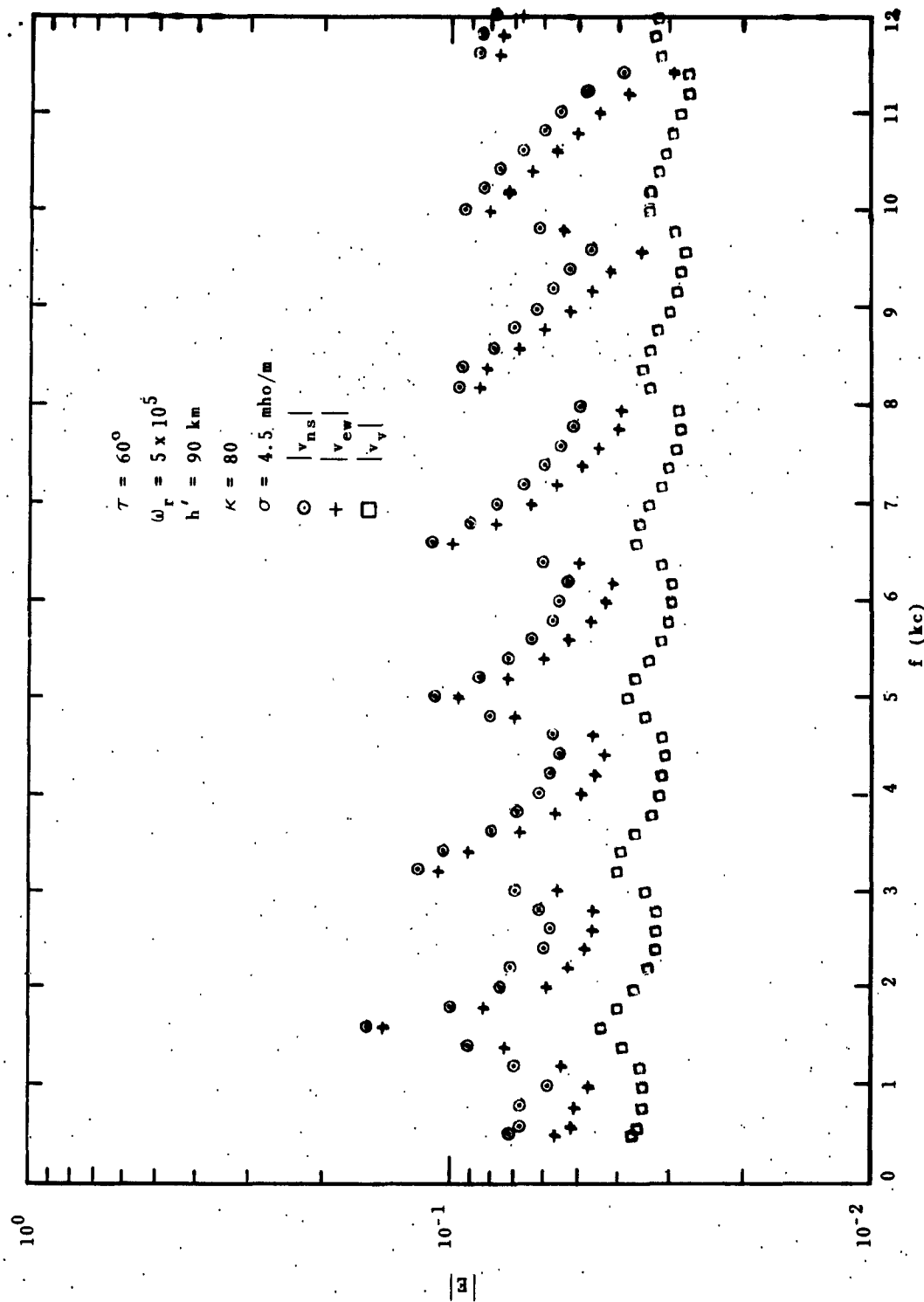
FIG. 3.64. MAGNITUDE OF E-FIELD RECEIVED BY NORMAL AND ABNORMAL VERTICAL LOOPS AND MONOPOLE VS FREQUENCY FOR D = 47.23 km, SEA WATER, AND SUMMER-NIGHT MODEL IONOSPHERE.
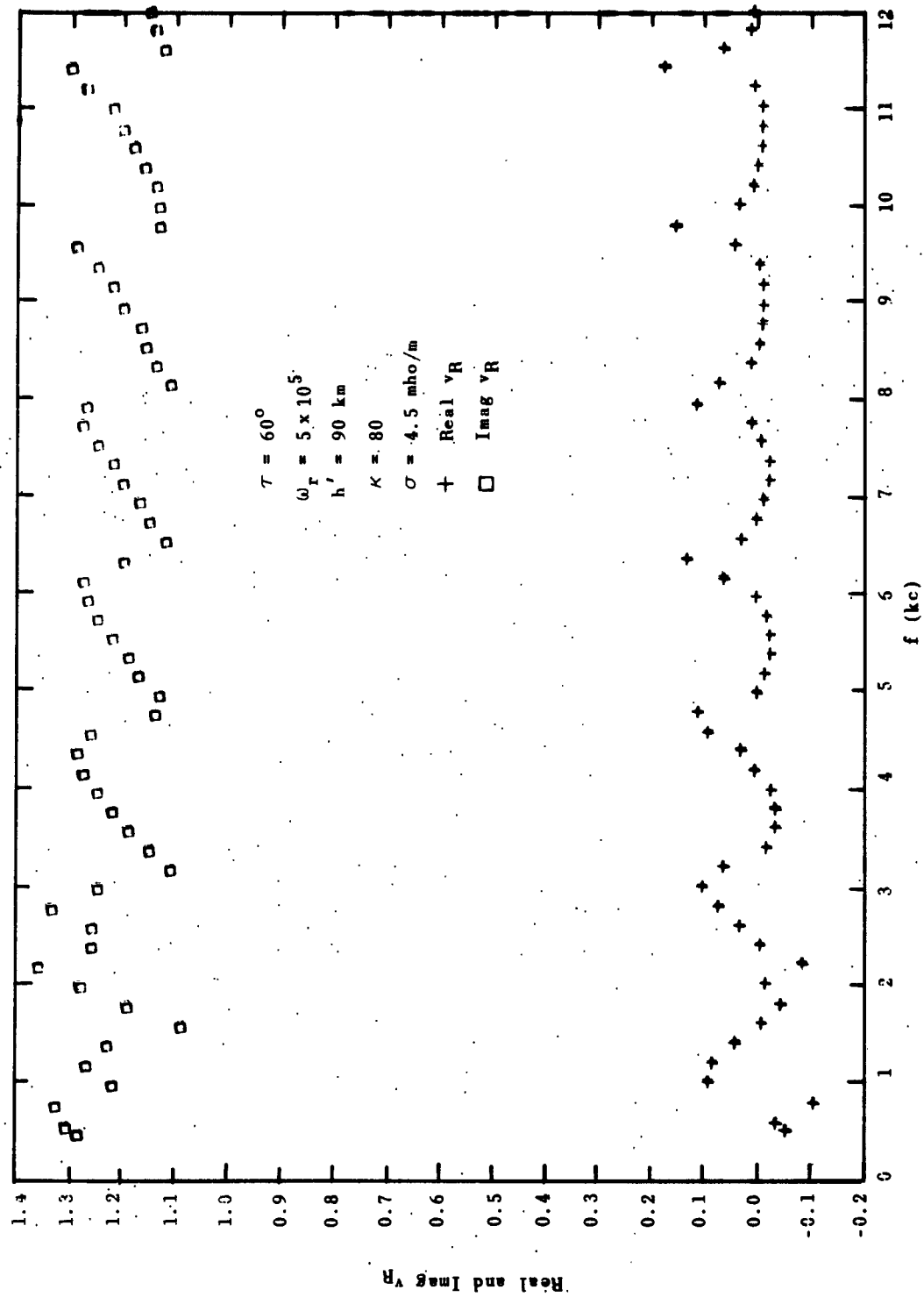
FIG. 3.65. REAL AND IMAGINARY PARTS OF CROSSED LOOP VOLTAGE RATIO VS FREQUENCY FOR D = 47.23 km, SEA WATER, AND SUMMER-NIGHT MODEL IONOSPHERE.

IV. THE d-f EXPERIMENT

A. SOURCE LOCATION BY d-f

As we have seen in Chapter I, it should be possible to determine the exit point at which whistler-mode energy is injected into the earth-ionosphere waveguide. There are several common methods for doing this. The two most common methods are called "inverse-Loran" or time delay location and "d-f" or direction finding.

The inverse Loran method requires the measurement of differences in phase or time of arrival of a signal at spaced stations. Each difference in arrival time at two stations will place the source on a hyperbola drawn with the two stations as foci. If more sets of differences are available, the location can be determined at the intersection of the proper hyperbolas. This method has the advantage of not requiring special goniometer equipment and antennas.

Large spacings, of the order of 150 km or more, are necessary for reasonable phase differences at vlf. The required precision is such that ordinary tape recording of signals produces too much error. The only practical way appears to be to relay signals to a central point for direct-recording. The problem of separation and identification of components in a whistler further complicates the measurement of relative phase. In addition, the phase velocity of earth-ionosphere waveguide signals is not precisely known,[34] which contributes more error. These complications led to the conclusion that this method should be used only if simpler methods were not successful.

The d-f method relies on direction-of-arrival measurements at different points to locate the exit point by triangulation. d-f systems utilizing loops or Adcock antennas are common at the higher frequencies. These are generally narrow-band systems and use some type of goniometer. The use of wideband d-f systems at vlf for the location of atmospherics has become widespread. Wideband systems have the advantage of providing better separation, in time, of the various sky wave components of impulsive signals, except for sources very close to the receiver. A narrow-band system often yields confused results because of its inherent ringing and slow rise time.

A wideband system would be advantageous, since a whistler is a wideband phenomenon. The problem is complicated by the existence of different components in the whistler which have traveled different paths and thus exhibit different arrival angles.

The use of a goniometer system for rapidly rotating the antenna pattern was suggested by the author in 1956,[*] but no practical method of recording and analyzing the output was available. It remained for J. M. Watts[**] to suggest that the wideband output of the goniometer be recorded on magnetic tape in the same manner as routine whistler recordings, and that a spectrum analyzer be used to separate the multiple components and to determine the location of the nulls. Watts was the first to perform this experiment.[41]

This system has the advantage of being simple enough to permit routine recordings of whistler phenomena. The goniometer system was thus selected for an experimental test program. It has the advantage that it can often utilize an antenna system which is normally used for routine vlf recordings. The present system utilizes the crossed vertical loops and vertical monopole antenna which were designed for routine recording on another experiment.

B. THE GONIOMETER SYSTEM RESPONSE

In order to discuss the goniometer system itself, it is necessary to examine the response to vlf signals of the two types of antennas. The loop antenna responds to the magnetic field threading it, and so the induced voltage may be expressed by:

$$v_\ell = - \frac{nd\varnothing}{dt} = - nA \frac{dB}{dt} \tag{4.1}$$

Now for sinusoidal variation, $\frac{dB}{dt} = - j\omega B$ and $B = \mu'H$

---

[*] The goniometer equations stated in this report are not correct, however.

[**] NBS Boulder Laboratories.

Therefore:

$$v_\ell = - j\omega nA\mu'H \qquad (4.2)$$

where:

    n = the number of turns of the loop

    A = the area of the loop in m^2

    μ' = the permeability of free space

    $\omega = 2\pi f$

    f = the wave frequency

    H = the magnetic field strength of the wave

    η = the intrinsic impedance of free space

Now, substituting $\eta = E/H$ yields:

$$v_\ell = - \frac{j\omega nA\mu'E}{\eta} \qquad (4.3)$$

or

$$v_\ell = h'_\ell E \qquad (4.4)$$

Where E is the electric field of the wave in v/m and $h'_\ell = -j\frac{\omega nA\mu'}{\eta}$ is the effective height of the loop in meters. Now the induced voltages may be expressed in terms of the parallel and perpendicular polarized components of a wave incident at azimuth $\emptyset$ and vertical angle $\theta(\theta = 90 - \beta)$. (See Fig. 2.2.) For the ns and ew loops, oriented at an angle $\emptyset$ to the plane of incidence and perpendicular to this plane, respectively, the induced voltages are:

$$v_{ns} = h'_\ell (E_{||}\cos\emptyset - E_\perp \cos\theta \sin\emptyset) \qquad (4.5)$$

$$v_{ew} = h'_\ell (E_{||} \sin\emptyset + E_\perp \cos\theta \cos\emptyset) \qquad (4.6)$$

The goniometer system utilizes a sine-cosine capacitor whose output voltage is given by:

$$v_g = v_{ns} \cos\emptyset_g + v_{ew} \sin\emptyset_g \qquad (4.7)$$

where $\emptyset_g$ is the goniometer coupling angle, measured clockwise from zero (or north). Without loss of generality we may now assume that h'_ℓ is equal to unity. When Eqs. (4.5) and (4.6) are substituted in Eq. (4.7)

and the equation simplified, the result is:

$$v_g = E_{||} \cos\emptyset \cos\emptyset_g - E_\perp \cos\theta\sin\emptyset_g + E_{||} \sin\emptyset\sin\emptyset_g + E_\perp \cos\theta\cos\emptyset\sin\emptyset_g$$

$$= E_{||} (\cos\emptyset\cos\emptyset_g + \sin\emptyset\sin\emptyset_g) - E_\perp \cos\theta(\sin\emptyset\cos\emptyset_g - \cos\emptyset\sin\emptyset_g)$$

$$= E_{||} \cos(\emptyset - \emptyset_g) - E_\perp \cos\theta\sin(\emptyset - \emptyset_g) \tag{4.8}$$

Therefore we see that the goniometer output is the same as that for v_{ns} with the angle $\emptyset$ in the original expression replaced by $\emptyset - \emptyset_g$, and that rotating the goniometer has the same effect as rotating the pattern of the antenna system or changing the direction of arrival with respect to the antenna.

Now let us express the output voltage in terms of the polarization Q of the wave, with the following results:

$$v_g = E_{||} [\cos(\emptyset-\emptyset_g) - Q\cos\theta\sin(\emptyset-\emptyset_g)] \tag{4.9}$$

where

$$Q = X + jY$$

From the form of this equation it is evident that the value of the complex polarization Q will have a great effect on the voltage of the goniometer system. Let us find the maximum and minimum points of this voltage with respect to $(\emptyset - \emptyset_g)$. The value of $(\emptyset - \emptyset_g)$ corresponding to the minimum is the bearing error angle. The maximum and minimum points are most easily found by taking the square of the magnitude of Eq. (4.9), dividing through by the square of the magnitude of $E_{||}$, and then differentiating with respect to $(\emptyset - \emptyset_g)$. This process yields the following equations:

$$|v|^2 = \left|\frac{v_g}{E_{||}}\right|^2 = [\cos(\emptyset-\emptyset_g) - X\cos\theta\sin(\emptyset-\emptyset_g)]^2 + Y^2\cos^2\theta\sin^2(\emptyset-\emptyset_g) \tag{4.10}$$

$$\frac{d|v|^2}{d(\emptyset-\emptyset_g)} = 0 = [\cos(\emptyset-\emptyset_g) - X\cos\theta\sin(\emptyset-\emptyset_g)][-\sin(\emptyset-\emptyset_g) - X\cos\theta\cos(\emptyset-\emptyset_g)]$$

$$+ Y^2\cos^2\theta\sin(\emptyset-\emptyset_g)\cos(\emptyset-\emptyset_g)$$

- 103 -

Then

$$\frac{d|v|^2}{d(\emptyset-\emptyset_g)} = - X\cos\theta[\cos^2(\emptyset-\emptyset_g)-\sin^2(\emptyset-\emptyset_g)]+\sin(\emptyset-\emptyset_g)\cos(\emptyset-\emptyset_g)[-1+(X^2+Y^2)\cos^2\theta]$$

Now the substitution of the trigonometric identities $\sin X \cos X = \frac{1}{2}\sin 2X$ and $\cos^2 X - \sin^2 X = \cos 2X$ yields:

$$0 = -X\cos\theta\cos 2(\emptyset-\emptyset_g)+ \frac{1}{2}[(X^2+Y^2)\cos^2\theta-1]\sin 2(\emptyset-\emptyset_g)$$

This equation may be rearranged to yield:

$$\tan 2(\emptyset-\emptyset_g)=+2X\cos\theta/(X^2+Y^2)\cos^2\theta - 1 \qquad (4.11)$$

This shows that the polarization affects the bearing error angle. Note especially the following property which is present in general and is important, as will later be shown. The sign of Y, the imaginary part of the polarization, determines the direction of the rotation of the phase shift Lissajous pattern when the two antenna voltages are compared. Note that Y appears only to an even power, which means that the direction of rotation does not affect the sign of the bearing error. The sign of X, the real part of the polarization, does affect the sign of the error since it appears to an odd power.

Two special cases are of interest. First, when $X = 0(Q = \pm jY)$, and θ does not equal zero, then the following results are obtained:

$$\tan 2 (\emptyset-\emptyset_g) = 0 \qquad (4.11a)$$

$$(\emptyset-\emptyset_g)1 = n\pi \qquad (4.11b)$$

$$(\emptyset-\emptyset_g)_2 = (2n - 1) \frac{\pi}{2} \qquad (4.11c)$$

where $n = 0, 1, 2, 3,...$

Taking the first values of each of the above solutions, the ratio of voltages obtained from Eq. (4.9) for these two values is:

$$\frac{v_{g2}}{v_{g1}} = Y \cos\theta$$

- 104 -

Thus, the null for $Y \cos\theta$ near unity is very shallow. The bearing error is either 0° or 90° when the magnitude of $Y \cos\theta$ is greater than, or less than, unity, respectively. For circular polarization ($Y = \pm 1$), the error is always 90°.

When the polarization is linear, $Y = 0$. For vertical polarization $X = 0$ also, and Eqs. (4.11a) to (4.11c) again apply. However, in this case, if the first value of each solution is taken, the result is:

$$\frac{v_{g1}}{v_{g2}} = \frac{\cos 0}{\cos \pi/2} \to \infty$$

Thus, the expected results, that the bearing error is zero and the minimum is a true null, are shown to be correct for the case of parallel polarization. Calculations of bearing error and null ratio have been made for a wide range of polarizations. The results are discussed on page 110.

C. THE GONIOMETER-VERTICAL SYSTEM

One logical improvement to the goniometer system would be to re-move the 180° ambiguity by some method of "sense". The polarity of the output voltage, as the goniometer rotates through half a revolution, will be opposite to that in the other half. Therefore, if the output of a vertical antenna, which does not change with the direction of arrival, were added to the goniometer voltage, one of the two minima would tend to be canceled and the other doubled in amplitude. The exact amount of cancellation would depend upon the vertical angle of arrival and the polarization, since the induced voltage in a vertical antenna system is given by:

$$v_v = h'_v E_{\parallel} \sin\theta \qquad (4.12)$$

We can assume here without loss of generality that h'_v is equal to unity. In this case if the angle θ is 90° and the polarization is parallel, the combined output voltage will have one null which is wider than the original goniometer null and one maximum which is twice as large as the

original goniometer maximum. The null ratio will therefore be twice that with the goniometer alone. If θ is less than 90°, two equally spaced nulls will appear on either side of the true direction of arrival.

On further consideration of the details of the response, another theoretical advantage appears. The best nulls would tend to result where the goniometer and vertical voltages are in exactly opposite phase. Consideration of Eq. (4.8) shows that this must occur for $(\emptyset - \emptyset_g)= \pi, 3\pi$, ...etc., or when the plane of the loop is in the plane of incidence of the signal, so that the loop has no response to the perpendicular component of electric field strength. It would therefore be expected that this system, under the condition of a single ray, would exhibit less polarization error and better nulls in general than the goniometer system alone, since there should always be an angle where the voltages are exactly out of phase, and this angle is the true null bearing. It is likely that subsidiary nulls would appear, due to minima caused by amplitude variations of the out-of-phase signals at other angles also. These would tend to be of lesser amplitude than the main null and should be relatively unimportant.

Let us determine the response of the system just described by the method used to determine the goniometer response. After adding Eqs. (4.9) and Eq. (4.12) the voltage of this system becomes:

$$v_{gv} = E_{\parallel} \left[\sin\theta + \cos(\emptyset-\emptyset_g) - Q \cos\theta\sin(\emptyset-\emptyset_g) \right] \qquad (4.13)$$

The simplest way of determining the nulls is again to take the square of the amplitude divided by the square of the amplitude of $E_{\parallel}$, which yields:

$$\frac{v_{gv}}{E_{\parallel}}^2 = \left[\cos(\emptyset-\emptyset_g)+\sin\theta-X\cos\theta\sin(\emptyset-\emptyset_g) \right]^2+Y^2\cos^2\theta\sin^2(\emptyset-\emptyset_g) \qquad (4.14)$$

Now let us make the substitution $\alpha = (\emptyset-\emptyset_g)$. Then, taking the derivative with respect to α and setting the result equal to zero, yields:

$$\left\{ \left[(X^2+Y^2)\cos^2\theta-1 \right]\sin\alpha-X\sin\theta\cos\theta \right\} \cos\alpha=+X\cos\theta(1-2\sin^2\alpha)+\sin\theta\sin\alpha$$

The next step is to substitute $\sqrt{1-\sin^2\alpha} = \cos\alpha$ and square the result, which yields:

$$\left\{ [(X^2+Y^2)\cos^2\theta-1]^2\sin^2\alpha-2X\sin\theta\cos\theta[(X^2+Y^2)\cos^2\theta-1]\sin\alpha+X^2\sin^2\theta\cos^2\theta \right\}$$

$$\cdot (1-\sin^2\alpha)$$

$$=X^2\cos^2\theta(1-2\sin^2\alpha)^2+2X\sin\theta\cos\theta(1-2\sin^2\alpha)\sin\alpha+\sin^2\theta\sin\alpha$$

When the multiplications are performed and the terms are collected the result is:

$$A \sin^4\alpha+B\sin^3\alpha+C\sin^2\alpha+D\sin\alpha+E = 0 \qquad (4.15)$$

where:

$$A = [(X^2+Y^2)\cos^2\theta-1]+4X^2\cos^2\theta$$

$$B = +\left\{2X\sin\theta\cos\theta[(X^2+Y^2)\cos^2\theta+1]\right\}$$

$$C = [(X^2+Y^2)\cos^2\theta-1]^2+X^2\cos^2\theta(4-\sin^2\theta)-\sin^2\theta$$

$$D = -2X\sin\theta\cos^3\theta(X^2+Y^2)$$

$$E = -X^2\cos^4\theta$$

This resulting equation, a quartic in $\sin\alpha$, is obviously more complicated than the result for the goniometer system, Eq. (4.11). Methods are available for solving quartic polynomials, and the method given by Milne-Thomson[27] was employed here.[*] The resulting solution yields four values of $\sin\alpha$, where α is $(\emptyset-\emptyset_g)$, the bearing error angle. There are eight possible values of α which satisfy this equation, of which four are maxima and minima. The other four solutions proved to be trivial. The suspected subsidiary "nulls" are therefore shown to exist. Extensive calculations of theoretical response to different polarizations and vertical angles of arrival were made. A typical example of the maximum and minimum positions is shown in Fig. 4.1 and the maximum-to-minimum ratios in Fig. 4.2. The positions of the maxima and minima for different values of Y vs the goniometer angle are shown in Fig. 4.1 for a single ray with

---

[*] The calculations were programed on a digital computer and are described in Appendix C.
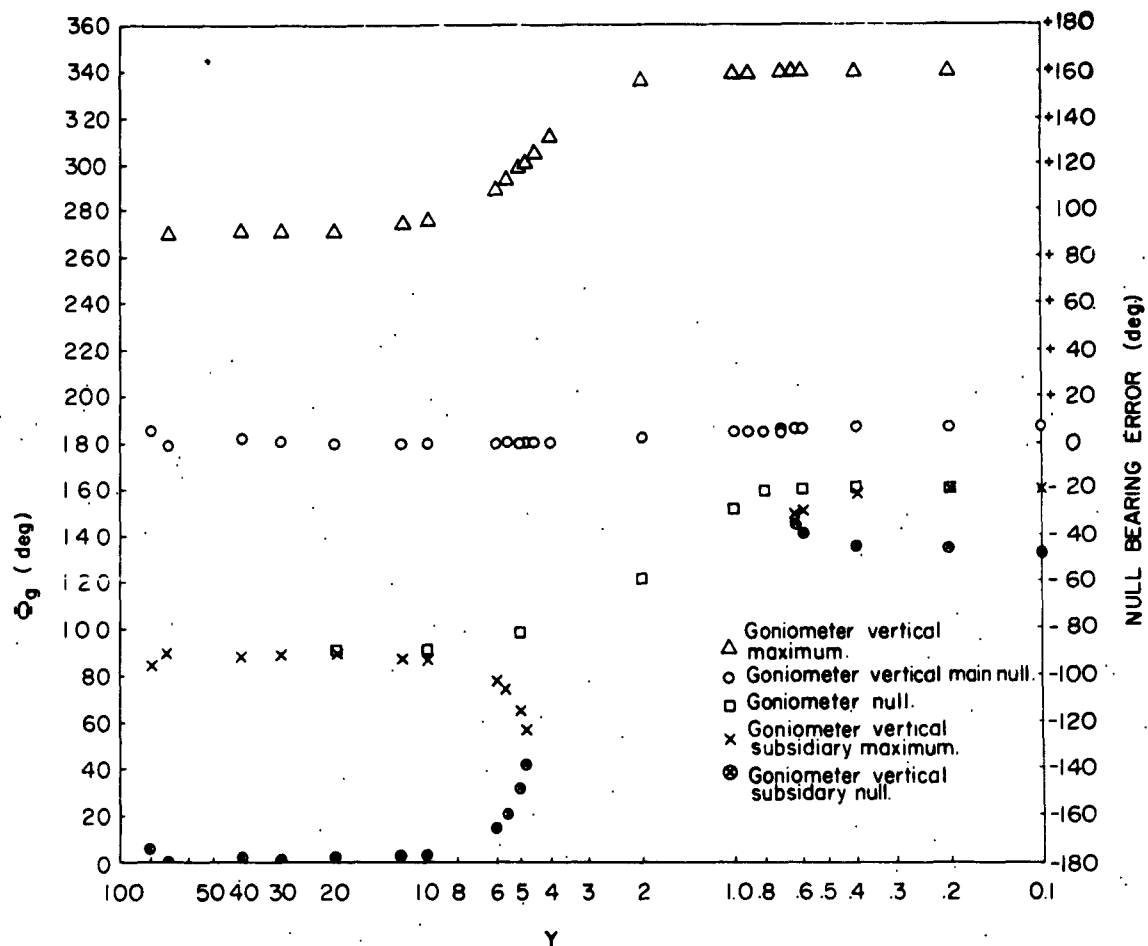
FIG. 4.1. CALCULATED BEARING ERROR OF GONIOMETER AND GONIOMETER-VERTICAL
SYSTEMS VS Y, FOR A SINGLE RAY WITH X = 1.0 AND θ = 70°.
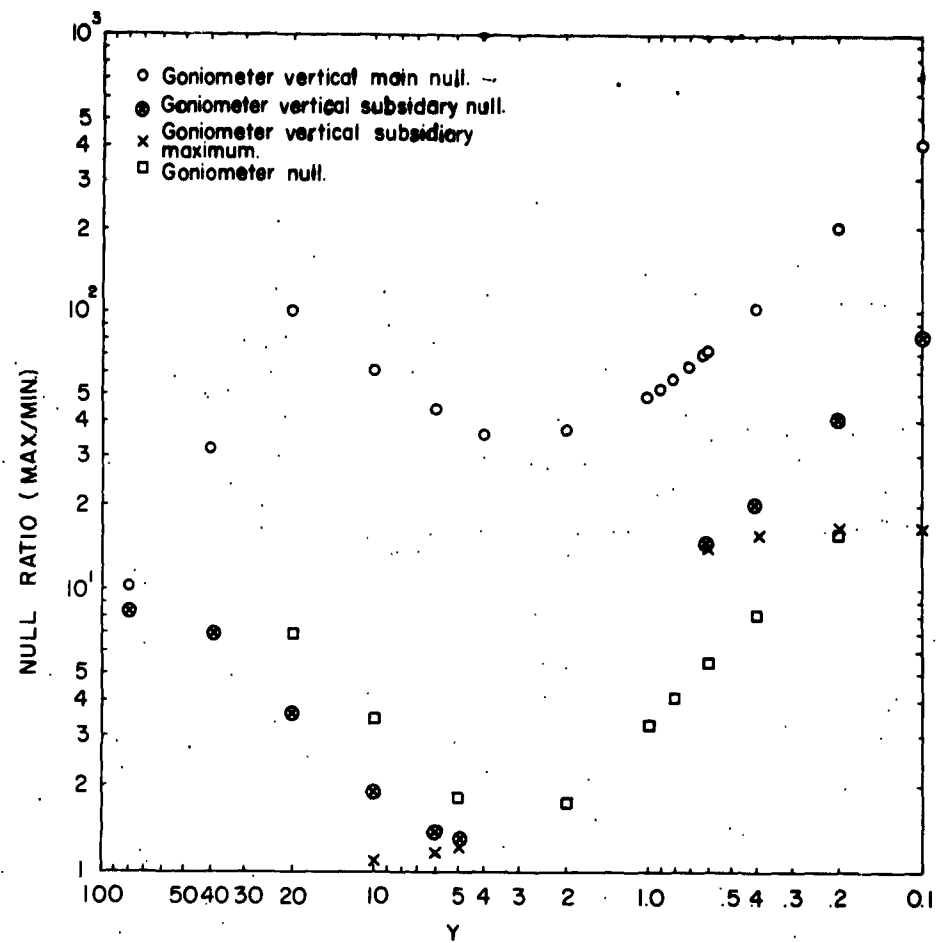
FIG. 4.2. CALCULATED MAX/MIN RATIO OF GONIOMETER AND GONIOMETER-VERTICAL SYSTEMS VS Y, FOR A SINGLE RAY, WITH X = 1.0 AND θ = 70°.

polarization X = 1.0 and θ = 70 degrees. Figure 4.2 shows the magnitude of the goniometer null ratio and the ratio of the goniometer-vertical maxima and minima to the main maximum. The correct bearing angle of the gonio-meter-vertical null would be 180 degrees. A scale is shown to indicate the actual null bearing error. The position of the goniometer null as a function of Y is shown, using the same null bearing error scale. The positions of the maxima and minima of the goniometer-vertical are shown by the ϕ_g scale as a function of Y.

The main null for the goniometer and vertical has a bearing error about half as great as the goniometer null, and the maximum-to-minimum ratio is improved by roughly a factor of ten over the goniometer.

The only general exception to this advantage is for the cases wherein two identical nulls appear. These are closely spaced and are of equal amplitude. They would be recognizable by their symmetry, however. The true bearing would be midway between them. The main minimum is much deeper than the subsidiary ones for the great majority of cases, and so the subsidiary minima are not likely to be significant. A further dis-cussion is given on page 143.

It was noted, in the section on the goniometer, that Y appears only in even powers while X appears in both odd and even powers. The odd powers occur only in coefficients of odd-power terms in $\sin\alpha$. The effect of a change in the sign of X will again, as in the case of the goniometer, reverse the pattern of maximum and minimum about the true bearing or, in other words, change the sign of the error. The significance of this property is discussed later, on page 141.

D. THE EXPERIMENTAL PROGRAM

Direction finding measurements, using a goniometer system of the type previously described, were made at Stanford, California, and at a site near Seattle, Washington. The Stanford station utilized the antenna and associated equipment built for Lissajous-pattern studies of whistlers and vlf signals and for whistler studies in the 30-60 kc range. The Seattle station utilized a standard two-channel IGY system. Regular operation of the two stations began in April 1960 after a trial period

:of several weeks, and continued until the end of January 1961. A similar experiment was started several months earlier by J. M. Watts of NBS Boulder Laboratories. Simultaneous observations among the three stations were obtained for a considerable time by mutual agreement. The goniometer-vertical system was added to the Stanford system at a later time.

1. EQUIPMENT. Figure 4.3 shows a block diagram of the Stanford equipment. The outputs of the goniometer and the goniometer-vertical were simultaneously recorded on a dual channel tape recorder. The operation was automatically programed to record on the standard IGY whistler recording schedule of 2 minutes per hour. A calibration signal was regularly inserted into the antenna circuit by the constant current method[5] as a test of the proper adjustment. The tape recordings were played back through a spectrum analyzer. A set of spectrograms is shown in Figs. 4.4 and 4.5. The spectrograms show voltage, measured by the relative darkness of the display, as a function of frequency and time. These spectrograms illustrate some of the best nulls obtained on the goniometer-vertical system.

The three spectrograms of Fig. 4.4 show the signals obtained simultaneously from the Stanford goniometer and goniometer-vertical and the Seattle goniometer system. The vertical bars on the spectrograms are the atmospherics from lightning discharges, which contain broadband energy. The broken, horizontal lines in the 15-20 kc region of all the spectrograms are the Morse code signals from navy vlf transmitters. The one in Fig. 4.5 is station NPG, 18.6 kc, located near Seattle, Washington. The recording level is varied on spectrograms so that the desired signal (in this case, the whistler) appears at the proper amplitude (or intensity). The vlf signals are therefore too strong, in this spectrogram, to show nulls.

The whistler shown in Fig. 4.4 is a good example of the multipath type of whistler which shows several traces with different delays which result from different propagation paths. The nulls for the different traces are easily seen to occur at different bearing angles.

Figure 4.5 shows a whistler with a single trace but a very regular null pattern which varies slightly with frequency.
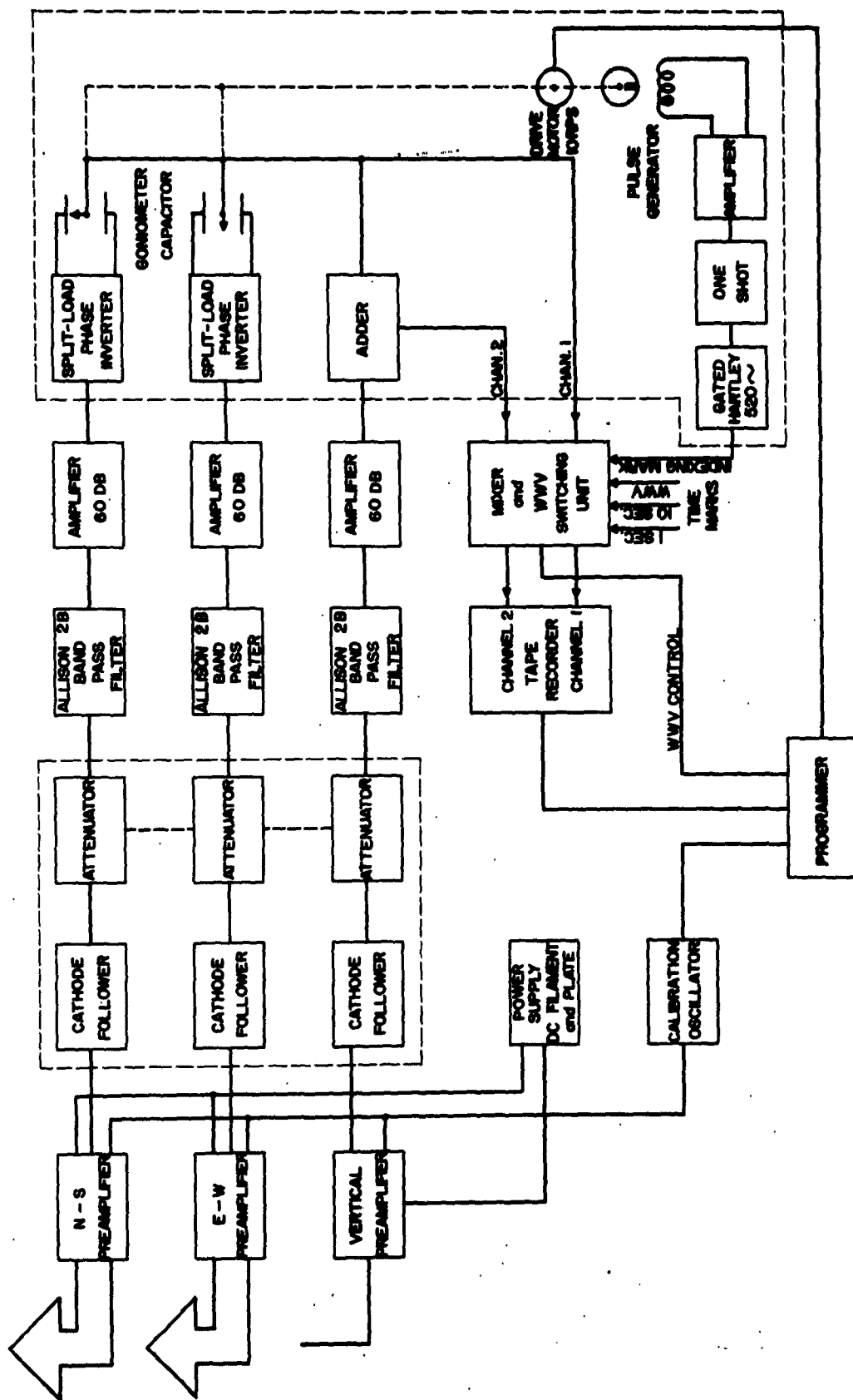
FIG. 4.3. BLOCK DIAGRAM OF STANFORD GONIOMETER AND GONIOMETER-VERTICAL SYSTEM.

3 JULY 1960   1436:29 UT

STANFORD

GONIOMETER-VERTICAL
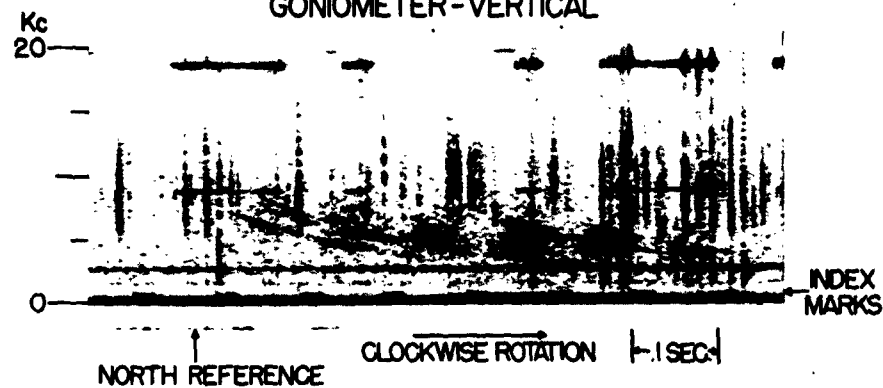
STANFORD

GONIOMETER
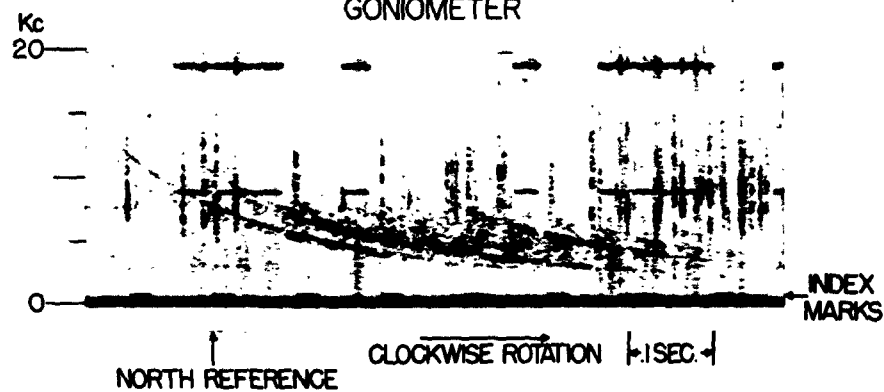
SEATTLE

GONIOMETER
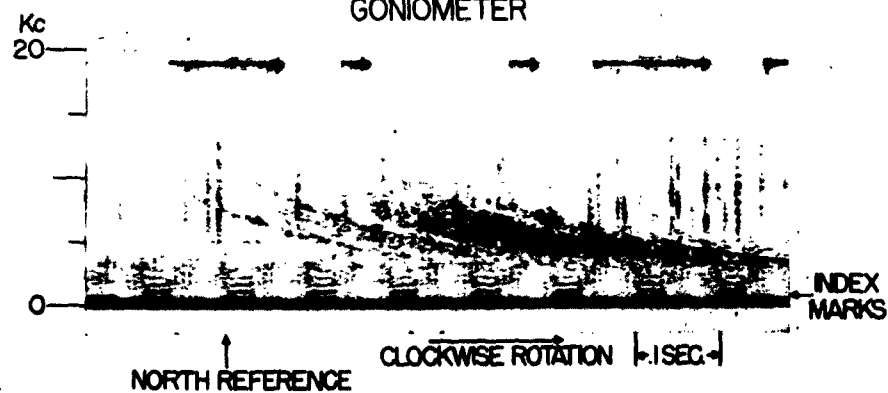
FIG. 4.4.   SPECTROGRAMS OF WHISTLER SHOWING DIFFERENCE BETWEEN NULLS ON THE GONIOMETER AND GONIOMETER-VERTICAL SYSTEMS AT STANFORD AND THE GONIOMETER SYSTEM AT SEATTLE.

STANFORD

8 JUNE 1960   11:35:38 UT

GONIOMETER
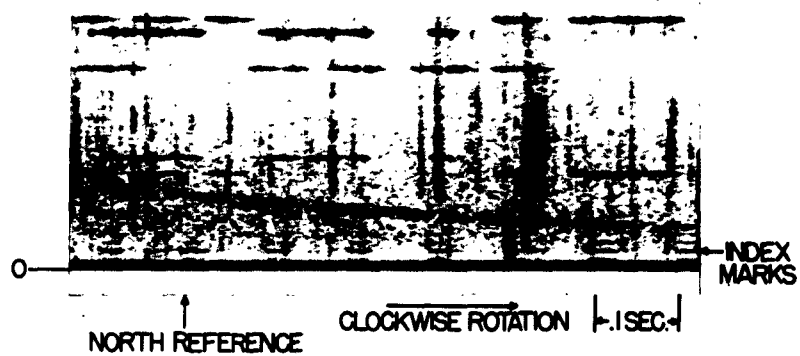
GONIOMETER-VERTICAL
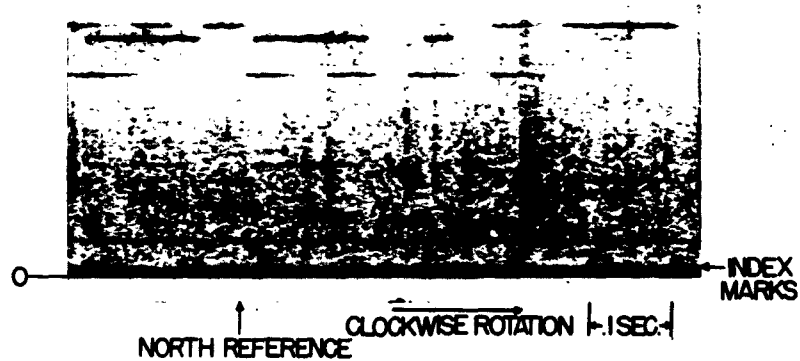
FIG. 4.5.   SPECTROGRAMS OF WHISTLER WITH WELL DEFINED NULLS ON
THE GONIOMETER-VERTICAL AND POOR NULLS ON THE GONIOMETER SYSTEM
AT STANFORD.

A variable-frequency signal from an oscillator is inserted, with equal amplitude and phase, into each antenna circuit. Typical calibration spectrograms made of this signal are shown in Fig. 4.6. The position of the nulls marks the coupling of equal and opposite signals from the two channels into the goniometer output, where the goniometer angle ϕ_g is $45°$. The series of marks near the bottom edge of the spectrogram (520 cps and harmonics) is the train of index marks. The goniometer is rotated at 10 rps by a synchronous motor. A pulse is generated by a magnet mounted on a disc rotating with the goniometer, and passing by a coil. The voltage induced in the coil is amplified, shaped and used to trigger the one-shot multivibrator shown in the block diagram. The resulting pulse turns on the "gated-Hartley" oscillator and produces an index mark once in each revolution. Bearings are scaled by measuring the position of a null, relative to the index marks, and converting this to angular position.

The calibration is used to determine the correction to the position of the index mark relative to the goniometer position and to check the equalization of the channels. Scaling of the calibration nulls at different frequencies shows that the shift of position with frequency is not significant compared to scaling error.

Recorded whistlers were analyzed on a regular basis, and a systematic search made for those with "nulls" at both stations so that bearings could be computed and the position of the exit-point triangulated from both stations. The error in the index-mark position, determined from the calibration spectrogram, was applied as a bearing correction factor during scaling. It is estimated that a high-quality spectrogram can be scaled to a maximum accuracy of $\pm$ 1 degree in bearing; the average scaling accuracy is estimated to be of the order of $\pm$ 2-4 degrees. The resulting error in position depends entirely upon the position of the "target" relative to the station. The worst cases occur when the "target" is close to one of the stations or the line joining them.

Several nulls are usually obtained on one whistler trace. Each of these gives a bearing for the corresponding frequency. The bearings obtained for the whistlers showing nulls at both stations are listed in Table I.

- 115 -

STANFORD
9 JANUARY 1961
GONIOMETER CALIBRATION
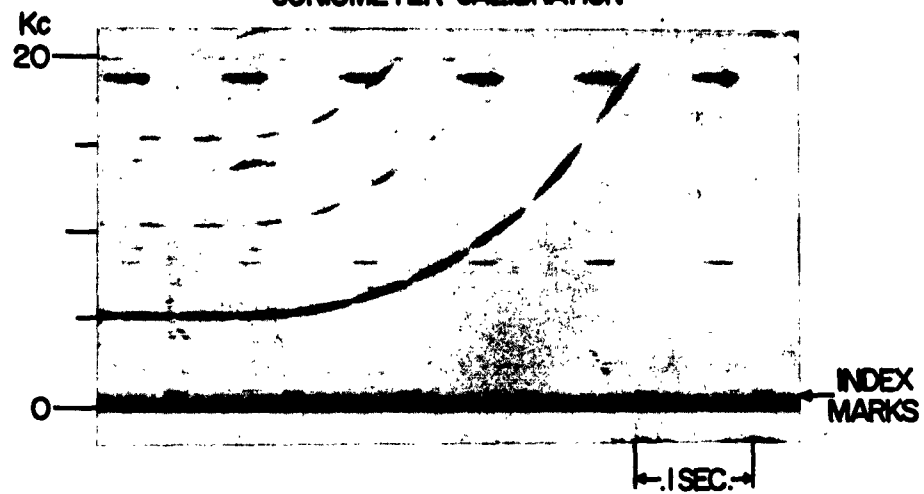
FIG. 4.6.   STANFORD GONIOMETER CALIBRATION SPECTROGRAM.

TABLE I. MEASURED NULL BEARINGS OF LOCATED WHISTLERS

Universal date and time	Seattle			Stanford		
	Sonagram number	Frequency	Bearing	Sonagram number	Frequency	Bearing
25 April 1960 1135/84	1A	8.8 7.0 5.0 4.2 3.5 3.0 2.8 2.5	135 119 140 113 116 140 122 124	1A 1D	9.0 7.4 5.5 4.5 4.1 3.8 4.0 3.8	60 55 62 54 62 56 60 51
		Average	126		Average	58
3 July 1960 1435/89	1A 1B	Trace A(1) 6.8 6.0 5.0 4.0 Trace D(4) 7.3 6.2 4.8 Trace D(4) 6.0 5.0 4.5	109 62 87 40 15 4 9 20 17 18	1A	Trace A(1) 9.0 8.0 6.2 5.2 4.8 4.0 Trace D(4) 6.0 5.2 4.5 4.0	144 114 140 127 104 163 153 147 150 162
		Average A Average D	98 9		Average A Average D	110 151
12 Aug 1960 1135/43	1A	6.2 5.2 4.2 3.7	154 134 168 157	1A	6.9 5.5 4.5 4.0 3.2 2.8 2.5 2.0	82 101 83 57 97 112 93 76
		Average	153		Average	88
26 September 1960 0435/43	1A	5.8 5.0 4.0 3.5 3.0 2.8 2.5	147 159 139 144 152 142 117	1B	8.5 6.5 5.0 3.7 3.0 1.6	124 105 147 139 125 131
		Average	143		Average	129
0735/24	1B	7.0 6.1 5.5 4.6 4.2 3.5	177 174 145 117 133 144	1C	5.4 4.2 3.3 2.5	154 127 118 140
		Average	148		Average	135
0835/29	1B	5.4 4.5 4.0 2.5 1.5	128 133 138 143 116		8.4 6.5 4.9 2.8	202 148 148 202
		Average	132		Average	175

TABLE I.   MEASURED NULL BEARINGS OF LOCATED WHISTLERS (Cont'd)

Universal date and time	Seattle			Stanford		
	Sonagram number	Frequency	Bearing	Sonagram number	Frequency	Bearing
0835/65	1B	5.8	149		10.3	150
		5.0	146		7.7	166
		4.4	142		5.7	187
		3.9	96.9		4.3	165
		3.4	155		3.2	189
		2.9	144		2.7	158
		2.6	150		2.0	168
		2.3	131			
		2.1	127			
		1.8	123			
		1.6	144			
		1.4	117			
		Average	135		Average	169
0835/109	1B	8.5	175		8.8	154
		7.7	108		6.2	197
		5.5	130		4.6	189
		3.5	153		3.5	192
		3.2	128		2.8	183
		2.8	153			
		2.5	134			
		2.2	108			
		2.0	129			
		1.7	109			
		Average	133		Average	183
1335/103	1A	4.5	175	2B	4.8	207
		4.0	182		2.0	224
		3.4	201		1.7	189
		3.0	185		1.3	198
		Average	186		Average	204

In a few cases, bearings were taken from two different spectrograms made at different level settings. This sometimes produces very different bearings at nearly the same frequencies. This is associated with poor signal-to-noise ratio and with errors such as flutter in the tape recording and reproducing process. The variation of the individual bearings about the average is very large, as is expected from the results of the calculations. This is discussed on page 141.

The average bearing for each trace is used. The locations are then determined by solving the spherical trigonometry on a digital computer.

E. EXPERIMENTAL RESULTS

During the measurements program, which lasted approximately 10 months, approximately 170 whistlers were recorded at Stanford; 130 of these showed scalable nulls. A total of only 10 whistlers yielded nulls on the same trace that were scalable at both Stanford and Seattle, as Table II shows. No whistlers were obtained which showed scalable nulls at Stanford or Seattle and also at the Boulder Station run by Watts.

The positions of the exit-point locations were plotted on a map from which the magnetic latitude of the position could be determined. The map is shown in Fig. 4.7.

The magnetic latitude of the path of propagation was also calculated by analysis of the spectrograms, using a method developed by Carpenter and Smith.[4,33] In their method the nose frequency is first calculated and then used to estimate the latitude of the path, assuming a dipole field and a particular form for the electron distribution.[4] Each location shown in Fig. 4.7 is connected by a line with the nearest point which has the magnetic latitude so determined. These two values are also compared in Table II.

TABLE II. COMPARISON OF MAGNETIC LATITUDE OF WHISTLER PATHS DETERMINED BY d-f LOCATION AND NOSE WHISTLER THEORY.

Ident. map no.	Date	UT	Trace	D-f θ_o (deg)	Nose θ_o (deg)	D-f-nose $\Delta\theta_o$ (deg)
1	25 Apr 60	1135/84	1	49.0	45.5	+3.5
2	3 Jul 60	1436/29	1	37.0	47.5	-10.5
3			4	46.0	54.5	-8.5
4	12 Aug 60	1135/43	1	44.0	46.0	-2.0
5	26 Sep 60	0435/43	1	30.0	47.0	-17.0
6		0735/24		29.0	47.0, 46.5	-17.8
7		0835/29	1	53.0	46.3, 46.5	+6.5
8		0835/65	1	54.0	46.0	+8.0
9		0835/109	1	52.0	45.5	+6.5
10		1335/103	1	40.0	46.0	-6.0
					Sum	-37.3
					Average	-3.73
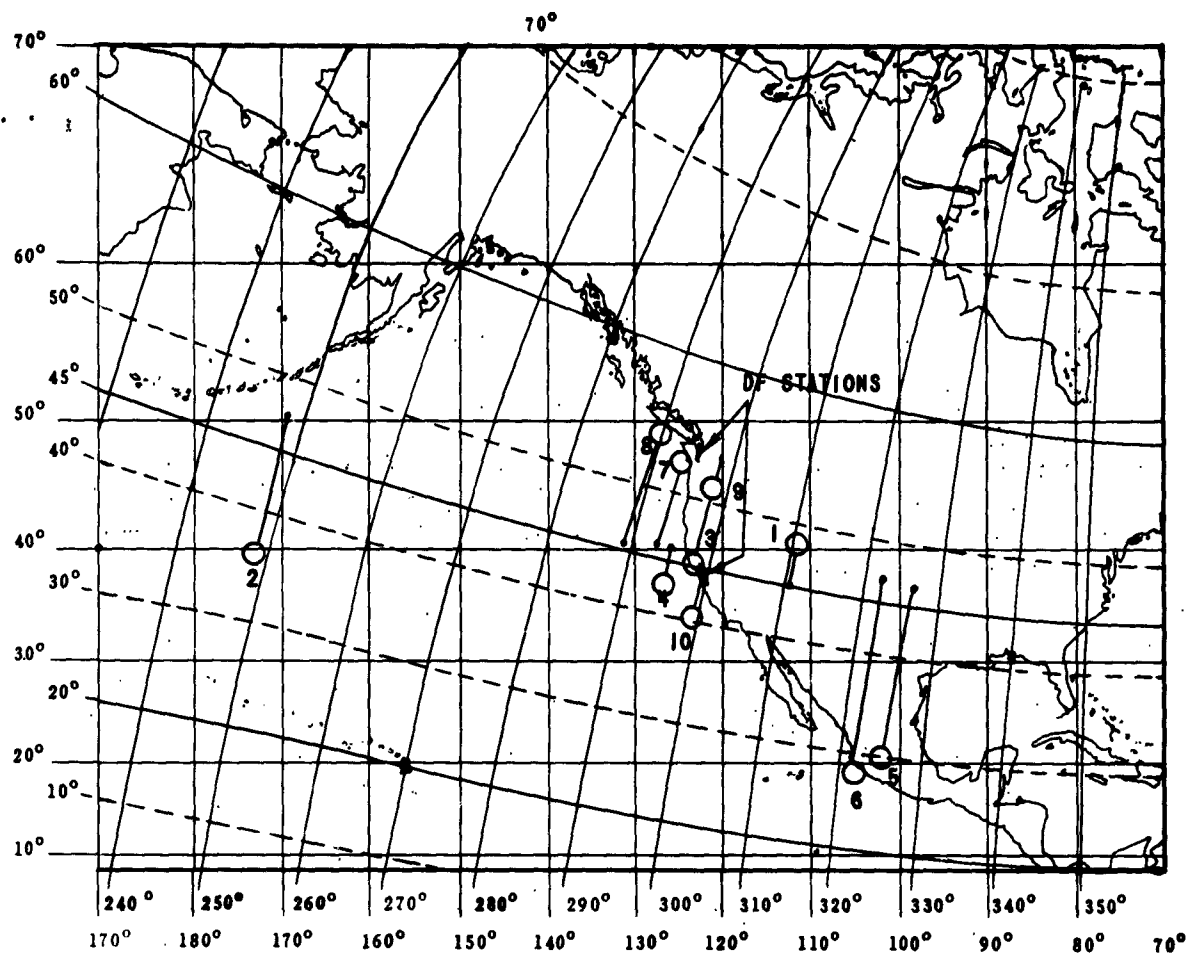
FIG. 4.7. LOCATION OF WHISTLER EXIT POINTS DETERMINED FROM STANFORD AND SEATTLE d-f BEARINGS.

The differences in latitude range from 2.1° to 17.8°. The average is -3.7° and the standard deviation is 9.2°. The number of cases is too small for the average to be statistically significant. In a large sample, it could be significant (see page 149).

A further result of the experiment is shown in Fig. 4.8. This curve indicates the range of 23 Stanford goniometer bearings for vlf station NSS (15.5 kc) at Annapolis. These data were taken on 4 different days spaced over a 3-month period. The scalings were made without prior knowledge of the true bearing. The average bearing for this set is 73.4°, and the standard deviation is 4.3°. The true great circle bearing is 72.99°. The measurement of vlf station bearings is generally more accurate than whistler bearing measurements, since the field strength is generally greater and always more constant. The results illustrate the improvement which may result from averaging bearings. The expected measuring error is $\pm$ 1 to 2 degrees. The remaining error can be attributed to polarization and lateral deviation error. Compared with whistlers, the error would be expected to be smaller since vlf stations generate vertically polarized waves.
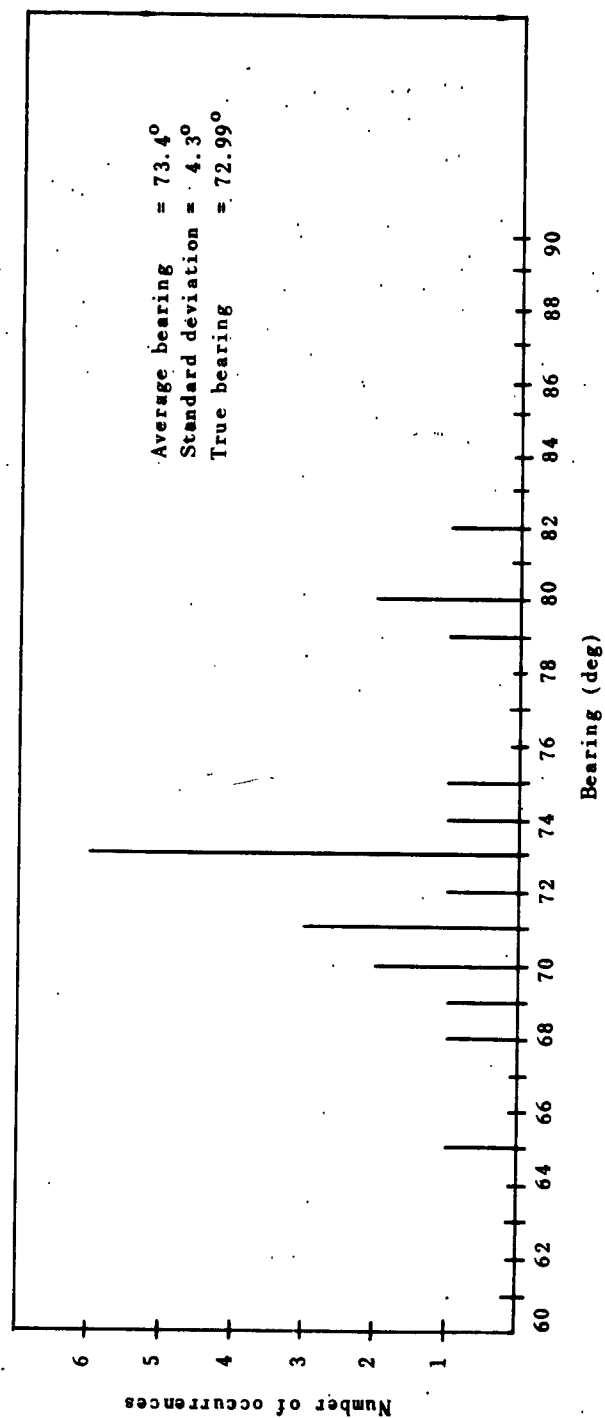
FIG. 4.8. VLF STATION NSS (15.5 kc) GONIOMETER BEARINGS. AT STANFORD.

V. DISCUSSION

A. THE EFFECT OF DIFFERENT ANTENNAS ON FIELD STRENGTH

The difference in the response of different antennas is one of the most striking features of the curves of field strength. It is evident that the loop and the vertical monopole measure different fields, even when the plane of the loop lies in the plane of propagation. An examination of the results shows that the field measured by the vertical antenna is less than that measured by the loop antenna by a factor of approximately 1 db for the majority of cases. Figure 3.4 shows one point where the difference is roughly 6 db in the opposite direction. Experimental measurements at Stanford have shown a discrepancy of this magnitude for vlf station NPG on 18.6 kc.

This difference in the fields is predicted by the equations for antenna response. The difference exists even when the incident field is vertically polarized. Consider the two equations for the response to the parallel component of electric field:

$$x_{3a} = \sum_n E_{\parallel}^{(n)} \left(1 + R_{\parallel n}\right) \tag{3.7}$$

$$x_{3v} = \sum_n E_{\parallel n} \left(1 + R_{\parallel n}\right) \cos \beta_n \tag{3.8}$$

It might seem at first that the magnitude of x_{3v} would always be less than the magnitude of x_{3a}, since $\cos \beta_n \leq 1$. Figure 5.1 shows the vector diagram of the two voltages for a typical case, in terms of the increments. For clarity, only the first 5 components are shown. For each n, the component of both fields will have the same phase angle (which measures time phase), since x_{3v} is merely x_{3a} multiplied by the scalar function $\cos \beta_n$. The two increments for each n will thus be parallel, with x_{3a} always longer than x_{3v}. The magnitude of each voltage is the distance from the origin. The example clearly shows that either voltage may have the greater magnitude.
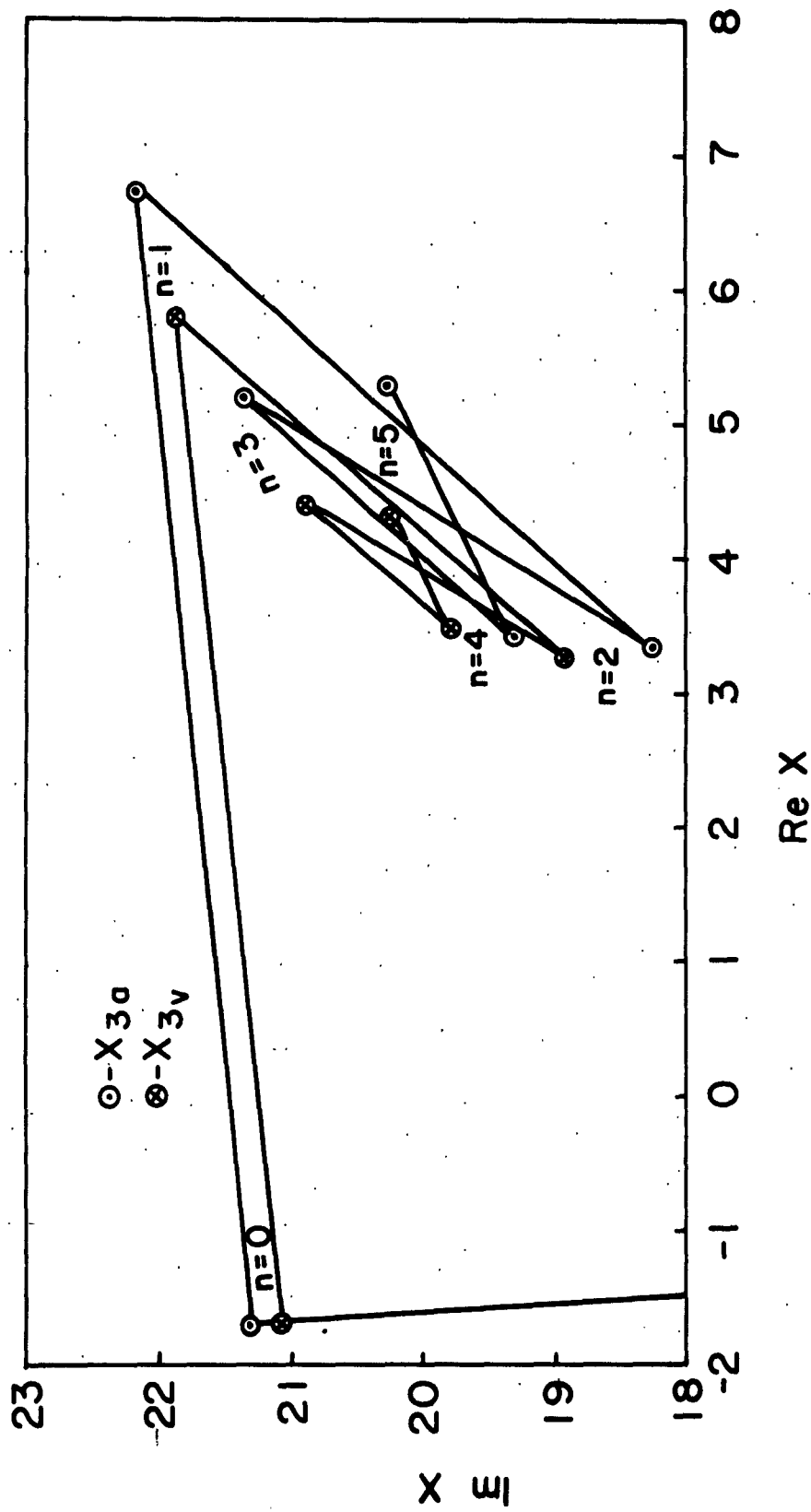
FIG. 5.1.   TYPICAL ADDITION OF RAYS ON NORMAL VERTICAL LOOP AND MONOPOLE.
FOR SUMMER-NIGHT MODEL IONOSPHERE, POOR GROUND, $D = 500$ km, $\phi_g = 0$, $f = 1$ kc.

The difference between the measured field strengths of vlf signals on vertical and loop antennas has been generally explained in terms of errors in the effective height values, site errors (ground irregularities, etc.), or polarization errors. However the difference in the response caused by this new factor should be considered.

The results of the calculations make possible an evaluation of different antennas for particular applications. One very important question that has often arisen in whistler work is the relative sensitivity, to whistler signals, of a vertical loop and a vertical monopole. This is best determined from Figs. 3.8 through 3.12, where field strength is plotted vs distance for 5 kc and 15.5 kc. It is evident that the response of the vertical antenna will be not more than 6 db below the normal loop response for D greater than about 60 km, for both 5 kc and 15.5 kc. The vertical is equally good for the great majority of whistler signals, therefore, and has the advantage that its response is independent of the azimuth of arrival. The choice can then be based on considerations of sensitivity to hum and other interference. Since the vertical cannot be nulled for hum or atmospheric noise, the interference may well be the deciding factor.

A second important question involves the orientation of a loop antenna. Figures 3.17 through 3.21 show the response of a loop vs frequency for different values of ϕ_g. It is evident that while the loop orientation affects the details of the response curves as a function of frequency or distance, the general behavior is the same for all orientations. An examination of Figs. 3.9 and 3.10 shows that the amplitude of the signal in the abnormal (EW) loop varies considerably, relative to that in the normal (NS) loop. It may be seen from Fig. 3.9, the curve for 5 kc, that the ratio of the NS to EW loops is not greater than 6 db for any distance. However, Fig. 3.10 for 15.5 kc shows that the ratio is generally greater than 6 db for distances greater than 600 km. This indicates that the loop orientation is important in the upper part of the vlf spectrum. There is some experimental evidence to support this theory. At Byrd Station, Antarctica, no "whistler mode" signals were received from station NSS at 15.5 kc until the loop antenna was oriented so that it pointed at the area where the ducts could be expected to terminate.

Whistler and vlf activity which occurs at the low frequencies was normal for this location.

B. FIELD STRENGTH VARIATIONS

Rapid variations of field strength with frequency are characteristic of all but the 0.1 km calculations. The shape of the curves for D = 0.1 km, shown in Figs. 3.1 and 3.2, is of special interest. The conditions are, of course, very close to vertical incidence. For this case, the earth-ionosphere waveguide appears to the transmitted wave as a transmission line with the earth as a termination at the end. If the ground is relatively good, as in sea water, the physical situation closely resembles the shorted transmission line, and a loop antenna on the ground would be measuring the equivalent of the magnetic field at the short. This analogy is demonstrated by expressing the magnetic field strength at the earth in terms of ordinary transmission line equations.

The transmission line equations represent the effect of the multiple reflections present in the line as a change in the impedance at the input to the transmission line. By contrast, the ray-theory method requires the determination of the effect of each ray. For this reason, the ray-theory calculation is very sensitive to small changes in the model. There are differences in the two situations, due to the assumed 1/R attenuation of the field and the imperfect ground in the ray-theory case. However, the situations are still very similar. A typical curve (based on ray theory) for the summer-night model and sea water ground is shown in Fig. 3.2. Figure 5.2 shows a portion of the shorted transmission line calculation for a perfect conductor at the short, with the summer-night model ionosphere constants. The similarity in the curves is obvious, and shows the analogy between the two viewpoints in this case.

Variations in the field strength similar to those shown in Figs. 3.2 and 5.2 have been seen in at least one whistler. This whistler shows several fairly sharp nulls in its pattern at anharmonic frequencies which are spaced by 0.8 - 1.2 kc in the frequency range below 5 kc.

- 126 -
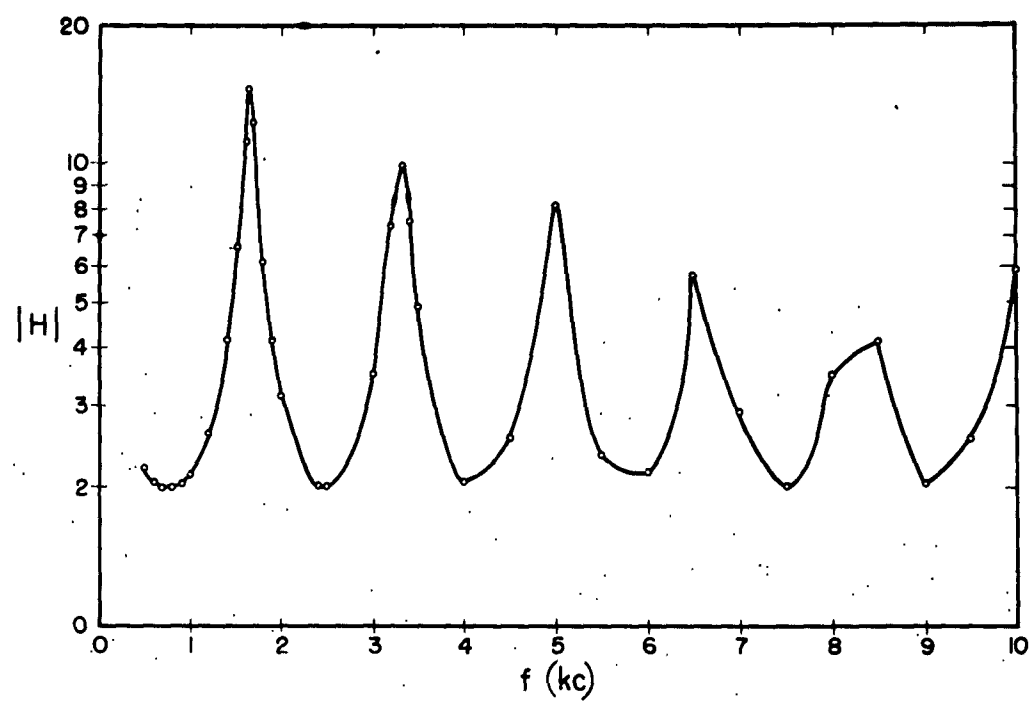
FIG. 5.2. MAGNETIC FIELD AT THE SHORT ON A TRANSMISSION LINE VS FREQUENCY FOR L = 90 km AND SUMMER-NIGHT MODEL REFRACTIVE INDEX.

This could be explained by the shape of the curves of field strength for vertical incidence. The minima in the field strength curves tend to be rather broad, however, while the nulls in the whistler are fairly sharp. The nulls could also be produced by beating of adjacent rays of different frequencies. It was shown in Section II-B that the difference at vertical incidence for a frequency of 10 kc and a typical dispersion of 100 $(sec)^{1/2}$ is about 13 cps. This difference is reduced to about 2 cps at 3 kc. The null separation is approximately correct for the variation due to the transmission line effect but the period is probably too short for beating effects at this frequency.

The beating effect alone would not produce very large variations, since the ray for n = 1 is weaker than that for n = 0 by at least a factor of three due to the increased propagation distance. It is therefore more likely that the cause is primarily the transmission-line effect. The appearance of these nulls is an easy way to identify short-distance propagation from routine spectrograms.

The behavior of the polarization and the crossed-loop Lissajous patterns is also unique for near-vertical incidence, and will be discussed on page 133.

The curves for greater distances show the characteristic rapid variations with frequency due to interference of different rays. A comparison of the curves in Figs. 3.4 and 3.7 shows that this effect is not noticeably greater at 2000 km than at 500 km. The most evident effect is that of changes in ionization density. The curve in Fig. 3.15 is for $\omega_r = 5 \times 10^4$, a factor of 10 lower than the summer-night model for the same distance (500 km) as in Fig. 3.3. This corresponds to a reduction in f_o of $\sqrt{10}$, or of 10 in the ion density. It is immediately evident that the rapid variations are much smaller and the field about 6 db weaker than for the summer-night model. The slope and position of the maxima and minima are also different. These changes are reasonable since the transmission coefficients decrease slightly with decreasing ω_r, while the reflection coefficients $_{||}R_{||}$ and $_{\perp}R_{\perp}$ decrease fairly rapidly with decreasing ω_r as shown in Figs. 3.38 through 3.55. The magnitude of the cross-coupling reflection coefficients $_{||}R_{\perp}$ and $_{\perp}R_{||}$ change very slowly with ω_r, and their magnitude is only of the order of

one-fourth that of the other two coefficients. Thus, the amplitude of the rays decreases much more rapidly with number of reflections, and a smaller number of rays contributes to the signal. This makes the interference patterns less complex.

The corresponding curve for an increased density, $\omega_r = 5 \times 10^6$, is shown in Fig. 3.16. As would be expected, the pattern is more complicated and the variations are more rapid.

Rapid variations in field strength are seen in experimental data. Figure 5.3 shows the signal voltage vs time for the parts of a whistler of 4 March 1956 at 0404 UT. An examination of a typical section shows that the field strength variation takes place in a minimum period of about 3 ms. The amplitude fades from the peak values down to noise level during these variations, covering a range of about 20 db. Fluctuations of this magnitude are very rare in the calculated results, and do not occur with such short periods.

It appears that these variations are due to some factor other than the interference between rays. The period of 3 ms corresponds to a frequency difference of about 300 cps if this were caused by "beating" of signals of different frequency. The whistler spectrogram, Fig. 5.4, shows that the whistler is about 1 kc wide at this frequency. It is quite possible that this variation is due to the interference of different frequency components. Such rapid variation cannot be seen on the observed crossed-loop Lissajous patterns probably because of the low sampling rate.

1. THE EFFECT OF GROUND. The electrical characteristics of the ground have little effect on the detailed variations in the calculated data. The main effect is, of course, the relative attenuation. Sea water adds about 0.2 db to the signal at 500 cycles, and 1 db at 20 kc, over poor ground at a distance of 0.1 km. At a distance of 2000 km, the increase is that 0.3 db at 500 cycles and 15 db at 20 kc. These values are typical in that the relative attenuation is low at low frequencies. One feature is immediately evident: that the curves for poor ground show a definite slope toward greater loss as the frequency is increased. This does not appear on the curves for sea water. The effect is especially evident on the curves for long distances, such as Fig. 3.6

FIG. 5.3. WAVEFORMS OF STANFORD WHISTLER OF 4 MARCH 1956, 0404 UT.

NORTH-SOUTH CHANNEL
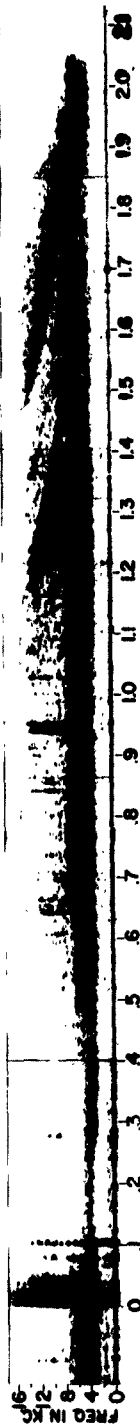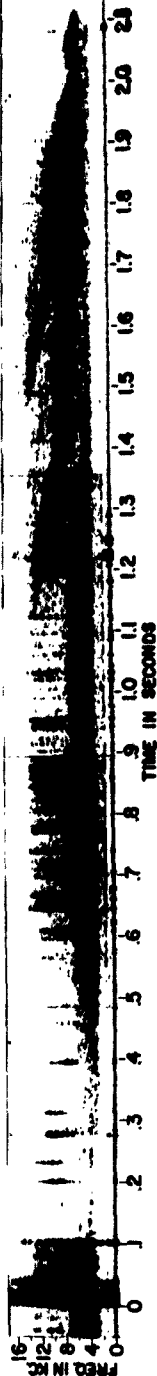
EAST-WEST CHANNEL

NORTH-SOUTH CHANNEL
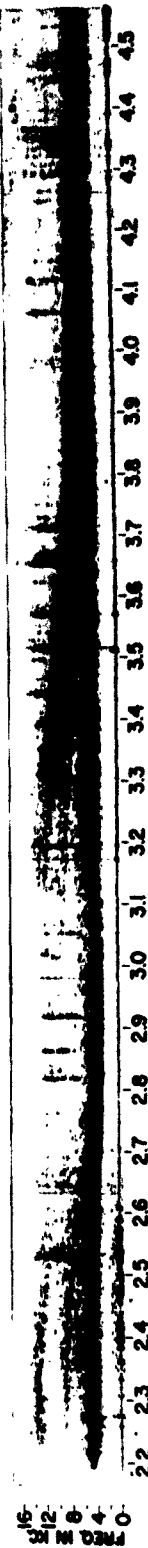
EAST-WEST CHANNEL
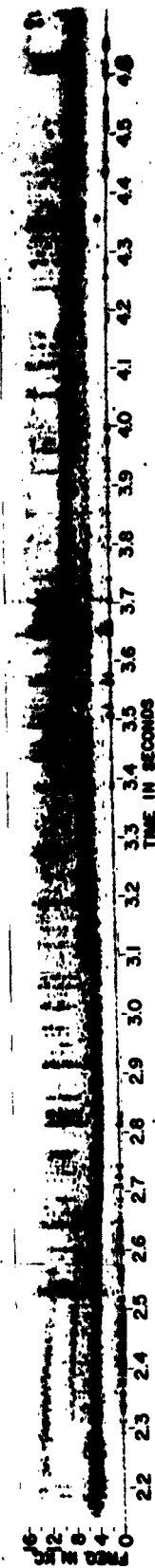
FIG. 5.4. SPECTROGRAM OF STANFORD WHISTLER OF 4 MARCH 1956, 0404 UT.

for 2000 km. This indicates that there is considerable advantage in locating middle- or low-latitude stations near a sea coast, especially when high frequency data, such as nose whistlers or vlf station echoes are desired. This finding agrees in general with the experimental data, indicating that the majority of whistler sources are generally over the ocean, to the west of Stanford.[30]

2. FREQUENCY EFFECTS. The curves of field strength vs frequency (Figs. 3.1 through 3.21) do not show any tendency to exhibit a peak in any part of the frequency range. Figures 3.38 through 3.59 show that no peak exists in the transmission or reflection coefficients. The rapidly varying nature of the curves of antenna voltage vs frequency make it difficult to define a figure for the loss at a particular frequency. It is evident that the loss always goes down near the low end of the frequency range, around 0.5 kc. A fairly deep null appears above this frequency in the curve, and the position and depth depend upon the distance, the ionosphere parameters, and the antenna orientation (for a loop). It is therefore very difficult to make general statements about transmission as a function of frequency. The experimental data on whistlers generally show a drop off in intensity at the low end of the spectrum near the "tweek" cutoff, where the earth-ionosphere waveguide becomes a half wave length in height. The interpretation of this fact is complicated by the energy spectrum of the source, which is known to drop off at low frequencies. This experimental effect could be produced by the null in the curves, together with the reduction in the excitation at low frequencies. The rise at lower frequencies could be masked by the equipment, which generally begins to roll off just above 0.5 kc, and by 60 cycle harmonic components.

3. EFFECTIVE AREA. The "effective area" of a whistler is defined as that area over which a whistler may be detected. This area is assumed to be circular, and the value of 1000 km has often been quoted for the radius as determined from experimental data.[1,2,3] If a reasonable value of 20 db is chosen for the range of detectable whistler amplitudes, the curves of Figs. 3.8 through 3.10 show that this change in amplitude occurs in approximately 1000 km.

C. THE CROSSED-LOOP LISSAJOUS PATTERNS

One of the results of the experimental studies was a number of recordings of the crossed-loop Lissajous patterns as a function of frequency. A particularly good example of this is the whistler of 4 March 1956, shown in Fig. 5.5. This shows the waveforms of the signal on two beams, and the resulting Lissajous pattern on the third beam of a multibeam oscilloscope. The beams are gated on only during the 200-μ sec sweep. The sweep repetition rate is 25 per second, which corresponds to 0.04-second intervals between sweeps. The whistlers were first tape-recorded on a carefully equalized tape recorder. They were then played back and filmed.

The upper strip shows a 10 kc calibration signal introduced into the system. The effects of tape flutter are evident in the changes in the axis ratio of the ellipses and in the amplitude of the waveforms. It is also evident that the flutter effects are small in comparison to the total changes. The striking thing about these records is the fairly regular change in the axis ratio and angle of the ellipse. Figure 5.6 shows the characteristics of the ellipse for different sweeps. The axis ratio varies from almost zero to about 0.8, and the angle varies from zero to almost 180 degrees. Periods in the range of 0.04 - 0.13 seconds are evident when this and other examples are examined. The isolated cases of opposite rotation are also of interest, as discussed on page 137.

The calculated real and imaginary parts of v_R, the voltage ratio of the NS and EW loops, are shown in Figs. 3.22 through 3.30 for various distances, ground parameters and ionosphere conditions. It is evident that the behavior is very complicated, except for very short distances. At a distance of 0.1 km, the polarization is circular and the loop voltages are essentially equal and 90 degrees out of phase. The imaginary part of v_R is then always equal to unity, and the real part is very small. When the distance is increased, the ratio departs from this constant value by only about 3% at 20 km. The difference increases to about 50% at 100 km. The behavior is characterized by rapid changes, as a function of frequency, for greater distances.
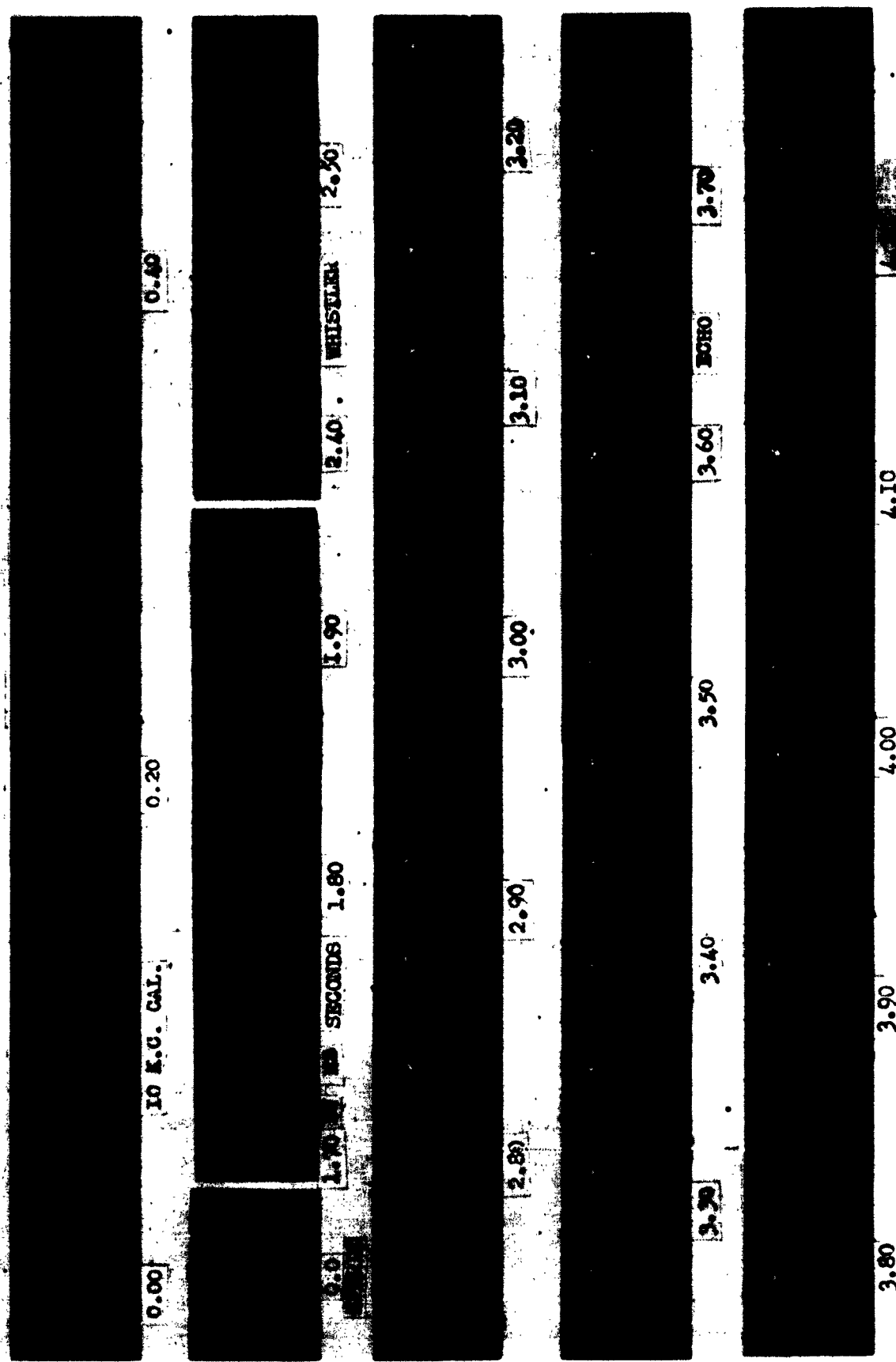
FIG. 5.5. WAVEFORMS AND LISSAJOUS PATTERNS OF STANFORD WHISTLER OF
4 MARCH 1956 0404 UT.
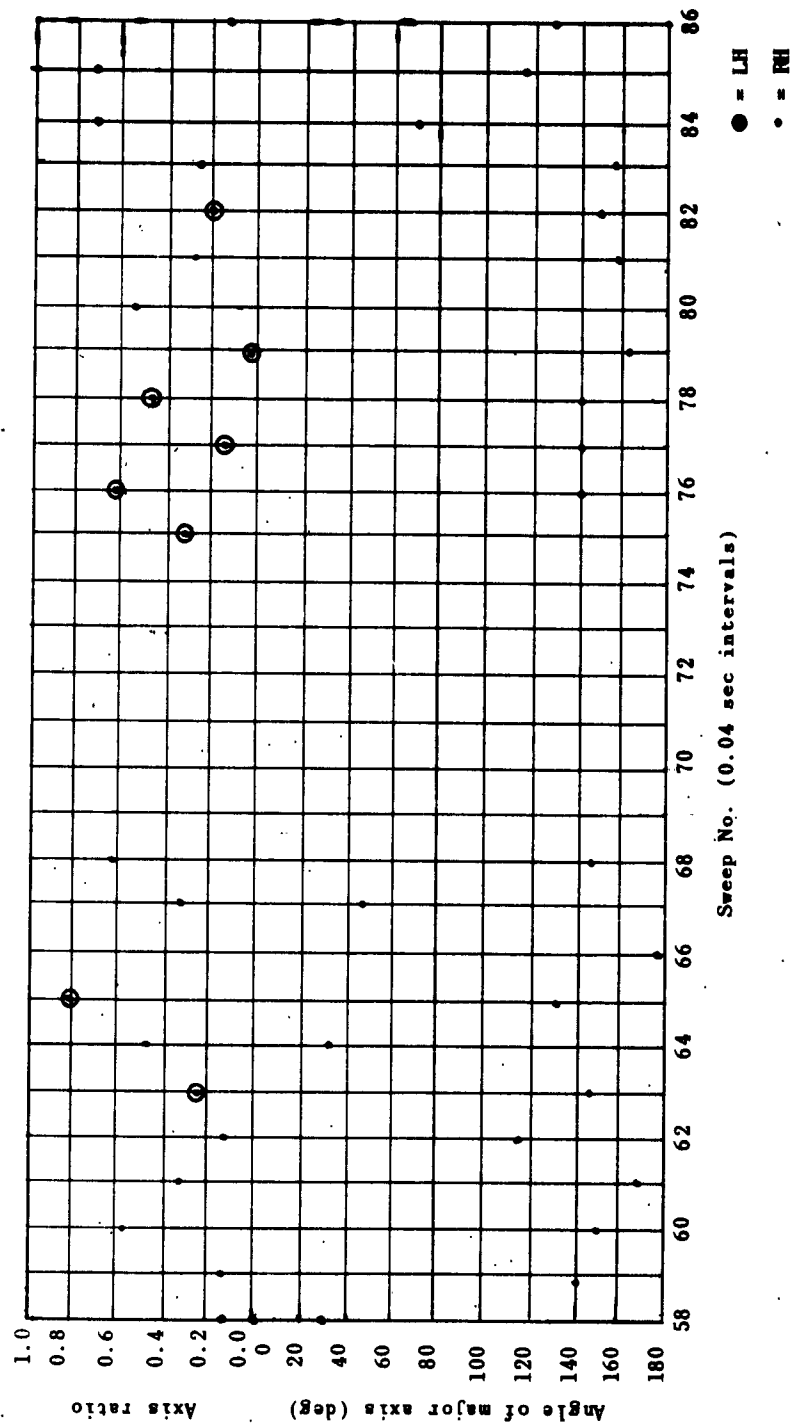
FIG. 5.6. CHARACTERISTIC OF LISSAJOUS PATTERN ELLIPSE OF STANFORD WHISTLER OF 4 MARCH 1956 0404 UT.

Let us consider the behavior of v_R in terms of the Lissajous pattern. Each time the real part changes sign from + to - it indicates a shift of the ellipse from the first and third quadrants to the second and fourth. Each change in sign of the imaginary part indicates a change in the direction of rotation, and would not be visible in the photographs, but can be determined from the waveforms. Appendix D gives details and curves for converting the real and imaginary (X and Y) notation to the axis ratio, ϵ, and tilt angle, $\emptyset$, of the major axis for any ellipse. Essentially linear polarization occurs where Y is very small compared to X. Circular polarization occurs where X is very small and Y is near unity. Both these cases occur in the calculated curves and in the experimental data.

A linear pattern occurs in Fig. 3.23 for 2.2 kc, and an essentially circular one for about 2.35 kc. The only features of the Lissajous pattern that can be called characteristic for any parameter are those for short distances and for low values of ω_r, such as in Fig. 3.29. The latter occurs for values of ω_r too low for actual ionosphere conditions.

The curves for D = 2000 km are considerably smoother than the 500-km and 1000-km curves, especially for the higher frequencies. The values sometimes fluctuate considerably, and sometimes form a fairly smooth curve over part of the frequency range. Consider Fig. 3.25. The curves are fairly smooth in the range around 10 kc. The pattern at 10.22 kc corresponds to a roughly linear polarization with $\emptyset = -58^\circ$ and $\epsilon = 0.12$. The pattern then changes smoothly with frequency, with X passing through 0 at f = 10.5 kc. This pattern would be an ellipse with the axis horizontal. The pattern remains approximately the same in a range around 12 kc, where $\emptyset \cong -60^\circ$ and $\epsilon \cong 0.40$. It then changes smoothly again until f = 14 kc, where the pattern is circular. It then passes through a very small linear pattern at f = 14.5 kc, and then starts more rapid changes. At 15.4 kc the pattern is tilted to $\emptyset \cong 85^\circ$ and $\epsilon \cong 0.3$. By 15.5 kc, it has changed to $\emptyset \cong +79^\circ$ and $\epsilon \cong 0.025$. This yields an ellipse with its axis almost vertical changing into a similarly oriented, almost linear pattern.

It is evident from the above description, that the variations in the calculated patterns very much resemble those seen in the experimental data, as in Fig. 5.4, which shows the Lissajous patterns of the 4 March 1956 whistler. The variations are sometimes fairly periodic, and a period which occurs in a frequency interval 1 to 1.5 kc can be identified. Let us determine the time interval involved.

The dispersion equation for a whistler is:[1]

$$D = t \sqrt{f}$$

where t = elapsed time from the occurrence of the initiating pulse in sec.

f = the instantaneous frequency in cps

D = the dispersion of the whistler in $\sec^{1/2}$

The variations of the 4 March 1956 whistler, shown in Fig. 5.4 and occurring at about 1.7 sec, correspond to the second trace of the whistler with a dispersion $\approx$ 175 $\sec^{1/2}$ and a frequency of about 10 kc. When values of the 1 and 1.5 frequency change are substituted into Eq. (5.1), the values of Δt are approximately 0.10 and 0.15 second. This is in the upper range of the experimental period of 0.04 - 0.13 second determined for the whistlers.

The isolated points in Fig. 5.6, which show a different direction of rotation of the ellipse from those on either side, are also of interest, as the same sort of behavior is evident at times in the calculated curves. The reversal of rotation occurs each time the imaginary part of v_R changes sign. Examples of the isolated points occur at 11.6 and 15.4 kc in Fig. 3.23. Other cases of reversal were evident on curves not reproduced here. The only feature of the experimental data on the Lissajous patterns that is not generally reproduced is that which occurred in the 13 September 1955 whistler. No reversal in the direction of rotation is apparent for that one whistler. Some reversal is generally expected. The only exception which would be expected in general is for whistlers close to vertical incidence, for which the pattern is essentially constant. This may mean that the distance was in the intermediate range, where not enough variation in the imaginary part of v_R is present, so that its sign does not change.

- 137 -

Another feature of interest is the algebraic signs of the real and imaginary parts of v_R. It might seem reasonable at first that the imaginary part should have the sign corresponding to the direction of rotation of the signal in the ionosphere. An examination of the curves shows that the calculated direction of rotation of the crossed-loop Lissajous pattern is as often of one sign as the other when the entire frequency range is considered.

Let us examine the meaning of the sign of the real part of v_R. It indicates which set of quadrants the ellipse occupies. Changing $\emptyset_g$ has the effect of rotating the ellipse relative to the coordinates. Therefore, the sign and range of the real part depends upon the direction of arrival relative to $\emptyset_g$. For a particular direction, then, it is possible that the value of the real part may have an average that is positive, negative, or zero.

The behavior of v_R is of interest also because of its effect on the error in goniometer systems. It was noted on page 104 and page 110 that the sign of the theoretical error in the goniometer and goniometer-vertical system was determined by the sign of X, the real part of the complex polarization. In the actual situation, the polarization is not defined for those conditions wherein there is no equivalent plane wave. If the meaning of the goniometer maximum/minimum ratio is considered, it is readily seen that the null occurs at the angular position of the minor axis of the crossed-loop Lissajous pattern ellipse. The Lissajous pattern ellipse is actually a representation of the goniometer voltage as a function of goniometer angle. There should be a relation between v_R and the bearing error. This relation will be examined in the next section.

D. GONIOMETER AND GONIOMETER-VERTICAL NULL CHARACTERISTICS

.Now let us consider the goniometer null bearings as calculated. Figures 5.7 and 5.8 show typical goniometer voltage curves. Figure 3.22 shows the real and imaginary parts of v_R vs frequency for the same conditions as in Figs. 5.7 and 5.8. A comparison of Figs. 5.7 and 5.8 with Fig. 3.22 shows that the bearing error changes sign when the real part of v_R changes sign. This is to be expected because of the analogy

- 138 -
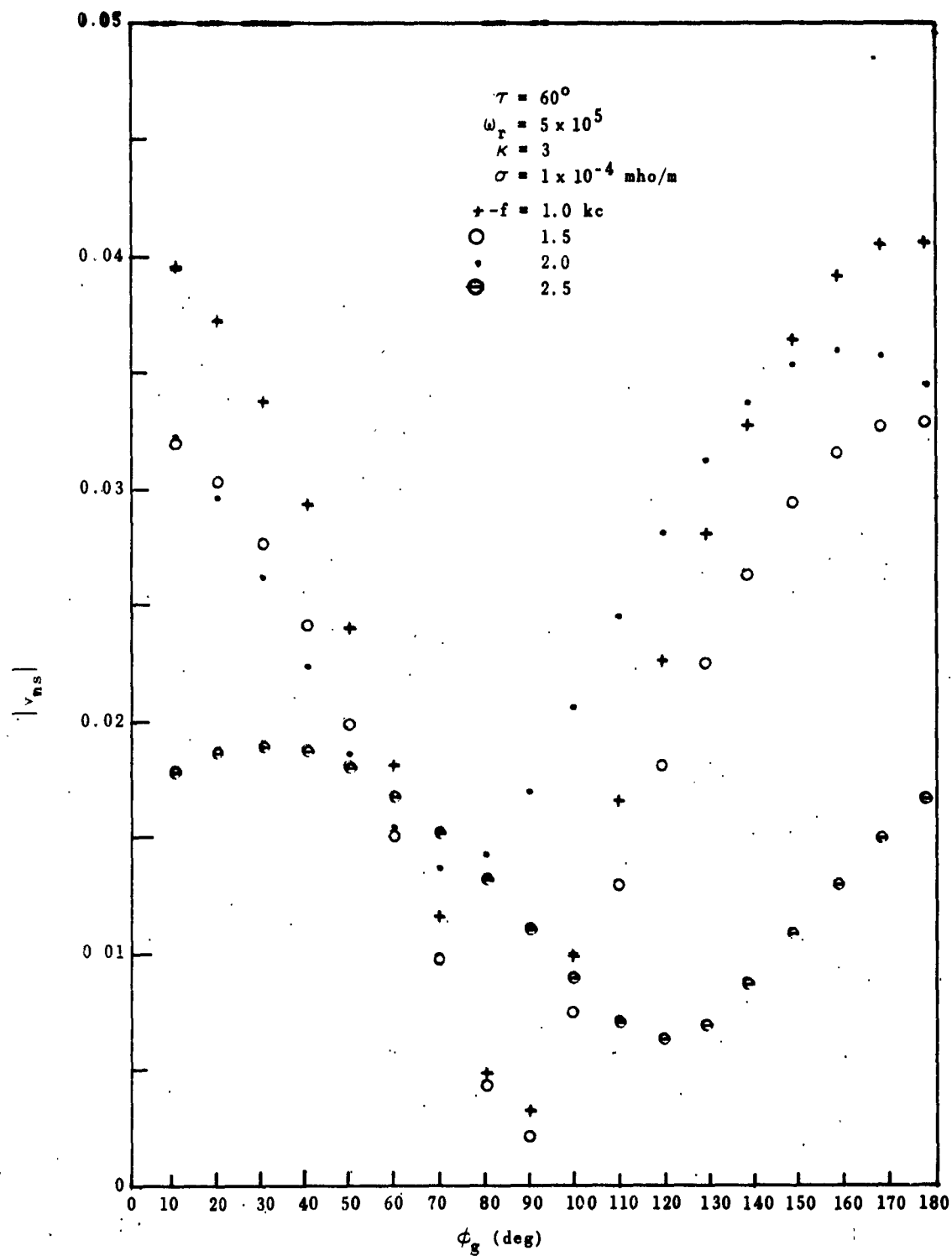
FIG. 5.7. CALCULATED MAGNITUDE OF GONIOMETER VOLTAGE VS ϕ_g, FOR f = 1.0, 1.5, 2.0, 2.5 kc SUMMER-NIGHT MODEL IONOSPHERE, POOR GROUND, D = 500 km.

- 139 -
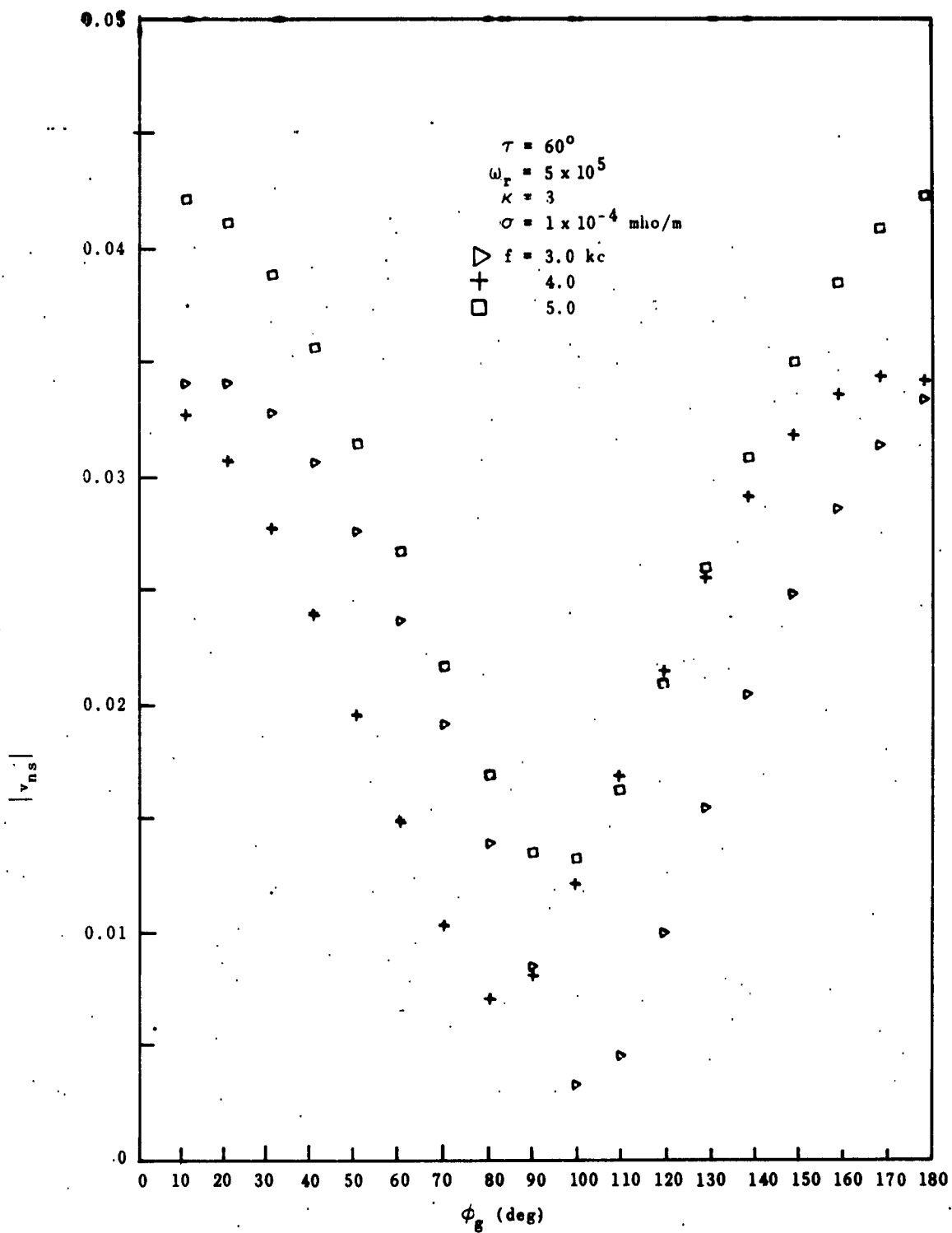
FIG. 5:8. CALCULATED MAGNITUDE OF GONIOMETER VOLTAGE VS ϕ_g, FOR
f = 3.0, 4.0, 5.0 kc, SUMMER-NIGHT MODEL IONOSPHERE, POOR GROUND,
D = 500 km.

between v_R and the Q used in the single-ray goniometer equations. The sign of the bearing error changes whenever the sign of X in the equations for bearing error is changed. The behavior of v_R is therefore significant, since the sign of the real part of v_R determines the sign of the bearing error. It was previously noted that the average value of the real part of v_R could tend toward any value. The average depends upon the distance, frequency, and all the waveguide parameters. The average error could therefore be improved if bearings of a single exit point are obtained over a wide range of conditions and frequencies.

Sometimes several whistlers are received over a period of several minutes to several hours. Each has the same characteristic frequency-vs-time variation. There is reason to believe that these arise from a single propagation path and from a single exit point. The goniometer nulls would occur at different frequencies on each whistler, since the rotation is random with respect to the time of occurrence. The averaging of bearings from these whistlers should reduce the error. This is not true in the case of the series of whistlers received on 26 September 1960. The exit-point is apparently near the line joining the two d-f stations and the d-f error is very large.

Figure 5.9 shows the deviation of the bearing of a whistler (Stanford 10 April 1960, 0941/46UT), obtained at different frequencies, from the average for that whistler. The bearing errors computed for conditions of Figs. 5.7 and 5.8 are also shown in Fig. 5.9. A wide variation in apparent direction occurs in both the measured and the calculated points. The standard deviation of the measured points is approximately 20 degrees, while that of the calculated points is approximately 10 degrees. This difference is too great to be explained by measuring error which was estimated on page 115 to be $\pm$ 2 - 4 degrees. The bearings on another whistler recorded an hour later had a standard deviation of 15.

The calculated results show that the bearing errors are a very complicated function of all the variables. The magnitude of the error varies widely under all conditions. The large variations of the measured bearings is what would be expected for any conditions other than nearly

- 141 -
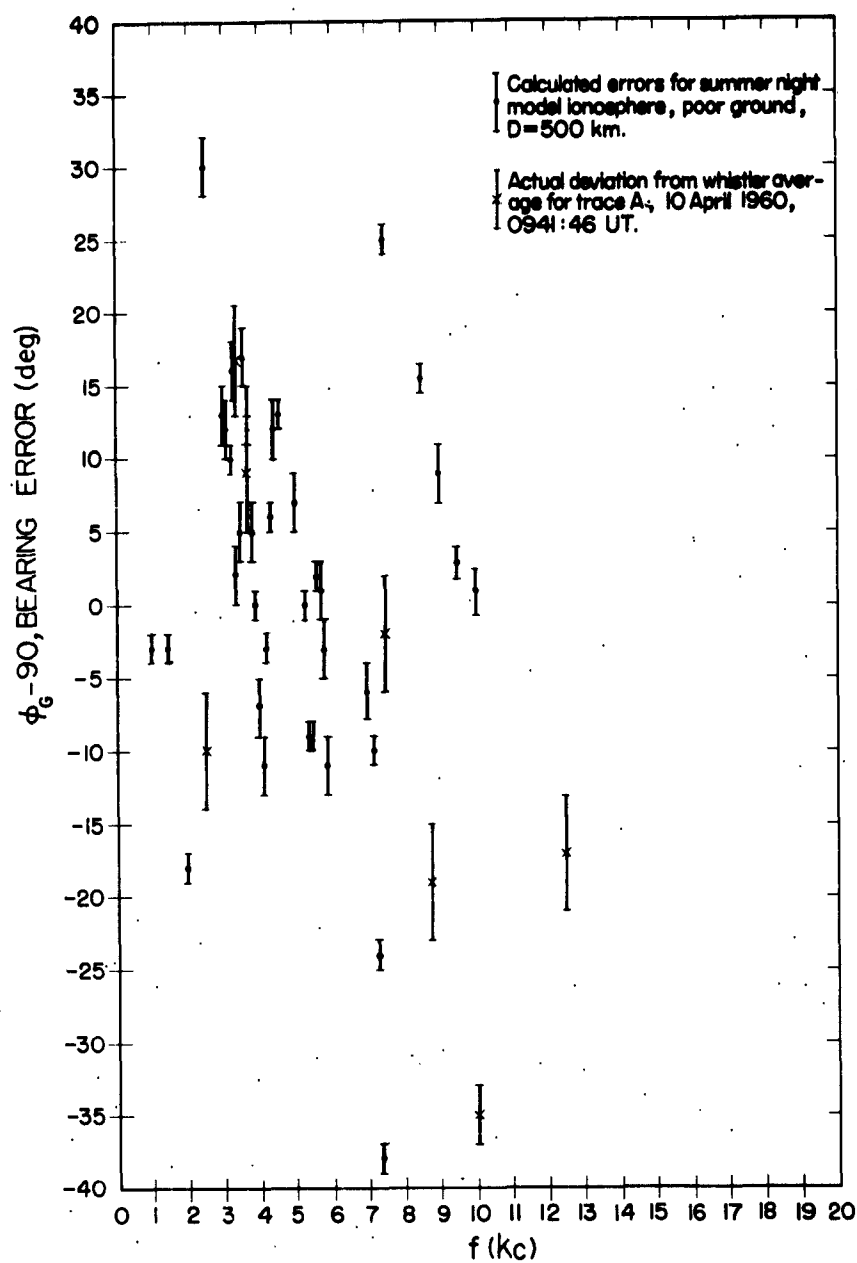
FIG. 5.9. CALCULATED BEARING ERRORS FOR SUMMER-NIGHT MODEL IONOSPHERE, POOR GROUND, D = 500 km, AND MEASURED BEARING ERRORS FOR WHISTLER OF 10 APRIL 1960 AT 0941:46 UT, VS FREQUENCY.

vertical incidence. This follows from the fact that the behavior is related to v_R and β_A, which vary widely with distance, ionosphere parameters, etc.

The next step is to compare some of the calculated bearing errors and null ratios for the goniometer system with those calculated for the goniometer-vertical system. Some typical curves for the latter are plotted in Fig. 5.10 for the same conditions as in Figs. 5.7 and 5.8 for the goniometer. These values are shown in Fig. 5.10 and compared in Table III. It is evident from Fig. 5.9 and Table III that a result not forseen from the simple plane-wave theory of the goniometer-vertical system has appeared here. The calculated errors for the goniometer-vertical are generally considerably larger than those for the goniometer alone. When the presence of multiple rays is considered, this result is reasonable. The main null of the goniometer-vertical depends upon the difference between the normal loop and the vertical monopole antenna voltages. When multiple rays are present, these voltages do not have a fixed relationship, in contrast to the single-ray situation. Since the null depends upon the difference between these voltages, the error would be expected to vary considerably. Note that the computed average bearing error is still of the order of the average scaling error $(2 - 4^\circ)$.

It will be noted, however, that the nulls are generally much deeper for the goniometer-vertical than for the goniometer alone. The nulls for the goniometer are always symmetrical and narrow. The nulls for the goniometer-vertical are generally broad and asymmetrical near the bottom, due to the multiple nature of the nulls.

The records must be analyzed on a spectrum analyzer. In normal operation it is the practice to reduce the signal to the level at which only the peaks of the desired signal are recorded. Interfering signals are reduced as much as possible in this manner. Spectrum analyzers always have a limited dynamic range. A value of 6 db is typical. Therefore, only the upper part of the pattern is generally evident on the spectrogram. If the measurement is made on the upper part, say the upper 6-db range, the asymmetry is almost removed. The error measured in this way is generally of the same order as the goniometer null error. The fourth column in Table III indicates this fact.

- 143 -
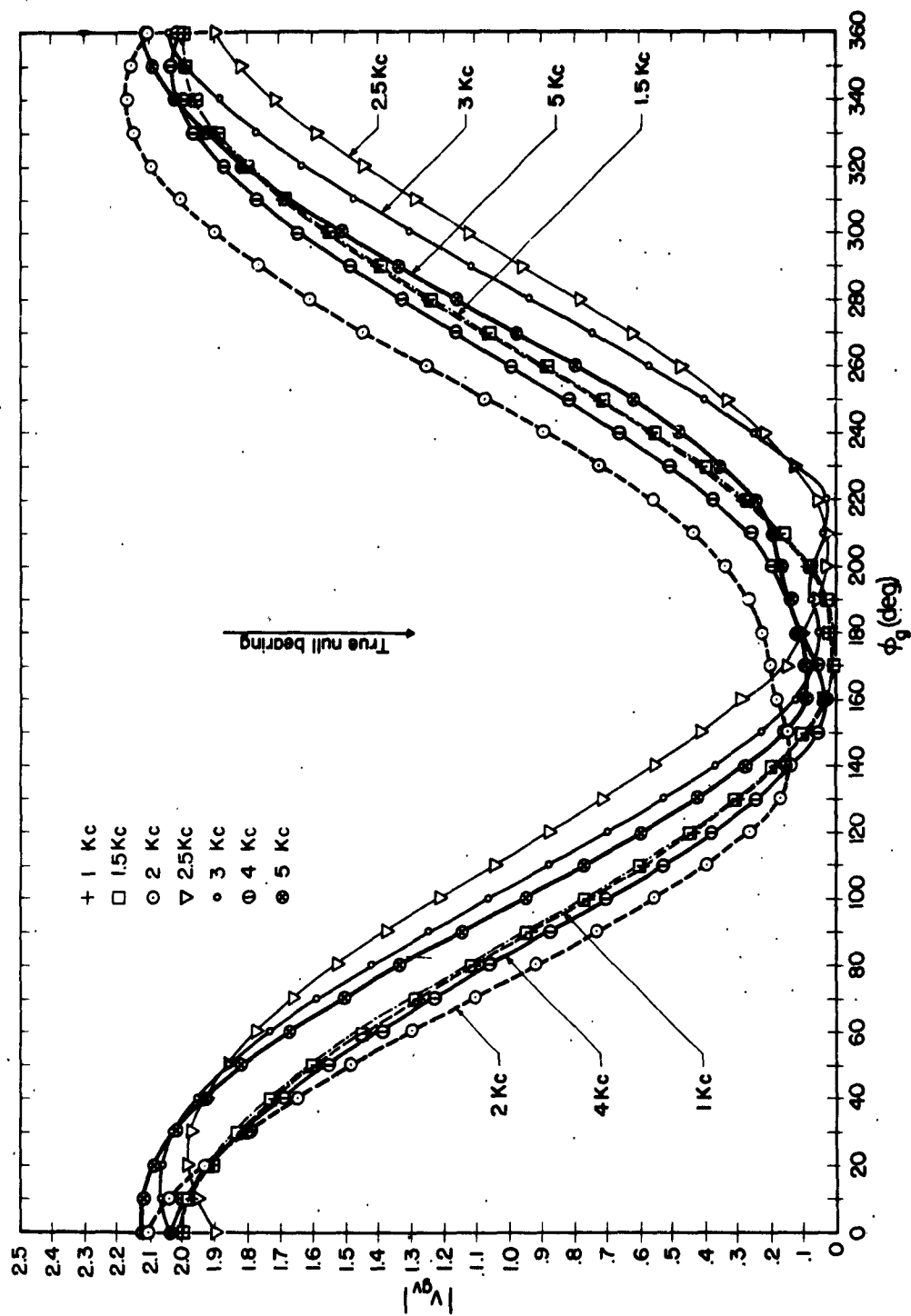
FIG. 5.10. CALCULATED MAGNITUDE OF GONIOMETER-VERTICAL VOLTAGE VS ϕ_g FOR $f = 1.0, 1.5, 2.0, 2.5, 3.0, 4.0$ kc AND 5.0 kc, SUMMER-NIGHT MODEL IONOSPHERE. POOR GROUND, $D = 500$ km.

f (kc)	Bearing error			Max/min ratio	
	Goniometer	Goniometer-vertical	-6 db goniometer-vertical	Goniometer	Goniometer-vertical
1.0	-3±1	-9±2	-3.5±2	16	154
1.5	-3±1	-8±2	-3.5±2.	19.5	500
2.0	-18±1	-38±2	-18.5±2	9.5	15
2.5	+30±2	+28±3	+1.5±3	3	74
3.0	+13±2	+40±2	+13.5±2	11	55.3
4.0	-7±2	-20±2	8.0±2	7	67.7
5.0	-7±2	-15±3	+5.0±3	3	23.7
Average	+0.7	-3.1	-1.9		

E. THE ANGLE ϕ_a AND LATERAL DEVIATION

The angle ϕ_a is the bearing angle of the equivalent plane wave as defined on page 34. It depends on the relative amplitudes and phases of the voltages from the three antennas. In general, it differs from the true bearing of the individual rays which are assumed to arrive from the great circle bearing. This phenomenon, which we shall call apparent lateral deviation, is separate from the polarization error, which is accounted for in Eqs. (2.81) through (2.88).

The phenomenon of lateral deviation has been observed over a wide range of frequencies for several years.[37,38] It is characterized as the arrival of a signal from a bearing apparently different from the great circle bearing. At vlf, this phenomenon is associated with the difference in the sums of the multiple rays that make up the total field at different antennas. The non-plane-wave character of the received field for some conditions is a related result. Apparent lateral deviation is the result of the presence of multiple rays. Polarization error can occur from a single ray.

The calculated angle ϕ_a is plotted as a function of frequency for different distances, ionosphere conditions, and ground constants in Figs. 3.35 through 3.45. It is readily apparent that the value of ϕ_a is highly variable. It is also apparent that its average value tends to zero (i.e., zero average error) for a large range of frequencies, distances and waveguide parameters. The significance of this is again that an average over a large number of measurements under varied conditions will approach the true bearing, even though individual errors may be large. This behavior is similar to the effect noted for goniometer bearing error. The errors due to apparent lateral deviation are sometimes difficult to separate from polarization error. The best example of this separation is in the case of D = 0.1 km. The variation in angle ϕ_a, shown in Fig. 3.36 is similar to the field strength variation, while the polarization is essentially constant.

F. THE CHARACTERISTICS OF A WAVE ARRIVING FROM THE MAGNETIC FIELD
    DIRECTION

A set of calculations was carried out for a distance of 47.23 km for sea water and summer-night model ionosphere. At this distance the n = 0 ray is parallel to the earth's magnetic field at the geomagnetic latitude of Stanford (44°N). This was done for the particular purpose of determining the characteristics of a wave arriving from the magnetic field direction. Such a signal would actually be made up of the n = 0 ray plus other higher-order rays of significant amplitude.

The fields are shown in Fig. 3.64 as a function of frequency. The patterns for the NS (normal) and EW (abnormal) loops are similar, with the EW loop voltage about 20% less than the NS loop. The pattern of the vertical-incidence field variation is quite well retained, with the peaking near the frequencies for which h' is an odd multiple of one-half wavelength. The apparent polarization is almost constant, as shown by Fig. 3.65. The Lissajous-pattern ellipse has an axis ratio of about 0.85 - 0.9 and its major axis is oriented within $\pm 15^{\circ}$ from the vertical for ϕ_g equal to zero.

The behavior of these curves is typical of a wide range of ionosphere and ground conditions. It is thus apparent that if a whistler came from the field direction, it would have the characteristics of short-distance propagation, with the distinctive apparent polarization pattern and variations in field strength. The latter should be apparent on spectrograms. In addition, the vertical-antenna voltage would be only about half the loop-antenna voltage. These facts make it quite apparent that only a very few whistlers have the field characteristics compatible with arrival from the magnetic field direction, and none has been observed with the proper apparent polarization. It is concluded therefore that whistlers do not arrive from the direction of the magnetic field.

G. WHISTLERS WITH FAIRLY CONSTANT APPARENT POLARIZATION

A few whistlers have been observed with fairly constant apparent polarization. The crossed-loop Lissajous patterns were observed visually by the author at Stanford on 27 May 1959, about 0730Z. All showed elliptical patterns on the crossed loops. The axis ratio varied from about 0.1 to 0.9. The major axis tended to be oriented at about 45° clockwise from north. There were some rapid variations in the pattern, but the visual integration effect made it difficult to notice details. The exit-point of these whistlers was probably nearby, to the northwest or southeast. Their pattern orientations were not compatible with the possibility of arrival from the magnetic field direction. One almost linear pattern was observed (axis ratio about 0.1) which was oriented almost due east-west. An explanation for this might be a long distance with low ionosphere reflection coefficients and poor ground conductivity. None of the available calculations explain this observation.

VI. CONCLUSIONS AND RECOMMENDATIONS

A. CONCLUSIONS

The ray-theory method used in this report utilizes the following simplifying assumptions: (1) each ray is a plane wave in the antenna area, (2) the ql approximation is valid (3) the ionosphere may be represented by an equivalent homogeneous model with a sharp lower boundary, (4) the necessary cone of plane wave energy is available for excitation, (5) all the rays are of a single frequency. This simplified method of adding multiple rays can still account for most of the previously unexplained characteristics found in a variety of experimental data. These include the variations with frequency in the shape and position of the crossed-loop Lissajous patterns, the changes in the direction of rotation of these patterns and the wide variation with frequency of the goniometer null bearings and ratios. This agreement with experimental data is not on a point-for-point basis. The behavior under specified conditions is an extremely complicated function of all the variables. It is possible that a correlation on a point-for-point basis might be found between a particular whistler and a particular set of conditions. The investigation of this possibility would be far too costly, and the required conditions might not be unique. The agreement is in the types of behavior, particularly that of the crossed-loop Lissajous patterns. This type of behavior was not explained prior to this work.

The results show that whistlers do not generally arrive from the direction of the magnetic field, contrary to the conclusion which has sometimes been reached from earlier theories. Any whistler which does arrive from the magnetic field direction can be identified by its characteristic variations in field strength and crossed-loop Lissajous pattern with frequency. The results are also consistent with the hypothesis that whistlers emerge from a relatively small area in the lower edge of the ionosphere, and that this exit point may be at a considerable distance from the receiver. The average difference between the measured d-f latitudes and those calculated independently from the dispersion characteristics is roughly what would be expected from the

calculated bearing **errors.** **Therefore, the exit** point **location, and**
presumably the path location, **is well described by this calculated**
magnetic latitude. The occasional large discrepancies between the d-f
and dispersion results can be accounted for by d-f error.

The variation in the observed bearings with frequency does not
indicate a variation in the exit point location, since the variation in
bearing is consistent with that calculated for a fixed location.

Consideration of the series of rays which determines the field com-
ponents for the vertical loops and monopole yields an explanation for
the phenomenon of apparent lateral deviation at vlf. No actual lateral
deviation need be present. The same effect produces the difference in
field strength measured from a normal loop and from a vertical monopole,
which is a previously unknown factor in the error in field-strength
measurement at vlf. A consideration of the total wave field present
should be made before interpreting measurements made with antenna
systems measuring more than one component of the total field. The
coupling of cross-polarized components due to the earth's magnetic field
is important in this case. Care must be exercised, when using the results
of measurements on fields generated from a single polarization component,
to predict the characteristics of a wave in which both components are
originally excited.

The results of the calculations show that a vertical monopole is
as effective as a vertical loop for whistler signals coming from all
distances beyond about 60 km, which includes almost all whistlers.
The orientation of a loop antenna is not important at the low frequencies
(around 5 kc) but can reduce the received signal by at least 6 db at the
higher frequencies (around 15.5 kc). The radius of the effective-area
circle for a whistler, for 20 db reduction in signal from the center to
the edge, is shown by the calculations to be approximately 1000 km.
This value is consistent with experimental data. The theoretical re-
sults for the goniometer and goniometer-vertical systems show that the
null bearing error in the case of a single ray is much smaller for the
goniometer-vertical system than for the goniometer. The calculations
show that the actual null bearing error of the goniometer-vertical in
the case of a series of incident rays is considerably greater than that

of the goniometer. This results from the fact that the parallel component of the field seen by the loop is different in both amplitude and phase from that seen by the vertical monopole. The calculated values of bearing error show that the two systems have nearly the same average error when the nulls are measured properly. The theoretical increase in null ratio of the goniometer-vertical system over the goniometer for a single ray is also realized for multiple rays. The calculated results show that the signal strength tends to be appreciably greater over a sea-water path compared with a path over poor ground at frequencies in the 15 - 20 kc range. This increase may amount to as much as 15 db for long distances (2000 km). At the lower frequencies, the difference is relatively small, being about 10 db at 5 kc.

The results show that the best d-f system would be one that utilized identical antennas. In this case the amplitude of the signal would be independent of the bearing of the signal. The bearing would therefore depend only upon the relative phases of the antenna voltages. A system that fits these requirements is an Adcock array, made up of four vertical monopoles arranged in a square. The difference between the signals from antennas in opposite corners is taken, and the two resulting differences applied to a goniometer to determine the bearings.

The errors in a properly adjusted Adcock array are more subtle than those in a loop system. The polarization and lateral-deviation errors are eliminated. The antennas respond only to the parallel component of the field seen by a vertical monopole. The difference in the signals obtained from a pair of antennas in the plane of an arriving plane wave is thepretically zero. Any null bearing error, therefore, must arise either from a non-plane wave front in the antenna area, or from site errors.

There are numerous practical problems involved in the Adcock system. The antenna spacing must be large enough to make voltages large compared to system noise. Small antenna spacings increase the relative errors due to unbalance in the system.

B. RECOMMENDATIONS FOR FUTURE WORK

1. Further study of ray theory is needed in order to establish in a more quantitative way the regions of validity. The possible advantages of mode theory for the study of whistler propagation should be studied. There is great need for a definitive work on this subject which states the restrictions on each method. More detailed physical interpretations of the ray and mode theories seem to be needed.

2. A more accurate model of the lower region of the ionosphere should be developed. The use of a homogeneous model with a sharp lower boundary at vlf is a rather rough approximation and probably results in significant errors for some conditions of interest, particularly at low frequencies. Consideration should be given to the use of a two or three slab model to account for the increased penetration at low frequencies and for absorbing regions below the reflection point.

3. The characteristics of propagation for conditions under which the ql approximation is not valid should be studied further. This should probably be done in combination with the multi-slab model, since both approximations are not necessarily applicable under some conditions of interest.

4. In problems for which the sharp-boundary homogeneous model and ql approximation are valid, better values of the parameters ω_r and τ are needed. It is suggested that total field information be obtained from ground-to-ground measurements to provide an experimental determination of τ.

5. The same ray-theory methods may also be used to calculate the excitation of a whistler duct by a series of rays transmitted into the ionosphere from the waveguide. The results would be valuable for the determination of transmission losses and duct sizes in whistler-mode propagation.

6. The effect of the difference in the frequency of the rays for a whistler at near-vertical incidence deserves more investigation. The steady-state calculations show regular sharp maxima and rather broad minima at harmonic frequencies. The introduction of different frequencies would undoubtedly change the shape of and displace the positions of the

maxima and minima. It would also produce an amplitude fluctuation of a
few db as a result of beating of different frequencies. It could be
studied by the present method if the exact frequency were used for each
ray and a very large number of calculations were made at very slightly
different frequencies. The cost of the calculation would be prohibitive
at present. It is probable that useful information could be obtained
by the use of a simple analog device, consisting of a shorted trans-
mission line.

7. Further studies of whistlers with the present antenna system
are not warranted. The accuracy is too limited to be of further interest.
The development of an Adcock system, as previously described, would be
of great interest. The increased accuracy of each bearing and the in-
crease in the number of whistlers showing nulls should make the project
well worth the development effort. The system could also be applied to
the study of whistler-mode echoes from fixed-frequency vlf transmitters.
Presentation of the Lissajous patterns from the two pairs of antennas
would provide a presentation like that of the standard d-f trace which
would be free of polarization error.

A recording technique using an intensity-modulated sweep triggered
by the goniometer indexing pulse would probably enable direction measure-
ments to be made on vlf transmitters when ordinary cw traffic is being
transmitted. This would permit continuous recording instead of requiring
special pulse programs as at present.

APPENDIX A. PATH GEOMETRY EQUATIONS

The path geometry equations used in this report are slightly modified versions of those used for the usual case of ground-to-ground transmission. The expressions for a single trip between earth and ionosphere are given by Helliwell[20] in this form:

$$P_n^2 = 2R(h' + R)[1 - \cos(180D/\pi R)] + h'^2 \qquad (A.1)$$

$$\theta_n = \tan^{-1}[\sin(180D/\pi R)/1 + h'/R - \cos(180D/\pi R)] \qquad (A.2)$$

$$\beta_n = 90 - \theta_n - (180D/\pi R) \qquad (A.3)$$

where

P_n = ray path distance for a single trip from ionosphere to ground.

θ_n = angle of incidence at the ionosphere in degrees.

β_n = angle of take-off or arrival at the earth, in degrees.

h' = virtual height of the ionosphere in km.

D = total ground distance in km.

R = mean earth radius, in km, equal to 6367.39 km.

These equations must now be generalized for the case of n reflections from the earth and ionosphere, with transmitter located at the ionosphere, and receiver at the ground. The situation is illustrated in Fig. 2.1, where the case of n = 2 is illustrated. It is readily seen that the equations may be generalized to this case by merely dividing the total distance by the factor $(2n + 1)$. The equations then become:

$$P_n^2 = 2R(h' + R)\left\{1 - \cos[180D/(2n+1)\pi R]\right\} + h'^2 \qquad (A.4)$$

$$\theta_n = \tan^{-1}\left\{\sin[180D/(2n+1)\pi R]/1 + h'/R - \cos[180D/2n+1)\pi R]\right\} \qquad (A.5)$$

$$\beta_n = 90 - \theta_n - 180D/(2n+1)\pi R \qquad (A.6)$$

Then the total path distance R_n and the phase $\angle T_n$ are given by

$$R_n = (2n+1)P_n \qquad\qquad (A.7)$$

$$\angle T_n = -R_n \left(\frac{360\,f}{c}\right) \text{ degrees}$$

These equations yield all the necessary information about the path geometry for solution of the problem.

APPENDIX B. THE REFLECTION COEFFICIENTS

The ionospheric reflection coefficients used in this report are those derived by Budden[12] and are listed in the form given by Wait:[13]

$$_\parallel R_\parallel = [(\mu_o + \mu_e)(C^2 - C_o C_e) + (\mu_o \mu_e - 1)(C_o + C_e)C]/D \tag{B.1}$$

$$_\parallel R_\perp = 2jC(\mu_o C_o - \mu_e C_e)/D \tag{B.2}$$

$$_\perp R_\parallel = 2jC(\mu_o C_e - \mu_e C_o)/D \tag{B.3}$$

$$_\perp R_\perp = [(\mu_o + \mu_e)(C^2 - C_o C_e) - (\mu_o \mu_e - 1)(C_o + C_e)C]/D \tag{B.4}$$

where

$$D = (\mu_o + \mu_e)(C^2 + C_o C_e) + (\mu_o \mu_e + 1)(C_o + C_e)C$$

$$C = \cos \theta_n$$

$$C_o = \cos \theta_o$$

$$C_e = \cos \theta_e$$

The subscripts o and e refer to the ordinary and extraordinary waves, respectively. As in Chapter II, the whistler mode is called the ordinary wave, in keeping with the notation and derivation used in the references.

The ground reflections are expressed by the Fresnel coefficients as given by Wait[42] and Jordan,[43] with the take off or arrival angle β_n substituted in the proper manner for the angle of incidence. This substitution yields:

$$R_\perp = \sin\beta_n + (N^2 - \cos^2\beta_n)^{1/2}/\sin\beta_n - (N^2 - \cos^2\beta_n)^{1/2} \tag{B.5}$$

$$R_\parallel = N^2 \sin\beta_n - (N^2 - \cos^2\beta_n)^{1/2}/N^2 \sin\beta_n + (N^2 - \cos^2\beta_n)^{1/2} \tag{B.6}$$

where

$$N^2 = \frac{\kappa}{\kappa_0} - \frac{j\sigma}{2\pi\kappa_0 f}$$

σ = conductivity of the ground in mho/m.

κ/κ_0 = dielectric constant of the ground.

κ_0 = permitivity of free space in fd/m.

f = wave frequency in cps.

The other conventions such as the field component indicated are the same as those in previous sections.

APPENDIX C. THE COMPUTER PROGRAM

The calculations of the total field and the antenna response were carried out at first on the IBM 650 digital computer at the Stanford Computation Center. The Bell system with a complex arithmetic subroutine was used. The running times were found to average at least 2 minutes per n, where n is the number of reflections for each reflection from the earth and ionosphere. The total time per calculation was therefore very long, the minimum being about 20 minutes. A hand calculation was performed as a check on the programing and operation. A standard test program was run regularly as a check.

During the calculations a Burroughs 220 computer became available. The program was then re-written for the 220, using the "Bleap" assembler system. A complex arithmetic subroutine was written for Bleap for this project. Intermediate data, including all the important path parameters, the results for each value of n, and the final results, were recorded on magnetic tape by the program. These results could later be taken off the tape, the decimal point fixed, and cards punched for use on an X-Y plotter. Considerable time was saved by reproducing most of the curves directly on Multilith mats with this machine.

The new program gave an approximate speeding-up factor of thirty to one in calculating time. The running times range from about fifty seconds for n = 4 to about 400 seconds for n = 50. The program can calculate a maximum n equal to 97.

The programing was organized in a system of subroutines to enable the use of these subroutines for other programs, if desired.

The calculations of the curves for the phase shift ellipse conversion were performed on the IBM 650, again using the Bell system routine. The calculations of theoretical null ratio and bearing error were also done in the same system on the 650.

The d-f location program was aided by another pair of routines, also written in the Bell system for the 650. These routines solved the spherical-trigonometry equations to determine: (1) the bearing and distance between any pair of points on the earth's surface, when the latitude and longitude are given; and (2) the latitude and longitude

of the "target" when the latitude and longitude of, and the bearing from, up to five stations are given. The equations are solved for each pair of stations giving bearings; for example: one location with two stations; three with three stations; six with four stations, etc. This solution was always accurate to at least the nearest one-tenth degree, so that the location accuracy was never limited by these calculations. The running times were 5 - 10 seconds and about 20 seconds for the two respective routines.

APPENDIX D. THE PHASE SHIFT ELLIPSE CHARACTERISTICS

A common problem in the use of Lissajous pattern ellipses is that of converting the pattern specified by an axis ratio ϵ and an orientation of the major axis into the equivalent complex form: $\frac{y}{x} = X + jY$. In order to facilitate this conversion, a pair of conversion formulas were derived in the following manner:

Let the vertical and horizontal deflections be given by:

$$y = A \sin \omega_t \tag{D.1}$$

$$x = A_x \sin (\omega_t + \theta) \tag{D.2}$$

Equation (D.2) can be expanded to yield:

$$x = A_x(\sin \omega_t \cos \theta + \cos \omega_t \sin \theta) \tag{D.3}$$

Now, substituting (D.1) in (D.3) and substituting $R = A_x/A$, rearranging and squaring, yields:

$$A_x = A_x \left(y \cos \theta + \sqrt{1 - \frac{y^2}{A^2}} \sin \theta \right)$$

$$A^2 x - AA_x y \cos \theta = A_x \sqrt{A^2 - y^2} \sin \theta$$

$$A^2(x - R_y \cos \theta) = AR \sqrt{A^2 - y^2} \sin \theta$$

$$A^2(x - R_y \cos \theta)^2 = R^2 \sin^2\theta(A^2 - y^2)$$

Substituting $Q = X + jY = R(\cos \theta + j \sin \theta)$ yields:

$$Y^2(A^2 - y^2) = (x - X_y)^2 \tag{D.5}$$

It can be shown that Eq. (D.5) describes an ellipse; so the next step is to rotate the coordinate axes so that the major axis is aligned with the x axis. A general rotation of $\emptyset$ degrees is expressed by:

$$x = x'\cos \emptyset + y' \sin \emptyset$$

$$y = x' \sin \emptyset + y' \cos \emptyset$$

After this substitution is made, the terms x and y are understood to mean the new coordinate system, which yields:

$$x^2 \left(-Y^2\sin^2\phi - \cos^2\phi - 2X\sin\phi\cos\phi - X^2\sin^2\phi\right)$$

$$+ \; xy \left(+2Y^2\sin\phi\cos\phi - 2\sin\phi\cos\phi + 2X\cos^2\phi - 2X\sin^2\phi + 2X^2\sin\phi\cos\phi\right)$$

$$+ \; y^2 \left(-Y^2\cos^2\phi - \sin^2\phi + 2X\sin\phi\cos\phi - X^2\cos^2\phi\right) + A^2Y^2 = 0 \qquad (D.6)$$

Now, to determine the angle of rotation, the xy term is equated to zero, which puts the equation almost in standard form. This step yields:

$$Y^2\sin2\phi - \sin2\phi + 2X\cos2\phi + X^2\sin2\phi = 0$$

$$\sin2\phi(X^2 + Y^2 - 1) = -2X\cos2\phi$$

$$\tan2\phi = \frac{2X}{1-X^2-Y^2} \qquad (D.7)$$

The tilt angle ϕ of the major axis is determined from Eq. (D.7). The next step is to find the functions of 2ϕ in terms of X and Y, which yields:

$$\cos^2 2\phi = \frac{1}{\sec^2 2\phi} = \frac{1}{\tan^2 2\phi+1} = \frac{(1-X^2-Y^2)^2}{4X^2+(1-X^2-Y^2)^2} = \frac{(1-X^2-Y^2)^2}{D} \qquad (D.8)$$

$$\sin^2 2\phi = \frac{1}{\csc^2 2\phi} = \frac{1}{\operatorname{cth}^2 2\phi+1} = \frac{4X^2}{4X^2+(1-X^2-Y^2)^2} = \frac{4X^2}{D} \qquad (D.9)$$

where

$$D = 4X^2+(1-X^2-Y^2)^2$$

When Eq. (D.8) and Eq. (D.9) are substituted into Eq. (D.6) the result is:

$$x^2\left[-Y^2\left(\tfrac{1}{2}-\tfrac{1}{2}\cos^2\phi\right)-\left(\tfrac{1}{2}+\tfrac{1}{2}\cos2\phi\right)-X\sin2\phi - X^2\left(\tfrac{1}{2}-\tfrac{1}{2}\cos2\phi\right)\right]$$

$$+ \; y^2\left[-Y^2\left(\tfrac{1}{2}+\tfrac{1}{2}\cos2\phi\right) - \left(\tfrac{1}{2}-\tfrac{1}{2}\cos2\phi\right) + X\sin2\phi - X^2\left(\tfrac{1}{2}+\tfrac{1}{2}\cos2\phi\right)\right]+A^2Y^2 = 0$$

- 160 -

$$x^2 \left[-\frac{Y^2}{2} + \frac{Y^2(1-X^2-Y^2)}{2\sqrt{D}} - \frac{1}{2} - \frac{(1-X^2-Y^2)}{2\sqrt{D}} - \frac{2X^2}{\sqrt{D}} - \frac{X^2}{2} + \frac{X^2(1-X^2-Y^2)}{\sqrt{D}} \right]$$

$$+ y^2 \left[-\frac{Y^2}{2} - \frac{Y^2(1-X^2-Y^2)}{2\sqrt{D}} - \frac{1}{2} + \frac{(1-X^2-Y^2)}{2\sqrt{D}} + \frac{2X^2}{\sqrt{D}} - \frac{X^2}{2} - \frac{X^2(1-X^2-Y^2)}{2\sqrt{D}} \right]$$

$$+ A^2 Y = 0$$

The results must now be manipulated into the standard form of $x^2/a^2 + y^2/b^2 = 1$ for an ellipse where a and b are the axes. This operation yields:

$$\frac{x^2}{\dfrac{A^2 Y^2}{(1+X^2+Y^2)\sqrt{4X^2+(1-X^2-Y^2)^2} + [4X^2+(1-X^2-Y^2)^2]}}$$

$$+ \frac{y^2}{\dfrac{A^2 Y^2}{(1+X^2+Y^2)\sqrt{4X^2+(1-X^2-Y^2)^2} - [4X^2+(1-X^2-Y^2)^2]}} = 1$$

The axis ratio ϵ may then be determined from:

$$\epsilon^2 = \frac{a^2}{b^2} = \frac{(1+X^2+Y^2) - \sqrt{4X^2+(1-X^2-Y^2)^2}}{(1+X^2+Y^2) + \sqrt{4X^2+(1-X^2-Y^2)^2}} \tag{D.10}$$

These two equations now make simple the conversion from the complex form to the ellipse constants. The reverse operation is still difficult. The best solution is to plot the curves. The result is Fig. D.1, which shows curves of constant X and Y as a function of ϵ and $\emptyset$. Note that the curves of constant X and Y are nearly orthogonal for most conditions and one
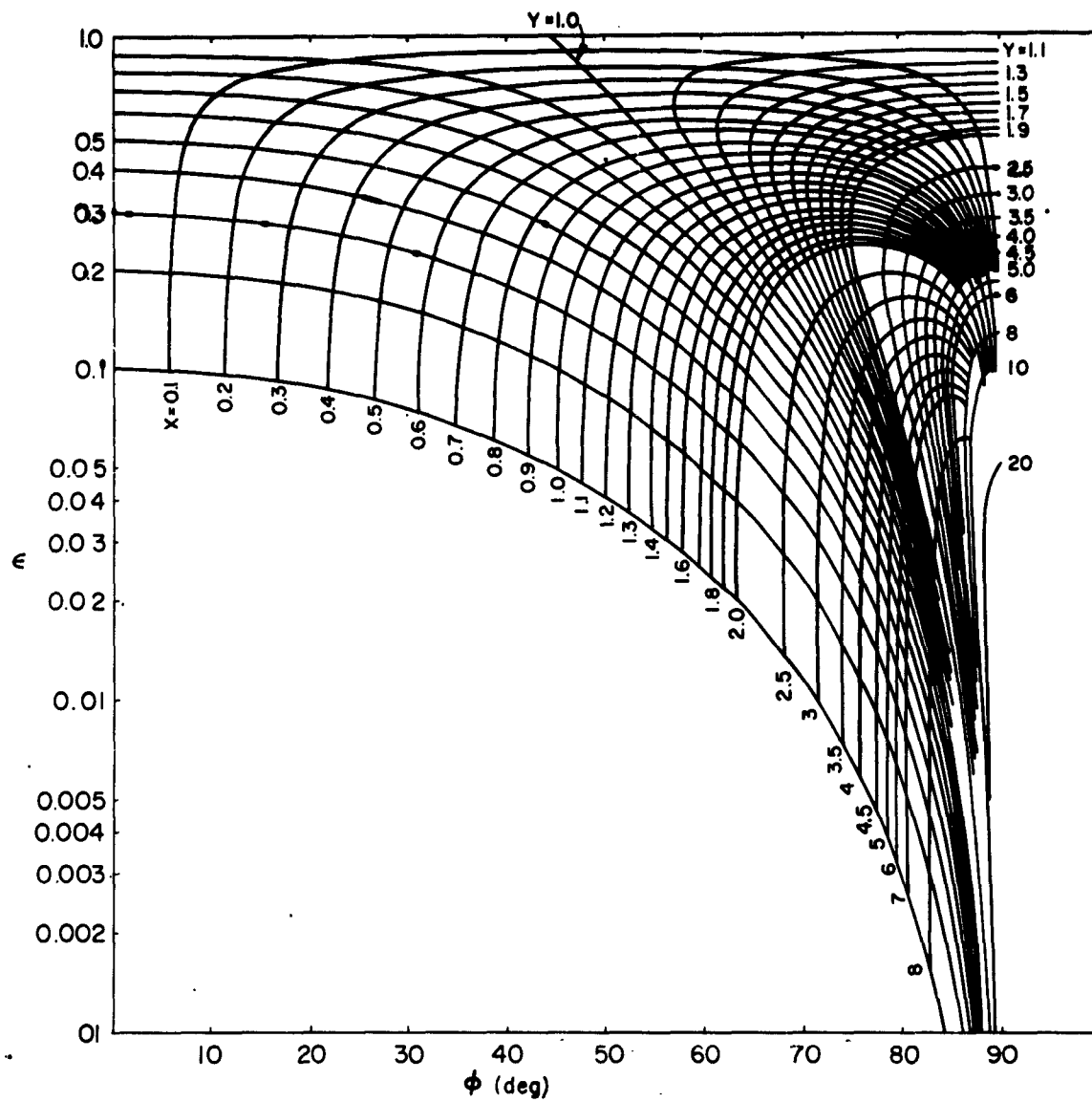
FIG. D.1.   PHASE SHIFT ELLIPSE CONVERSION CHART.

sheet can be used for both directions of conversion. The result is plotted for positive X and Y. It is evident from Eq. (D.7) that a change in the sign of Y has no effect on $\emptyset$ or ϵ, and a change in the sign of X merely changes the sign of $\emptyset$. This curve is therefore usable for all cases.

APPENDIX E.   THE TRANSMISSION COEFFICIENT APPROXIMATION

The derivation of the transmission coefficients for the V field of
whistler-mode waves traveling from the ionosphere into free space is
given in Section II-E, page 16. The derivation uses two facts which
follow from the ql approximation. The practical necessity for using the
ql approximation arises from the fact that the refractive index in the
general case is a function of the wave normal angle. This case would
require solution of a complicated equation[17] for each transmission angle,
which would complicate the solution, for several rays, to an impractical
point. The ql approximation was shown to be a valid approximation for
most of the whistler range.

When the ql assumption is applied, the refractive index becomes
independent of the wave normal. As a consequence, the two characteristic
waves are circularly polarized with opposite rotation. It is clear that
for vertical incidence, the ordinary-wave whistler energy would excite
no reflection of the other characteristic wave. For angles other than
the vertical, the amount of the other wave excited should still be small.
It was thus assumed that the field of the other characteristic reflected
wave would be negligible. A measure of the quality of this approximation
may be determined by finding the corresponding reflection coefficients
for the assumed ordinary wave. Since the $\parallel$ and $\perp$ field components in
the incident wave are equal in magnitude, the actual polarization of the
reflected ordinary wave calculated under these assumptions will be
determined by the ratio of the reflection coefficients, which we shall
label $R_\perp$ and $R_\parallel$. $R_\perp$ may be easily found from Eqs. (2.17) and (2.20a),
and $R_\perp$ from Eq. (2.18) and Eq. (2.19a).

$$R_\perp = \frac{E_{\perp r}}{E_{\perp i}} = \frac{\mu_o C_o - C_t}{\mu_o C_o + C_t} \tag{E.1}$$

$$R_\parallel = \frac{E_{\parallel r}}{E_{\parallel i}} = \frac{C_o - \mu_o C_t}{C_o + \mu_o C_t} \tag{E.2}$$

The ratio is then:

$$Q_r = \frac{R_\perp}{R_{\parallel}} = \frac{(\mu_o C_o - C_t)}{(\mu_o C_o + C_t)} \frac{(C_o + \mu_o C_t)}{(C_o - \mu_o C_t)}$$

$$= \frac{\mu_o^2 C_o C_t - \mu_o C_t^2 + \mu_o C_o^2 - C_o C_t}{-\mu_o^2 C_o C_t - \mu_o C_t^2 + \mu_o C_o^2 + C_o C_t}$$

$$\vdots$$

$$= \frac{C_o C_t (\mu_o^2 - 1) + \mu_o (C_o^2 - C_t^2)}{C_o C_t (\mu_o^2 - 1) - \mu_o (C_o^2 - C_t^2)} \tag{E.3}$$

The magnitude of this quantity will be very close to unity for large μ_o and angles of incidence not too large. The range of validity therefore is approximately that of the ql approximation.

APPENDIX F. THE CRITICAL ANGLE EFFECT IN THE IONOSPHERE

The ionosphere is assumed in this report to be homogeneous with a vertical magnetic field, with losses represented by ν, the effective collisional frequency. Not very much is known about refraction and transmission at vlf in such a medium. The assumption of infinite plane waves is not strictly correct, because of the loss factor.

The refraction properties of such a medium are treated by Stratton.[18] He considers the case of transmission from a dielectric medium (2) into a medium possessing conductivity (1). The wave which is transmitted into the refracting medium is what he calls an "inhomogeneous plane wave", in which the planes of constant amplitude are parallel to the interface. The normals to the planes of constant phase which define the direction of propagation, are inclined at an angle ψ to the normal to the interface.   The angle ψ is defined by:

$$\cos \psi = \frac{q}{\sqrt{q^2 + \alpha_2^2 \sin^2 \vartheta_o}}$$

$$\sin \psi = \frac{\alpha_2 \sin \theta_o}{\sqrt{q^2 + \alpha_2^2 \sin \theta_o}}$$

where θ_o = the angle of incidence in medium (2)

θ_1 = the angle of refraction in medium (1) as given by Snell's law

$k_1^2 = \omega^2 \epsilon_1 \mu_1 + i\omega\sigma_1\mu_1 = (\alpha_1 + j\beta_1)^2$, the square of the propagation constant in medium (1)

$k_2^2 = \omega^2 \epsilon_2 \mu_2$, the square of the propagation constant in medium (2).

$\cos\theta_1 = \rho e^{i\gamma} = \sqrt{1 - \sin^2\theta_1}$

$p = \rho(\beta_1 \cos\gamma + \alpha_1 \sin\gamma)$

$q = \rho(\alpha_1 \cos\gamma - \beta_1 \sin\gamma)$

The above equation from Stratton may be simplified by further substitution. The first step is to express $\tan \psi$ as follows.

$$\tan \psi = \frac{\sin \psi}{\cos \psi} = \frac{\alpha_2 \sin \theta_o}{q} \tag{F.1}$$

The quantity q is easily seen to be the real part of $k_1^2 \cos \theta_1$. Therefore:

$$\tan \psi = \frac{\alpha_2 \sin \theta_o}{Re k_1 \cos \theta_1}$$

$$= \frac{\alpha_2 \sin \theta_o}{Re k_1 \sqrt{1 - \sin^2 \theta_1}}$$

$$= \frac{\alpha_2 \sin \theta_o}{Re \sqrt{k_1^2 - k_1^2 \sin^2 \theta_1}} \tag{F.2}$$

Now, by the use of Snell's law, this yields:

$$\tan \psi = \frac{\alpha_2 \sin \theta_o}{Re \sqrt{\dfrac{k_1^2}{k_2^2} - \sin^2 \theta_o}} \tag{F.3}$$

Now, substitute for the propagation constants $k = \frac{\omega \mu}{c}$, where μ is the refractive index of the medium. If medium (2) is free space and we assume that medium (1) is the ionosphere, then for the whistler mode:

$$\tan \psi = \frac{\sin \theta_o}{Re \sqrt{\mu_o^2 - \sin \theta_o}} \tag{F.4}$$

This expression is readily evaluated by using the ql approximation and Eq. (2.9) for μ_o.
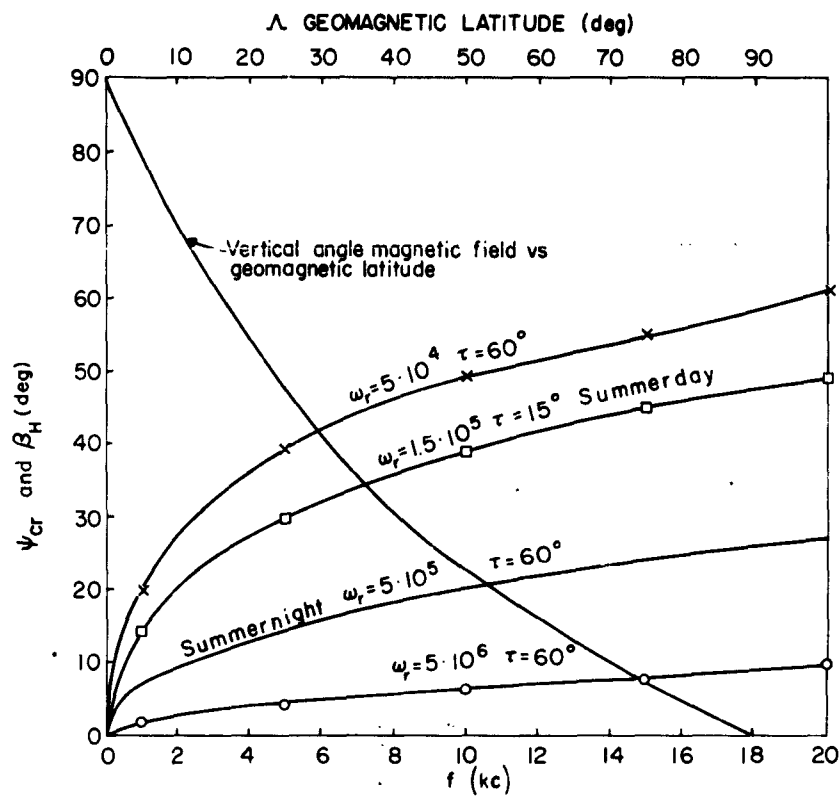
- 167 -

FIG. F.1. CRITICAL ANGLE VS FREQUENCY FOR VARIOUS IONOSPHERE MODELS
AND ANGLE OF EARTH'S MAGNETIC FIELD FROM VERTICAL VS GEOMAGNETIC
LATITUDE.

The critical angle ψ_{cr} is given when $\theta_o = 90°$, and is plotted in Fig. (F.1) for the summer-night model ionosphere, the summer-day model, and two variations of ω_r from the summer-night model. In addition, the angle of the earth's magnetic field β_H, measured from the vertical, is shown as a function of geomagnetic latitude Λ.

This figure shows several interesting features. The summer-night model curve intersects the magnetic field curve at $f \cong 10.6$ kc, and $\Lambda \cong 53°$ for $\psi_{cr} = 20.8$. Let us consider the effect on whistler excitation. Suppose that a field-aligned duct is present which may trap waves with normals reasonably close to the field angle, say 5 degrees. Trapping would then be possible over a range of latitudes above 29 degrees and for frequencies above 5.8 kc. If the trapping angle were very limited, the trapping could be confined to frequencies and latitudes above 10.6 kc and $53°$, respectively. In the opposite case, of transmission into the wave-guide, this effect could also limit the number of rays which contribute to the field at an antenna, and would modify the assumption about the exciting energy; it could cause complete cutoff in some cases. The trapping area or the exciting area would correspond to the intersection of two cones of angles, one around the field direction corresponding to the trapping angle, and the other around the vertical corresponding to the angles of refraction. Partial intersections would cause marked directional effects.[*]

Next let us consider the effect of changes in the ion density. Note that a decrease in the ion density shifts the curve upward, as shown by the curve for $\omega_r = 5 \times 10^4$, $\tau = 60°$. This would have the effect of lowering the minimum latitude for trapping. A decrease in the ionization density should cause a lowering of the minimum latitude and of the average latitude of received whistler traces. Such a decrease in density may occur after magnetic storms,[39] and the number of low-latitude whistlers received at Byrd Station, Antarctica, does indeed increase.[40] Other factors could cause this same effect, however.

---

[*]Some details of the trapping cones and the directional effect were given by R. A. Helliwell in the paper "Synoptic observations of whistler mode signals from vlf transmitters." URSI-IRE meeting, Washington D.C., May 1961.

REFERENCES

1. R. A. Helliwell, "Low frequency propagation studies, part I: Whistlers and related phenomena", Final report, Contract AF19(604)-795, AFCRC-TR-56-189 ASTIA Document AD 110184, June 15, 1953 to September 30, 1956 (revised May 28, 1958).

2. L. R. O. Storey, "An investigation of whistling atmospherics", Phil. Trans. Roy Soc. A, London, vol. 246, 1953, pp. 113-141.

3. L. R. O. Storey, "An investigation of whistling atmospherics", Ph.D. Dissertation, Cambridge University, England.

4. R. L. Smith, "The use of nose whistlers in the study of the outer ionosphere", TR No. 6, Contract AF18(603)-126, Radioscience Laboratory, Stanford Electronics Laboratories, Stanford University, July 11, 1960.

5. R. L. Smith, J. H. Crary, W. T. Kreiss, "IGY instruction manual for automatic whistler recorders", Radioscience Laboratory, Stanford Electronics Laboratories, Stanford University, January 1958.

6. R. A. Helliwell, D. L. Carpenter, "Whistlers-west IGY-IGC synoptic program", National Science Foundation Grants IGY 6.10/20 and G-8839, Radioscience Lab., Stanford University, March 20, 1961.

7. R. A. Helliwell, and E. Gehrels, "Observations of magneto-ionic duct propagation using man-made signals of very low frequency", Proc. IRE, vol 46, April 1958, pp. 785-7.

8. J. H. Crary, "Measurement and interpretation of the polarization and angle of arrival of whistlers", Paper No. 21, Symposium on the propagation of vlf radio waves, Boulder, Colorado, January 23-25, 1957.

9. M. Jean Delloue, "Contribution a l'etude de la propagation des atmospheriques siffleurs. Application a la connaissance de la tres haute atmosphere", ScD Thesis, University of Paris.

10. G. R. A. Ellis, "Directional observations of 5 kc/s radiation from the earth's outer atmosphere",J.Geophys Res., vol. 65, no. 3, March 1960, p. 839.

11. G. R. A. Ellis, "Geomagnetic disturbances and 5 kilocycles per second electromagnetic radiation", J. Geophys. Res., vol. 65, no. 6, June 1960, p. 170.

12. K. G. Budden, "The reflection of very low frequency radio waves at the surface of a sharply bounded ionosphere with superimposed magnetic field", Phil. Mag., vol. 42, 1951, pp. 833-850.

13. J. R. Wait and A. Murphy, "Multiple reflections between the earth and ionosphere in vlf propagation", Proc. IRE, vol. 45, 1957, p. 754.

14. J. R. Wait and A. Murphy, "The geometrical optics of vlf sky wave propagation", Proc. IRE, vol. 45, no. 6, June 1957.

15. J. R. Wait, "Influence of source distance on the impedance character-
    istics of vlf radio waves", Proc. IRE, vol. 48, no. 7, July
    1960, p. 1338.

16. K. G. Budden, "The propagation of a radio-atmospheric", Phil. Mag.,
    vol. 42, no. 324, January 1951, p. 1.

17. I. W. Yabroff, "Reflection and transmission at a sharply-bounded
    ionosphere", TR No. 1, Stanford Electronics Laboratories,
    Stanford University, AFOSR-TN-57-466, ASTIA Document No.
    AD 136 457, July 29, 1957.

18. J. A. Stratton, Electromagnetic Theory, McGraw Hill, New York, 1941.

19. J. R. Johler, L. C. Walters, C. M. Lilley, "Low and very low radio-
    frequency tables of ground wave parameters for the spherical
    earth theory: the roots of Riccati's differential equation",
    NBS Technical Note No. 7, 1959.

20. R. A. Helliwell, "Graphical solution of sky-wave problems",
    Electronics, Feb. 1953, pp. 150-152.

21. J. R. Wait and Alyce M. Conda, "On the diffraction of electromagnetic
    pulses by curved conducting surfaces", Can. Jour. Phy., vol. 37,
    1959, p. 1384.

22. J. R. Wait and Alyce M. Conda, "On the computation of diffraction
    fields for grazing angles", in Electromagnetic Wave Propagation,
    Edited by M. Desirant and J. L. Michiels, Academic Press, 1960.

23. F. L. Griffin, Mathematical Analysis, Higher Course, Houghton
    Mufflin, New York, 1927.

24. J. J. Gibbons and A. H. Waynick, "The normal D region of the iono-
    sphere", Proc. IRE, vol. 47, no. 2, February 1959, p. 160.

25. Sir Edward V. Appleton, "The normal E region of the ionosphere",
    Proc. IRE, vol. 47, no. 2, February 1959, p. 155.

26. J. R. Wait and L. B. Perry, "Calculations of ionospheric reflection
    coefficients at very low radio frequencies", J. Geophys. Res.,
    vol. 62, no. 1, March 1957, p. 43.

27. L. M. Milne-Thomson, Jacobian Elliptic Function Tables, Dover
    Publications, Inc., New York, 1950.

28. D. G. Cartwright, "Direction-finding on diffuse sources of electro-
    magnetic radiation", Austral. J. Phys., vol. 13, 1960, pp. 712-
    717.

29. James R. Wait, "A new approach to the mode theory of vlf propagation",
    NBS J. of Res. Ser. D, Radio Propagation, 65D, No. 1, January-
    February 1961, pp. 37-46.

30. R. A. Helliwell, W. L. Taylor, and A. G. Jean, "Some properties of
    ligntning impulses which produce whistlers", Proc. IRE, vol. 40,
    no. 10, October 1958, pp. 1760-1762.

REFERENCES (Cont'd)

31. J. R. Wait, "Discussion on sferics and whistlers", Symposium on the Propagation of vlf Radio Waves, NBS, Boulder, Colorado, vol. 4, January 1957, p. 23.

32. F. E. Terman, Electronic and Radio Engineering, McGraw-Hill, New York, 1955.

33. R. L. Smith and D. L. Carpenter, "Extension of nose whistler analysis", TR No. 8, Stanford Electronics Lab., Stanford University, Contract AF 18(603)-126, April 26, 1961.

34. J. R. Wait, Discussion in vlf Session, URSI-IRE Meeting, San Diego, California, October 1960.

35. J. A. Ratcliffe, The Magneto-Ionic Theory and its Applications to the Ionosphere, Cambridge University Press, 1959.

36. K. G. Budden, Radio Waves in the Ionosphere, Cambridge University Press, 1961.

37. Donald S. Bond, Radio Direction-Finders, McGraw-Hill, New York, 1944.

38. R. A. Barfield and W. Ross, "The measurement of the lateral deviation by means of a spaced-loop direction finder", J. Inst. Elec. Eng. (London), vol. 83, July 1938, p. 98.

39. D. L. Carpenter, "Whistler data on the change of base-level ionization in the whistler medium following magnetic storms", Joint meeting of URSI and IRE, Washington, D. C., May 1-4, 1961.

40. L. H. Martin, "Studies of vlf phenomena in the antarctic", Joint meeting of URSI and IRE, Washington, D. C., May 1-4, 1961.

41. J. M. Watts, "Direction-findings on whistlers", J. Geophys. Res., vol. 64, no. 11, November 1959, pp. 2029-30.

42. J. R. Wait, "A basis of a proposed method to measure the characteristics of an arbitrary downcoming radio wave", NBS report 3587, May 1956.

43. E. C. Jordan, Electromagnetic Waves and Radiating Systems, Prentice Hall, New York, 1950.

44. J. R. Wait and K. Spies, "Influence of earth curvature and the terrestrial magnetic field on vlf propagation", J. Geophys. Res., vol. 65, 1960, p. 2365.

45. J. R. Wait, "The mode theory of vlf ionospheric propagation for finite ground conductivity", Proc. IRE, vol. 45, no. 6, June 1957, pp. 760-767.

46. W. C. Forsythe, Smithsonian Physical Tables, Ninth revised ed., Smithsonian Institution, Washington, D. C., 1954.

47. J. Johler and L. C. Walters, "On the theory of reflection of low and very low radiofrequency waves from the ionosphere", J. Res. NBS, vol. 64D, May-June 1960, pp. 269-285.

48. J. R. Johler, L. C. Walters, and C. M. Lilley, "Transfer characteristics of radio waves propagated between the ionosphere and the earth at very low frequencies", NBS report 6002, September 15, 1958.